FEARS STRUCTURAL ENGINEERING LABORATORY

1054

subject 2: Connections - End Plate
subject 3: Computer Analysis

School of Civil Engineering and Environmental Science
University of Oklahoma
Norman, Oklahoma 73019

SPLICE RESEARCH

Progress Report

FINITE ELEMENT ANALYSIS OF TWO TENSION BOLT FLUSH END-PLATE CONNECTIONS

subject 1

by

Ali Abolmaali

and

Anant R. Kukreti — author 1

Thomas M. Murray — author 2

Co-Principal Investigators

Sponsored by

Metal Building Manufacturers Association

and

American Institute of Steel Construction

Report No. FSEL/MBMA 84-01

July 1984

FEARS STRUCTURAL ENGINEERING LABORATORY

School of Civil Engineering and Environmental Science

University of Oklahoma

Norman, Oklahoma 73019

ACKNOWLEDGMENTS

The research reported here was sponsored by the Metal Building Manufacturing Association and the American Institute of Steel Construction. Appreciation is extended to the MBMA Splice Research Subcommittee chairmen, Mr. Dennis Watson and to the members of the Subcommittee. Appreciation is also extended to Dr. Duane Ellifritt of the Metal Building Manufacturing Association and Mr. Nestor Iwankiw of the American Institute of Steel Construction. A special thanks is due to Star Manufacturing Company for providing the test specimens.

The contents of the paper are the same as the thesis submitted by Ali Abolmaali to the faculty of the School of Civil Engineering and Environmental Science, University of Oklahoma, in partial fulfillment of the requirements for the degree of Master of Science.

TABLE OF CONTENTS

LIST OF FIGURES

LIST OF TABLES

ABSTRACT

This study involves the development of a design methodology for flush end plate connections with a single row of bolts in the tension region. This geometric configuration results in a highly indeterminate problem. Thus, an analytical study which models the connection as an assemblage of finite elements was conducted. A two-dimensional mathematical model and three partial three-dimensional models using eight noded isoparametric elements for the end plate were analyzed to select the best possible finite element model for the study. A correlation factor between the two-dimensional model and partial three-dimensional model results for end-plate separation was also developed.

A sensitivity and feasibility study was conducted with information from sufficient cases so as to select parameters, within practical ranges, from pertinent geometric and force related variables governing the connection behavior. Two-dimensional finite element analyses were carried out for fifty cases and the results were regressed to provide prediction equations for maximum end-plate separation and bolt force. The results of the analytical study were compared to experimental laboratory tests on similar specimens. Finally, the prediction equations were used to develop a design methodology. An analytical equation was also obtained to predict maximum tensile force in the web of the beam using stress plots along the beam depth obtained from two-dimensional finite element analyses results.

This study was restricted to grade 50 steel and A325 high strength bolts. Based on comparison of experimental and analytical results, it was concluded that the prediction equations developed, adequately represent the connection behavior for these materials.

ELASTO-PLASTIC FINITE ELEMENT MODELING AND ANALYSIS OF A FLUSH-END-PLATE CONNECTION

CHAPTER I

INTRODUCTION

1.1 General

End-Plate connections of the typical configurations shown in Figure 1.1 are increasingly used as moment-resistant connections in framed structures. The popularity of this connections is due to economics, ease of fabrication and the assumption that they provide a rigid moment connection. A typical end-plate connection is composed of a steel plate shop welded to the end of the beam section with field attachment to an adjacent member made using rows of tensioned high strength bolts. A connection in which the end-plate projects beyond the beam flanges, as shown in Figure 1.1(c), is called an extended unstiffened end-plate connection. If an additional plate is welded to the part extended in the plane of the beam web, as shown in Figure 1.1(d), then the connection is referred to as an extended stiffened end-plate connection. A connection in which the end-plate depth is equal to the depth of the beam, as shown in Figures 1.1(a) and 1.1(b), is called a flush-end-plate connection. The above connections may be used to provide a connection between two beams, called a "splice plate connection", as shown in Figure 1.2(a), or between a beam and a column, as shown in Figure 1.2(b).

Considerable research results, of both analytical and experimental nature, are available for extended end-plate connections. In most cases, the end-plates were quite thick because the connection was designed to deliver the full moment capacity of the beam. Probably because of its lesser moment capacity, the so called "flush" end-plate connection has received much less attention. Douty and McGuire[1] studied both "extended" and "flush" end-plate connections and concluded that the behavior and strength of these two connections differ greatly, and that the findings and design methods developed for the former cannot be applied to the latter. For this reason, the voluminous literature for "extended" end-plate connections has little applicability for design of "flush" end-plate connections.

The objective of this study is to investigate the strength and stiffness of "flush" end-plate connections with one row of bolts in the tension region, with the aim of developing design procedures for such connections. The behavior of such a connection is highly indeterminate and complex and depends upon the geometric arrangement of the bolts, beam depth, beam web thickness, end-plate thickness, weld sizes and bolt and end-plate strengths.

There are at least three alternative approaches that can be used to develop the necessary design criteria:

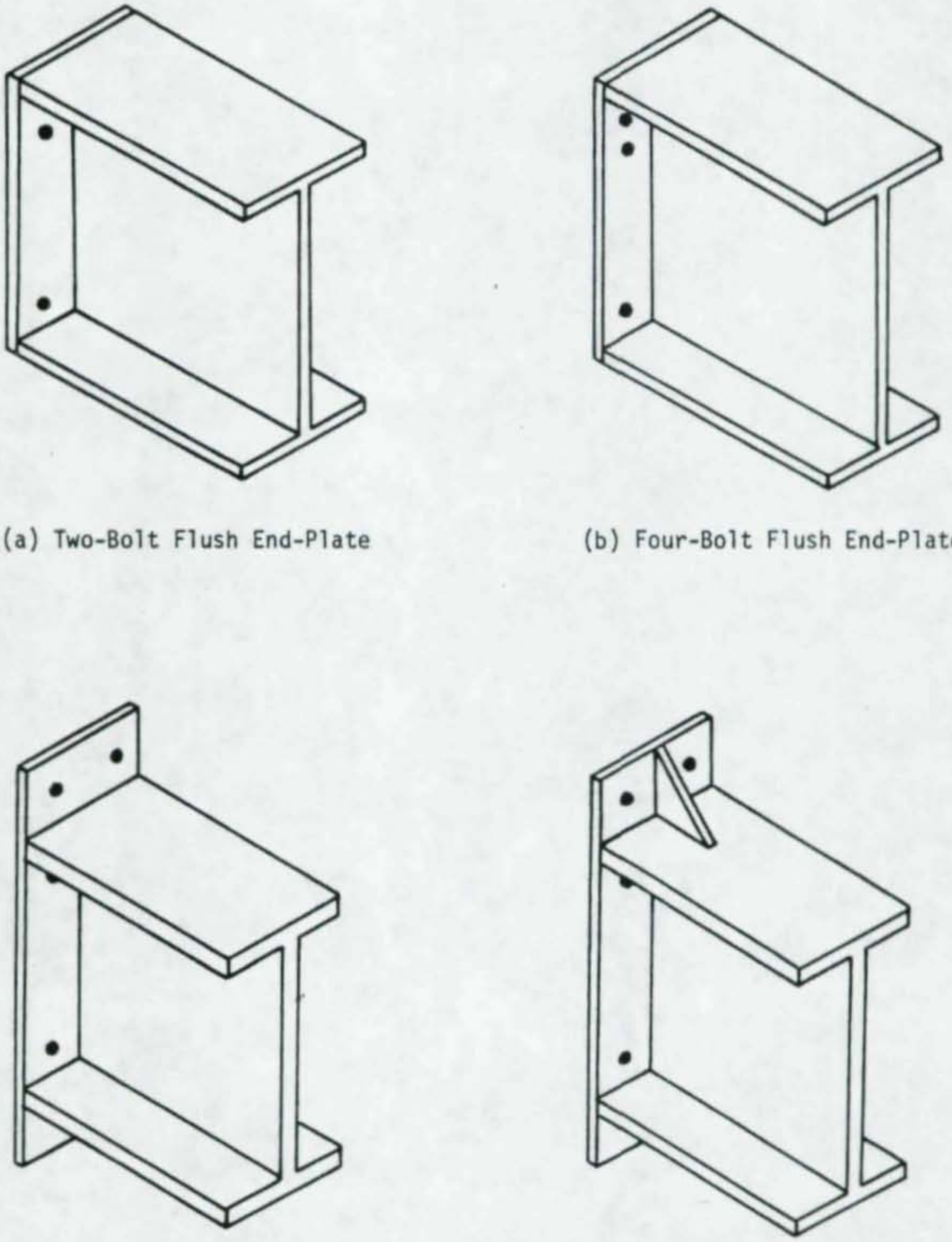

(a) Two-Bolt Flush End-Plate

(b) Four-Bolt Flush End-Plate

(c) Unstiffened Extended End-Plate

(d) Stiffened Extended End-Plate

Figure 1.1 Typical End-Plate Configurations

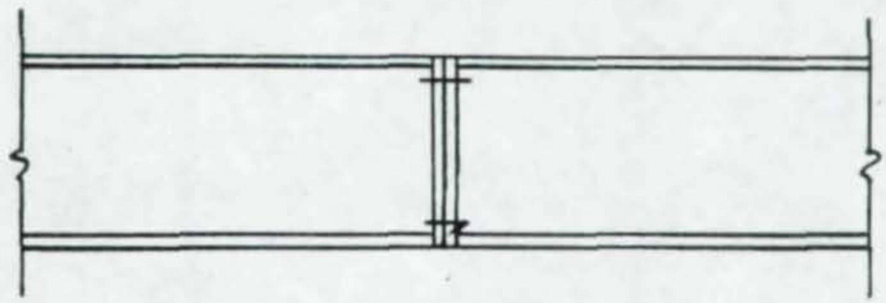

(a) Beam-to-Beam Connection (Splice Connection)

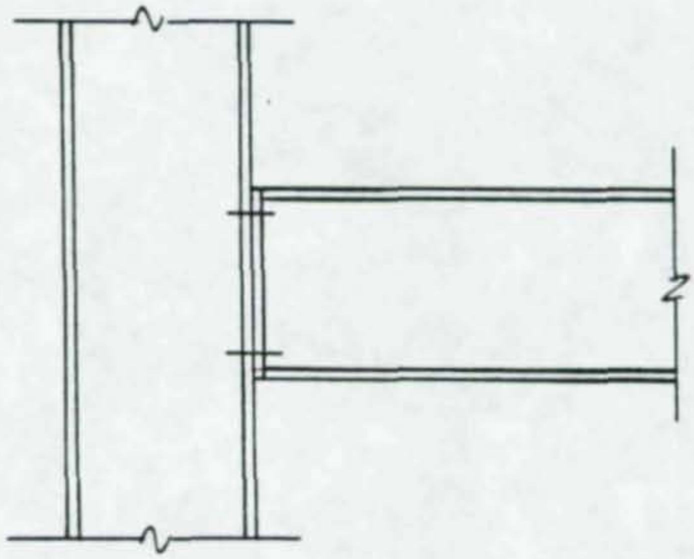

(b) Beam-to-Column Connection

Figure 1.2 Typical Uses of Flush End-Plate Connections

1. Perform regression analysis using data, such as maximum displacement and bolt force, obtained either by experimental measurements or from analytical results for many connection geometries. Analytical results may be obtained by conducting finite differences or finite element analysis. Tests are time consuming, and expensive and data gathered from them are generally limited to surface measurements giving more justification for using analytical techniques.

2. Use yield line analysis of possible mechanisms in a typical connection.

3. Combinations of 1 and 2.

It was decided to conduct two separate studies: one using finite element analyses results and the other using yield line analyses. This study reports the findings of the former approach. A separate test program on prototype connections was conducted to verify the validity of the finite-element models used in the study and also to verify the results obtained from the equations developed. The yield line study, conducted by Srouji(2), has also been completed and the findings of this study are also compared with it.

1.2 Literature Review

Douty and McGuire(1), who based their findings on a limited test series of five flush end-plate connections attached to W16x36 beams, have shown the importance of end-plate thickness on the behavior and strength of the connection. They concluded "..... except where relatively thick end-plates are used, flexure of the plate limits the effectiveness of the tension bolts removed from the immediate vicinity of the tension flange". Unfortunately, insufficient tests were performed to quantify this conclusion. From their study, they have proposed a formula to determine the flush end-plate thickness based on the assumption that the end-plate cantilevers from the nearest row of tension bolts under the action of tension flange forces. They also suggested use of maximum stress level in the plate equal to the yield stress of the plate material when the stress in the beam flange is also at its yield point.

Bockley[3] used a yield line pattern for which the beam was assumed to apply the entire bolt force to the end-plate. He has suggested the flush end-plate thickness for two rows of bolts in the tension region.

The German[4] and French[5] specifications present formulas to find the moment capacity of the connection for a known flush end-plate thickness. The presumption is that, if the tension bolts are not allowed to exceed the proof load of the bolt, the formulas can be rearranged to determine the thickness of the flush end-plate. In the German specification, it is assumed that the flange force is transferred only to the bolts adjacent to the tension flange and the bolt proof load is twice the allowable limit. The French specification formula was determined on the bases of 171 test results.

Zoetermeijer[6] carried out a theoretical analysis using yield-line theory for an infinitely long plate bounded by two fixed edges and one free edge and loaded with a concentrated force. However, it was noted that the analytical model was only an approximation, hence necessitating comparison with experimental test results. As a result of this research, a chart was developed by which the ultimate load of a stiffened column flange or a flush end-plate can be determined knowing the distance from the bolt to the beam flange and web. The study also compared the situation of one row of bolts and two rows of bolts below the tension flange by varying various geometric parameters, e.g., gage, pitch and end-plate thickness.

Packer and Morris[7] utilized curved yield line mechanisms to predict end-plate capacity with testing directed at failure of the colum flange. Due to limited experimental data, the study did not give any conclusive results. Subsequently, Phillips and Packer[8] conducted a series of tests to detect the effect of end-plate thickness on moment-rotation and end-plate collapse mechanism. They also investigated connections with two rows of bolts in the tension region to study the influence of the second row on stiffness of the conection. They concluded that flush end-plates with two-rows of two bolts at the tension flange are more suitable for semi-rigid constructions, and that the second row of bolts is effective but to a much lesser extent than expected. Also, it was seen that for practical end-plate thicknesses, the yield capacity of such connections is typically less than that of the beam yield capacity. This is contrary to the assumption made by Douty and McGuire[1]. Phillips and Packer[8] also concluded that the French specification best predicts the connection moment capacity when the bolt proof load can be reached before the plate failure occurs.

Krishnamurthy[9] performed finite element analyses of extended and flush end-plate connections. His results clearly documented the importance of end-plate bending, and its effect on the bolt forces in multiple rows; in general, he demonstrated the ineffectiveness of all but the outermost bolts, thus verifying the conclusions of Douty and McGuire[1]. Krishnamurthy concluded that additional rows of tension bolts beyond two bolt rows decreased both stiffness and strength of end-plate connections. This surprising result needs experimental verification before it can be accepted.

As stated before, the research on end-plate connections, which has been extensive in the past ten years, has focused primarily on the extended end-plate connections. Early attempts (prior to 1970) to develop a design methodology for such end-plate connections were based on tee-stub analogy. All the early research on extended end plate design resulted in large end-plate thicknesses and large bolt diameters. The reason being that a prying force was conservatively assumed to act at the edge of the end-plate. One of these methods, as quoted before, was developed by Douty and McGuire[1] and was presented in 7th edition of the AISC manual of steel construction[10]. Other significant methods using the tee-stub analogy were suggested by Kato and McGuire[11] and Nair et al[12]. Along with other methods, the aforementioned methods are summarized by Fisher and Stuik[13]. More recently, methods based on refined yield line analyses have been suggested by Zoetermeijer[6], Mann and Morris[13] and Kennedy et al[15].

Krishnamurthy[16] developed the finite-element methodology, specifically for the analyšis of unstiffened, four bolt extended end-plate connections (see Figure 1.1(c)). Based on finite-element analyses of a large number of geometric configurations of the connection along with a series of experimental tests, he developed the design methodology found in the 8th edition of the AISC manual of steel construction[17]. Krishnamurthy's theoretical results clearly showed that even enough prying action is presented, it is too conservative to assume it to be acting at the edge of the end-plate since this results in thicker than necessary plates. Krishnamurthy[18] also investigated to a limited extent, the behavior of stiffened tee-stubs as it applied to the stiffened extended end-plate connections. The study showed that by providing the stiffener a reduction in the end-plate thickness can be achieved.

Ahuja[19] investigated the behavior of stiffened extended end-plate connections with two rows of bolts on either side of the tension flange of the beam. Such connections can be used for large capacity beams where a one bolt row configuration on either side of the beam flange would result in either too thick plates or require large size bolts than can be practically used for economical, erection and fabrication reasons. Ahuja developed a prediction equation for maximum end-plate separation considering linear material behavior and finite element analyses results for 32 practical cases. He has also recommended to limit the maximum end-plate separation to 0.02 in., which can be used to size the thickness of the end-plate.

Ghassemieh[20] extended Ahuja's study to incorporate nonlinear material behavior of the end-plate and the bolts. Prediction equations were developed for maximum stress in the end-plate and forces in the bolts. A design methodology is also suggested using these prediction equations. In this study the finite element results are compared with experimental results for tee-hanger models and full scale tests. Good correlation is reported.

Srouji[2] studied the development of a methodology for the design of four types of end-plate configurations using yield-line-analysis. The four types of end-plates considered are: flush with two bolt rows in tension region, flush with four bolt rows in tension region, unstiffened extended with two bolt rows on either side of tension flange, and stiffened extended with two bolt rows on either side of tension flange. He developed prediction equations for the bolt forces including prying action. Experimental verification of the yield line analysis was conducted by Srouji for the two-bolt flush end-plate and the four bolt flush end-plate connections. He recommended the design methods for these connections using both strength and stiffness of the connection. Since stiffness data was only available for the two-bolt and the four bolt flush end-plate connections, complete design procedures for the extended end-plates were not recommended in this study.

It is evident from the aforementioned literature that considerable research results, of both analytical and experimental nature, are available for extended end-plate connections. These cannot be directly applied to flush-end-plate connections. Although several design procedures have been suggested to determine the plate thickness for flush-end-plate connections, using yield line theory and experimental test data, but the variations between the various methods is significant. Hence it is difficalt to recommend any particular method for design and additional research is needed. Further, no substantial information is available on the moment-rotation (M-θ) relationships and tensile force in the beam web for flush end-plate configurations. Hence the following research program was undertaken.

1.3 Objectives and Scope of the Research

The main objective of this study is to develop a design methodology that can be used to determine end-plate thickness and bolt size considering nonlinear material behavior for the flush end-plate connection. The secondary objective of the study is to develop a prediction equation to calculate the maximum tensile force in the beam web. As a part of the main objective, the moment-rotation characteristics and the force carried by the bolts of a typical connection would be studied.

The literature review (Section 1.2) suggests that the following geometric related variables are potentially important for flush end-plate connections:

1. Thickness of end-plate,
2. location of bolt relative to beam flange and web,
3. web thickness,
4. beam depth,
5. width of end-plate (= beam flange width),
6. bolt size, and
7. end plate weld size.

In order to focus attention on the major variables, the study was limited to following restrictions:

1. Only the effects of pure moment are studied. While it can be

be expected that end-plate splices may be used in regions in which both moment and shear act together, such combinations are not considered in the study.

2. It is postulated that the connection shall be so designed that failure will occur by either excessive yielding of the end-plate or bolt rupture. Excessive yielding failure is said to occur when the strain in the plate becomes equal to twelve times the yield strain of the plate material. Rupture of the bolt is said to occur when the strain in the bolt shank becomes equal to its ultimate value (=0.00693 in./in. for A325 bolts).

3. The study will be limited to 50 ksi grade steel and A325 bolts.

4. Small displacement theory is valid.

Keeping these in view, the study was addressed on six fronts:

1. Development of a finite element model for the connection which gives good results when compared to laboratory tests on similar specimens. Investigate the effect of mesh refinement and effect of failure criterion on the connection behavior.

2. Conduct a parametric study to investigate the pertinent geometry and force related variables that effect the behavior of connection. These will be grouped in five categories: beam dimensions, plate dimensions, bolt sizes and locations, material properties and load level.

3. Development of prediction equations for maximum deflection of end-plate and force in tension bold considering nonlinear material behavior. The prediction equation for maximum deflection of end-plate will be used to obtain the moment-rotation relationship for the connection.

4. Comparison of the analytical results obtained from the

individual finite element analysis and the prediction equations to laboratory test results and yield line results obtained by Srouji[2].

5. Formulation of a design methodology for the flush end-plate connection under study using the prediction equations developed.

6. Development of an analytical equation to predict maximum tensile force in the web of the beam using stress plots along the depth obtained from two-dimensional finite element analyses results.

A computer program formulated by Ghassemieh[20], was extensively modified to conduct the parametric study needed in this research effort. The basic finite element modeling technique and the related computer programming details are presented in Chapter II. For the parametric study, the variables were limited to practical ranges and finite element analyses of fifty cases were conducted. The development of the "best fit" prediction equations for maximum end-plate separation and force in the tension bolts are presented in Chapter III. In Chapter IV, the comparison of analytical and experimental studies are discussed. The development of the design methodologies using the prediction equations (for maximum end-plate separation and bolt force and the connection moment-rotation curve are presented in Chapter V. Finally, Chapter VI concludes the research study and also presents recommendations for future work.

CHAPTER II

FINITE ELEMENT ANALYSIS

2.1 Introduction

In this chapter, the finite element model used to analyze the behavior of a typical flush end-plate connection with two bolts in the tension region is explained. The problem is obviously three dimensional (3-D) in nature. A 3-D finite element analysis is much more complicated than a two-dimensional (2-D) analysis, and more demanding in effort of input preparation, output evaluation, and above all, in electronic time and machine requirements. It was therefore decided to conduct a 2-D finite element analysis on a plane stress model taken parallel to the plane of the web. Elements of different widths normal to the vertical plane of symmetry, (flanges, web, etc.) are treated as in-plane components with corresponding thicknesses. Transverse variations of deformations and stresses connot be represented in this model, thus for comparison purposes, it was decided to conduct 3-D finite element analyses for certain "bench mark" connections considered representative of common fabrication and construction practices. These models were developed using 3-D elements for the end-plates (where transverse geometry such as separate bolts at specified gages can be closely represented in the model and transverse variations of deformations and stresses can be determined in the solution) and 2-D elements for the beam flange and 2-D elements for the beam web. These finite element models are referred to as "partial 3-D" models in this study. The development and solution of the 2-D and partial 3-D finite element models are discussed in Sections 2.2 and 2.3, respectively. A finite element computer program incorporating nonlinear material properties, called NONEPAP (Nonlinear End-Plate Analysis Program), was developed for the study. Description of the failure criteria used to check yielding in elements is presented in Section 2.5. The salient features of the finite-element program and its flow chart are presented in Section 2.6. Finally, selection and adequacy of the 2-D and partial 3-D mathematical models are discussed in Section 2.7.

2.2 Two-Dimensional Finite Element Model Development

The configuration of the 2-D finite element model used in most analyses is shown in Figure 2.1. A length of the beam flange equal to the depth of the beam is chosen as adequate for inclusion in the analysis domain. Thus the end-plate connection is idealized as a plane stress model parallel to the web, with flanges, web, plate and bolt widths represented as elements with different thicknesses. The effect of welds was not incorporated in this model.

The bolts near the tension flange are simulated by modeling the bolt shanks as separate elements, connected to the end-plate element nodes at the plate surface, and by constraining the bolt centerline nodes against vertical displacement, as shown in the typical mesh configuration of Figure 2.1(a). For the 2-D analysis, the bolt area in a row is assumed

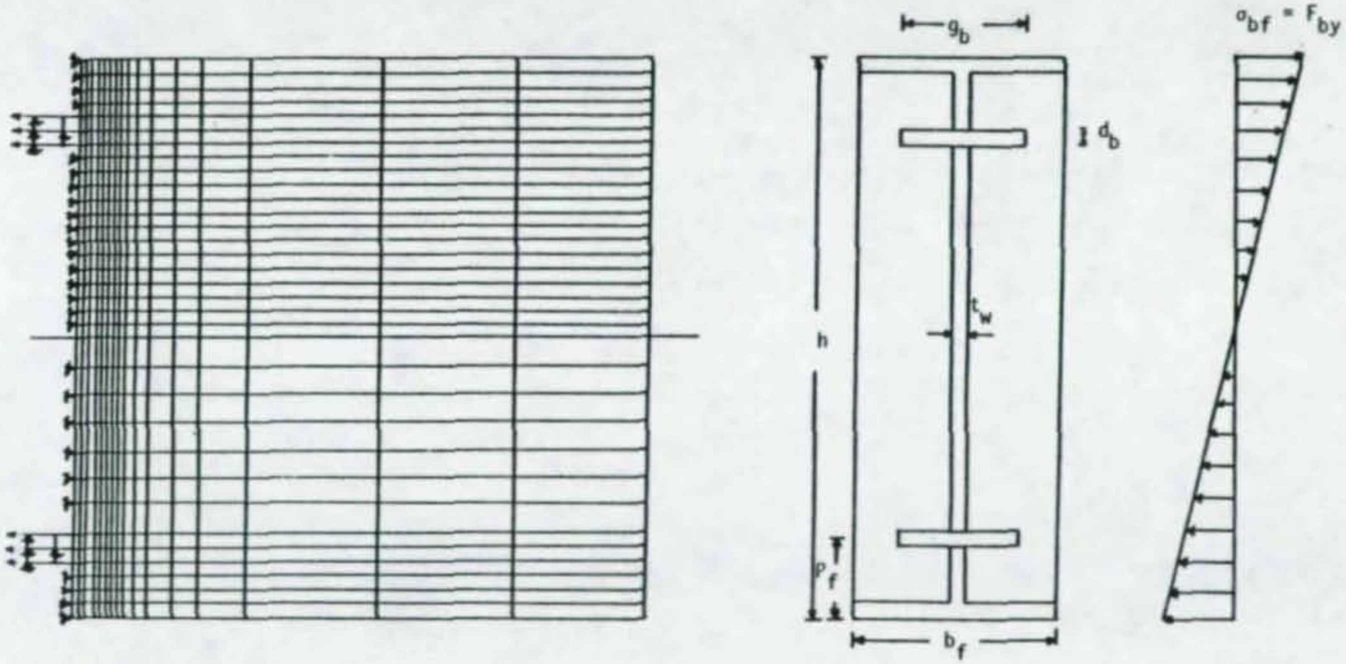

(a) Typical 2-D Mesh Configuration

(b) Section

(c) Assumed Stress Distribution

Figure 2.1 Two-Dimensional Finite Element Mesh Configuration to be uniformly spread across part of the width (in a rectangle) as shown in Figure 2.1(b). The equivalent bolt area for both the tension or the compression regions is calculated by setting the yield strength of one-third of the beam section equal to the strength of two bolts in one row (refer to Appendix G for details). Thus, bolt areas are calculated to match the strength of the beam according to the following expressions:

$$(A_B F_{by})/3 = A_{be} F_{yb} \tag{2.2.1}$$

$$A_{be} = (1/3)\ (A_B\ F_{by})/\ F_{yb} \tag{2.2.2}$$

$$(g_b)(d_b) = (1/3)\ (A_B\ F_{by})/\ F_{yb} \tag{2.2.3}$$

where A_B = area of the beam, A_{be} = equivalent area of one row (zone) of bolts, F_{yb} = yield stress of bolt material, g_b = width of equivalent bolt rectangular area and d_b = bolt diameter. Using Equation (2.2.3), the width g_b of the equivalent bolt area can be obtained and is used as the thickness of elements representing the bolts.

The effect of bolt pretensioning caused by bolt tightening is incorporated by the application of forces to the bolt shank end nodes and by imposition of the resulting displacements of these nodes in subsequent load runs. The analysis sequence is explained in detail in Section 2.6.

The moment loading on the connection is simulated by the application of forces at the nodes on the end of the beam stub as shown in Figure 2.1(c). In this figure, the extreme fibre stress is shown as αF_{by}, where F_{by} = yield stress of beam material and α is a scalar number. As will be discussed later, loads are applied on the beam section in increments of α varying from 0.1 to 1.0, in increments of 0.1.

The typical 2-D mesh of Figure 2.1 contains 560 elements, 626 nodes and 1252 degrees-of-freedom (d.o.f.). This mesh requires approximately 6 minutes of CPU (Central Processor Unit) time for analysis. Comparison of results of this model with experimental results is found in Section 2.7.

2.3 Partial Three-Dimensional Models

The accurate and ideal selection of any finite element problem is obviously a 3-D mesh. However, it is not necessarily the best choice, computer costs associated with the required number of d.o.f. in a 3-D model increases rapidly. To satisfy both economy and accuracy, a partial 3-D model was developed to study the one bolt row flush end-plate connection. Three partial 3-D models were investigated to obtain the one which best predicts results closest to the experimental results obtained by tests performed on similar specimens. Since the primary objective of the study was to simulate the end-plate behavior as accurately as possible, in all three models the end-plate was modeled with 8-noded isoparametric element developed by Levy[21], as shown in Figure 2.2. In this figure, the x, y, and z coordinates denote the global cartesian right-handed rectangular coordinates system used to describe the geometry and ξ, η, ζ coordinates are a set of skew parametric coordinates set in the element such that their values are either +1 or -1 on the faces. Besides the eight corner nodes, this element also has nine internal d.o.f., which are highly effective in eliminating the "shear error" and thus permitting the use of fewer elements than conventionally required. The 3-D elements are used where most accuracy was needed, i.e., the end plate, bolt heads and bolt shanks. Either 2-D subparametric quadrilateral or 2-D eight d.o.f. hybrid

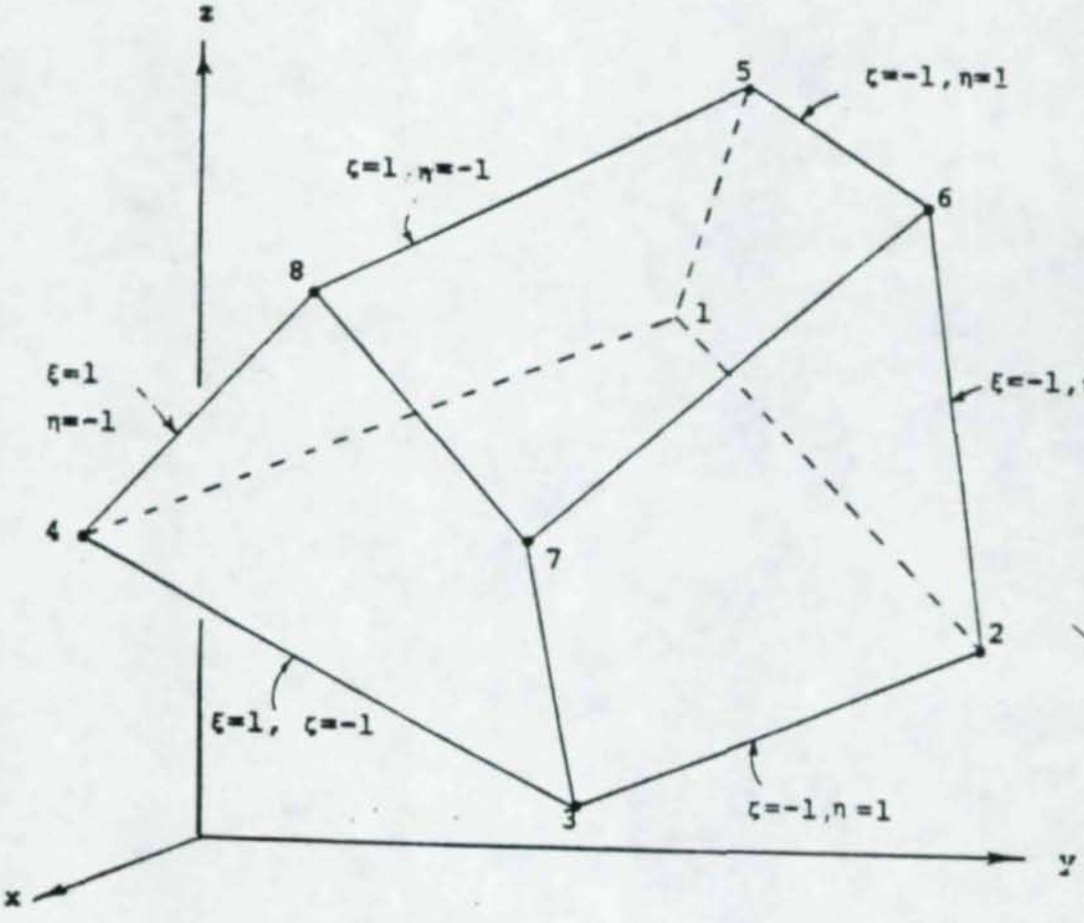

Figure 2.2 Typical 8-noded Isoparametric Element Showing Rectangular and Parametric Coordinate Systems

plane stress rectangular element developed by Turner, et al.[22] are used elsewhere, except in one model (Mesh-III) where the beam flange is also modeled using 3-D elements. In standard fabrication practice the gage of the bolt is much larger than pitch (distance of bolt from beam flange). Thus more load is transferred to the bolt directly from the beam flange through the beam web. So the weld used at the intersection of the beam flange and the end-plate is of relative more importance and was also modeled using the 3-D elements. All other welds are modeled using the 2-D elements.

The configurations of the three models investigated are described in the subsequent sections. The connection is symmetrical about the plane passing through the mid-thickness of the beam web, as shown in Figure 2.3(a). Thus only half of the connection needs to be considered in the finite element modeling and all nodes which lie on the plane of symmetry are to be constrained so as not to move normal to the plane of symmetry.

Pretensioning force is applied as nodal force on the four free bolt shank nodes. As explained before, the moment loading on the connection is simulated by the application of forces at the nodes on the end of the beam stub, as shown in Figure 2.1(c). For the Partial 3-D model, it was seen that not considering loads on the nodes of the web elements did not effect the results within the significant digits printed out in the computer output. So it was decided to only consider the loads acting on the nodes of tension and compression flange. The comparison of analytical and experimental results are presented in Section 2.7.

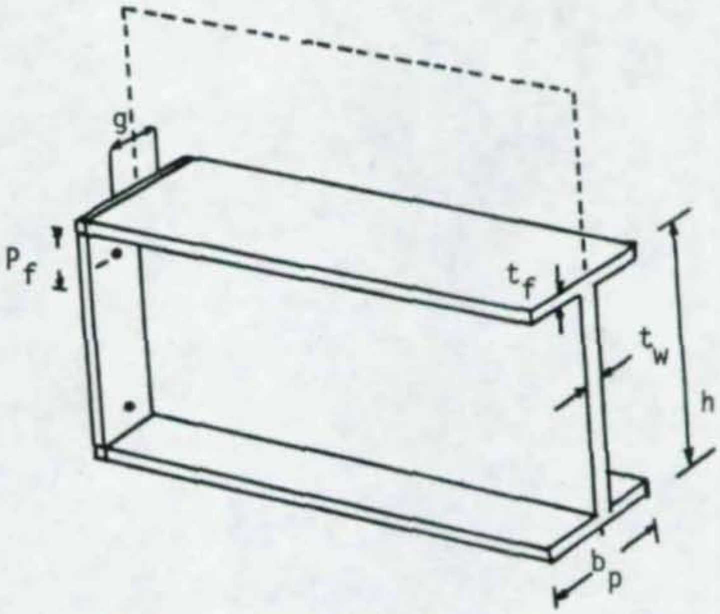

(a) Full Connection Configuration

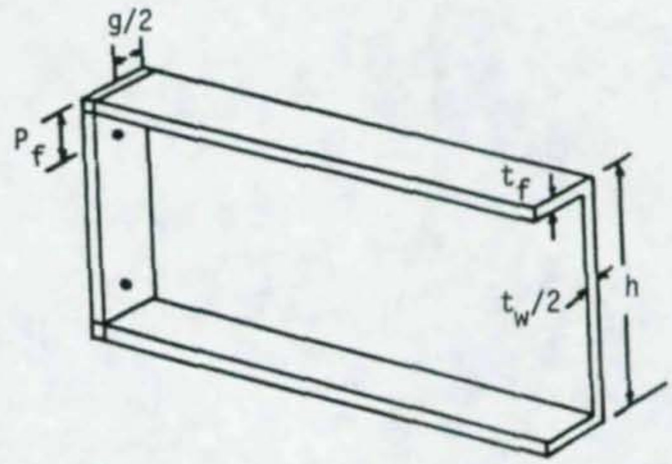

(b) Symmetrical Half Section Used

Figure 2.3 Connection Configuration and Plane of Symmetry

00728

2.3.1 Partial 3-D Mesh-I

The artial 3-D Mesh-I is shown in Figure 2.4. This mesh contains 304 elements, 470 nodes and 1222 d.o.f. It requires approximately 35 minutes of CPU time for a typical solution. In this model, the plane containing the 2-D elements is to be located so that it passes through the mid-thickness of each 2-D element. Therefore, the 2-D web elements are placed in a plane parallel to the actual plane of symmetry but located at a distance $t_w/4$ from it, in order to use $t_w/2$ as the thickness for 2-D web elements. This modeling approximation effects the other geometric dimensions which are perpendicular to plane of the web, such as width of end plate ($b_p/2 - t_w/4$ instead of $t_w/2$) as illustrated in Figure 2.5. The same modeling approximation occurs for the 2-D beam flange elements. These 2-D elements have a thickness equal to flange thickness, t_f, which can be achieved by locating the 2-D beam flange elements parallel to the beam flange and in a plane at a distance $t_f/2$ from the top and bottom flange surfaces. This modeling approximation effects the geometric dimensions perpendicular to the plane of flange elements as follows:

i) The depth of the connection in the model is $(h-t_f)$ instead of h, as shown in Figure 2.5; and

ii) The pitch of the bolt is $(p_f-t_f/2)$ instead pf p_f as shown in Figure 2.5.

Modeling of the bolt shank and the bolt head is shown in Figure 2.5 along with end-plate detail. As shown in this figure, the bolt head node 'a' is connected to the end-plate node 'a' and bolt shank

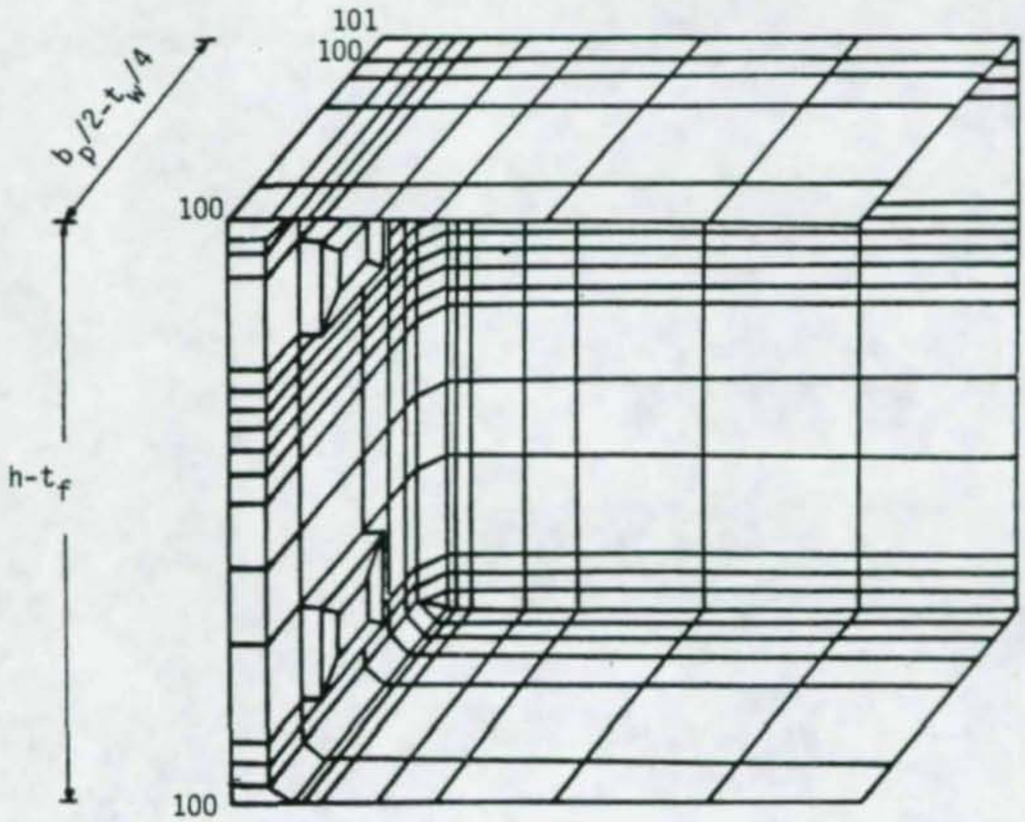

Figure 2.4 Configuration for Partial 3-D Mesh-I

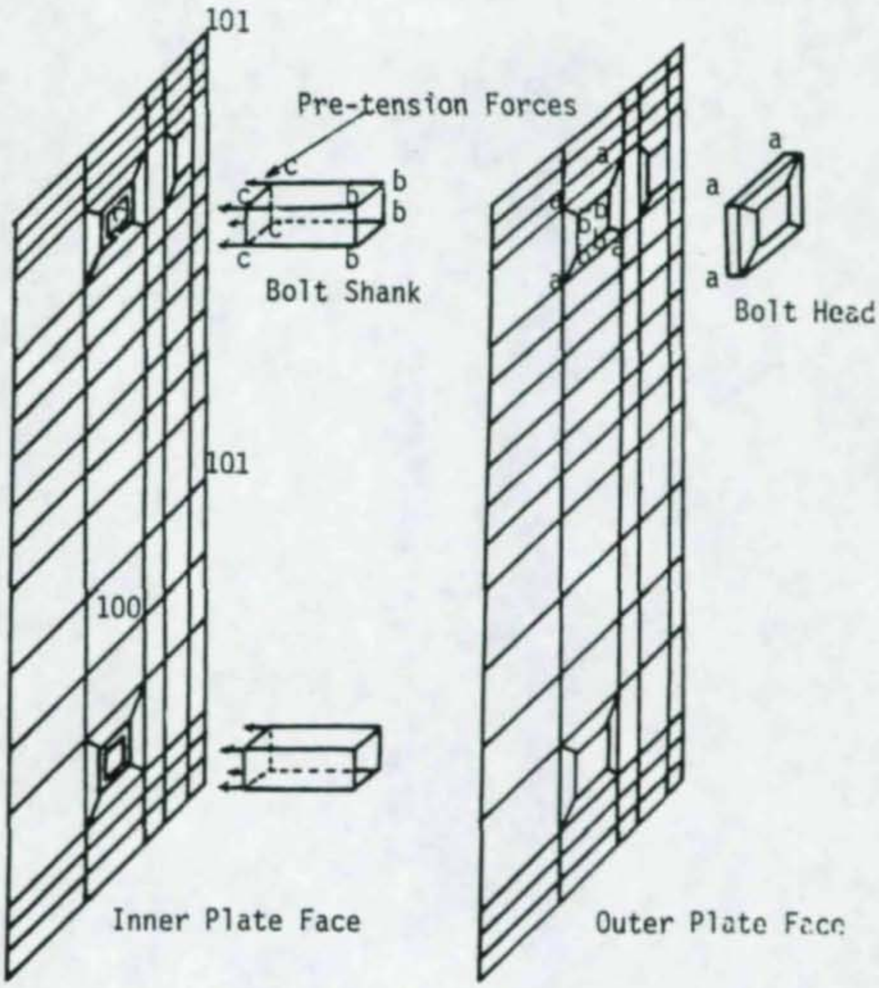

Figure 2.5 Detail of End-Plate in Partial 3-D Mesh-I

node 'b' is connected to the end-plate node 'b'. The influence of the bolt shank was carefully considered in the model. The nodes of the shank at the back of the end-plate are distinct from those of the end-plate even though they have the same coordinates, as shown in Figure 2.5. Thus, the nodes of the bolt shank are free to move in the x-direction (axial) at the bolt pretension level. To model the necking action of the shank, one of the four nodes of the shank can move in the y- and z- direction as well. The node diagonally opposite to this node is constrained to move in both the y- and z- directions while one of the adjacent nodes can move only in the y- direction. The fourth node is constrained to move only in the z-direction.

To simplify data preparation, a mesh processor was written to generate nodes information, boundary conditions, pretension loads on bolts (tension bolt and compression bolt) and applied loads at the end of beam stub (as either triangular stress distribution or as flange forces). Comparison of the results from this model with experimental results is presented in Section 2.7.

2.3.2 Partial 3-D Mesh-II

From the results of the partial 3-D Mesh-I analyses, it was concluded that it is a very flexible model. Therefore, it was decided to develop a finer finite element mathematical model (mesh) called Mesh-II, as shown in Figure 2.6. In this mesh more elements were used in the end-plate, especially on the tension side. This mesh contains 530 elements, 818 nodes and 2142 d.o.f. It requires approximately 60 minutes of CPU time for a typical solution. The modeling of end-plate, bolt shanks,

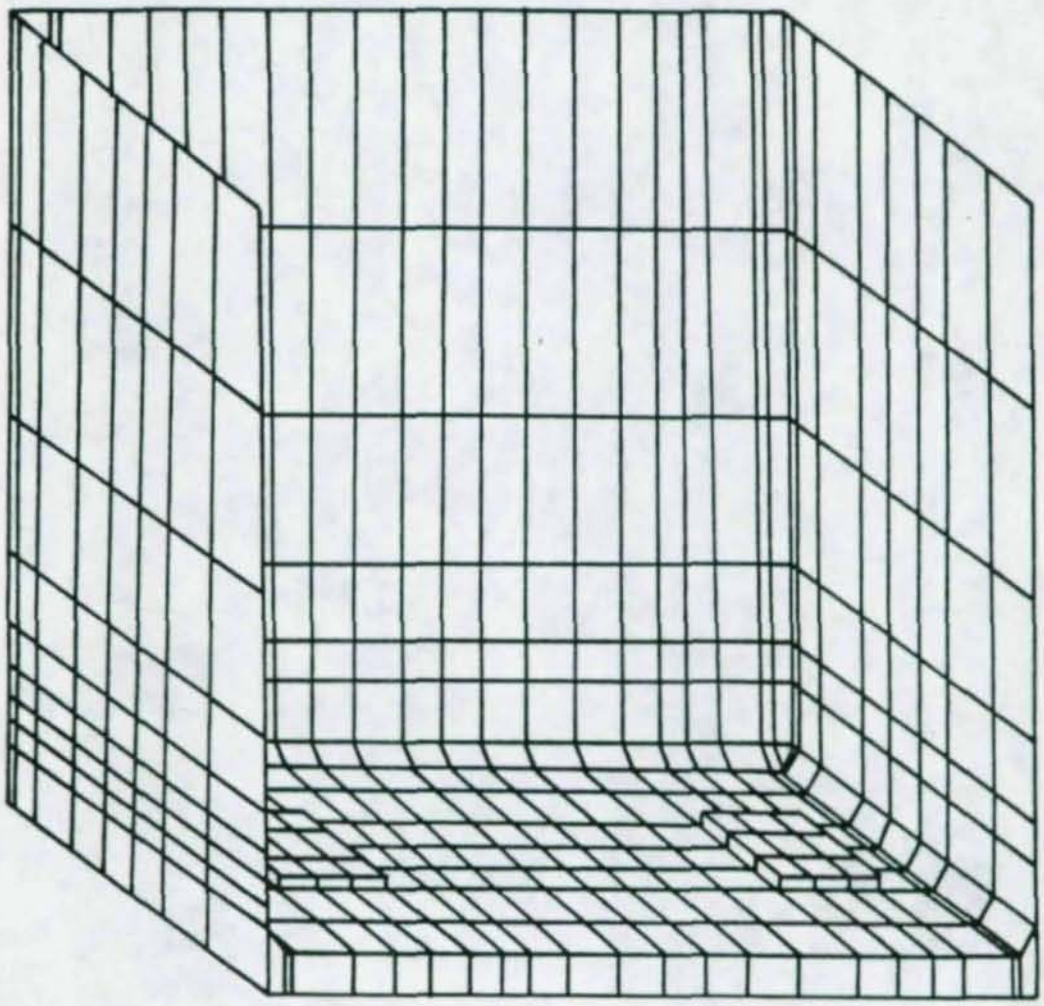

Figure 2.6 Configuration of the Partial 3-D Mesh-II

welds, web and beam flange is the same as for Mesh-I. Comparison of the results of this model with experimental results is presented in Section 2.7.

2.3.3 Partial 3-D Mesh-III

Upon careful examination of the previous partial 3-D models, it was concluded that because of a modeling approximation an important part of end-plate is not being considered in these partial 3-D models. Since the 2-D flange elements are located in a plane parallel to the beam flanges, but at a distance of $t_f/2$, and the 2-D web elements are placed at $t_w/4$. Therefore, using 2-D flange elements will lead to a loss of end-plate material in the direction of the beam depth. In the partial 3-D Mesh-III model, 3-D elements are used to model the beam flanges, end-plate, bolt shanks and bolt heads, shown in Figure 2.7. Therefore, the only 2-D elements used in this mesh are the beam web elements. This mesh contains 546 elements, 998 nodes and 2810 d.p.f. It requires approximately 150 minutes of CPU time for a typical solution. Comparison of the results of this model with experimental results is presented in Section 2.7.

2.4 Inelastic Material Properties

2.4.1 Maximum Distortion Energy Theory

Several theories of failure for yielding are discussed in mechanics of materials texts, but the one most used for steel is the maximum distortion energy theory developed by R. Von Mises[23]. In this research study, the effective stress-strain relationship of steel plates such as the end-plate, beam flanges and beam web are taken to be elastic-

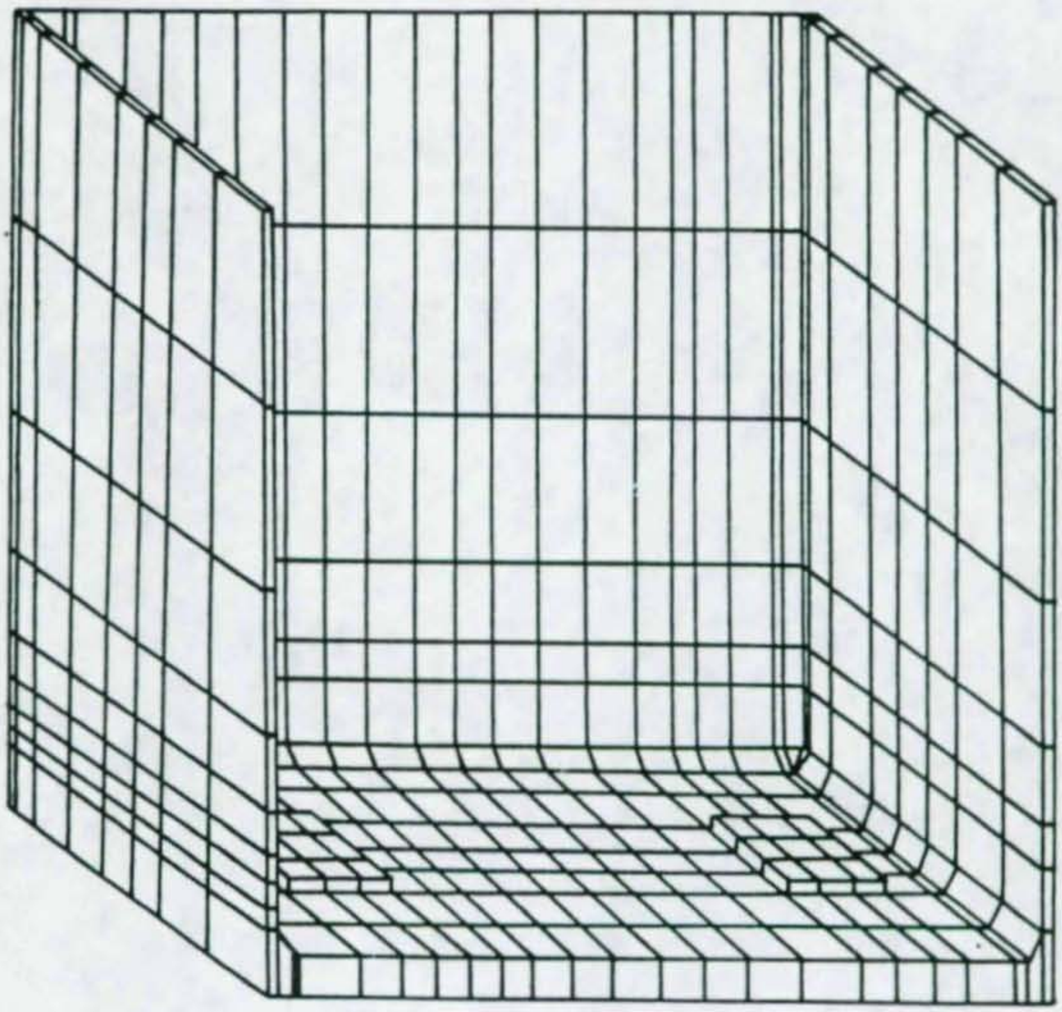

Figure 2.7 Configuration of the Partial 3-D Mesh-III

perfectly-plastic as illustrated in Figure 2.8(a). The effective stress-strain behavior of the steel bolt material is represented by a bilinear stress-strain curve as shown in Figure 2.8(b).

Based on this Maximum Distortion Energy Theory, a material is yielded when the following relationship is true:

$$(\sigma_1-\sigma_2)^2 + (\sigma_2-\sigma_3)^2 + (\sigma_3-\sigma_1)^2 > 2\sigma_y^2 \qquad (2.4.1)$$

$$\sigma_{eff}=1/\sqrt{2}\{(\sigma_1-\sigma_2)^2 + (\sigma_2-\sigma_3)^2 + (\sigma_3-\sigma_1)^2\}^{1/2} > \sigma_y \qquad (2.4.2)$$

where σ_1, σ_2, and σ_3 are the principal stresses ($\sigma_1>\sigma_2>\sigma_3$) and σ_y is the yield stress of material obtained from a uniaxial tensile test. When $\sigma_{eff} > \sigma_y$, then the element is said to have yielded. To consider the nonlinear behavior, it is convenient to convert stresses to strains, since for the plate material, the stresses remains constant upon yielding. The principal stresses are transferred to principal strains by the following relationships:

$$\sigma_1= \mu\{(1-\nu)\ \varepsilon_1 + \nu\varepsilon_2 + \nu\varepsilon_3\} \qquad (2.4.3a)$$

$$\sigma_2= \mu\{\nu\varepsilon_1 +(1-\nu)\ \varepsilon_2 + \nu\varepsilon_3\} \qquad (2.4.3b)$$

$$\sigma_3= \mu\{\nu\varepsilon_1 + \nu\varepsilon_2 + (1-\nu)\ \varepsilon_3\} \qquad (2.4.3c)$$

where ν is the Possions's ratio and μ is calculated using the following relationship.

$$\mu= E/\ \{(1+\nu)(1-2\nu) \qquad (2.4.4)$$

and ε_1, ε_2 and ε_3 are the principal strains ($\varepsilon_1>\varepsilon_2>\varepsilon_3$). Substituting Equation (2.4.3a to b) into Equation (2.4.2), gives

$$(\sigma_1-\sigma_2)^2+(\sigma_2-\sigma_3)^2+(\sigma_3-\sigma_1)^2=\left(\frac{\varepsilon}{1+\nu}\right)^2 \{(\varepsilon_1-\varepsilon_2)^2+(\varepsilon_2-\varepsilon_3)^2+ (\varepsilon_3-\varepsilon_1)^2\}\leq 2(\varepsilon y)^2 \qquad (2.4.5)$$

or

$$\frac{\sqrt{2}}{2(1+\nu)} \{(\varepsilon_1-\varepsilon_2)^2 + (\varepsilon_2+\varepsilon_3)^2 + (\varepsilon_3-\varepsilon_1)^2\}^{\frac{1}{2}} \leq \varepsilon_y \qquad (2.4.6)$$

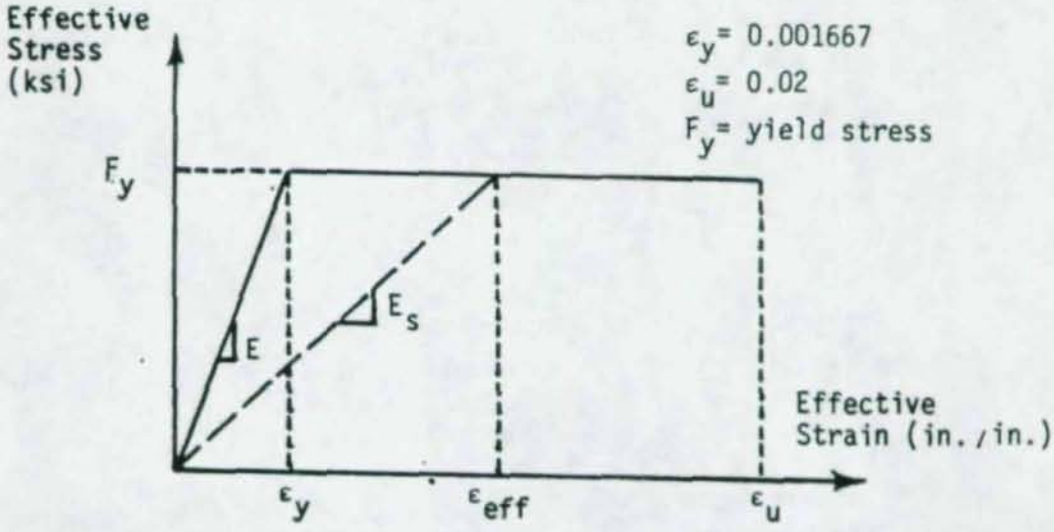

(a) Idealized Stress-Strain Diagram and Secant Modulus for End-Plate

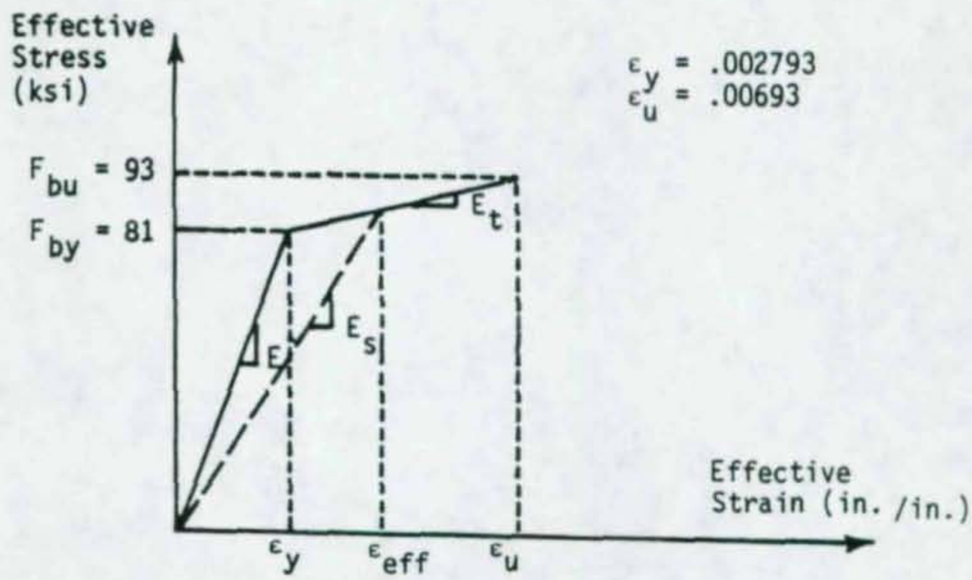

(b) Idealized Stress-Strain Diagram and Secant Modulus for A325 Bolt

Figure 2.8 Idealized Non-linear Stress-Strain Used where ε_y is the yield strain of the material from a uniaxial tensile test. Taking $\nu = 0.5$ for the plastic region, Equation (2.4.6) reduces to

$$\frac{\sqrt{2}}{3}\{(\varepsilon_1-\varepsilon_2)^2+(\varepsilon_2-\varepsilon_3)^2+(\varepsilon_3-\varepsilon_1)^2\}^{\frac{1}{2}} \leq \varepsilon_y \qquad (2.4.7)$$

Therefore, the effective strain, ε_{eff}, in any element of the end-plate is calculated in terms of principal strains of the element, as follows:

$$\varepsilon_{eff} = \frac{\sqrt{2}}{3}\{(\varepsilon_1-\varepsilon_2)^2+(\varepsilon_2-\varepsilon_3)^2+(\varepsilon_3-\varepsilon_1)^2\}^{\frac{1}{2}} \qquad (2.4.8)$$

If ε_{eff} is found to be greater than ε_y, then the element is said to have yielded and the elastic modulus, E, cannot be used to formulate the stiffness matrix of such an element since E=0. (A singular system stiffness matrix will result.) Hence, for yielded elements the reduced modulus of elasticity is taken as the secant modulus of elasticity, E_s, which can be calculated from (see Figure 2.8a):

$$E_s = \frac{\sigma_y}{\varepsilon_{eff}} \qquad (2.4.9)$$

In each cycle, the elastic modulus of the yielded elements (i.e., when $\varepsilon_{eff} > \varepsilon_y$) is set to their secant values.

To check for yielded elements, principal strains are calculated based on two methods:

1. Principal strains are calculated at each node and the average of these values taken as ε_1, ε_2, and ε_3 for each respective element to be used to compute ε_{eff} from Equation (2.4.8).

2. Principal strains are calculated at centroid of each element and these are used for each respective element to compute ε_{eff} from Equation (2.4.8).

For the 2-D model, both the options implemented, but for 3-D models only the second option was used.

2.5 Finite-Element Program

The Finite element program used in this research study was written in FORTRAN language and implemented on the University of Oklahoma's IBM-380 model D computer. This computer program is essentially the same as the one described by Ghassemieh[20], with nonlinear capability being incorporated for both 2-D and 3-D elements and direct access files used to minimize costs. The modified program was called "Nonlinear End Plate Analysis Program" (NONPAP), and is written specifically for the purpose of analyzing bolted end-plate connections considering nonliner material behavior and takes into account the pretension force applied to the bolts. It also considers the possibility of plate separations.

The program is a relatively large program with approximately 2000 records and requires about 8 seconds of CPU time for compilation alone. The core memory requirements are of the order of 292 and 423k for 2-D and 3-D typical runs, respectively. The program requires two input and one output units for operation. In addition direct access files are used throughout the program.

The program execution begins with reading the basic geometry of the mesh along with the material properties of the element. Then the main program calls the pre-processor subroutine for generating node coordinates, element definition and material properties of the elements. Data is processed and all elements are identified with their appropriate boundary conditions. The main program then calls subroutine STIFF to formulate the system stiffness matrix.

In subroutine STIFF, first the element number (MM), d.o.f.

number (MID) and element type (MDF) are written on direct access File 15. Then the element subroutines, bar (BARSP), Triangle (TRIAN), rectangle (RECT), quadrilateral (QUAD) or solid (SOLID) are called to generate the element stiffness matrices, depending on the type of element used. In addition, the element stiffness matrices are also written on a new File 17, which is retained so as to store the elastic stiffness matrix of each element. In the QUAD subroutine, the displacement-stress transformation matrices (DB) of the 4 corner nodes of the element are also written on the direct access Files 20 and 21 before the element stiffness matrix is written. Similarly, in the SOLID subroutine, the displacement-transformation matrices (BB) and displacement-stress transformation matrices (DB) evaluated at the corner nodes (or at the centroid when a yield check is made at the centroid) of the element are also written on the direct access Files 18 and 19 before the element stiffness matrix is written. After formulating the element stiffness matrices, these are stuffed into the system stiffness matrix using compatibility relationships between element nodes. Similarly, the load vector which is read in the main routine, for each loaded element (concentrated nodal loads only considered) is stuffed into the system load vector.

The resulting stiffness matrix will be symmetric for a stable structure and banded with the size: (NDOF x IBD), where NDOF = total number of d.o.f. and IBD = band width. Thus the stiffness matrix contains (2xIBD-1)xNDOF non-zero elements. Using the symmetry of this matrix, the core storage can be reduced by storing only the upper (NDOFx IBD) portion of the system stiffness matrix, which is a rectangular matrix. But, since the finite-element model for the whole connection gives a large number of system equations (specially for partial 3-D models), even this method of storing the system stiffness matrix is inadequate, and an alternative procedure was to be developed. The problem was solved in the subroutine STIFF by dividing the system matrix into many blocks and having two blocks in the computer core at a time, while the remaining portions are kept in sequential file. Thus, in the subroutine STIFF two blocks are used with lower one being moved up at the upper one is being read from the file. Determination of the block size and number of blocks is automated. The block size is computed as NBD-3 (maximum node difference + 1) , where NBD = maximum difference in d.o.f. numbers in any element + 1. The number of blocks required to subdivide the system stiffness matrix is computed from NBL = 1 + (NDOF-1)/ NBD . In a "Do-Loop" covering all NBL, elements associated with the d.o.f. in a certain block are stored in that block. Modification is also made in the load vector for changes made in the boundary conditions of the back nodes of the end-plate.

The main routine then calls the subroutine BANSOL to obtain the solution of the system stiffness equilibrium equation for nodal displacement. The modified Guass elimination technique is utilized to solve the banded equations which are stored in the blocks. Finally, subroutine STREAC is called by the main program to calculate the stresses and reactions.

In the subroutine STREAC, the following files read in a "Do-Loop" covering all the element:

1) The element number, d.o.f. numbers, and element type are read from File 15.

2) Strain-displacement matrices and stress-displacement matrices are read from File 18 and 20.

3) Elastic stress-displacement matrices are read from File 21.

To consider the inelastic effect, the element stiffness matrix of those elements whose effective strain exceeds the yield strain will have to be modified. The effective strain for each element is calculated using Equation (2.4.8), where for the first option, the principal strains are calculated (using strain-displacement matrices) first at each corner node and then an average value used to check yielding. In the second option, where a yield check is made at the centroid, the effective strain is calculated directly at the centroid only. If element is yielded, then the element stiffness matrix is adjusted by an appropriate scaling factor (SF) which is found from the following equation:

$$SF = E_s/E \tag{2.5.1}$$

For a yielded element, n, the new element stiffness matrix, $(K)^n$, is then computed from

$$(K)^n_{new} = SF\ (K)^n_{elastic} \tag{2.5.2}$$

From Equation (2.5.2), it is found that the element elastic stiffness matrices are required to compute the modified (or new) element stiffness matrices in each cycle to consider nonlinear material behavior. If an element has not yielded, then the program proceeds without changing the element stiffness matrix. The updated stiffness matrix replaces the old one on the direct access File 16 for further computation. For a yielded element, the stress-displacement matrices, $(DB)^n$, also have to be modified in the same way as stiffness matrix, i.e.,

$$(DB)^n_{new} = SF\ (DB)^n_{elastic} \tag{2.5.3}$$

The updated stress-displacement matrices and strain-displacement matrices are replaced on the direct access Files 18 and 20 in adequate places. Finally, the stress, $\{\sigma\}^n$, and reactions, $\{Rec\}^n$, for each element are calculated from the deflection vector, $\{\sigma\}^n$, for the element, i.e., from

$$\{\sigma\}^n = (DB)^n_{new}\ \ \{\sigma\}^n \tag{2.5.4}$$

and

$$\{Rec\}^n = (K)^n_{new}\ \{\sigma\}^n \tag{2.5.5}$$

Thus, the new direct access Files 16, 18 and 20 contain information regarding the updated stiffness matrices and the appropriate updated transformation matrices of the elements.

The value of the ratio SF for an element indicates the degree of yielding in the element. Failure in a plate element is said to occur due to excessive yielding if the strain becomes equal to 0.02 (i.e., SF=1/12). For the bolt shank element, failure is said to occur due to rupture if strain is equal to or exceeds 0.00693 (i.e., SF = 0.40). If any of these failure modes occur then the execution is stopped and a message is printed defining which criteria was violated. The variation of load versus SF for a typical element is shown in Figure 2.9. One of the corner nodes of this element experiences the maximum end-plate separation. As shown for this connection, at load level 4 (when $\sigma_{bf} = 0.4\sigma y$, also see Figure 2.1(c)) the connection fails due to excessive yielding in the end-plate.

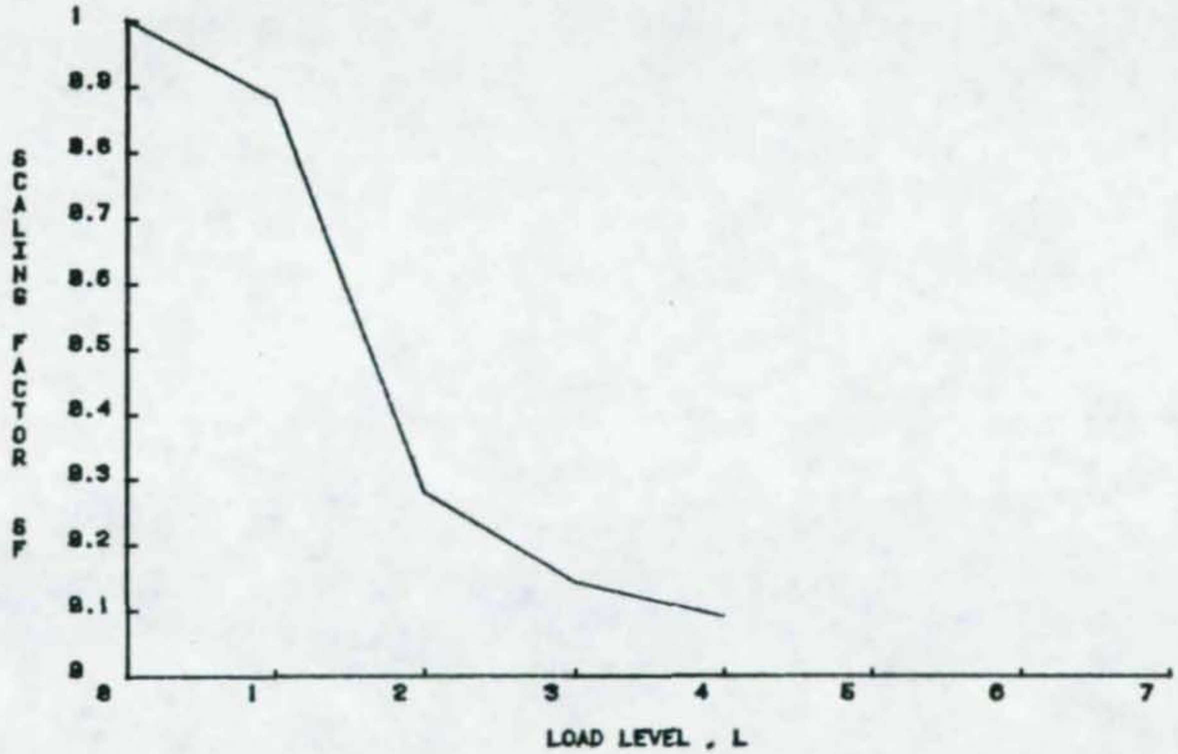

Figure 2.9 Load Level Versus Scaling Factor, SF

A typical analysis sequence is as follows: The pretension caused by the bolt tightening is first applied as forces at the bolt end nodes. Displacements of bolt nodes and the back of the end-plate are then determined. The resulting bolt elongations and displacements are applied as specified displacements for the subsequent external loadings, thus simulating bolt tightening process and subsequent iteration with the other components. When the pretension load is applied, the back of the end-plate is assumed to be in contact with the support, and the actual deformed shape is determined by an automated trial and error procedure. At the end of each cycle, the displacements and reactions of the nodes at the back of end-plate are checked, nodes tending to move away from supports are released; previously released nodes which moved into the support region are constrained. The process of analysis and checking support modifications is repeated until no changes occur.

The flow chart of the program is shown in Figure 2.9 and the associated variables are defined in Table 2.1.

2.6 Comparison of 2-D and Partial 3-D Results

Upon comparison of the results of the 2-D and partial 3-D finite element analyses with eight sets of experimental test results (discussed in Chapter IV), it was found that the partial 3-D model that best compared with experimental results required approximately 150 minutes of CPU time. The similar 2-D model required about 6 minutes of CPU time. It is obvious that the 2-D model is much more suitable for regression analysis than the 3-D model because of computer time associated cost. Figures C.3 and C.4 in Appendix C shows a close correlation between 2-D and

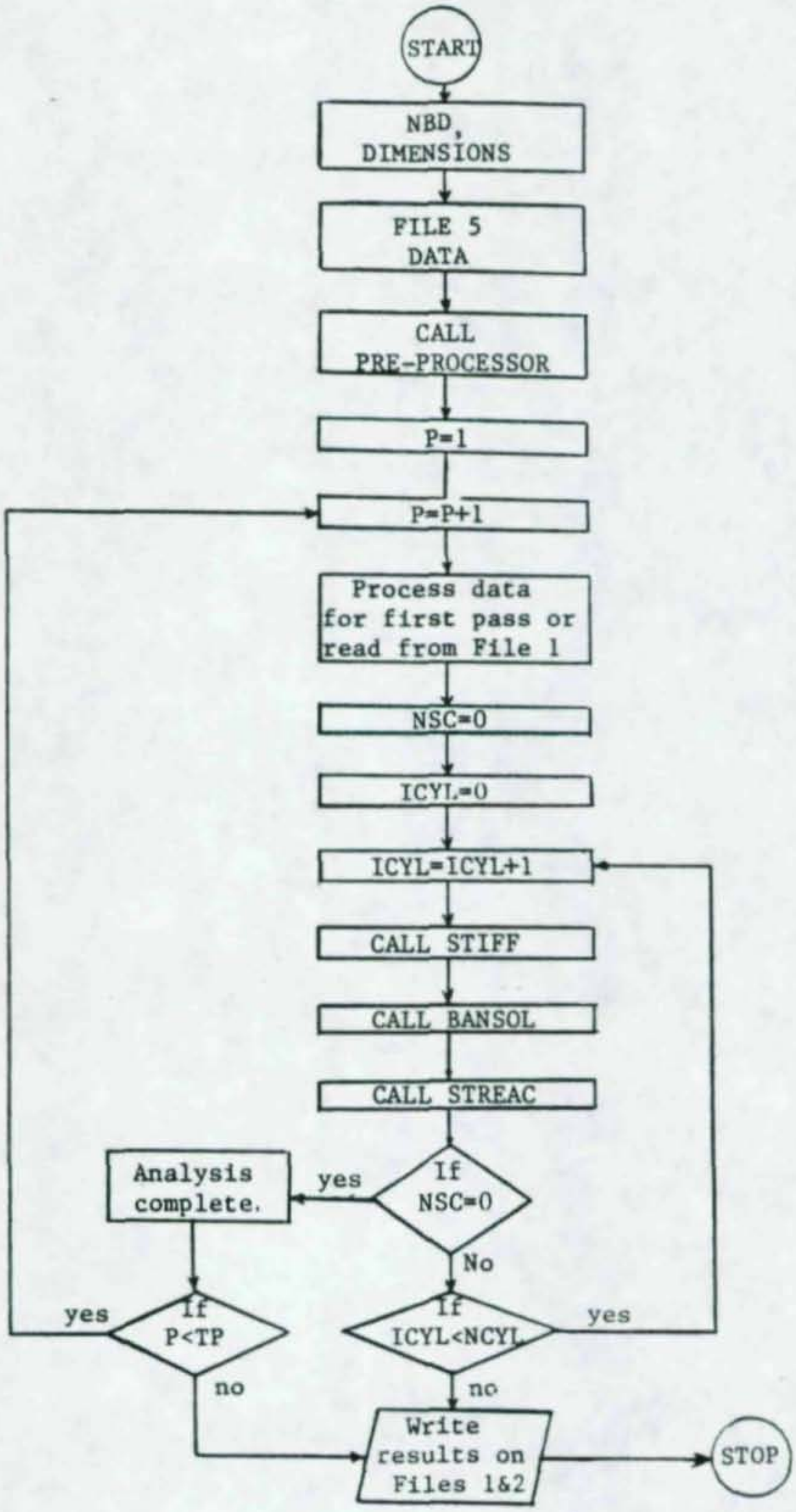

(a) MAIN Routine

Figure 2.10 Macro Flow Chart for Finite Element Program

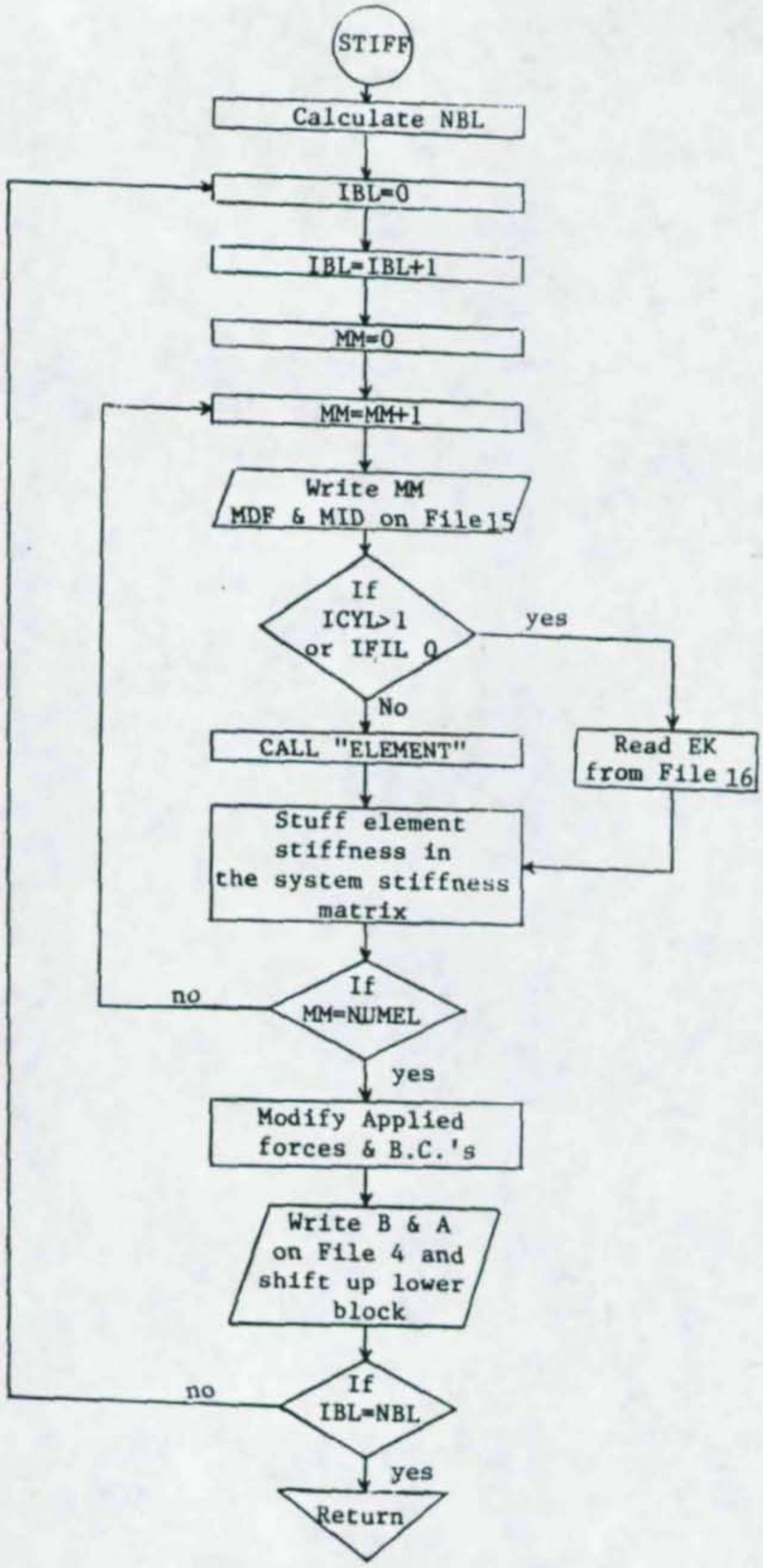

(b) STIFF Subroutine

Figure 2.10 Macro Flow Chart for Finite Element Program (continued)

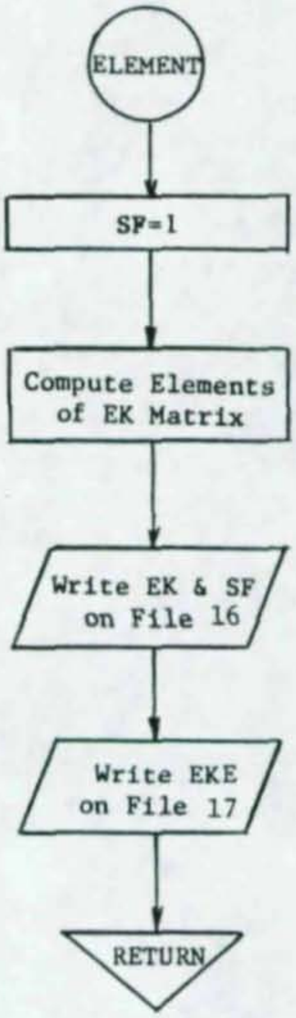

(c) BARSP, TRIAN and REST Element Subroutines

Figure 2.10 Macro Flow Chart for Finite Element Program (continued)

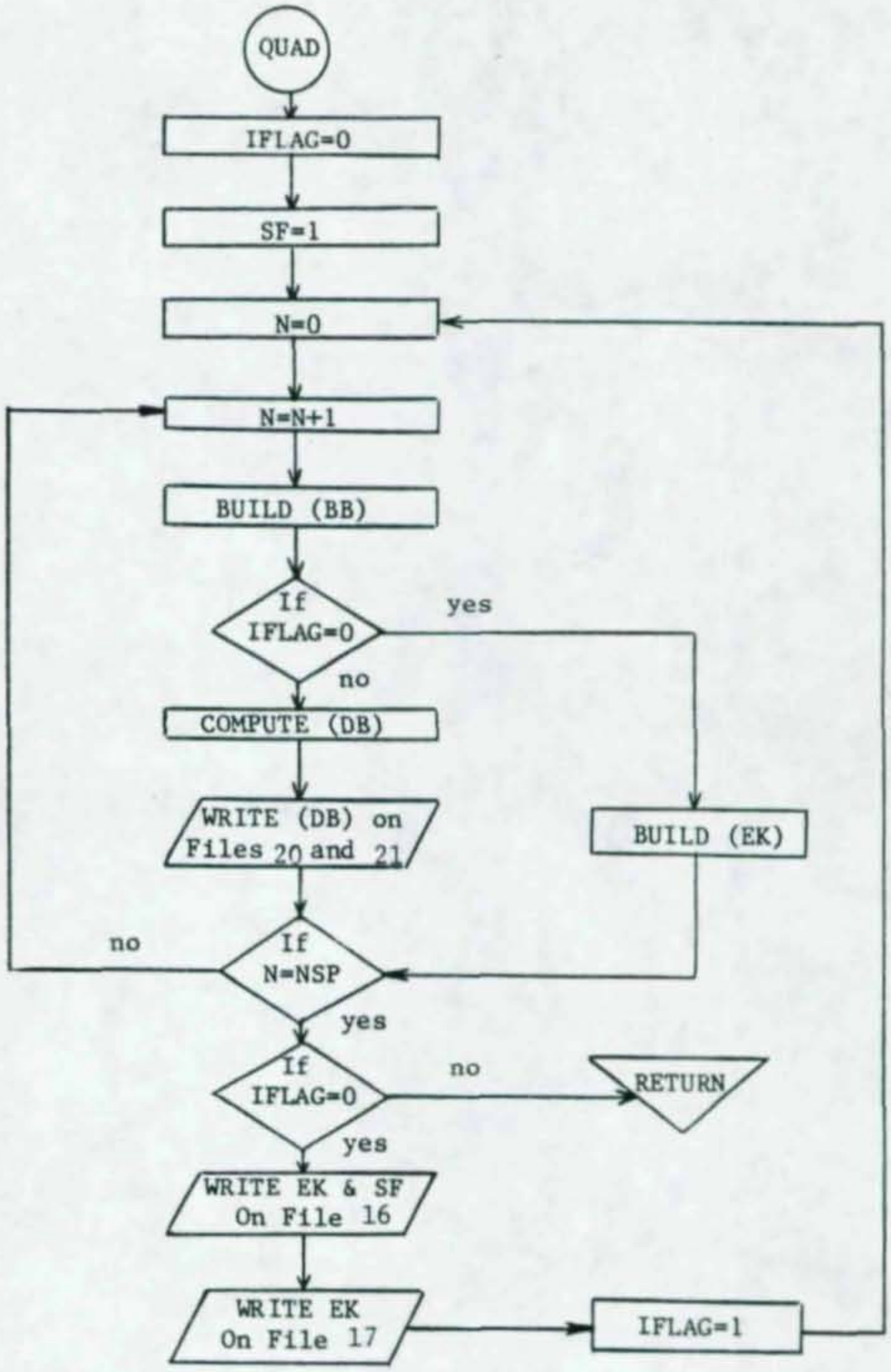

(d) QUAD Element Subroutine

Figure 2.10 Macro Flow Chart for Finite Element Program (continued)

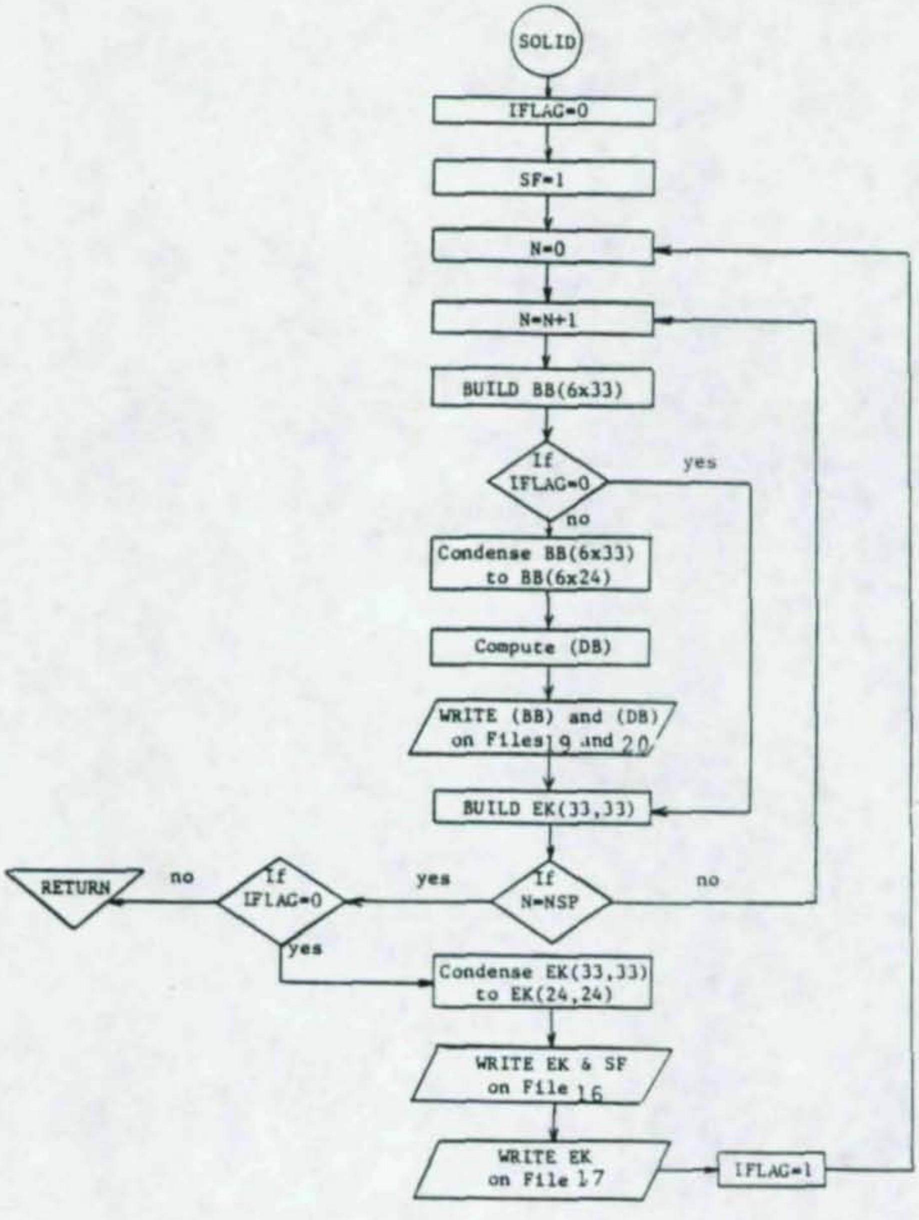

(e) SOLID Element Subroutine

Figure 2.10 Macro Flow Chart for Finite Element Program (continued)

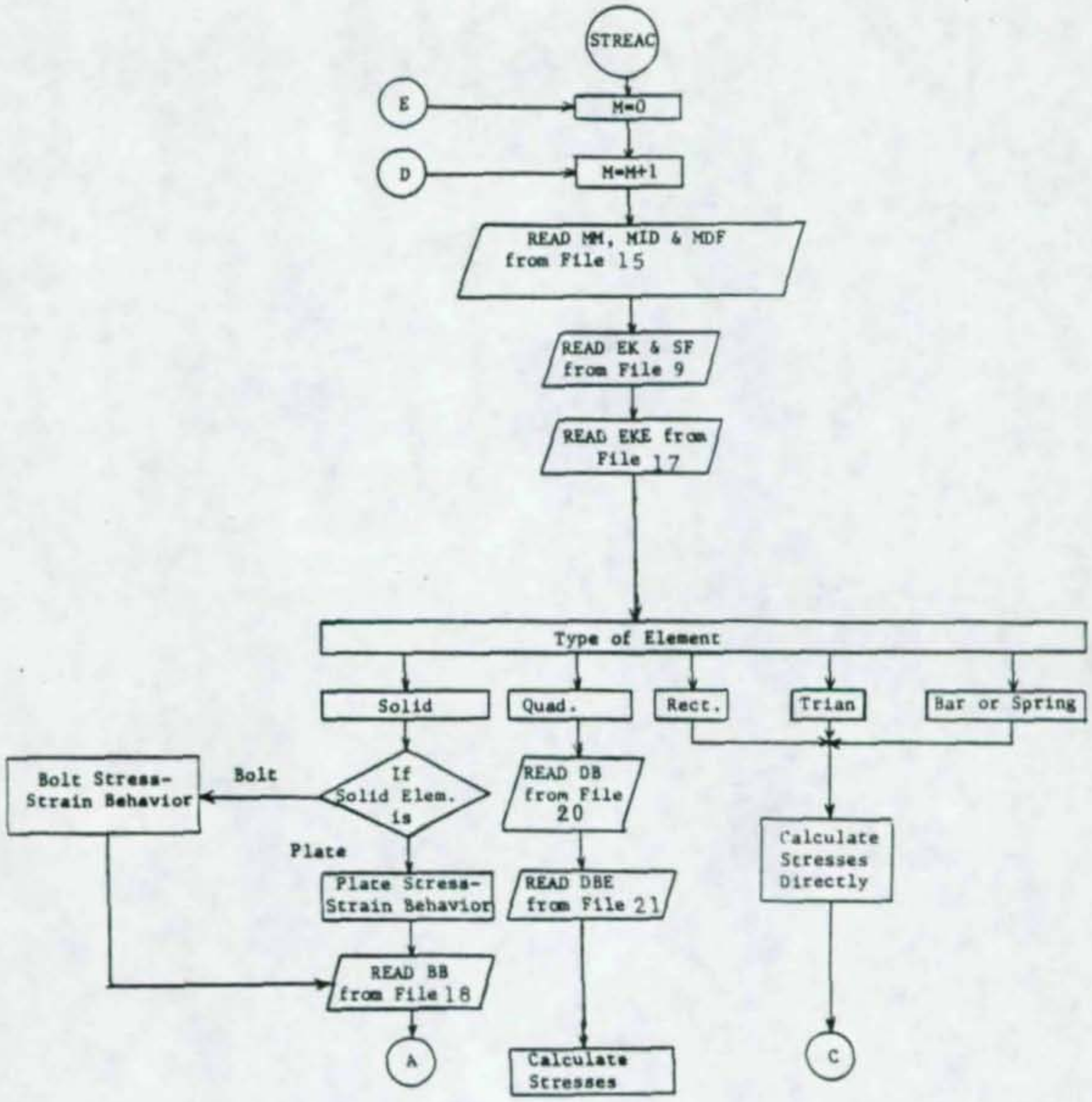

(f) STREAC Subroutine

Figure 2.10 Macro Flow Chart for Finite Element Program (continued)

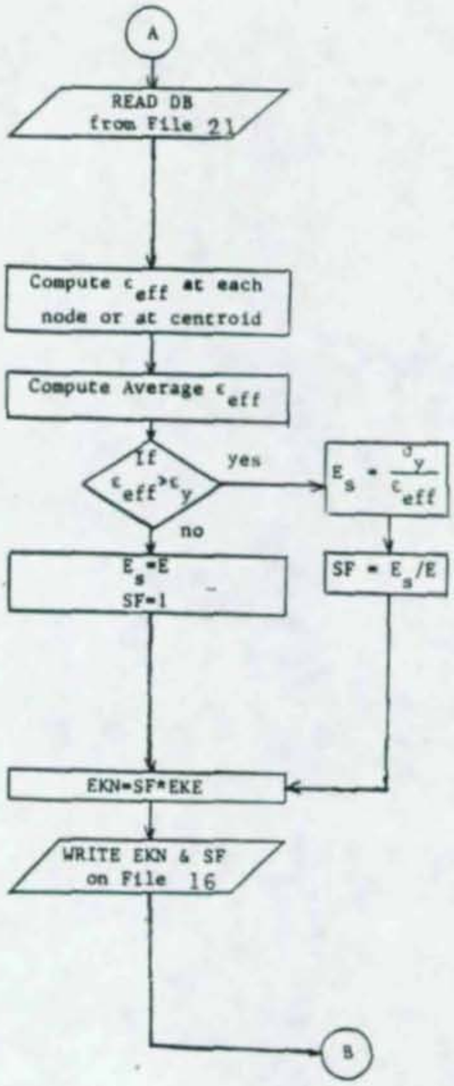

(f) STREAC Subroutine, Cont.

Figure 2.10 Macro Flow Chart for Finite Element Program (continued)

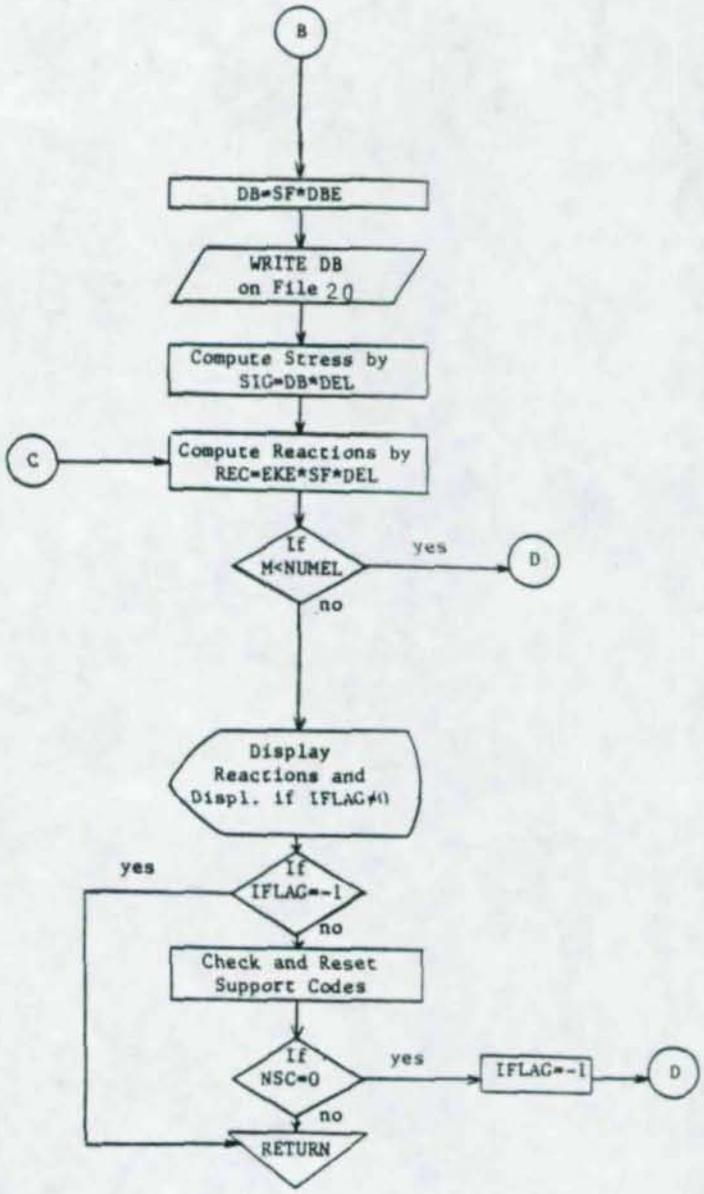

(f) STREAC Subroutine, Cont.

Figure 2.10 Macro Flow Chart for Finite Element Program (continued)

Table 2.1 Definition of Symbols Used in Figure 2.10

(a) MAIN Routine

NBD - Maximum band width

File 5 - Unit responsible for reading title card which also contains various specifications of number of elements and cards for various loading cases

NDOF - Number of d.o.f.

P - Loading case

NSC - Number of support changes

ICYL - Cycle number

NCYL - Total number of cycles specified

STIFF - Subroutine to calculate element and system stiffness matrix

BANSOL - Subroutine to perform a "banded solution" of the stiffness matrix and applied forces

STREAC - Subroutine to calculate stresses and reactions

TP - Total number of loading cases

File 1 - Stores information for elements and boundary conditions of the deformed configuration of end-plate to be used in the next load level

File 2 - Used as back-up for File 1

(b) STIFF Subroutine

IBD - Half of band-width

NBL - Total number of blocks into which system stiffness matrix is divided

IBL - Block number

MM - Element number

00754

Table 2. Definition of Symbols Used in Figure 2.10

MDF - Total degrees of freedom for that element

MID - Keeps track of d.o.f. numbers associated with a particular element

ICYL - Cycle number

IFIL - Code for generating or using data

NUMEL - Maximum number of elements

EK - Element stiffness matrix

B - Boundary force vector

A - System stiffness matrix

File 4 - Unit that contains boundary force vector and system stiffness matrix

(c) Element Subroutines

IFLAG - Flag to keep track of number of passes. Stress computations skipped in 1st pass

BB - Displacement-strain transformation

DB - Displacement-stress transformation

EK - Same as in STIFF

NSP - Number of corner nodes

DBE - Elastic displacement - stress transformation

EKE - Elastic element stiffness matrix

Table 2.1 Definition of Symbols Used in Figure 2.10

(d) STREAC Subroutine

MID - Same as in STIFF

EK - Same as in STIFF

NUMEL - Same as in STIFF

MM - Same as in STIFF

NSC - Same as in MAIN

DB - Same as in "Element"

DBE - Same as in "Element"

BB - Same as in "Element"

NSC - Number of support changes

ϵ_{eff} - Effective strain

ϵ_y - Yield strain

σ_y - Yield stress

E - Modulus of elasticity

E_s - Modified modulus of elasticity

SF - Modification factor for element stiffness matrix

EKN - Modified element stiffness matrix

EKE - Same as in "Element"

SIG - Nodal stress

REC - Nodal reaction

DEL - Nodal deflection

IFLAG - Flag to keep track of number of passes. Stress computations are at last pass.

Partial 3-D models at lower load levels for moment versus plate separation. Only at the failure load level does the partial 3-D model represent more closely the true behavior of end-plate when compared with experimental results.

Table 2.2 shows the separation relationship between 2-D and Partial 3-D models. From this data, it was decided to use the 2-D model, with a correction factor of 1.5 applied to the plate separation at the failure load level for further work.

2.7 Comparison of Analytical and Experimental Results

The comparison of analytical and experimental results are presented in detail in Section 4.2 of Chapter IV. However, a brief discussion follows.

Comparison of the 2-D finite element model results with experimental results for moment versus plate separation and bolt force versus moment is shown in Figure B.1 through B.16 in Appendix B. For moment versus plate separation (Figures B.1 through B.8), it is observed that good correlation is obtained at lower load level between the 2-D finite element and experimental results (maximum difference of 5-10%). At higher load levels, when the plate fails due to excessive yielding, the 2-D model cannot explain the behavior of the connection accurately. Figures B.9 through B.16 are bolt force versus moment plots which show good correlation between analytical and experimental results (differences of 10-15% for various load levels).

Comparison of the partial 3-D Mesh-I results with experimental results for moment versus plate-separation as well as bolt force versus

Table 2.2

Comparison of Plate Separation from Partial 3-D and 2-D Models

Experimental Case	Load Level	Ratio or Partial 3-D Separation/2-D Separation
F-3/4-1/2-16	1	1.15
	2	1.07
	3	1.12
	4	1.5
F-5/8-1/2-10	1	0.98
	2	1.00
	3	1.01
	4	1.56
F-5/8-1/2-16	1	1.2
	2	1.2
	3	1.3
	4	1.6
F-3/4-1/2-24A	1	1.2
	2	1.2
	3	1.23
	4	1.51

moment are shown in Figures C.1 and C.2, respectively, in Appendix C. The plate separation predicted by this mesh is much more flexible than that obtained from experimental results (a maximum difference of 60%). The bolt force plot versus moment plot indicates good correlation between analytical end experimental results (a maximum difference of 15%).

Comparison of the partial 3-D Mesh-II results with experimental results for moment versus plate separation as well as bolt force versus moment are shown in Figures C.1 and C.2, respectively. Comparing these results with results from the partial 3-D Mesh-I, partial 3-D Mesh-II, gives less flexible results which are closer to experimental results than the partial 3-D Mesh-I results. However, Mesh-II results for moment versus plate separation are still more flexible in comparison to the experimental results (a maximum difference of 30%).

Comparison of the partial 3-D Mesh-III results for moment versus plate separation (a maximum difference of 15%).

2.8 Conclusions

The 2-D finite element model of the connection is a more stiff representation of actual end-plate behavior since it does not account for the effect of transverse bending of the plate. On comparing the 2-D finite element moment versus plate separation results with experimental results on similar specimens, it is found that good correlation with test results is obtained for lower load levels, but for higher load levels the model is excessively stiff. However, the 2-D model predicts the bolt force in the tension bolts very close to the experimentally observed values.

Out of the three partial 3-D finite element models studied, it was concluded that it is essential to model the end-plate, bolt shanks, bolt heads, welds connecting end-plate to the beam and the beam flanges with 3-D elements. The web may be modeled with 2-D elements. If the beam flanges is also modeled using 2-D elements a portion of the plate is not considered in the model, which predicts a much more stiff behavior in comparison to that obtained from experimental observations. From the discussion in Section 2.3, it was concluded that the partial 3-D Mesh-III with 546 elements, 998 nodes and 2810 d.o.f. gives the best results when compared to experimental results on similar specimens. Thus this model was used to develop a correction factor between Partial 3-D and 2-D results and was found to be equal to 1.5 at the failure load level.

To conduct the feasibility and sensitivity study and to develop the prediction equations characterizing the connection behavior, finite element analyses of a number of cases are needed. For a typical connection, the computer costs associated with partial 3-D Mesh-III is much higher (30 to 40 times) than that of a 2-D mesh. Because of costs involved, it is not feasible to conduct the parametric study completely based on partial 3-D Mesh-III. Based on comparison of 2-D, partial 3-D Mesh-III and experimental results, it was found that if a correction factor of 1.5 is applied to the failure load level, the 2-D model results for end-plate separation are adequate.

In summary, it was concluded that the 2-D finite element model, with 560 elements, 626 nodes and 1252 d.o.f. can be used for the analyses needed for the parametric study. The prediction equations for maximum end-plate separation and maximum bolt force in the tension bolt will be developed from the 2-D results. Finally, a correction factor equal to 1.5 needs to be applied to the 2-D prediction equation for maximum end-plate separation.

CHAPTER III

PARAMETRIC STUDY BASED ON

TWO-DIMENSIONAL FINITE ELEMENT MODEL

3.1 Introduction

A parametric study was conducted to determine the effect of the various parameters on the behavior of the flush end-plate connection with two bolts in the tension region. Parameters describing the geometry of the connection and the force applied were chosen as independent parameters and the maximum separation in the end-plate and force in the tension bolt were chosen as dependent parameters. The 2-D finite element model and the computer program 'NONPAP', described in Section 2.5 of Chapter II, were used to conduct this parametric study. The finite element results from sufficient cases were regressed to develop prediction equations for the dependent parameters. The prediction equations developed using the 2-D finite element results are corrected using the scaling factor developed in Section 2.6 of Chapter II so as to characterize the behavior of the more realistic 3-D model.

In this chapter, independent parameters, dependent parameters, selection of cases and development of the "best-fit" prediction equation for the dependent parameters are presented. Independent and dependent parameters are discussed in Section 3.2. Selection of cases is explained in Section 3.3. The salient features of the regression technique used are presented in Section 3.4. The development of the prediction equations is presented in Section 3.5. Selection of the "best-fit" set of prediction equations for maximum end-plate separation and force in tension bolt are presented in Section 3.6. Finally the conclusions of the parametric study are summarized in Section 3.7.

3.2 Definition of Parameters

3.2.1 Independent Variables:

The primary geometric related variables for the 2-D model of the flush end-plate connection are identified as follows: t_p = thickness of the end-plate, p_f = pitch of the bolt (distance from top of the flange to the centerline of the bolt), t_w = thickness of the web, h = depth of the beam, d_b = nominal bolt diameter, b_p = width of the end-plate, g = gage of the bolts (centerline distance between two bolts) and g_b = width of equivalent rectangular bolt area. The variable g_b is calculated by using the following expressions (refer to Section 2.2 of Chapter II):

$$g_b = (1/3)\ (F_{by}/F_{yb})\ (A_B/d_b) \tag{3.2.1}$$

where A_B = area of beam cross-section and d_b = nominal bolt diameter.

With the exception of gage (distance between bolt centerline in the same row), all other geometric variables which were used in the partial 3-D model were determined as functions of the aforementioned primary independent variables. The edge distance, d_e, was set at

$$d_e = 1.75\ d_b \tag{3.2.2}$$

Exact dimensions of the bolt head diameter, d_h, and bolt head height, h_t, are found in Reference 25. The relationship between d_h and h_t with d_b are approximated as

$$d_h = 1.75\ d_b \tag{3.2.3}$$

$$h_t = 0.7\ d_b \tag{3.2.4}$$

The size of the fillet welds, w_s, connecting the end-plate to the beam flanges and the beam web was computed to develop the yield capacity of the two equivalent bolts, i.e.,

$$2(w_s/\sqrt{2}\ )\ b_p\ F_{by} = 2A_b\ F_{yb} \tag{3.2.5}$$

or

$$w_s = \sqrt{2}\ (\frac{A_b}{b_p})\ (\frac{F_{yb}}{F_{by}}) \tag{3.2.6}$$

where $(w_s/\sqrt{2}$ is the throat size of fillet weld, A_b is the gross area of bolt, F_{by} is the yield stress of the beam material and F_{yb} is the yield stress of the bolt based on gross area.

The force related independent variables in the study were taken as M = applied moment on the beam stub calculated from double triangular stress-distribution, according to simple bending theory and P_T = pretension force as specified in Table 1.23.5 of Reference 13. However, the pretension force, P_T, is omitted because it is related to the bolt diameter, d_b, and the yield stress of the bolt, F_{yb}, as follows:

$$P_T = 0.7\ (\frac{\pi}{4}\, d^2{}_b)\ F_{yb} \tag{3.2.7}$$

3.2.2 Independent Parameters

Two sets of independent paramenters were considered in the study. In the first case, the seven primary geometric variables were non-dimensionalized with respect to plate width, b_p, to give six independent parameters as follows:

$$\Pi_1 = t_p / b_p, \text{ the plate thickness parameter;} \tag{3.2.8}$$

$$\Pi_2 = p_f / b_p, \text{ the bolt pitch parameter;} \tag{3.2.9}$$

$$\Pi_3 = t_w / b_p, \text{ the beam web thickness parameter;} \tag{3.2.10}$$

$$\Pi_4 = t_f / b_p, \text{ the beam flange thickness parameter;} \tag{3.2.11}$$

$$\Pi_5 = h / b_p, \text{ the beam depth parameter; and} \tag{3.2.12}$$

$$\Pi_6 = d_b / b_p, \text{ the bolt diameter parameter.} \tag{3.2.13}$$

In the 2-D finite element model the width g_b of the equivalent rectangular area representing the row of bolts in the tension and the compression region was an input variable. So, in addition to the aforementioned six geometric related parameters, one additional non-dimensionalized parameters was incorporated

$$\Pi_7 = \frac{g_b}{b_p} \tag{3.2.14}$$

Ghassemieh[20], after numerous attempts, found that incorporation of bending parameters representing the bending stiffness of the end-plate, greatly improved the prediction equations characterizing the behavior of extended end-plate connections. Since a 2-D model is considered in this study, only one bending parameter was considered, which was defined as follows:

$$\Pi_8 = \frac{p_f^{\,3}}{b_p \, t_p^{\,3}} \tag{3.2.15}$$

This parameter has unit of (length) $^{-1}$.

The force related variable was defined as

$$\Pi_9 = M \qquad (3.2.16)$$

This parameter has unit of (force x length).

The nine parameters described were used to obtain the first set of regression equations described in Section 3.5.

In the second case, the seven primary geometric variables and g_b were non-dimensionalized with respect to beam depth, h. In this case two sets of independent parameters were considered: The one is obtained by non-dimensionalizing the basic geometric variables and the additional parameters obtained by considering combinations of the basic geometric variables. The basic parameters obtained from the primary geometric variables, g_b and force variables are as follows:

$\Pi_{10} = t_p/h$, the plate thickness parameter; (3.2.17)

$\Pi_{11} = p_f/h$, the bolt pitch parameter; (3.2.18)

$\Pi_{12} = t_w/h$, the beam web thickness parameter; (3.2.19)

$\Pi_{13} = t_f/h$, the beam flange thickness parameter; (3.2.20)

$\Pi_{14} = b_p/h$, the width of plate parameter; (3.2.21)

$\Pi_{15} = d_b/h$, the bolt diameter parameter; and (3.2.22)

$\Pi_{16} = g_b/h$, the width of rectangular bolt zone parameter. (3.2.23)

The following additional parameters were also considered for use in attempts to arrive at compact expressions by regression analysis:

$\Pi_{17} = \frac{r_b}{h}$, the radius of gyration parameter; (3.2.24)

$$\Pi_{18} = \frac{I_p}{h^4}\text{, the end-plate moment of inertia parameter;} \quad (3.2.25)$$

$$\Pi_{19} = \frac{I_B}{h^4}\text{, the beam moment of inertia parameter;} \quad (3.2.26)$$

$$\Pi_{20} = \frac{M}{M_y}\text{, the applied moment over yield moment parameter;}$$

and (3.2.27)

$$\Pi_{21} = \frac{M}{M_p}\text{, the applied moment over plastic moment parameter.} \quad (3.2.28)$$

where

$$r_B = \sqrt{\frac{I_B}{A_B}}, \quad (3.2.29)$$

$$I_p = \left(\frac{1}{12}\right)(t_p)(b_p)^3, \quad (3.2.30)$$

$$I_B = \frac{1}{12}(t_w)(h-2t_f)^3 + 2(b_p)(t_f)\frac{(h-t_f)^2}{2}, \quad (3.2.31)$$

A_B = area of the beam,

M_y = yield moment capacity of beam cross-section, and

M_p = plastic moment capacity of beam cross-section.

3.2.1 Dependent Parameters

The primary concern of this study is to develop prediction equations for the maximum deflection in the end-plate and force in the tension bolt. Therefore, two dependent parameters were chosen as follows:

$$\Pi_a = (\delta)_{max}\text{, the maximum end-plate separation, and} \quad (3.2.32)$$

$$\Pi_b = B_F\text{, the force in tension bolt.} \quad (3.2.33)$$

These have units of length and force, respectively.

3.3 Selection of Cases

To conduct the parametric study, it was decided to limit the geometric variables to practical ranges based on usual detailing practices, as given in Table 3.1. Based on the ranges of variables defined in this table, the following procedure was adopted to select the beam dimensions:

1. Four values of beam depth, h, were selected based on maximum and minimum value of h given in Table 3.1. The four values selected were 10 in., 16 in., 24 in. and 30 in.

2. For each value of beam depth, four values of beam flange width, b_f (=b_p, end-plate width), were considered as follows: h/6, h/5, h/4 and h/3. However, a limitation was put on b_f so that $b_f \geq 2$ in.

3. For each value of beam flange width, four values of beam flange thickness, t_f, were considered as follows: $b_f/35$, $b_f/26$, $b_f/16$ and $b_f/16$. A limitation was put on t_f so that $t_f \geq 0.1$ in.

4. For each value of beam depth, four values of beam web thickness, t_w, were considered as follows: h/160, h/153, h/107 and h/180. A limitation was put on t_w so that $t_w \geq 0.1$ in.

Based on this procedure for choosing the values of h, b_f and t_w, a total of 256 different beam cross-sections can be chosen which will fall within the range of the variables given in Table 3.1. A computer program was written to develop cross-section properties for these 256 cases.

Performing finite-element analyses for the flush-end-plate connections corresponding to the 256 beam cross-sections and then regressing the results to develop the prediction equations would have been very time consuming and costly. So it was decided to select 50 beam cross-

Table 3.1

Practical Ranges for Various

Geometric Parameters (in.)

Parameter	Low	Intermediate	High
g	2 1/4	2 3/4	3 1/2
d_b	5/8	3/4	1.00
p_f	1 1/8	1 3/4	2 1/2
b_p	5	7	10
t_p	5/16	1/2	3/4
t_f	.18	.375	.50
t_w	.10	.1875	.25
h	10	24	30

sections for further analysis. The following automated procedure was used to select these 50 cases:

1. The value of yield moment, M_y, was calculated for all the 256 beam cross-sections using the following expression:

$$M_y = SF_{by} \tag{3.3.1}$$

where S = elastic section modulus and F_{by} = yield stress of the beam material.

2. Choose number of beam cross-section, say n, to be considered in the study. The value of n was taken as 50.

3. A moment interval, ΔM, was computed based on the following expression:

$$\Delta M = \frac{(M_y)_{max} - (M_y)_{min}}{n} \tag{3.3.2}$$

where $(M_y)_{max}$ = maximum yield moment calculated in step 2 and $(M_y)_{min}$ = minimum yield moment calculated in step 2.

4. For each case, the beam cross-section is chosen such that its moment carrying capacity is given by

$$M_m = (M_y)_{min} + (m-1)\ \Delta m \leq (M_y)_{max} \text{ for } m = 1, 2, 1, \ldots\ldots, n \tag{3.3.3}$$

For each of the aforementioned 50 cases, the end-plate thickness and bolt diameter was computed using the experessions developed by Srouji[2]. The expression for end-plate thickness, t_p, used is:

$$t_p = \left[\frac{M_u/F_{py}}{C\,(\frac{h-P_t}{P_f}) + 2(\frac{h-P_t-P_f}{g} + 1) + (\frac{h-P_t}{2})\pi + x} \right]^{1/2} \tag{3.3.4}$$

where $c = (b_f-g)/z$ = end-plate bolt edge distance, M_u = ultimate moment applied to the connection, F_{py} = yield stress of plate material, h = depth of beam cross-section, P_t = pitch measured from top of flange to centerline of bolts, P_f = pitch measured from bottom of flange to centerline of bolts and x is given by

$$x = (h-t_f)\ \Pi/2\ \mathrm{Sec}^2\ \tan^{-1} 2\ l_n\ (\frac{2\ P_t/g}{\Pi}) \tag{3.3.5}$$

where l_n = length of yield line n

The expression used for bolt diameter, d_b, is

$$d_b = \sqrt{2B_F/\Pi F_a}\ , \tag{3.3.6}$$

where B_F = bolt force and F_a = allowable bolt stress.

3.4 Regression Analysis

Some of the considerations in developing the regression equations are discussed in this section. In statistics, regression equations are developed from sample data collected from experiments conducted to determine the values of the dependent parameters for preset values of independent parameters. However, the finite element analysis are not experiments in the true sense, since the results for each case are completely deterministics and reproducible.

To perform the regression analysis, it is a common procedure to represent the response or dependent parameter as a function of the independent parameters. In the parametric study, the maximum end-plate separation, Π_a, and force in tension bolt, Π_b, are the two responses measured (or here, obtained by computer solutions) as functions of the independent variables Π_1 through Π_9. The independent variables Π_1 through Π_9 for the 50 cases selected, as described in Section 3.3, were the input data to the computer program described in Chapter II, which eventually were solved for the maximum end-plate separation of the back of the end-plate and the force in the tension bolt. Thus the objective of the regression analysis was to develop equations to describe the connection behavior in the forms:

$$\Pi_a = f_1\,(\Pi_1, \Pi_2, \Pi_3, \Pi_4, \Pi_5, \Pi_6, \Pi_7, \Pi_8, \Pi_9) \qquad (3.4.1)$$

$$\Pi_b = f_2\,(\Pi_1, \Pi_2, \Pi_3, \Pi_4, \Pi_5, \Pi_6, \Pi_7, \Pi_8, \Pi_9) \qquad (3.4.2)$$

Determination of the functions f_1 and f_2 is discussed in general terms as follows. Let

$$x = f\,(\Pi_1, \Pi_2, \Pi_3, \ldots. + \Pi_n) \qquad (3.4.3)$$

be a function of n independent parameters, intended to fit data collected from a study. A linear (or sum) regression model for the function is written as

$$\begin{aligned} x = C_o &+ C_1\Pi_1 + C_2\Pi_2 + C_3\Pi_3 + \ldots\ldots\ldots + C_n\Pi_n + C_{12}\Pi_1\Pi_2 \\ &+ C_{23}\Pi_2\Pi_3 + \ldots\ldots C_{n1}\Pi_n\Pi_1 + C_{123}\Pi_1\Pi_2\Pi_3 + \ldots\ldots \\ &+ C_{123\,\ldots\ldots\,n}\,(\Pi_1\Pi_2\,\ldots\ldots\,\Pi_n) \end{aligned} \qquad (3.4.4)$$

This technique yields information on the relative significance of not only the main parameters Π_1, Π_2, ..., Π_n, but also the interactions $\Pi_1\Pi_2$, $\Pi_2\Pi_3$, ..., $(\Pi_1\Pi_2 \ldots\ldots \Pi_n)$. However, in most practical problems, such as the one reported, many of the higher-order interactions may be eliminated on the basis of physical and intutive considerations. Likely interactions must, however, be included in the model. The flush end-plate connection behavior is so complex that it is not easy to completely define all the interactions.

If a linear regression model is not found satisfactory, an alter-ternative is the nonlinear (or product) regression model of the form:

$$x = C_o \Pi_1^{C_1} \Pi_2^{C_2} \ldots\ldots \Pi_n^{C_n} \tag{3.4.5}$$

This may be reduced to a linear regression model if logarithms are taken of both sides, i.e.,

$$\text{Ln } x = \text{Ln } C_o + C_1 \text{Ln}\Pi_1 + C_2 \text{Ln}\Pi_2 + C_n L_n \Pi_n \tag{3.4.6}$$

Denoting the logarithms of the various parameters by prime superscripts, Equation (3.4.6) becomes

$$x' = C'_o + C_1\Pi'_1 + C_2\Pi'_2 + \ldots\ldots + C_n\Pi'_n \tag{3.4.7}$$

which is similar to the first group of terms in Equation (3.4.3). It should be noted that in Equation (3.4.7) product terms of the form Π'_1, Π'_2, Π'_3, Π'_4, etc., do not occur, so no interactions are present.

In this study the coefficient C'_o and the exponents C_1, C_2, ..., C_n in Equation (3.4.6) are determined by multiple regression analysis, so as to obtain the best least square fit to the data. In this method the best fit regression equation is taken as the one which minimizes the sum of the sqaures of the deviations of the data points from the equation fitted to the data. To demonstrate the basic principles, say the value of the dependent variable predicted from the best fit equation is x'_i, for any particular set of values. Π'_{1i}, Π'_{2i}, Π'_{3i} ..... Π'_{ni}, while it is measured (or directly determined) value is $\bar{x}_i$. Deviation of the predicted value from the measured value is given by

$$\bar{x}_i - x'_i = \bar{x}_i - (C'_o + C_1 x'_{1i} + C_2 x'_{2i} + \ldots\ldots + C_n x'_{ni}) \tag{3.4.8}$$

sum of the squares, S, for (say) m data is given by

$$S = \sum_{i=1}^{m} (\bar{x}'_i - x'_i)^2 \qquad (3.4.9)$$

The unknown coefficients C'_o, C_1, C_2, ... C_n are determined by minimizing the quality S with respect to each coefficient, i.e., by setting

$$\frac{\partial S}{\partial C'_o} = 0, \frac{\partial S}{\partial C_1} = 0, \frac{\partial S}{\partial C_2} = 0, \ldots\ldots, \frac{\partial S}{\partial C_n} = 0 \qquad (3.4.10)$$

This will result in $(n + 1)$ linear simultaneous equations from which the coefficients C'_o, C_1, C_2, ..., C_n can be determined. To determine C_o, the anti-logarithm of C'_o must be found.

A "goodness of fit" of the prediction equation is a comparison of S, sum of the squares, for the deviations for the constant term C_o above. The constant term model is

$$S = C'_o \qquad (3.4.11)$$

and the sum of the squares of this model can be written as

$$S_o = \sum_{i=1}^{m} (\bar{x}_i - x'_o)^2 \qquad (3.4.12)$$

in which x'_o is the mean. The difference between S_o and S is called as "sum of squares due to regression" and the ratio $(S_o - S)/S_o$ is called as "coefficient of multiple determination", R^2, i.e.,

$$R^2 = 1 - S/S_o \qquad (3.4.13)$$

A value of $R^2 = 1$ implies that S is zero and the regression prediction equation passes through all the data points. A value of $R^2 = 0.80$ means that 80% of the sum of squares of the deviations of the observed (or directly determined) $\bar{x}'_i$ values about their x'_o can be explained by the prediction equation obtained.

In the parametric study conducted no estimate of the experimental error was available, since in all cases the parameters were input in the finite element computer program, NONPAP, and the output was the response of the dependent parameters. Therefore, rerun of the same case would have given the same value of the response, thus not providing any information regarding the variance in the response. Not knowing how accurate the data was, the standard error of estimate was of very little help in checking the accuracy of the prediction equations obtained. The coefficient of multiple determination, R^2, thus was the sole criterion used to measure the adequacy of the prediction equation to characterize the behavior of the typical connection. Also, it was decided to examine the effect of each variable appearing in the prediction equation, and check to determine if it gives consistant results, when compared to actual observed behavior, by varying it within the practical range.

All the regression analyses were conducted using the computer program SAS[24] (Statistical Analysis System) available in the system library of the University of Oklahoma Computer Center. The SAS computer program is greatly used to conduct statistical studies in the area of social studies, psychology and mathematics.

3.5 Prediction Equations

Using the 2-D finite element model described in Section 2.2 and the computer program NONPAP explained in Section 2.6, the 50 cases selected in Section 3.3 were analyzed. The results of the analyses were regressed, using the procedure explained in Section 3.4, to develop the prediction equation for maximum end-plate separation, Π_a, and force in the tension bolt, Π_b.

Two sets of prediction equations were developed. In the first set the parameters Π_1 through Π_9 were considered and in the second set the parameters Π_8 through Π_{21} were considered as independent parameters. In all cases the nonlinear form of the regression equation, i.e., Equation (3.4.5), was used. A total of 37 different "cases" or combination of the independent parameters as listed in Table 3.2 were tested.

In formulating some of the cases combinations of the basic geometric and force related variables are used. For example in case 9, the following parameters are considered as independent parameters: Π_{10}, Π_{11}, Π_{19}, Π_8, Π_{20}. Comparing this case with case 2, it can be seen that the parameters connected with beam geometric variables, i.e., t_f, t_w, $b_f(=b_p)$ and h, are replaced by parameter $\Pi_{19} = I_B/h$, where I_B = moment of inertia of beam cross-section. Similarly the geometric variable I_p, defined in case 22 is used to replace variables defining end-plate cross-sectional geometry, such as t_p and $b_p(=b_f)$. In some cases applied load is defined using Π_{20}, while in other cases it is replaced by Π_{21}. The input information for all the basic independent parameters (Π_1 to Π_6) and the corresponding dependent parameters used to perform the regression analysis are given in Appendix E.

The values of the constants and exponents obtained from the regression analyses for the maximum end-plate separation, Π_a, and the force in the tension bolt, Π_b, for all the cases are listed in Table 3.3 and 3.4, respectively. The value of R^2 for each prediction equation obtained is also given in these tables.

Table 3.2

Various Independent Parameter Combinations Tested

Case	Independent Parameters	R^2 for Π_a Equation	R^2 for Π_b Equation
1	$\Pi_1, \Pi_2, \Pi_3, \Pi_4, \Pi_5, \Pi_6, \Pi_7, \Pi_8, \Pi_9$	0.94	0.90
2	$\Pi_{10}, \Pi_{11}, \Pi_{12}, \Pi_{13}, \Pi_{14}, \Pi_{15}, \Pi_{16}, \Pi_{20}$	0.89	0.88
3	$\Pi_{10}, \Pi_{11}, \Pi_{12}, \Pi_{13}, \Pi_{14}, \Pi_{15}, \Pi_{16}, \Pi_8, \Pi_{20}$	0.94	0.90
4	$\Pi_{10}, \Pi_{11}, \Pi_{13}, \Pi_{14}, \Pi_{20}$	0.88	0.85
5	$\Pi_{10}, \Pi_{11}, \Pi_{13}, \Pi_{14}, \Pi_8, \Pi_{20}$	0.85	0.83
6	$\Pi_{10}, \Pi_{11}, \Pi_{16}, \Pi_{19}, \Pi_{20}$	0.89	0.83
7	$\Pi_{10}, \Pi_{11}, \Pi_{16}, \Pi_{19}, \Pi_8, \Pi_{20}$	0.89	0.84
8	$\Pi_{10}, \Pi_{11}, \Pi_{14}, \Pi_{16}, \Pi_{19}, \Pi_8, \Pi_{20}$	0.89	0.85
9	$\Pi_{10}, \Pi_{11}, \Pi_{19}, \Pi_8, \Pi_{20}$	0.85	0.84
10	$\Pi_{10}, \Pi_{11}, \Pi_{16}, \Pi_{17}, \Pi_{20}$	0.89	0.86
11	$\Pi_{10}, \Pi_{11}, \Pi_{16}, \Pi_{17}, \Pi_8, \Pi_{20}$	0.89	0.84
12	$\Pi_{10}, \Pi_{11}, \Pi_{14}, \Pi_{16}, \Pi_{17}, \Pi_8, \Pi_{20}$	0.94	0.90
13	$\Pi_{10}, \Pi_{11}, \Pi_{17}, \Pi_8, \Pi_{20}$	0.89	0.82
14	$\Pi_{11}, \Pi_{16}, \Pi_{19}, \Pi_{18}, \Pi_{20}$	0.85	0.84
15	$\Pi_{11}, \Pi_{16}, \Pi_{19}, \Pi_{18}, \Pi_8, \Pi_{20}$	0.86	0.84
16	$\Pi_{11}, \Pi_{14}, \Pi_{16}, \Pi_{19}, \Pi_{18}, \Pi_8, \Pi_{20}$	0.89	0.84
17	$\Pi_{11}, \Pi_{19}, \Pi_{17}, \Pi_8, \Pi_{20}$	0.80	0.84
18	$\Pi_{11}, \Pi_{16}, \Pi_{17}, \Pi_{18}, \Pi_{20}$	0.87	0.80
19	$\Pi_{11}, \Pi_{16}, \Pi_{17}, \Pi_{18}, \Pi_8, \Pi_{20}$	0.88	0.87
20	$\Pi_{11}, \Pi_{14}, \Pi_{16}, \Pi_{18}, \Pi_8, \Pi_{20}$	0.87	0.84
21	$\Pi_{11}, \Pi_{17}, \Pi_{18}, \Pi_8, \Pi_{20}$	0.85	0.84
22	$\Pi_{11}, \Pi_{16}, \Pi_{19}, \Pi_{18}, \Pi_{21}$	0.86	0.85

Table 3.2 (continued)

Various Independent Parameter Combinations Tested

Case	Independent Parameters	R^2 for π_a Equation	R^2 for π_b Equation
23	$\pi_{11}, \pi_{16}, \pi_{19}, \pi_{18}, \pi_8, \pi_{21}$	0.86	0.85
24	$\pi_{11}, \pi_{14}, \pi_{16}, \pi_{19}, \pi_{18}, \pi_8, \pi_{21}$	0.92	0.85
25	$\pi_{11}, \pi_{19}, \pi_{18}, \pi_8, \pi_{21}$	0.83	0.86
26	$\pi_{11}, \pi_{16}, \pi_{17}, \pi_{18}, \pi_{21}$	0.87	0.86
27	$\pi_{11}, \pi_{16}, \pi_{17}, \pi_{18}, \pi_8, \pi_{21}$	0.88	0.86
28	$\pi_{11}, \pi_{14}, \pi_{16}, \pi_{17}, \pi_{18}, \pi_8, \pi_{21}$	0.89	0.85
29	$\pi_{11}, \pi_{17}, \pi_{18}, \pi_8, \pi_{21}$	0.88	0.84
30	$\pi_{10}, \pi_{11}, \pi_{16}, \pi_{19}, \pi_{21}$	0.35	0.04
31	$\pi_{10}, \pi_{11}, \pi_{16}, \pi_{19}, \pi_8, \pi_{21}$	C.90	0.85
32	$\pi_{10}, \pi_{11}, \pi_{14}, \pi_{16}, \pi_{19}, \pi_8, \pi_{21}$	0.94	0.90
33	$\pi_{10}, \pi_{11}, \pi_{19}, \pi_8, \pi_{21}$	0.87	0.84
34	$\pi_{10}, \pi_{11}, \pi_{17}, \pi_{21}$	0.84	0.83
35	$\pi_{10}, \pi_{11}, \pi_{17}, \pi_8, \pi_{21}$	0.89	0.86
36	$\pi_{10}, \pi_{11}, \pi_{16}, \pi_{17}, \pi_8, \pi_{21}$	0.90	0.86
37	$\pi_{10}, \pi_{11}, \pi_{14}, \pi_{17}, \pi_8, \pi_{21}$	0.94	0.90

Table 3.3

Constants and Exponents Obtained from

Regression Analysis for Maximum End Plate

Separation Prediction Equation

Case	C_0	C_1	C_2	C_3	C_4	C_5	C_6	C_7	C_8	C_9	C_{10}	C_{11}	C_{12}	C_{13}	C_{14}	C_{15}	C_{16}	C_{17}	C_{18}	C_{19}	C_{20}	C_{21}	R^2
1	-8.336	7.620	-6.932	-0.501	-0.038	-1.613	-0.850	-0.518	3.053	1.355													0.94
2	-5.895										-1.843	2.051	-0.837	0.319	-0.023	-0.052	0.8132				1.354		0.89
3	-6.002								-0.0994		-4.483	5.188	-0.547	0.403	-0.708	-0.142	-0.519				1.356		0.94
4	-6.334										-3.522	2.420		0.741	0.258						1.357		0.88
5	-5.716								-0.197		-2.917	1.760		0.551	0.315						1.355		0.85
6	-6.170										-2.653	1.960					-1.767			0.512	1.358		0.89
7	-5.484								-0.125		-2.194	2.260					-1.390			0.606	1.358		0.89
8	-5.073								-1.290		-5.854	6.214			-1.487		-1.666			1.357	1.358		0.89
9	-5.945								-0.403		-3.005	3.225								-0.035	1.362		0.85
10	-3.814										-0.375	2.098					-0.421	1.312			1.359		0.89
11	-4.409								0.331		-1.324	3.036					-0.522	1.205			1.360		0.89
12	-2.028								3.423		8.732	-8.049			3.277		0.355	4.506			1.356		0.94
13	-4.300								-0.285		-1.574	3.070						1.421			1.361		0.89
14	-3.769											1.381					-1.777		-0.030	0.247	1.356		0.85
15	-3.769											0.588					-1.774		0.012	0.530	1.355		0.86
16	-19.612								1.290			6.213			16.077		-1.665		-5.854	1.357	1.358		0.89
17	-4.187								0.329			0.585							0.152	-0.476	1.360		0.83
18	-1.830											1.399					-1.069	2.544	-0.109		1.353		0.87
19	-1.489								0.433			0.362					-0.455	3.612	-0.027		1.353		0.88

Table 3.3 (continued)

Constants and Exponents Obtained from

Regression Analysis for End-Plate

Separation Prediction Equation

Case	C_0	C_2	C_3	C_4	C_5	C_6	C_7	C_8	C_9	C_{10}	C_{11}	C_{12}	C_{13}	C_{14}	C_{15}	C_{16}	C_{17}	C_{18}	C_{19}	C_{20}	C_{21}	R^2
20	-13.923							-1.082			5.470			13.132		0.355	4.506	-4.876		1.357		0.87
21	-0.831							0.605			-0.059						4.646	-0.032		1.352		0.85
22	-3.810										1.394					-1.345		-0.031	0.018		1.365	0.86
23	-3.961							0.306								0.646		0.0094	-1.343		1.356	0.86
24	-19.143							-1.254			6.085			15.546		-1.239		-5.663	1.086		1.361	0.92
25	-4.125							0.301			0.645							0.114	-0.476		1.395	0.83
26	-2.445										1.398					-1.053	1.635	-0.110			1.353	0.87
27	-2.104							0.432			0.362					-0.439		-0.028	2.703		1.352	0.88
28	-14.586							-1.089			5.490		13.181			0.374		-4.806	3.597		1.356	0.89
29	-1.468							0.598			-0.044							-0.033	3.525		1.351	0.88
30	-7.024							-0.074		-2.094	2.130					-1.448					0.653	0.35
31	-5.465							-0.122		-2.107	2.243					-0.970			0.355		1.364	0.90
32	-5.069							-1.254		-5.664	6.085			6.085		-1.239			1.086		1.361	0.94
33	-5.762							-0.316		-2.668	2.914								-0.093		1.387	0.87
34	-3.612									-1.345	1.565						2.716				1.357	0.84
35	-3.731							0.059		-1.977	1.774						2.516				1.356	0.89
36	-3.869							0.019		-1.119	1.856					-0.142	2.281				1.356	0.90
37	-2.644							-1.089		-4.806	5.490			-1.236		-1.236	3.597				1.356	0.94

Table 3.4

Constants and Exponents Obtained from

Regression Analysis for Force in Tension

Bolt Prediction Equation

Case	C_0	C_1	C_2	C_3	C_4	C_5	C_6	C_7	C_8	C_9	C_{10}	C_{11}	C_{12}	C_{13}	C_{14}	C_{15}	C_{16}	C_{17}	C_{18}	C_{19}	C_{20}	C_{21}	R^2
1	-2.062	16.427	-16.823	-0.347	0.049	-2.984	-2.391	0.436	5.655	2.568													0.90
2	2.456										-5.132	4.132	-0.605	0.785	-1.325	-0.432	-2.061				2.565		0.88
3	2.355								-2.013		-6.498	6.136	-0.511	0.886	-1.081	-0.513	2.0571				2.568		0.90
4	3.227										-1.413	-0.309		1.007	0.527		2.057				2.563		0.85
5	3.550								3.370		-1.655	0.654		0.567	3.214						2.570		0.83
6	5.840										-1.950	0.540					0.153			0.595	2.567		0.83
7	6.471								-0.383		-2.064	0.678					0.187			0.706	2.570		0.84
8	4.164								-2.348		-8.237	7.346			-2.508		-0.278			1.974	2.569		0.85
9	3.533								-0.346		-1.955	0.548								0.792	2.570		0.84
10	6.377										1.006	-0.022					1.645	2.275			2.570		0.86
11	6.474								-2.240		1.212	-0.315					1.712	2.640			2.565		0.84
12	8.546								4.443		12.800	-13.210			4.366		2.644				2.568		0.90
13	4.538										11.440	-8.755						3.570			2.570		0.87
14	5.310											-0.714					0.426		-0.118	-0.935	2.565		0.84
15	5.369								-0.119			-0.422					-0.427		-0.134	0.831	2.566		0.88
16	-16.304								-2.348			7.346			22.203		-0.278		-8.237	1.974	2.569		0.84
17	5.306								-0.118			-0.423							-0.101	0.588	2.567		0.88
18	8.893											-0.653					1.516	5.234	-0.191		2.563		0.80
19	8.150								-2.145			-0.750					1.935	6.254					

Table 3.4 (continued)

Constants and Exponents Obtained from

Regression Analysis for Force in Tension

Bolt Prediction Equation

Case	C_0	C_2	C_3	C_4	C_5	C_6	C_7	C_8	C_9	C_{10}	C_{11}	C_{12}	C_{13}	C_{14}	C_{15}	C_{16}	C_{17}	C_{18}	C_{19}	C_{20}	C_{21}	R^2
20	-8.035							-2.049			6.267			17.897		2.644		-6.672		2.568		0.84
21	6.678							-0.566			0.733						2.390	-0.169		2.565		0.84
22	5.225										-0.689					0.387		-0.119	0.504		2.577	0.85
23	5.301							-0.153			-0.314					0.386		-0.139	0.369		2.578	0.85
24	-15.401							-2.281			7.104			21.200		0.527		-8.786	1.462		2.574	0.85
25	5.348										-0.3136							-0.170	0.588		2.569	0.86
26	7.729										-0.654					1.547	3.511	-0.193			2.562	0.86
27	7.742							0.015			-0.691					1.569	3.550	-0.190			2.562	0.86
28	-9.290							-2.061			6.305			17.986		2.679	4.770	-6.709			2.568	0.85
29	5.469							-0.578			0.762						0.609	-0.172			2.563	0.84
30	0.556							-0.287		-1.874	0.432					0.076			0.796			0.04
31	3.504							-0.378		-1.898	0.646					0.979			0.233		2.580	0.85
32	4.170							-2.281		-7.876	7.104			-2.429		0.527			1.461		2.573	0.90
33	3.803							-0.183		-1.331	-0.030								0.686		2.556	0.84
34	3.967									-0.815	0.969						-0.564				2.565	0.83
35	3.543							-0.632		-0.993	1.041						-0.454				2.567	0.86
36	5.261							0.141		-1.711	0.014					1.785	2.491				2.567	0.86
37	-7.381							-2.061		-6.709	6.305			-2.141		2.678	4.770				2.568	0.90

Next an effort was made to select the best-fit prediction equations which realistically characterizes the behavior of a typical connection. This procedure is discussed in the next section.

3.6 Selection of Best Prediction Equations

3.6.1 Elimination Based on Value of Coefficient of Multiple Determination, (R^2)

Although no error estimates were available to determine goodness of fit, the value of $R^2 = 0.90$ was considered satisfactory under the circumstances, allowing for 90% of the variation of Π_a and Π_b about their mean value. From Table 3.2, cases in which R^2 has a value greater than or equal to 0.90 are selected for end-plate separation and bolt force prediction equations. So based on this criterion, five sets of equations for Π_a and Π_b (cases 1, 3, 12, 32 and 37) and one equation for Π_a (case 24) are selected as the best-fit prediction equations as follows:

Case 1

$$\Pi_a = (\delta)_{max} = (e)^{-8.336} \left(\frac{t_p}{b_p}\right)^{7.620} \left(\frac{p_f}{b_p}\right)^{-6.932} \left(\frac{t_w}{b_p}\right)^{-0.501} \left(\frac{t_f}{b_p}\right)^{-0.038} \left(\frac{h}{b_p}\right)^{-1.613} \left(\frac{p_f^{\,3}}{b_p t_p^{\,3}}\right)^{3.053} \left(\frac{g_b}{b_p}\right)^{-0.518} (M)^{1.355}$$

$(R^2 = 0.94)$ (3.6.1)

$$\Pi_b = (e)^{-2.062} \left(\frac{t_p}{b_p}\right)^{16.427} \left(\frac{p_f}{b_p}\right)^{-16.823} \left(\frac{t_w}{b_p}\right)^{-0.347} \left(\frac{t_f}{b_p}\right)^{0.049} \left(\frac{h}{b_p}\right)^{-2.984} \left(\frac{d_b}{b_p}\right)^{-2.391} \left(\frac{p_f^{\,3}}{b_p t_p^{\,3}}\right)^{5.655} \left(\frac{g_b}{b_p}\right)^{0.436} (M)^{2.568}$$

$(R^2 = 0.90)$ (3.6.2)

<u>Case 3</u>

$$\Pi_a = (\delta)_{max} = (e)^{-6.002} \left(\frac{t_p}{h}\right)^{-4.483} \left(\frac{p_f}{h}\right)^{5.188} \left(\frac{t_w}{h}\right)^{-0.547} \left(\frac{t_f}{h}\right)^{0.403} \left(\frac{d_b}{h}\right)^{0.142} \left(\frac{b_p}{h}\right)^{-0.789} \left(\frac{n_b}{h}\right)^{-0.519} \left(\frac{p_f^3}{b_n t_p^3}\right)^{-0.944} \left(\frac{M}{M_y}\right)^{1.356}$$

$(R^2 = 0.94)$ (3.6.3)

$$\Pi_b = (e)^{2.355} \left(\frac{t_p}{h}\right)^{-6.498} \left(\frac{p_f}{h}\right)^{6.136} \left(\frac{t_w}{h}\right)^{-0.511} \left(\frac{t_f}{h}\right)^{0.886} \left(\frac{d_b}{h}\right)^{0.513} \left(\frac{b_p}{h}\right)^{-1.081} \left(\frac{g_b}{h}\right)^{2.057} \left(\frac{p_f^3}{b_p t_p^3}\right)^{-2.013} \left(\frac{M}{M_y}\right)^{2.568}$$

$(R^2 = 0.90)$ (3.6.4)

<u>Case 12</u>

$$\Pi_a = (\delta_x)_{max} = (e)^{-2.028} \left(\frac{t_p}{h}\right)^{8.732} \left(\frac{p_f}{h}\right)^{-8.049} \left(\frac{b_p}{h}\right)^{3.277} \left(\frac{g_b}{h}\right)^{0.355} \left(\frac{r_B}{h}\right)^{4.506} \left(\frac{p_f^3}{b_p t_p^3}\right)^{3.423} \left(\frac{M}{M_y}\right)^{1.356}$$

$(R^2 = 0.94)$ (3.6.5)

$$\Pi_b = (e)^{8.546} \left(\frac{t_p}{h}\right)^{12.80} \left(\frac{p_f}{h}\right)^{-13.210} \left(\frac{b_p}{h}\right)^{4.366} \left(\frac{g_b}{h}\right)^{2.644} \left(\frac{r_b}{h}\right)^{6.492} \left(\frac{p_f^3}{b_p t_p^3}\right)^{4.443} \left(\frac{M}{M_y}\right)^{2.568}$$

$(R^2 = 0.90)$ (3.6.6)

Case 24

$$\Pi_a = (\delta)_{max} = (e)^{-19.143} \left(\frac{p_f}{h}\right)^{6.085} \left(\frac{b_p}{h}\right)^{15.476} \left(\frac{p_f^3}{b_p t_p^3}\right)^{-1.254} \left(\frac{g_b}{h}\right)^{-1.239} \left(\frac{I_p}{h^4}\right)^{-5.663} \left(\frac{I_B}{h^4}\right)^{1.086} \left(\frac{M}{M_p}\right)^{1.361}$$

$(R^2 = 0.90)$ (3.6.7)

Case 32

$$\Pi_a = (\delta_x)_{max} = (e)^{-5.069} \left(\frac{b_p}{h}\right)^{-5.664} \left(\frac{p_f}{h}\right)^{6.085} \left(\frac{b_p}{h}\right)^{6.085} \left(\frac{g_b}{h}\right)^{-1.239} \left(\frac{I_B}{h^4}\right)^{1,086} \left(\frac{p_f^3}{b_p t_p^3}\right)^{-1.254} \left(\frac{M}{M_p}\right)^{1.361}$$

$(R^2 = 0.94)$ (3.6.8)

$$\Pi_b = (e)^{4.170} \left(\frac{t_p}{h}\right)^{-7.876} \left(\frac{p_f}{h}\right)^{7.104} \left(\frac{b_p}{h}\right)^{-2.429} \left(\frac{g_b}{h}\right)^{0.527} \left(\frac{I_B}{h^4}\right)^{1.461} \left(\frac{p_f^3}{b_p t_p^3}\right)^{-2.281} \left(\frac{M}{M_p}\right)^{2.573}$$

$(R^2 = 0.90)$ (3,6.9)

Case 37

$$\Pi_a = (\delta_x)_{max} = (e)^{-2.644} \left(\frac{t_p}{h}\right)^{-4.806} \left(\frac{p_f}{h}\right)^{5.490} \left(\frac{b_p}{h}\right)^{-1.236} \left(\frac{g_b}{h}\right)^{-1.236} \left(\frac{r_B}{h}\right)^{3.597} \left(\frac{p_f^3}{b_p t_p^3}\right)^{-1.089} \left(\frac{M}{M_p}\right)^{1.356}$$

$(R^2 = 0.94)$ (3.6.10)

$$\Pi_b = (e)^{-7.381} \left(\frac{t_p}{h}\right)^{-6.709} \left(\frac{p_f}{h}\right)^{6.305} \left(\frac{b_p}{h}\right)^{-2.141} \left(\frac{g_b}{h}\right)^{2.679} \left(\frac{r_B}{h}\right)^{4.770} \left(\frac{p_f^3}{b_p t_p^3}\right)^{-2.061} \left(\frac{M}{M_p}\right)^{2.568}$$

$$\Pi_b = (e)^{-7.381} \left(\frac{t_p}{h}\right)^{-6.709} \left(\frac{p_f}{h}\right)^{6.305} \left(\frac{b_p}{h}\right)^{-2.141} \left(\frac{g_b}{h}\right)^{2.679} \left(\frac{r_B}{h}\right)^{4.770} \left(\frac{p_f^{\,3}}{b_p t_p^{\,3}}\right)^{-2.061} \left(\frac{M}{M_p}\right)^{2.568}$$

$(R^2 = 0.90)$ (3.6.11)

3.6.2 Elimination Based on Predicted Versus Actual Plots

To obtain the best-fit set of equations, using Equations (3.6.1) through (3.6.11) it was next decided to plot input or (actual) end-plate displacement versus predicted end-plate displacement and input bolt force versus predicted bolt force. These plots are illustrated in Figures 3.1 through 3.11. To investigate the scatter of the points obtained from the regression analysis a line with slope of 1:1 has been drawn along with two other lines denoting $\pm$ 25% deviation from abovementioned line. Equations in which most of the points either lie on or are close to the line with slope of 1:1 are taken as the best fit equations. From Figures 3.1, 3.3, 3.4 and 3.7 it can be seen that there is too much scatter of the points beyond the $\pm$ 25% deviation lines. These four figures correspond to the prediction equations, Equations (3.6.1), (3.6.2) and (3.6.7), which correspond to the maximum end-plate separation and bolt force equations for Case 1 and the maximum end-plate separation equation for Cases 12 and 24 of Table 3.2. Therefore, based on these plots, it was decided to eliminate Equations (3.6.1), (3.6.2), (3.6.5) and (3.6.7) from equations selected in Section 3.6.1. The remaining equations (Equations (3.6.3), (3.6.4), (3.6.6), (3.6.8), (3.6.9), (3.6.10), and (3.6.11) need to be further scrutinized to obtain the best-fit equations.

The abovementioned seven equations are functions of either Π_{20} ($=M/M_y$) or Π_{21}($=M/M_p$). To obtain a design equation, the end-plate

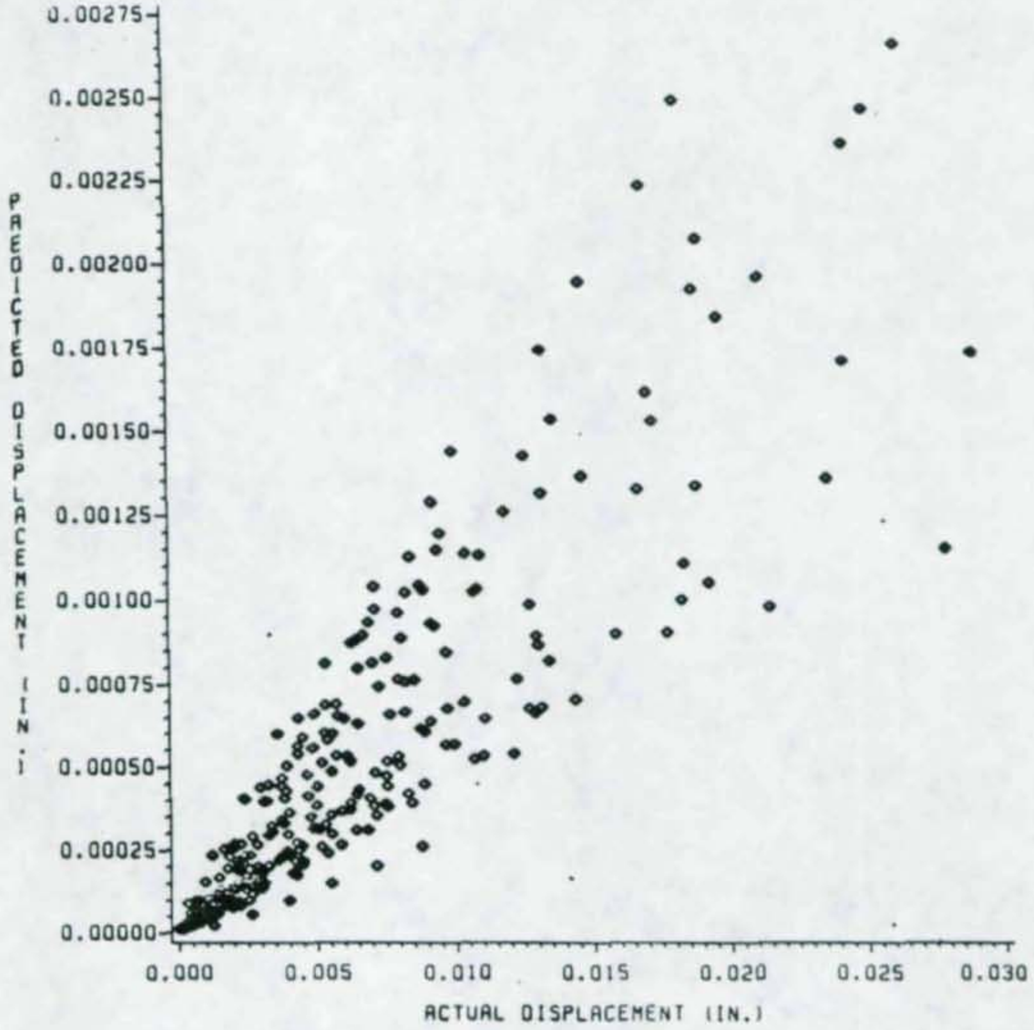

Figure 3.1 Predicted End-Plate Displacement vs. Input (or Actual) End-Plate Displacement for Case 1

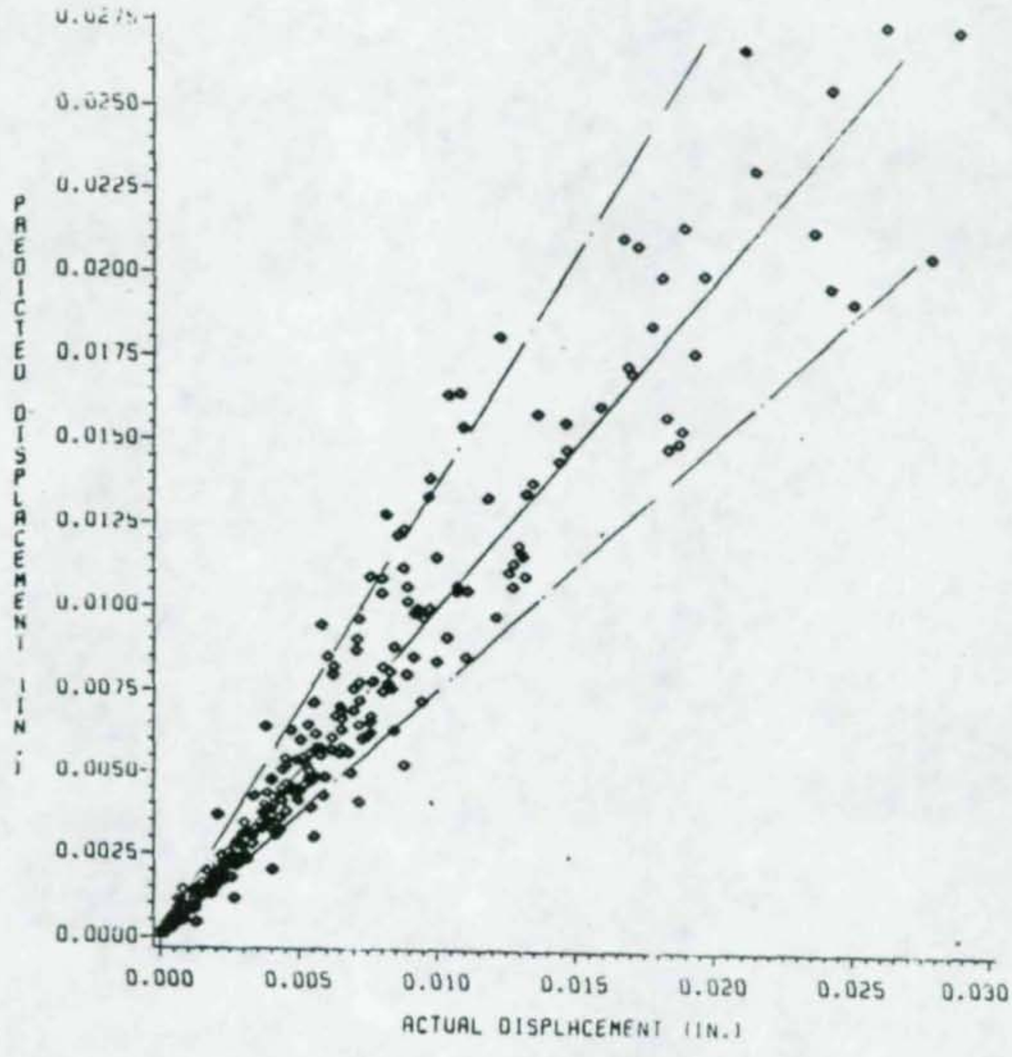

Figure 3.2 Predicted End-Plate Displacement vs. Input (or Actual) for Case 3.

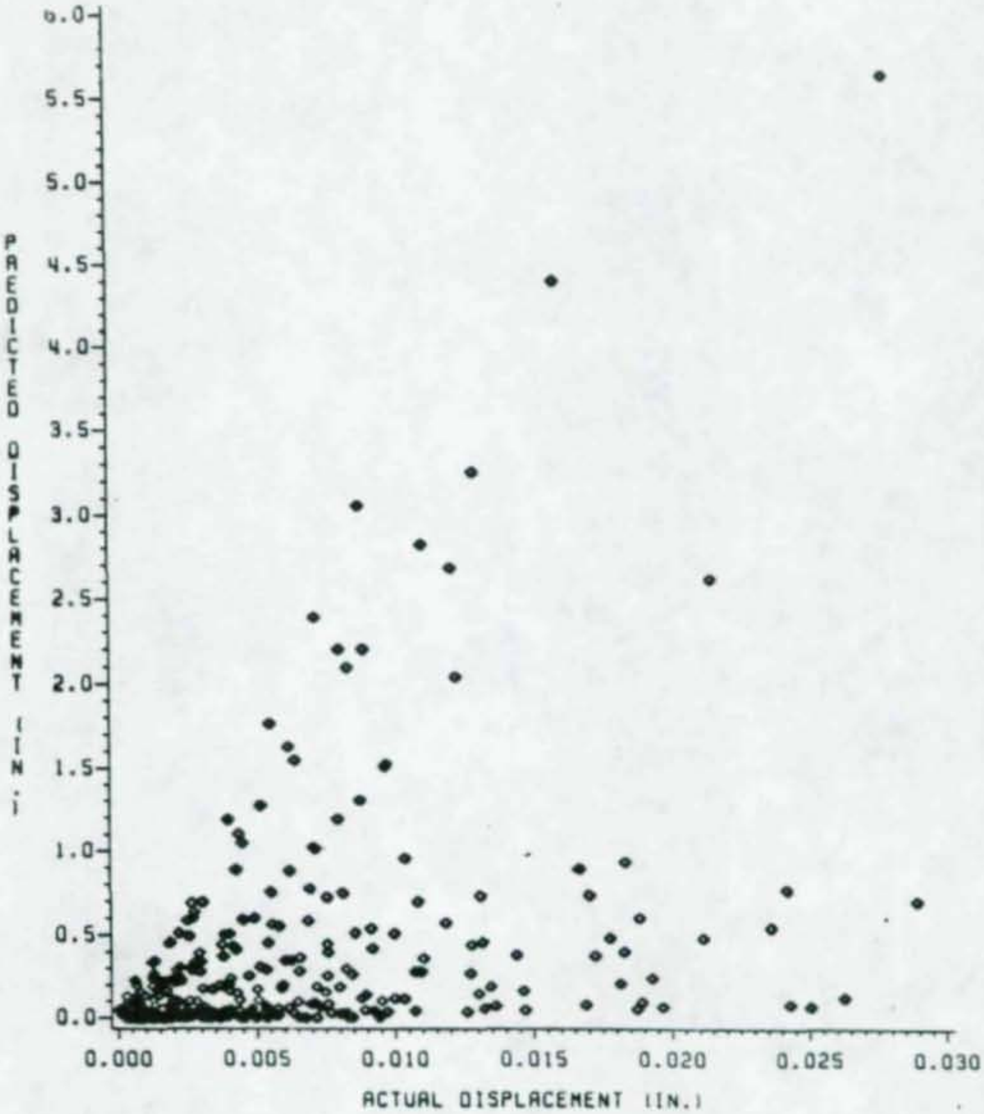

Figure 3.3 Predicted End-Plate Displacement vs. Input (or Actual) Displacement for Case 12

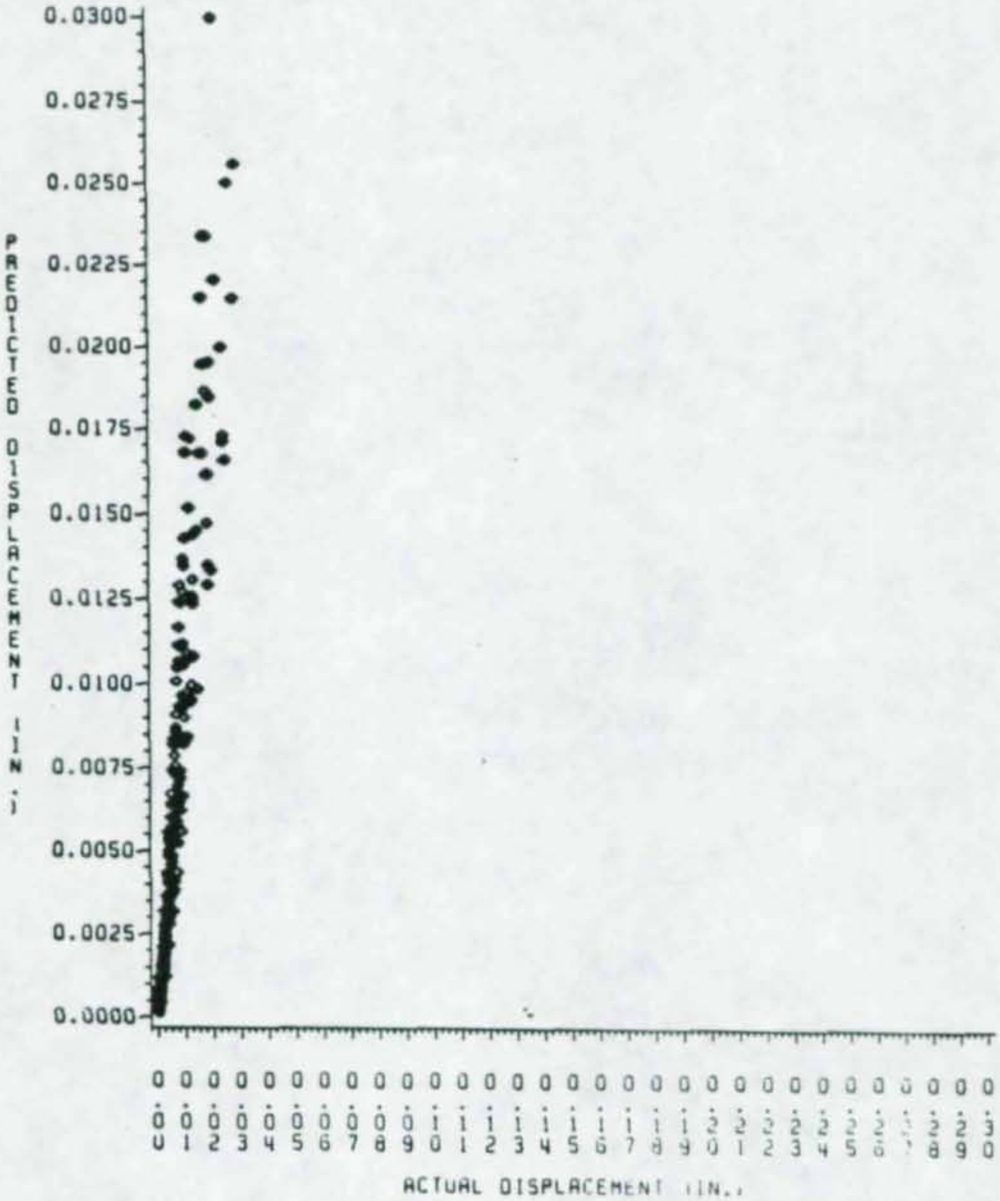

Figure 3.4 Predicted End-Plate Displacement vs. Input (or Actual) Displacement for Case 24

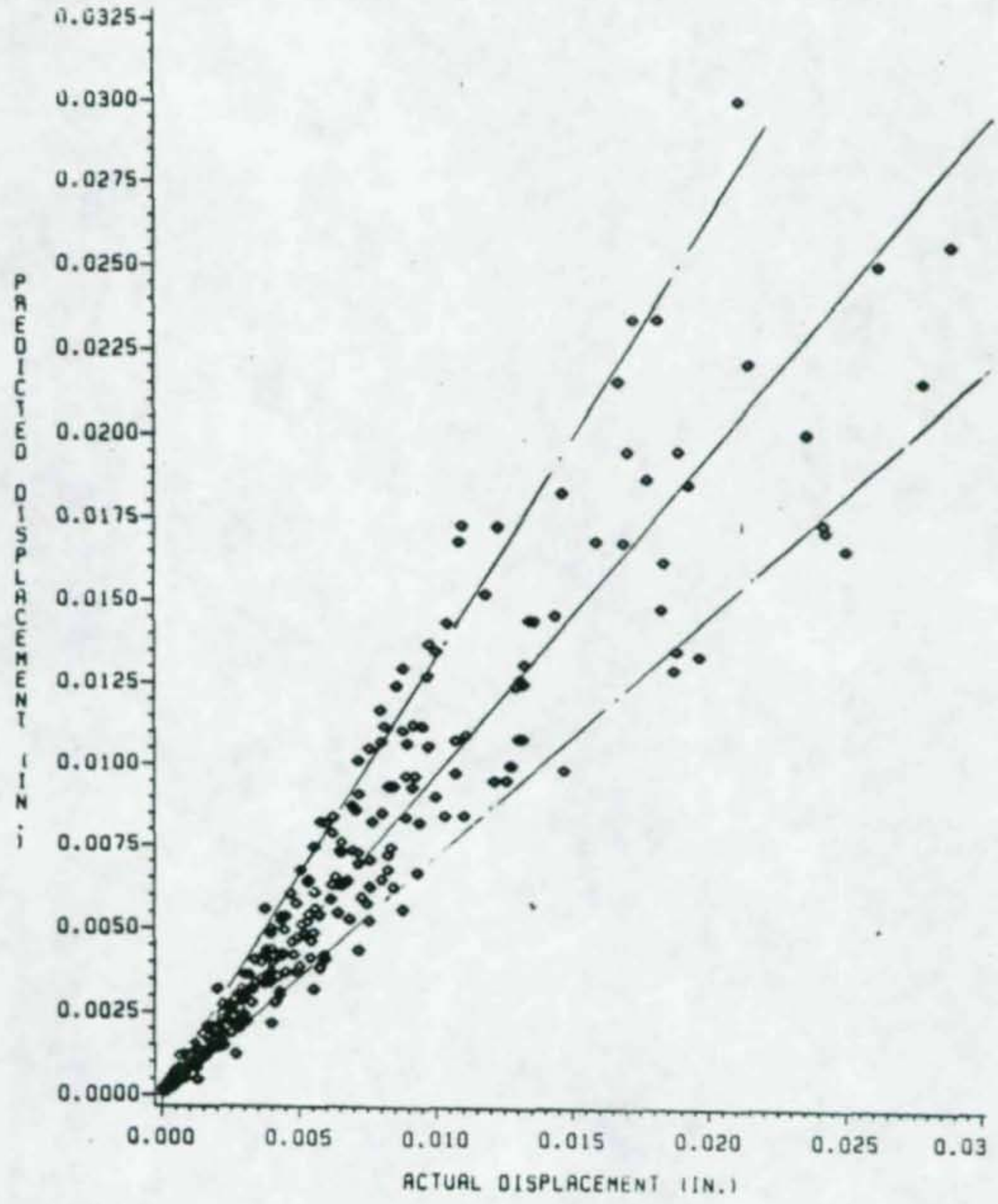

Figure 3.5 Predicted End-Plate Displacement vs. Input (or Actual) Displacement for Case 32

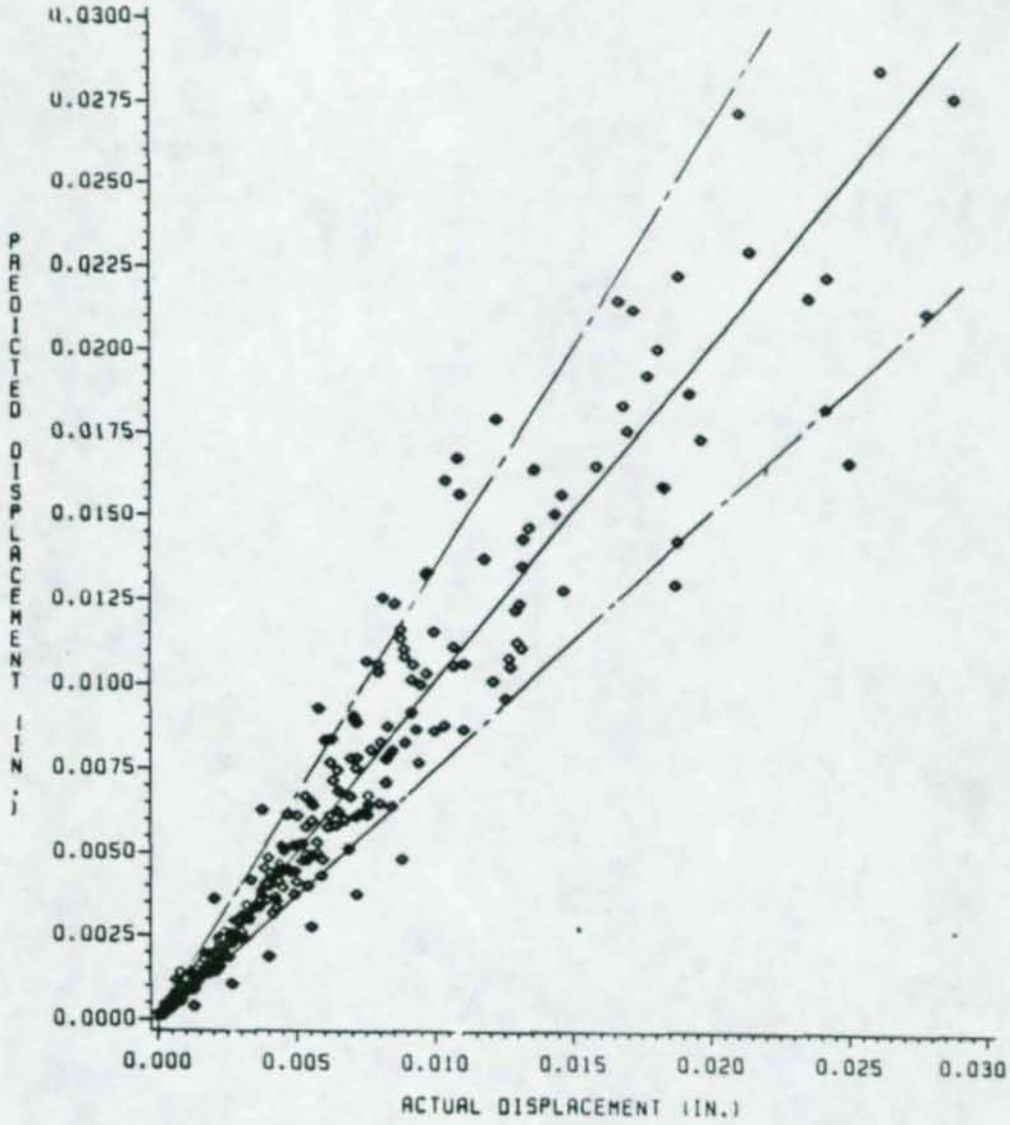

Figure 3.6 Predicted End-Plate Displacement vs. Input (or Actual) Displacement for Case 37

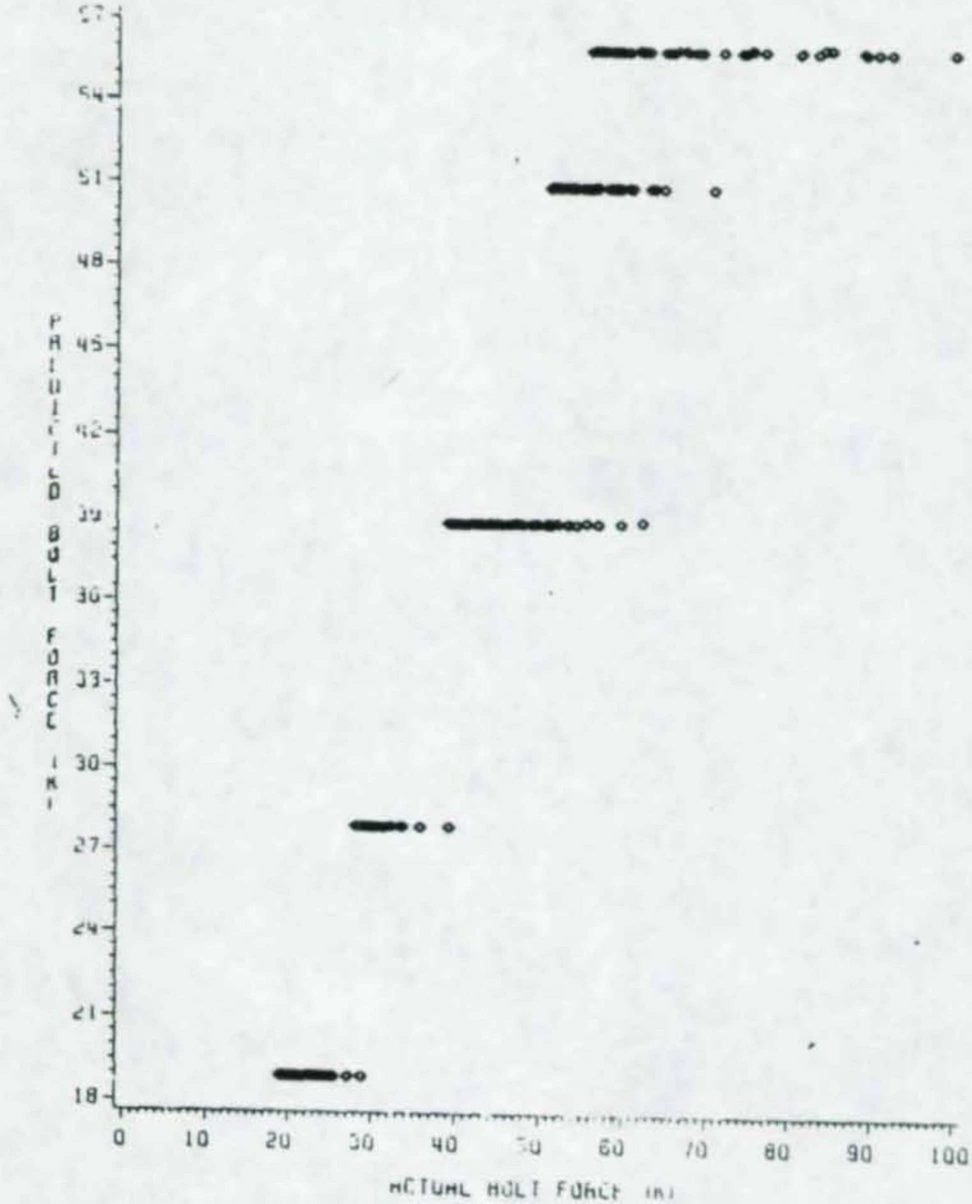

Figure 3.7 Predicted Bolt Force vs. Input (or Actual) Bolt Force for Case 1

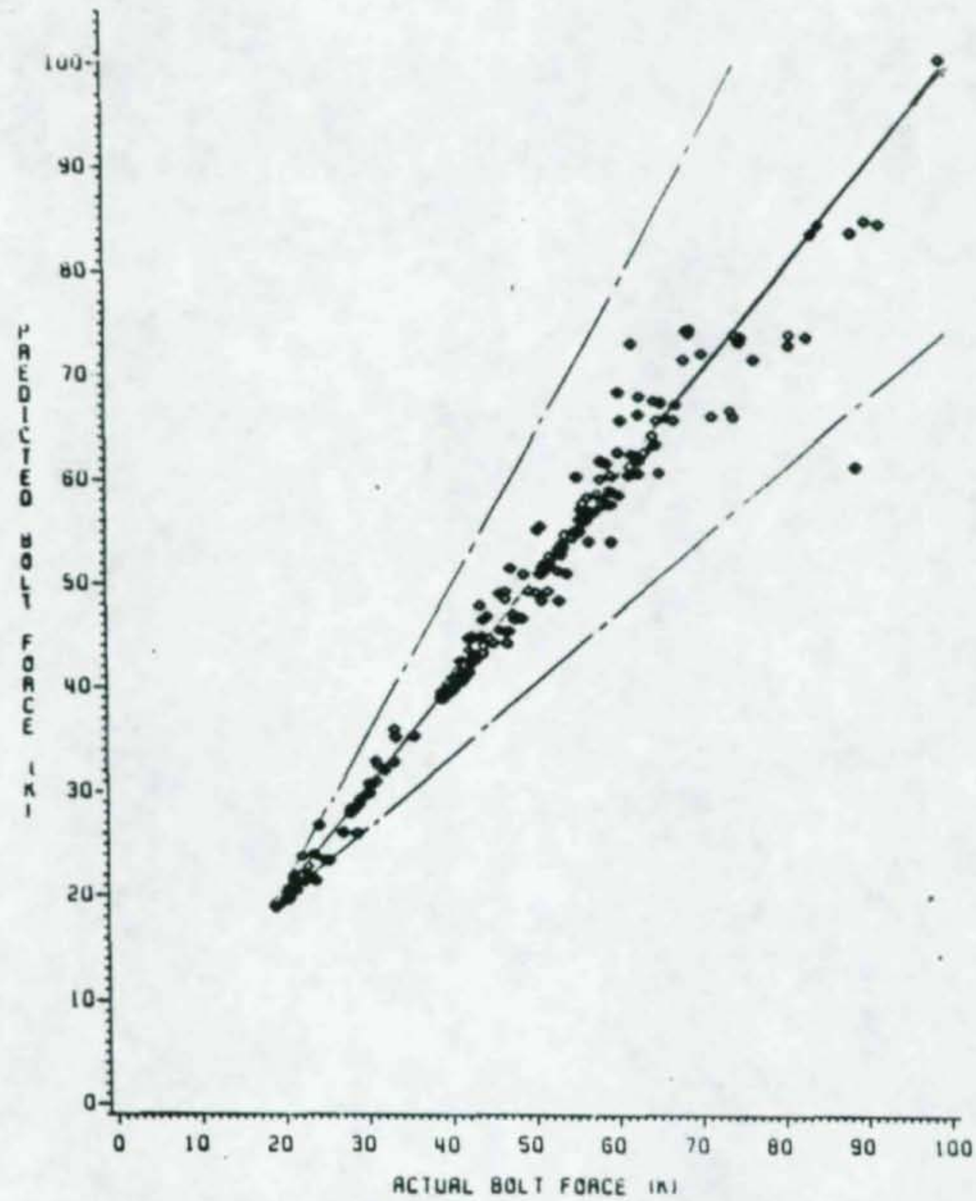

Figure 3.8 Predicted Bolt Force vs. Input (or Actual) Bolt Force for Case 3

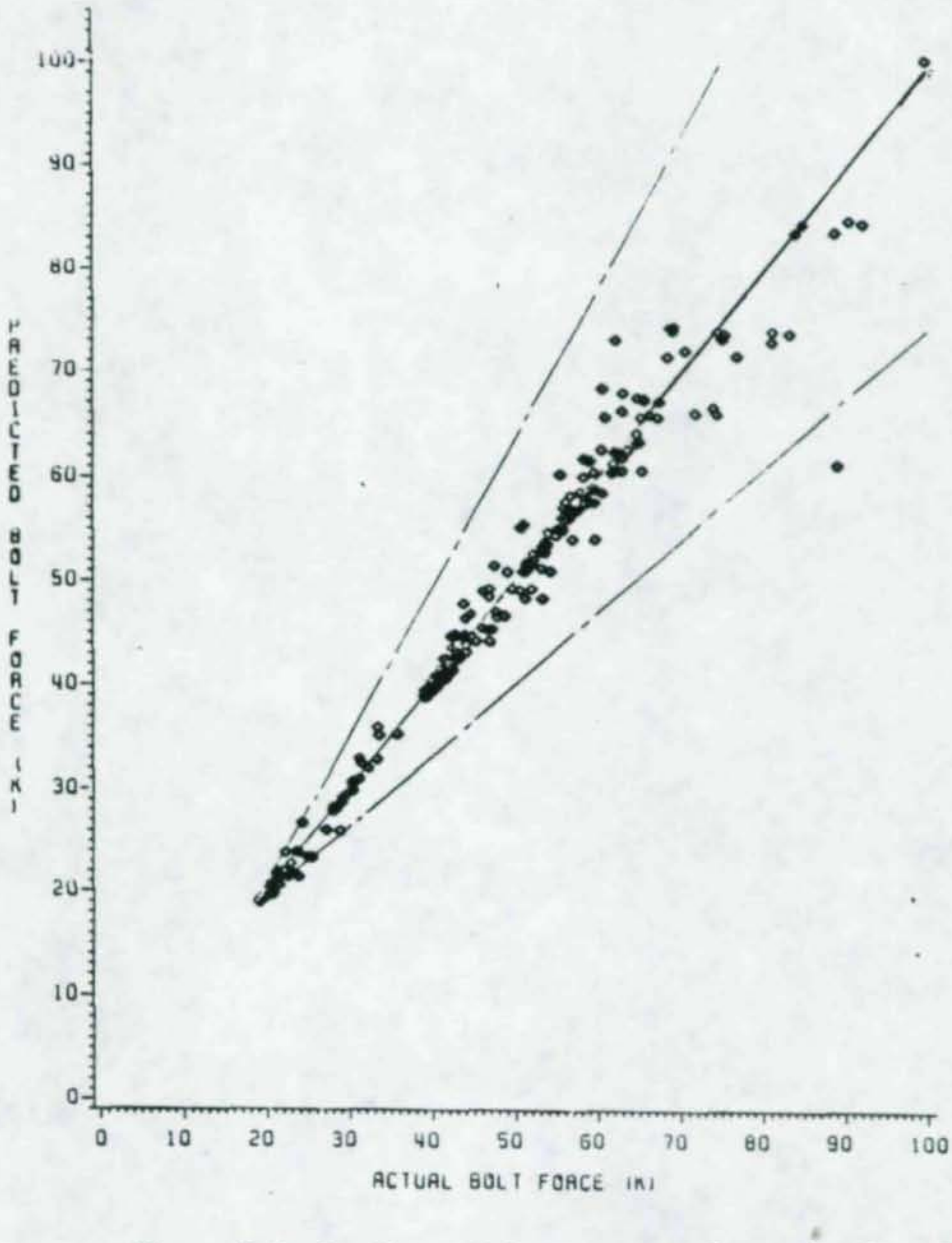

Figure 3.8 Predicted Bolt Force vs. Input (or Actual) Bolt Force for Case 12

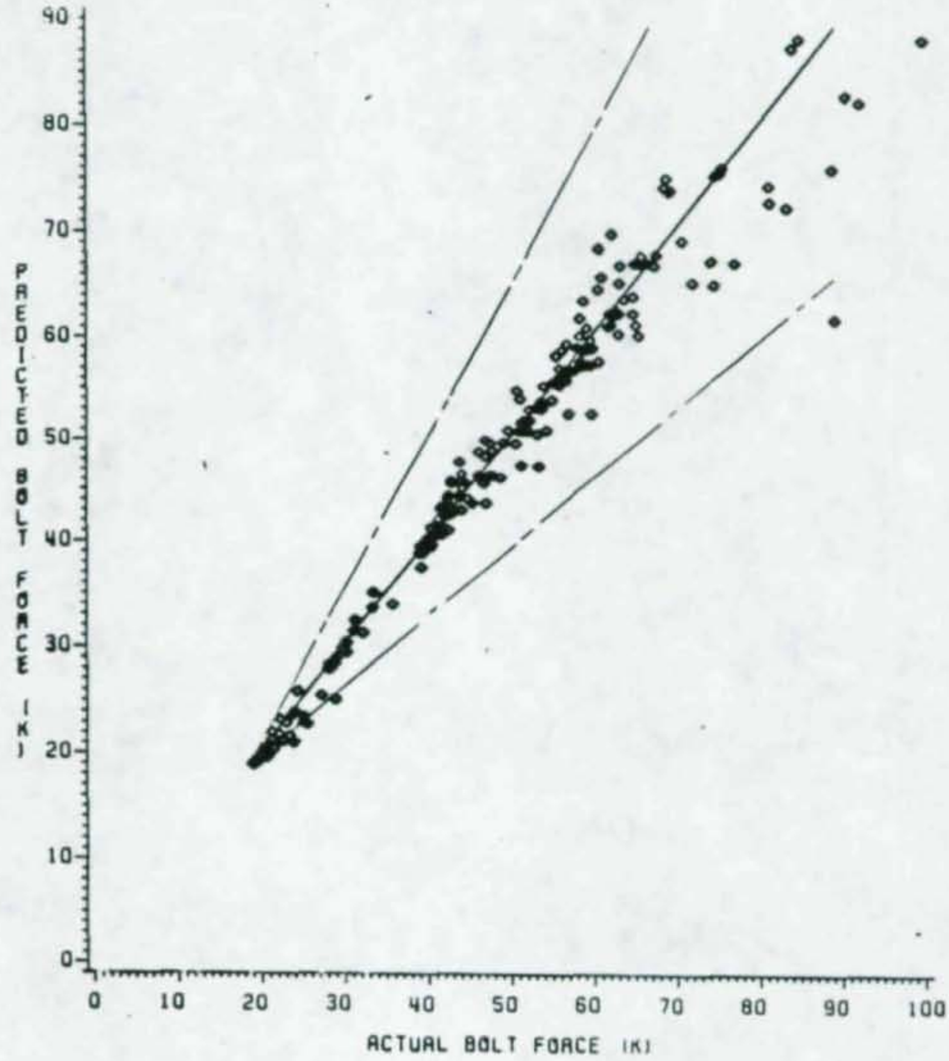

Figure 3.10 Predicted Bolt Force vs. Input (or Actual) Bolt Force for Case 32

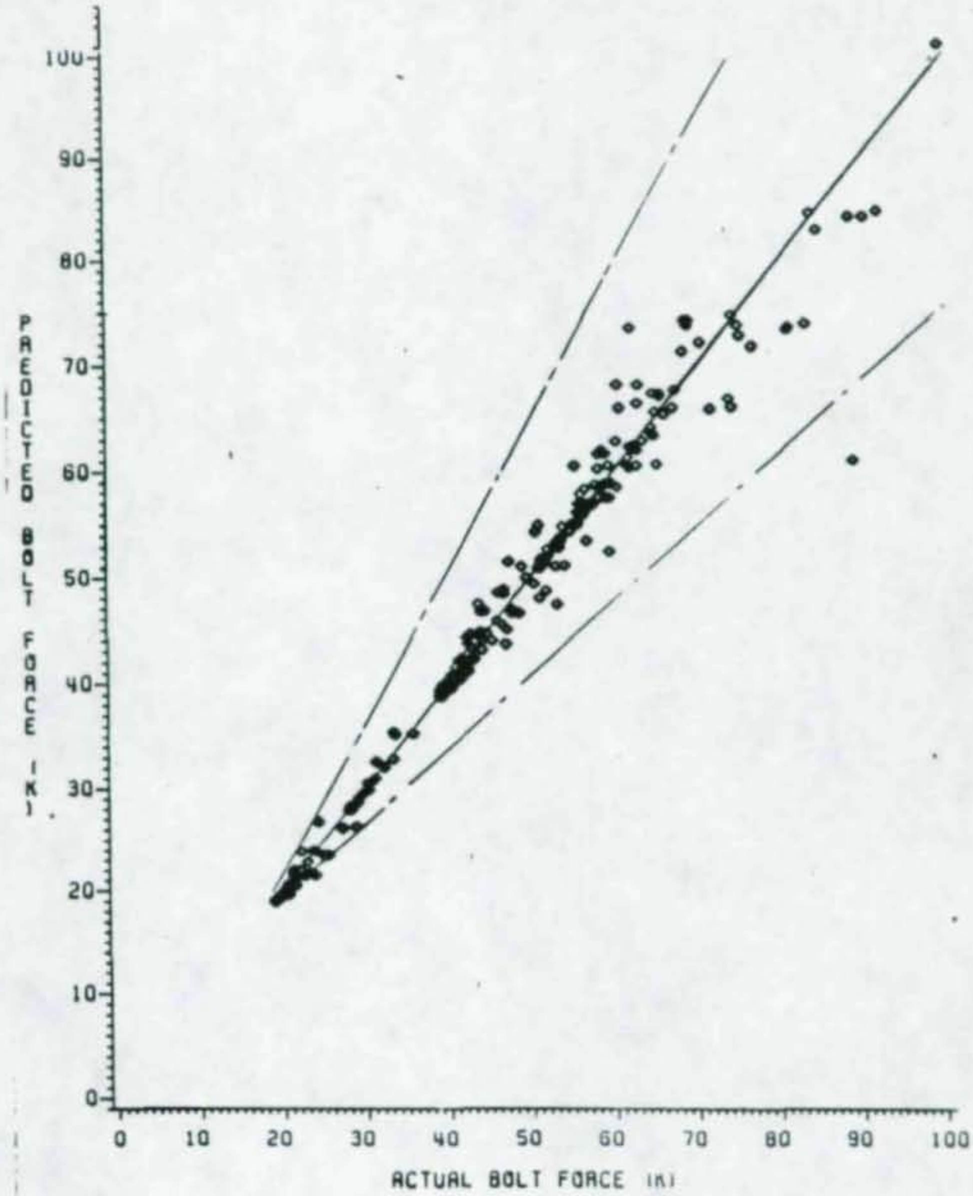

Figure 3.11 Predicted Bolt Force vs. Input (or Actual) Bolt Force for Case 37

separation equation needs to be solved for plate thickness. For example, if Equation (3.6.6) is solved for t_p, the resulting equation is

$$t_p = \frac{(1.827)\ p_f^{3.460}\ h^{0.350} b_p^{2.180} d_b^{0.094}}{(\delta)_{max}^{0.667}\ \ t_w^{0.364}} \left(\frac{M_y}{M}\right)^{0.900} \qquad (3.6.12)$$

From this equation it can be seen that for a particular value of moment applied to the connection (i.e., M), if the beam size is increased (i.e., M_y is increased), then t_p will also increase. This observation will be true for all maximum end-plate separation prediction equations involving $\frac{M}{M_y}$ or $\frac{M}{M_p}$. Hence, it was concluded that it may be better to keep the load parameter as a function of the moment applied to the connection only and not correlate it to the beam size. So it was decided to perform new regression analyses to obtain Equations (3.5.3), (3.5.4), (3.5.6), (3.5.8), (3.5.9), (3.5.10) and (3.5.11) in terms of applied moment, M, instead of $\frac{M}{M_y}$ or $\frac{M}{M_p}$. The resulting equations are as follows:

<u>Case 3</u>. In Case 3, Π_{20} has been changed to Π_9 which results in:

$$\Pi_a = (\delta_x)_{max} = (e)^{-8.336} \left(\frac{t_p}{h}\right)^{7.620} \left(\frac{p_f}{h}\right)^{-6.932} \left(\frac{t_w}{h}\right)^{-0.501} \left(\frac{t_f}{h}\right)^{-0.032} \left(\frac{b_p}{h}\right)^{2.885} \left(\frac{d_b}{h}\right)^{-0.849} \left(\frac{g_b}{h}\right)^{-0.519} \left(\frac{p_f^3}{b_p t_p^3}\right)^{3.053} (M)^{1.356}$$

$(R^2 = 0.94)$ (3.6.12)

$$\Pi_b = P_T \neq (e)^{-2.062} \left(\frac{t_p}{h}\right)^{16.428} \left(\frac{p_f}{h}\right)^{-16.824} \left(\frac{t_w}{h}\right)^{-0.349} \left(\frac{t_f}{h}\right)^{0.049} \left(\frac{b_p}{h}\right)^{5.612} \left(\frac{d_b}{h}\right)^{-2.391} \left(\frac{g_b}{h}\right)^{0.441} \left(\frac{p_f^3}{b_p t_p^3}\right)^{5.655} (M)^{2.568}$$

$(R^2 = 0.90)$ (3.6.13)

<u>Case 12</u>. In Case 12, only bolt force equation needs to be modified since plate separation equation has been eliminated. In this case Π_{20} is changed to Π_9 which results in:

$$\Pi_b = P_T + (e)^{-1.284} \left(\frac{t_p}{h}\right)^{13.830} \left(\frac{p_f}{h}\right)^{-15.213} \left(\frac{b_p}{h}\right)^{4.817} \left(\frac{g_b}{h}\right)^{-0.657} \left(\frac{r_B}{h}\right)^{-0.223} \left(\frac{p_f^{\,3}}{b_p t_p^{\,3}}\right)^{5.229} (M)$$

$(R^2 = 0.90)$ (3.6.14)

<u>Case 32</u>. In Case 32, Π_{21} has been changed to Π_9 which results:

$$\Pi_a = (\delta_x)_{max} = (e)^{-7.952} \left(\frac{t_p}{h}\right)^{6.366} \left(\frac{p_f}{h}\right)^{-6.007} \left(\frac{g_b}{h}\right)^{-1.667} \left(\frac{I_B}{h^4}\right)^{-0.0004} \left(\frac{p_f^{\,3}}{b_p t_p^{\,3}}\right)^{2.783} \left(\frac{b_p}{h}\right)^{2.568} (M)^{1.358}$$

$(R^2 = 0.94)$ (3.6.15)

and

$$\Pi_b = P_T + (e)^{-1.284} \left(\frac{t_p}{h}\right)^{6.366} \left(\frac{p_f}{h}\right)^{-6.007} \left(\frac{g_b}{h}\right)^{-1.667} \left(\frac{I_B}{h^4}\right)^{-0.0004} \left(\frac{p_f^{\,3}}{b_p t_p^{\,3}}\right)^{2.783} \left(\frac{b_p}{h}\right)^{2.568} (M)^{1.358}$$

$(R^2 = 0.90)$ (3.6.16)

<u>Case 37</u>. In Case 37, Π_{21} has been changed to Π_9 which results in:

$$\Pi_a = (\delta_x)_{max} = (e)^{-7.223} \left(\frac{t_p}{h}\right)^{6.041} \left(\frac{p_f}{h}\right)^{-5.873} \left(\frac{r_B}{h}\right)^{0.959} \left(\frac{p_f^{\,3}}{b_p t_p^{\,3}}\right)^{2.760} \left(\frac{g_b}{h}\right)^{-1.385} \left(\frac{b_p}{h}\right)^{2.438} (M)^{1.339}$$

$(R^2 = 0.94)$ (3.6.17)

$$\Pi_b = P_T + (e)^{-1.228} \left(\frac{t_p}{h}\right)^{13.830} \left(\frac{p_f}{h}\right)^{15.213} \left(\frac{r_B}{h}\right)^{-0.223} \left(\frac{p_f^{\,3}}{b_p t_p^{\,3}}\right)^{5.229} \left(\frac{g_b}{h}\right)^{-0.657} \left(\frac{b_p}{h}\right)^{4.817} (M)^{2.535}$$

$(R^2 = 0.90)$ (3.6.18)

Equation (3.6.18) is the same as Equation (3.6.14). Equations (3.6.5) and (3.6.6) are similar except for the last terms, which are $\frac{M}{M_y}$ and $\frac{M}{M_p}$, respectively. Therefore, when $\frac{M}{M_y}$ or $\frac{M}{M_p}$ is changed to M then both equations will yield the same prediction equations.

The input (or actual) versus predicted plots for Equations (3.6.12) through (3.6.18) were again checked. They all were similar to the corresponding plots shown in Figures 3.1 through 3.11.

3.5.3 Elimination Based on Behavior Prediction from Varying the Variables Individually

To further investigate, whether the equations obtained at the end of Section 3.5.2, correctly depict the behavior of a typical flush end-plate connection with a single row of bolts in the tension region, it was decided to vary one variable through low, intermediate, and high values (values given in Table 3.1) and hold the others at the intermediate level. Since the prediction equation for maximum end-plate separation, i.e., $\pi_a = (\delta)_{max}$, was intended to be used for designing the end-plate thickness, t_p, in this investigation Equations (3.6.11), (3.6.15) and (3.6.17) were solved for end-plate thickness. In solving for t_p, the value maximum end-plate separation $(\delta)_{max}$ was set equal to 0.01 in. Since according to the 2-D finite element analysis of eight test specimens, the average value of maximum end-plate separation found to be equal to 0.01 in. (the solution of equation in terms of t_p is illustrated in Chapter V).

In the 2-D finite element model, the two most important variables that effect the design of the end-plate are the pitch, p_f, of the tension bolt and diameter, d_b, of the bolt. The effect of these two parameters was investigated first. Figures F.1 through F.6 of Appendix F show the plots of moment versus plate thickness obtained by varying p_f and d_b through low, intermediate and high values in Equations (3.5.11), (3.5.15), and (3.5.17), respectively. The observations made from these plots are summarized in Table 3.5. From this table it can be seen that Equations (3. 6.15) and (3.6.17) both predict that in a connection as the bolt diameter is increased, the end-plate thickness required will also increase. This

Table 3.5

End-Plate Thickness Prediction by Varying

P_f and d_b

Equation	Observations	
	By varying p_f	By varying d_b
3.6.11	t_p increases significantly as p_f is increased	t_p decreases, though not significantly, as d_b is increased
3.6.15	t_p increases significantly as p_f is increased	t_p increases as d_b increased
3.6.17	t_p increases significantly as p_f is increased	t_p increases as d_b is increas-ed

is contradictory to the true behavior. With increase in bolt diameter, the end-plate thickness required should actually decrease. So based on this investigation it was concluded that Equation (3.6.11) predicts best the maximum end-plate separation. For this equation, the effect of variation of other variables, (beam web thickness, t_w, beam flange, t_f, width of end-plate, b_p, and beam depth, h, on the end-plate thickness) with applied moment are shown in Figures F.7 through F.10 of Appendix F, respectively. From these figures the following is observed:

1) As t_w is increased, the required t_p decreases.
2) As t_f is increased, the required t_p decreases.
3) As b_p is increased, the required t_p decreases.
4) As h is increased, the required t_p decreases.

These results show that as each individual variable in the beam cross-section is increased more load is carried by the beam, therefore, the load going to the plate is less, thus decreasing the end-plate thickness. However, if the beam cross-section is increased (i.e., heavier beam is used) due to higher moment applied to the connection, the plate thickness will increase. Figures F.7 through F.10 of Appendix F soley represents the effect of varying one individual variable at a time and keeping the other variables constant at their intermediate values.

A similar procedure was used to select the best prediction equation for bolt force from Equations (3.6.13), (3.6.16) and (3.6.16). Figures F.11 through F.17 of Appendix F show the plots for moment versus bolt force less pretension (B_F - P_T) obtained by varying d_b, p_f, t_p, t_w and h, respectively, through low, intermediate and high values in

Equation (3.6.16). Figures F.18 through F.24 and F.25 through F.31 show similar plots for Equations (3.6.16) and (3.6.13), respectively. The observation made from all these plots are summarized in Table 3.6.

From Table 3.6 it is concluded that Equation (3.6.13) is the best fit prediction equation for bolt force since it represents the true behavior of the connection. For Equation (3.6.13) the following observations are made from Table 3.6:

1. As d_b increases, $(B_F - P_T)$ increases, which is correct, since a larger diameter bolt would be less stressed (Column 1 of Table 3.6).

2. As p_f, b_p and t_f increaase, $(B_F - P_T)$ increases, which is correct, since by increasing each of these variables one at a time, the bending in the plate increases which results in less back nodes of the end-plate to be in contact, thus generating less reactive force at the back of the end-plate and so more load is transferred to the bolt (Columns 2, 3 and 5 of Table 3.6, respectively).

3. As t_p, t_w and h increases, $(B_F - P_T)$ decreases, which is correct, since the bending in the end-plate decreases causing more back nodes of the end-plate to be in contact, thus generating more reactive force at the back of end-plate and so less load is transferred to the bolts (Columns 4, 6 and 7 of Table 3.6, respectively).

Equation (3.6.16) does not agree with the aforementioned arguments for Columns 1 and 3. Therefore, it is eliminated since it does not correctly characterize the connection behavior. Similarly Equation (3.6.18) is also eliminated, since it does not agree with Equation (3.6.13) for Columns 1 and 5.

Table 3.6

Trend of $(B_F - P_T)$ from Varying the Basic Geometric Variables

Equation	Effect on $(B_F - P_T)$ by increasing						
	d_b (1)	p_f (2)	b_p (3)	t_p (4)	t_f (5)	t_w (6)	h (7)
3.6.13*	decreases	increases	increases	decreases	increases	decreases	decreases
3.6.16**	no effect	increases	decreases	decreases	increases	decreases	decreases
3.6.18***	increases	increases	decreases	decreases	decreases	decreases	decreases

* Refer to Figures F.11 through F.17 of Appendix F

** Refer to Figures F.18 through F.23 of Appendix F

*** Refer to Figures F.24 through F.30 of Appendix F

3.7 Conclusions

Based on the process of elimination described in Section 3.6, it is concluded that the two best-fit regression equations which correctly describe the behavior of the flush-end-plate for end-plate separation and bolt force are Equations (3.6.12) and (3.6.13), respectively. Both these equations are based on the 2-D finite element results and have an R^2 value greater than or equal to 0.9.

CHAPTER IV

EXPERIMENTAL VERIFICATION

4.1 Introduction

A series of tests were conducted to obtain necessary data to evaluate the finite element modeling and also to verify the results of the parametric study. In Section 4.2, the testing program which includes test set up, testing procedure, instrumentation and loading are discussed. In Section 4.3, comparison of analytical and experimental results is presented.

4.2 Testing Program

4.4.1 Test Set Up and Procedure

To verify the analytical procedure described for the flush end-plate connection, a series of tests were conducted by Srouji[2]. His tests consisted of eight one-row flush end-plate specimens, grouped into three series. The test set-up was as shown in Figures 4.1, 4.2 and 4.3. The end-plates were welded to two beams and tested as splice connections under pure moment. The beam and end-plate material was A572 Gr50 steel and bolts were A325. Table 4.1 lists the nominal geometry of the one-row flush end-plate specimens tested. The table also lists the measured yield stress obtained using coupons cut from identical plate material.

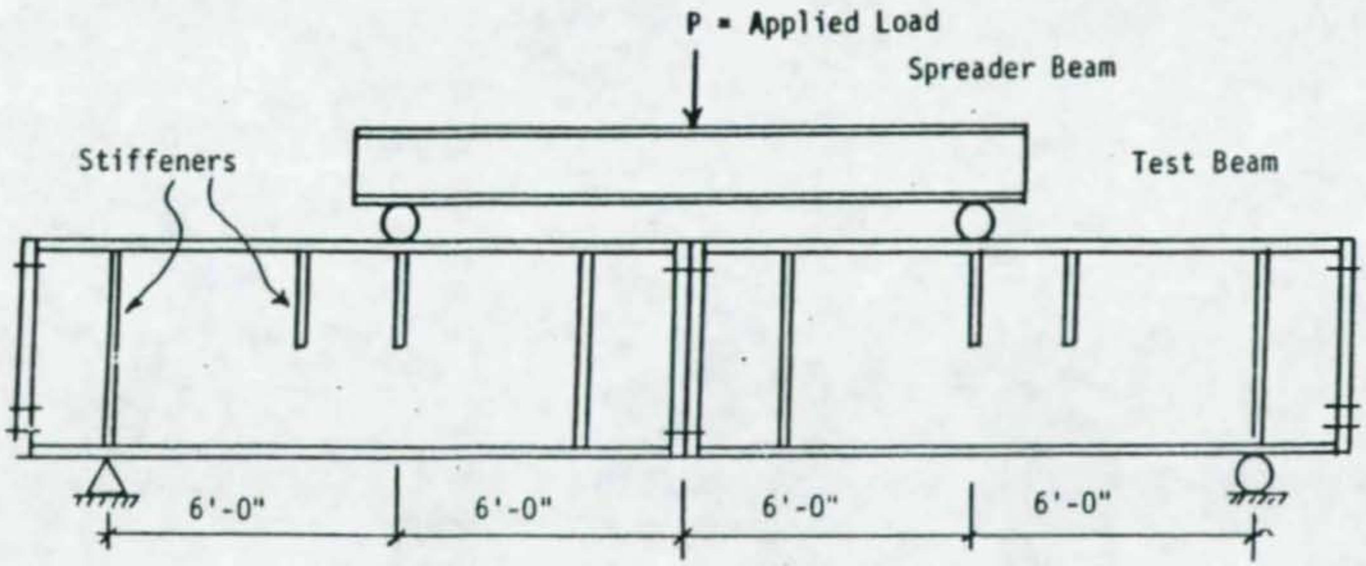

Figure 4.1 Elevation of Test Set-up

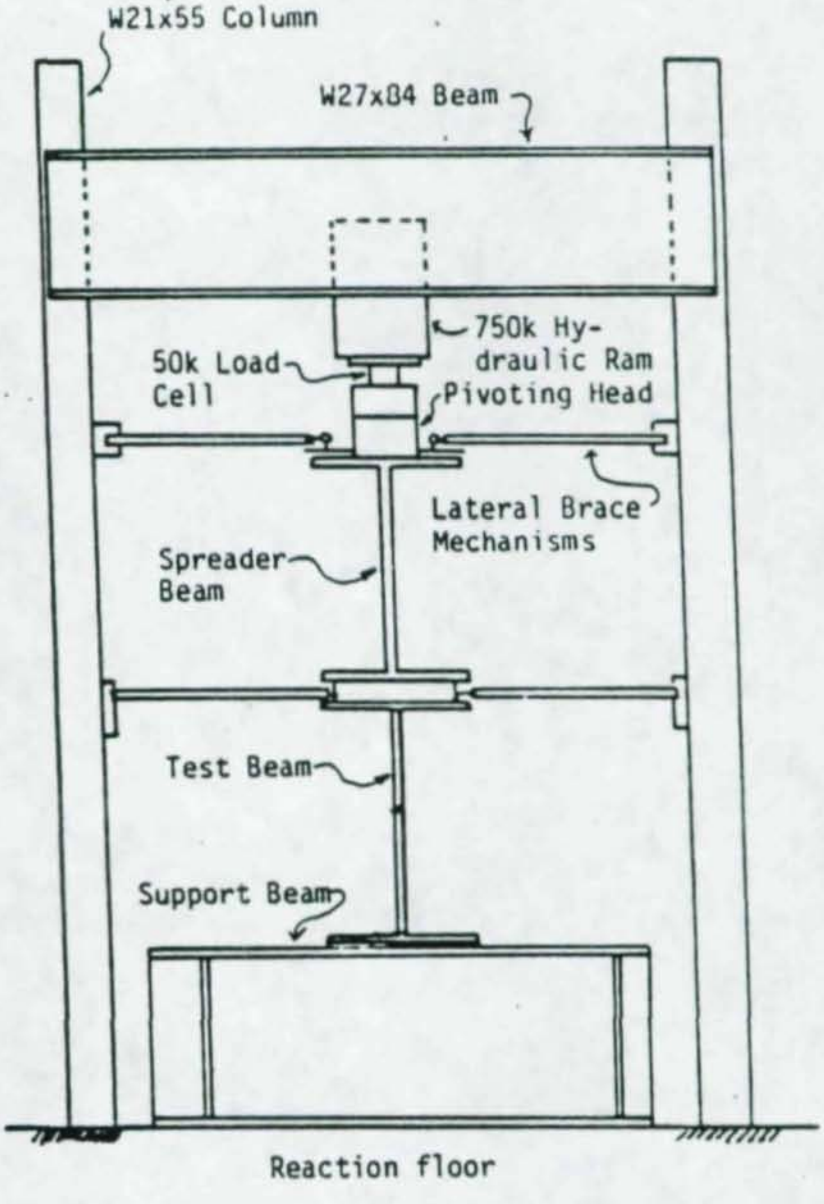

Figure 4.2 Cross-Section of Test Set-up

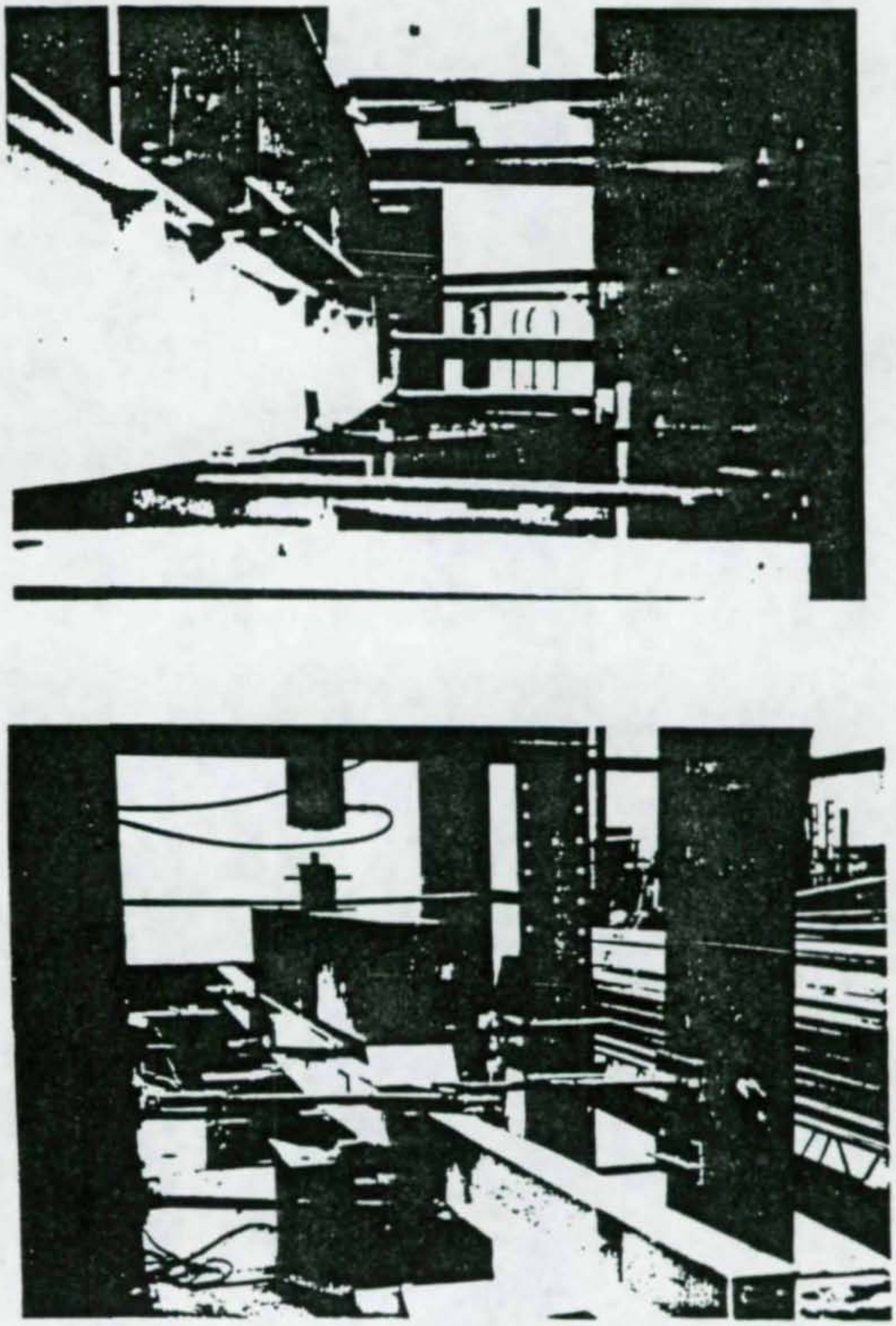

Figure 4.3 Photographs of Test Set-up

60800

Table 4.1
Two-Bolt Flush End-Plate Parameters

Test No.	Test Designation	Bolt Diameter d_b (in)	End-Plate Thickness t_p (in)	Beam Depth h (in)	Flange Width b_f (in)	Pitch p_f (in)	Gage g (in)	Yield Stress (ksi)
1	F1-3/4-1/2-16	3/4	1/2(.505)	16	6	1 1/2	3 1/2	55.48
2	F1-3/4-3/8-16	3/4	3/8(.383)	16	6	1 1/2	3 1/2	59.45
3	F1-5/8-1/2-16	5/8	1/2(.508)	16	6	1 7/8	3 3/4	53.98
4	F1-5/8-3/8-16	5/8	3/8(.385)	16	6	1 3/8	2 3/4	56.95
5	F1-5/8-3/8-10	5/8	3/8(.384)	10	5	1 1/4	2 1/4	51.90
6	F1-5/8-1/2-10	5/8	1/2(.506)	10	5	1 1/2	3	55.80
7	F1-3/4-1/2-24A	3/4	1/2(.504)	24	6	1 3/4	3 1/4	57.53
8	F1-3/4-1/2-24B	3/4	1/2(.502)	24	6	1 3/8	2 3/4	57.53

Notes: Flange and web thicknesses for all tests were 1/4 in.
(.xxx) indicates measured thickness.

The test designations shown in Table 4.1 are to be interpreted as follows: F1-3/4-1/2-16 designates a flush end-plate with one row of 3/4 in. diameter bolts near the tension flange. The end-plate thickness is 1/2 in. and the beam depth is 16 in. In this set, tests were conducted using 10 in., 16 in., and 24 in. deep beams.

In the test set up, the load for the first set of tests (Tests 1, 2, 3 and 4 of Table 4.1) and the first two sets in the second set (Tests 5 and 6 of Table 4.1) was applied using a hydraulic ram powered by an electric pump. The load was monitored using a load cell and standard indicator. For the last tests (Tests 7 and 8 of Table 4.1) a closed loop hydraulic testing (MTS system) was used. The test beams were supported laterally at three locations using lateral brace mechanism. The spreader beam was also laterally supported at centerline (see Figures 4.1, 4.2 and 4.3).

4.1.2 Instrumentation

Instrumentation consisted of wire displacement transducers, calipers, strain gages, and instrumented bolts. For all the tests a HP349A data acquisition/control unit was used with a HP85 desk top computer to collect and record the data. One wire displacement transducer was attached to the end-plate to measure the vertical deflection, two more were attached on the top and the bottom flange of the test beam to measure the lateral displacement close to the end-plate. Calipers were used to measure the end-plate separation at the tension flange. One of the calipers was placed at the centerline of the plate while the others were attached to the edges.

Strain gages were used to measure the strain in the web and flange. In the first set of tests, (one-row bolts) strain gages were placed at two cross-sections 2 in. and 16 in. from the face of the end plate.

4.1.3 Loading Procedure

At the beginning of each test the specimen was loaded to approximately 20% of the expected maximum load to check the test set up and instrumentation. Load versus beam deflection and load versus end-plate separation curves were plotted simultaneously using an HP7470A graphic plotter. The specimen was then unloaded and initial readings recorded at zero load.

The first two sets conducted (F1-3/4-1/2-16 and F1-3/4-3/8-16) were loaded continuously in approximately 2 kips increments to failure and then unloaded. Data was recorded at every load level using the data acquisition system. For all the other tests that were loaded using the hydraulic ram, the specimens were loaded to approximately 2/3 of the expected failure load at varying increments depending on the expected failure load of each test. The specimens were then unloaded at increments 5 kips or more to a load of 2 or 5 kips, taking readings at every step while unloading. The load was then increased to the previous load, and then increased 5 to 10%. For the tests that were loaded using closed loop hydraulic testing system, the test beams were deformed to preselected vertical deflection instead of a particular load. The load required to impose the deflection was obtained by the internal load cell of the system. The vertical deflection was controlled by the actuator of the closed loop hydraulic system. The same cyclic pattern of loading was used and the data was recorded using the same data acquisition system.

4.2 Comparison of Analytical and Experimental Results

As mentioned before, eight specimens were tested in this study. Four of these were conducted using a 16 in. deep beam, two tests were conducted using a 10 in. deep beam, and two others using a 24 in. deep beam. The moment versus end-plate separation and moment versus bolt force plots obtained from experimental tests and finite element results were compared. These results were also compared with corresponding values obtained from the prediction equations (Equation (3.6.11) and (3.6.12) of Chapter III).

Table 4.2 illustrates the strength data of the connection. In this table the maximum applied moments from experimental test specimens, finite element analysis and prediction equation are compared for all the eight test specimens. The maximum predicted applied moment is calculated based on prediction equation (3.6.11) by solving the equation for moment and setting maximum end-plate separation at 0.01 in. (as discussed in Section 5.2 of Chapter V). In Table 4.2 two values are reported for experimental maximum applied moment: the ultimate (failure moment) and the moment resulting for an end-plate separation equal to 0.01 in. In the yield line study conducted by Srouji[2], the failure in the connection was defined as the moment which results in sufficient yield lines in the end-plate so as to result in a collapse mechanism in the end-plate. So the ultimate moment carrying capacity of the end-plate was determined

Table 4.2

Comparison of Maximum Applied Moment Between

Experimental, F.E.M., Predicted and Yield Line

Test No. (1)	Test Designation (2)	Maximum Applied Moments (ft-kips)					Ratios		
		Experimental		F.E.M* (5)	Predicted** (6)	Yield Line (7)	$\frac{\text{F.E.M.}}{\text{Exp.}}$ (8)	$\frac{\text{Predicted}}{\text{Exp.}}$ (9)	$\frac{\text{Predicted}}{\text{F.E.M.}}$ (10)
		Ultimate (3)	At 0.01 in. Separation (4)						
1	F-3/4-1/2-16	92.50	54.0	67.73	64.40	90.12	1.25	1.19	0.95
2	F-3/4-3/8-16	53.96	40.0	41.26	46.47	54.33	1.03	1.16	0.85
3	F-5/8-1/2-16	77.08	52.0	68.77	40.78	80.04	1.32	0.78	0.60
4	F-5/8-3/8-16	64.75	52.0	55.02	50.19	62.02	1.06	0.97	0.91
5	F-5/8-1/2-10	39.47	21.5	25.2	22.30	38.36	1.17	1.04	0.73
6	F-5/8-3/8-10	33.92	24.67	31.67	23.0	31.30	1.28	0.93	0.88
7	F-3/4-1/2-24A	120.2	98.0	122.30	92.46	145.2	1.24	0.94	0.63
8	F-3/4-1/2-24B	154.2	110.0	122.30	130.0	164.5	1.11	1.18	0.88

* These are for partial 3-D Mesh III (refer to Section 2.3 of Chapter II)

** M calculated from Equation (3.6.12) of Chapter III using $(\delta)_{max} = 0.01$ in.

which was used to compute the end-plate thickness. To compare the yield-line analysis results with experimental results, the tests were continued till sufficient yielding occurred in the end-plate so as to result in a yield mechanism. This maximum moment recorded in the experiments is tabulated as "ultimate" in Table 4.2. On the other hand, in the finite element analysis, the failure of the end-plate due to yielding is taken to occur when the maximum effective strain in an element, computed from Von Mises yield criterion, becomes greater or equal to 12 times the yield strain for the material. As discussed in Section 5.2 of Chapter V, based on the partial 3-D finite element analyses of the eight test specimens, it was seen that a failure of the end-plate occurs when separation is between 0.0087 in. to 0.01407 in., giving an average value of about 0.01 in.

Column 6 of Table 4.2 gives the ratio between the maximum applied moment obtained from finite element analysis and the experimental values based on 0.01 in. end-plate separation. This ratio varies from 1.03 to 1.32 indicating the difference between finite element analysis and experimental to be within +3% to +32%. Column 7 of Table 4.2 gives the ratio between maximum applied moment using the prediction Equation (3.6.11) and the experimental value based on 0.01 in. end-plate separation differ by -22% to +19% (negative implying lesser predicted value). Column 8 of Table 4.2 gives the ratio between predicted maximum applied moment and maximum applied moment based on finite element results. These ratios indicate how close the predicted values are to the finite element values. Differences lie within -5% to +17%, except for test numbers 3 and 7 for which the difference increases to -40% and -37%, respectively.

This value shows that a value of $(\delta)_{max}$=0.01 in. is too conservative for test numbers 3 and 7.

As was mentioned before, based on the partial 3-D finite element analyses of eight test specimens, the maximum end-plate separation, $(\delta)_{max}$, obtained at failure varied from 0.0087 in. to 0.014A in. In Table 4.3, the values of maximum moment obtained from analytical and experimental results, corresponding to the value of $(\delta)_{max}$ for each test specimen, are compared. In this table, Column 7 gives the ratio between the maximum moment from finite element analyses and experimental values. It can be seen that differences between finite element and experimental results lies within the range +6% to +30%. Column 8 gives the ratio between predicted maximum moment and experimental values. It can be seen that the difference between predicted and experimental results lies within the range -5% to +20%. Column 9 gives the ratio of predicted maximum applied moment and finite element result. It should be noted that by using more realistic $(\delta)_{max}$ value for test numbers 3 and 7, the difference between predicted and finite element results is decreased to +26% and 20%, respectively, from 40% and 37%, respectively, as shown in Table 4.2.

In Figures B.1 through B.8 of Appendix B, the moment versus maximum end-plate separation obtained from the eight test specimens are compared with the results of the 2-D finite element analyses. These plots indicate a good correlation at lower load levels (10% to 15% difference between 2-D finite element and experimental results), whereas at failure the 2-D finite element results deviate significantly from the experimental results (difference varies between 50% to 60%). This is because in the 2-D finite element model, the transverse variation of deformations and stresses of the end-plate

Table 4.3

Comparison of Maximum Applied Moment Between

Experimental, Finite Element and Predicted Values

for Maximum End-Plate Separation

Test No. (1)	Test Designation (2)	δ_{max} (in.) (3)	Maximum Applied Moment (ft-kips) Experimental (4)	F.E.M. (5)	Predicted (6)	Ratios $\frac{F.E.M.}{Experimental}$ (7)	$\frac{Predicted}{Experimental}$ (8)	$\frac{Predicted}{F.E.M.}$ (9)
1	F-3/4-1/2-16	0.0120	59.0	67.73	71.00	1.14	1.20	0.95
2	F-3/4-3/8-16	0.0094	39.0	41.26	44.00	1.06	1.12	0.94
3	F-5/8-1/2-16	0.01467	54.0	68.77	54.00	1.27	1.00	1.27
4	F-5/8-3/8-16	0.0116	52.0	55.02	56.00	1.06	1.07	0.93
5	F-5/8-3/8-10	0.0087	21.0	25.2	20.00	1.20	0.95	1.26
6	F-5/8-1/2-10	0.0095	24.19	31.67	28.84	1.30	1.19	1.10
7	F-3/4-1/2-24A	0.01152	99.0	122.30	102.00	1.23	1.03	1.20
8	F-3/4-1/2-24B	0.010	111.00	122.30	130.00	1.10	1.17	0.94

cannot be represented. To correct for this a scaling factor (=1.5) was developed in Section 2.5 of Chapter II, which when applied to the failure load of the 2-D finite element model results gives more realistic results closer to both partial 3-D finite element model results and experimental results. The plots obtained after applying the scaling factor are shown in Figures C.7 through C.14 in Appendix C. The maximum difference between the experimental and modified 2-D finite element results now varies between 1% to 18% at the various load levels for the eight test cases.

In Figures B.9 through B.16 of Appendix B, the moment versus bolt force plots obtained for the eight test specimens are compared with the results of 2-D finite element analyses. From these figures it can be seen that good correlation is obtained between experimental and analytical results, with a difference of less than 20%. This shows that the 2-D finite element model predicts the bolt force behavior reasonably well for the flush-end-plate connection.

Figures C.1 through C.6 of Appendix C shows comparison of the experimental and the 2-D, partial 3-D Mesh-I, Partial 3-D Mesh-II, and Partial 3-D Mesh III finite element results for test specimens designated as F-3/4-1/2-16 and F-3/4-1/2-24A. Comparisons are shown only for these two tests, similar results were obtained for the remaining six tests also. These plots indicate that the best finite element mesh, which best represents the true behavior of the connection for end-plate separation, is the partial 3-D Mesh III (see Figures C.3 and C.4 of Appendix C) and results obtained by this model differ from experimental observed values by 2% to 15% at different load levels. Figures C.1 of Appendix C shows that the Partial 3-D Mesh-I and Mesh-II do not give good correlation between analytical and experimental results for end-plate separation. The end-plate separation obtained by finite element analysis and experimental results at any load level differ by more than 60% and 35% for the partial 3-D Mesh-I and Partial 3-D Mesh-II, respectively. Figures C.2, C.5, and C.6 of Appendix C show that moment versus bolt force plots for the 2-D model, partial 3-D models, and experimental results compare well (difference between analytical and experimental values at various load levels varying between 5% to 20%).

Figures D.1 through D.8 of Appendix D shows comparison of the experimental and prediction equation results for moment versus maximum end-plate separation. The prediction Equation (3.6.11), which was developed in Chapter III, is used. Figures D.9 through D.16 of Appendix D shows comparison of the experimental and the prediction equation results for moment versus bolt force. The prediction equation, Equation (3.6.12), which was developed in Chapter III, is used. From these figures it can be concluded that the difference between prediction equation and experimental results for end-plate separation and bolt force varied between 1% to 21% and 1% to 18%, respectively, at various load levels.

CHAPTER V

PROPOSED DESIGN METHODOLOGY

5.1 Introduction

The prediction equations obtained by regressing the finite element results of the fifty 2-D cases with application of a suitable correction factor to account for 3-D effects have been shown to adequately explain the behavior of typical "flush" end-plate connections. These equations predict maximum end-plate separation and force in the tension bolts. The maximum end-plate separation prediction equation is used in Section 5.2 to develop an equation to compute the end-plate thickness. Further, in Section 5.3 an analytical equation is also developed to predict the maximum tensile force in the web of the beam. A design procedure is explained in Section 5.4. Finally a design example is presented in Section 5.5.

5.2 Development of Design Equations for the End-Plate

To develop a design equation, Equation (3.6.12) of Chapter III, is solved for plate thickness, t_p, for a known value of the allowable maximum end-plate separation $(\delta)_{max}$. The maximum end-plate separation defined in Equation (3.6.12) is obtained from the 2-D finite element analyses and is not a true representation of the 3-D behavior of the end-plate. However, the partial 3-D finite element model, presented in Section 2.3 of Chapter II, is seen to give acceptable results for maximum end-plate separation (also refer to Appendix C). As was shown in Section 2.6 of Chapter II, at failure the relationship between maximum end-plate separation for a typical 2-D and partial 3-D model is as follows:

$$(\delta_{max})_{2D-3D} = 1.5(\delta_{max})2D \tag{5.2.1}$$

$$(\delta_{max})2D = (\delta_{max})_{2D-3D}/1.5 \tag{5.2.2}$$

Substituting Equation (5.2.2) into Equation (3.6.12), results in

$$\frac{(\delta_{max})_{2D-3D}}{1.5} = (e)^{-8.336}\left(\frac{t_p}{h}\right)^{7.620}\left(\frac{p_f}{h}\right)^{-6.932}\left(\frac{t_w}{h}\right)^{-0.501}\left(\frac{t_f}{h}\right)^{-0.038}\left(\frac{b_p}{h}\right)^{2.835}\left(\frac{d_b}{h}\right)^{-0.849}\left(\frac{g_b}{h}\right)^{-0.519}\left(\frac{p_f^{\,3}}{b_p t_p^{\,3}}\right)^{3.053}(M)^{1.356} \tag{5.2.3}$$

Solving Equation (5.2.3) for end-plate thickness, gives

$$t_p = \frac{(p_f)^{1.447}}{(\delta_{max})_{2D-3D}^{0.650}(h)^{1.050}(t_w)^{0.325}(t_f)^{0.025}(d_b)^{0.551}(g_b)^{0.551}(b_p)^{0.141}}(M)^{0.881} \tag{5.2.4}$$

All variables appearing in Equations (5.2.4) were defined in Section 3.2 of Chapter III. However, the variable g_b is redefined as follows:

$$g_b = \left(\frac{1}{3}\right)\left(\frac{A_B}{d_b}\right)\left(\frac{F_{by}}{F_{yb}}\right) \tag{5.2.5}$$

where A_B = area of beam cross-section, d_b = bolt area, F_{by} = yield stress of beam material, and F_{yb} = yield stress of bolt material. Hence, the maximum end-plate separation $(\delta_{max})_{2D-3D}$ appearing in Equation (5.2.4) will simply be called $(\delta)_{max}$. For the eight laboratory test specimens using the partial 3D finite element model (refer to Section 4.1 of

Chapter IV), it was seen that $(\delta)_{max}$ varied from 0.0087 to 0.0147 in. So if the designer can establish a limit on the maximum allowable end-plate separation, then Equation (5.2.4) can be used to compute the plate thickness required. However, if such information is not available then based on laboratory test and finite element results, it is proposed that a conservative value of δ_{max} = 0.01 in. be adopted. Substituting $(\delta)_{max}$ = 0.01 in. into Equation (5.2.3), gives the following equation:

$$t_p = 0.115526 \frac{(p_f)^{1.447}}{(h)^{1.050} (t_w)^{0.325} (t_f)^{0.024} (d_b)^{0.551} (g_b)^{0.337} (b_p)^{0.141}} (M)^{0.881} \tag{5.2.6}$$

The behavior characteristic of steel connections can also be represented by its moment-rotation (M-Θ) relationship. The degree of rigidity of a moment-connection can be also chosen as a design criterion to design the connection. The rotation, Θ, of the flush end-plate connection at any load can be found from the following expression:

$$\Theta = \frac{(\delta)_{max}}{h} \tag{5.2.7}$$

Substituting Equation (5.2.3) into Equation (5.2.7), gives

$$\Theta = C\, M^n \tag{5.2.8}$$

where

$$C = (0.000359) \frac{(p_f)^{2.227}}{(h)^{2.616} (t_w)^{0.501} (t_f)^{0.038} (d_b)^{0.849} (g_h)^{0.519} (b_p)^{0.218} (t_p)^{1.539}} \tag{5.2.9}$$

is a coefficient dependent on the end-plate thickness, beam dimensions, bolt diameter and pitch of the tension bolt. The value of n for the single bolt row flush end-plate is found to be equal to 1.356 (refer to Equation (5.2.3)). Equation (5.2.8) represents the moment-rotation relationship for this particular connection. Generally, to represent this relationship graphically, Θ is measured on the horizontal axis and M on the vertical axis, as shown in Figure 5.1, with the equation of the curve taken as

$$M = C' \Theta^{1/n} \tag{5.2.10}$$

where $C' = 1/C$. This curve is called the "connection curve". For the flush end-plate connection, this curve is nonlinear and is close to linear for small loads, but flattens out at larger loads. A "perfectly rigid" connection is a connection with no relative rotation between the two connected parts. The connection curve coincides with the M-axis. For a "perfectly flexible" or pinned connection, the connection curve coincides with Θ axis. However, for all practical or real connections the curves are between the two axes, as shown in Figure 5.1.

A typical flush end-plate connection is not perfectly rigid and the restraining moment at the beam end is less than the fixed end moment. This reduced moment capacity, M_c (see Figure 5.1), and the actual rotation, Θ_c, depends not only on the end-plate configuration but also on the beam dimensions. The interaction between the two can be found by plotting the beam line and connection curve as shown in Figure 5.1. In this figure the intercept Θ_s represents the simple beam end rotation under the specified loading and the intercept M_f represents the fixed-end moment at the beam end and under the same loading. For a beam of span, L, with uniformly distributed loading, w,

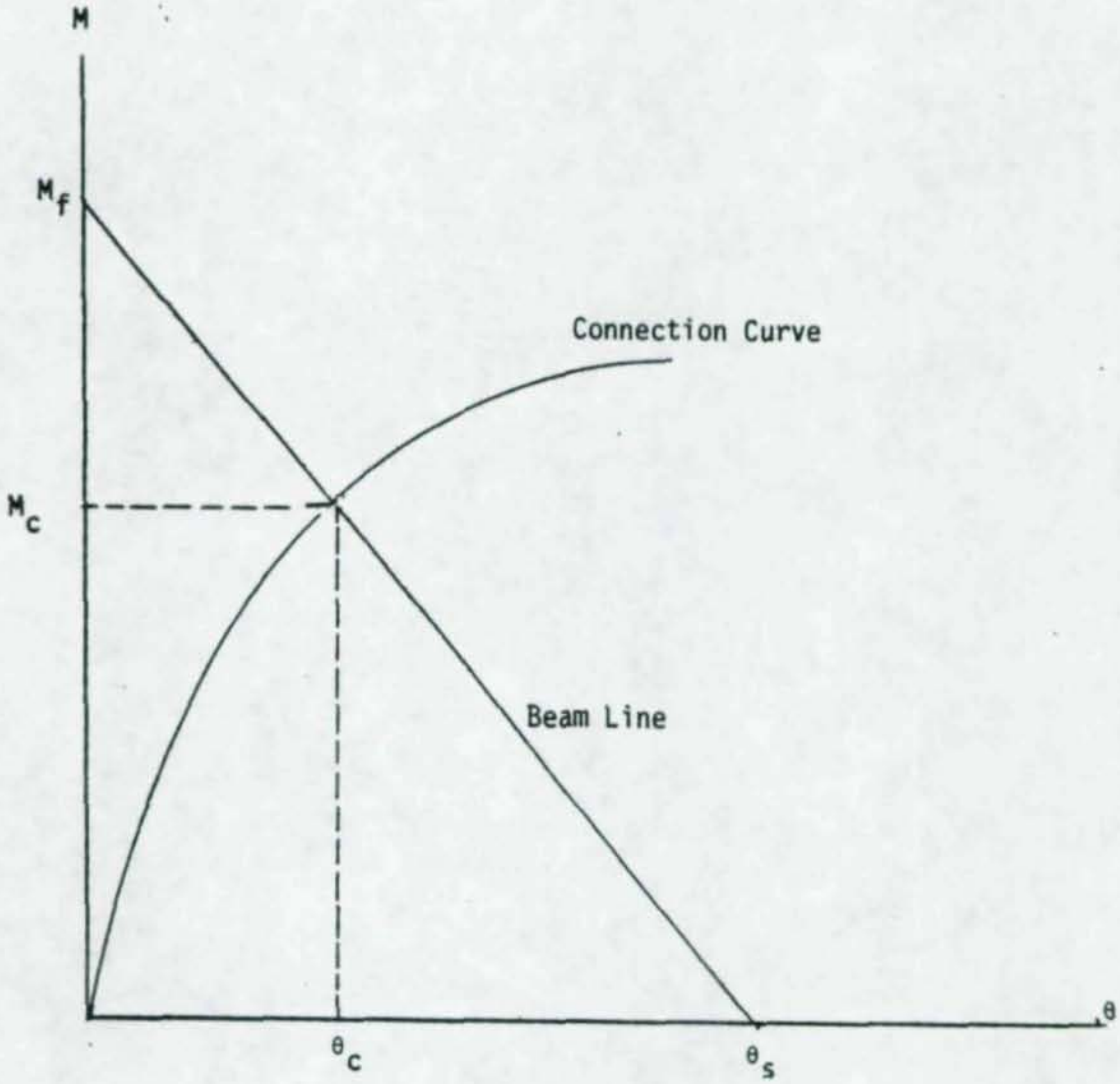

Figure 5.1 Connection Curve and Beam Line

$$\theta_s = wL^3/(24EI) \tag{5.2.11}$$

$$M_f = wL^2/12 \tag{5.2.12}$$

The "degree of rigidity", α_r, of the connection is defined as

$$\alpha_r = M_c/M_f \tag{5.2.13}$$

Similarly the "degree of flexibility", α_f, for the connection can be defined as

$$\alpha_f = \theta_c/\theta_s \tag{5.2.14}$$

From similar triangles of the beam line, the following is concluded:

$$\alpha_r + \alpha_f = \frac{M_c}{M_f} + \frac{\theta_c}{\theta_s} = \left(\frac{\theta_s - \theta_s}{\theta_s}\right) + \frac{\theta_c}{\theta_s} = 1 \tag{5.2.15}$$

For other than "perfectly rigid" connections, the connection can be designed by either computing iteratively M_c and θ_c as the intersection values of the beam line and the connection M-θ curve for a given loading or by taking a certain total rigidity, α_r. For example $\alpha_r = 0.9$, i.e., by taking total rigidity of 90% or total flexibility of 10%. In the former approach the connection geometry must be assumed to start the design process. In the latter approach, a value for total rigidity, α_r, (or for α_f) must be assumed. A 90% value for α_r is recommended by McGuire[26].

In Section 5.4, a design methodology is developed assuming that the connection resisting moment is known.

5.3 Development of an Equation to Predict Tensile Force in Web

In this section an equation is developed to predict the maximum tensile force in the web of the beam utilizing stress plots along the beam depth as obtained from 2-D finite element analyses. Figures 5.2 through 5.5 show the variation of normal stress across the beam depth in the beam web for different load levels (shown as L1, L2, L3, etc.) for four selected cases. Each case was analyzed for a different web thickness, t_w. Maximum stress occurs at point marked 6 in these figures; points 5 and 7 are adjacent. From Figures 5.2 through 5.5, it can be seen that the stress distribution is a pressure bulb around the tension bolt under pretension alone. The pressure bulbs increase in size with increasing moment. The free edge of the plate remains stress free.

Based on the stress plots shown in Figures 5.2 through 5.5, the force in the web corresponding to points 5, 6 and 7 is calculated using the following expression:

$$T_w = \{(\frac{\sigma_5 + \sigma_6}{2})d_1 + (\frac{\sigma_6 + \sigma_7}{2})d_2\}t_w \tag{5.3.1}$$

where T_w = force in the web corresponding to web material volume covered by points 5, 6 and 7; σ_5, σ_6 and σ_7 = stress at points 5, 6 and 7, respectively; d_1 = distance between points 5 and 6; d_2 = distance between points 6 and 7; and t_w = thickness of the web. The distances d_1 and d_2 equal the bolt diameter, i.e.,

$$d_b = d_1 + d_2 \tag{5.3.2}$$

With the tension force, T_w, and the bolt force, B_F, (from a 2-D finite element analysis), a parameter, ϕ, is defined as follows:

$$\phi = \frac{T_w}{B_F} \tag{5.3.3}$$

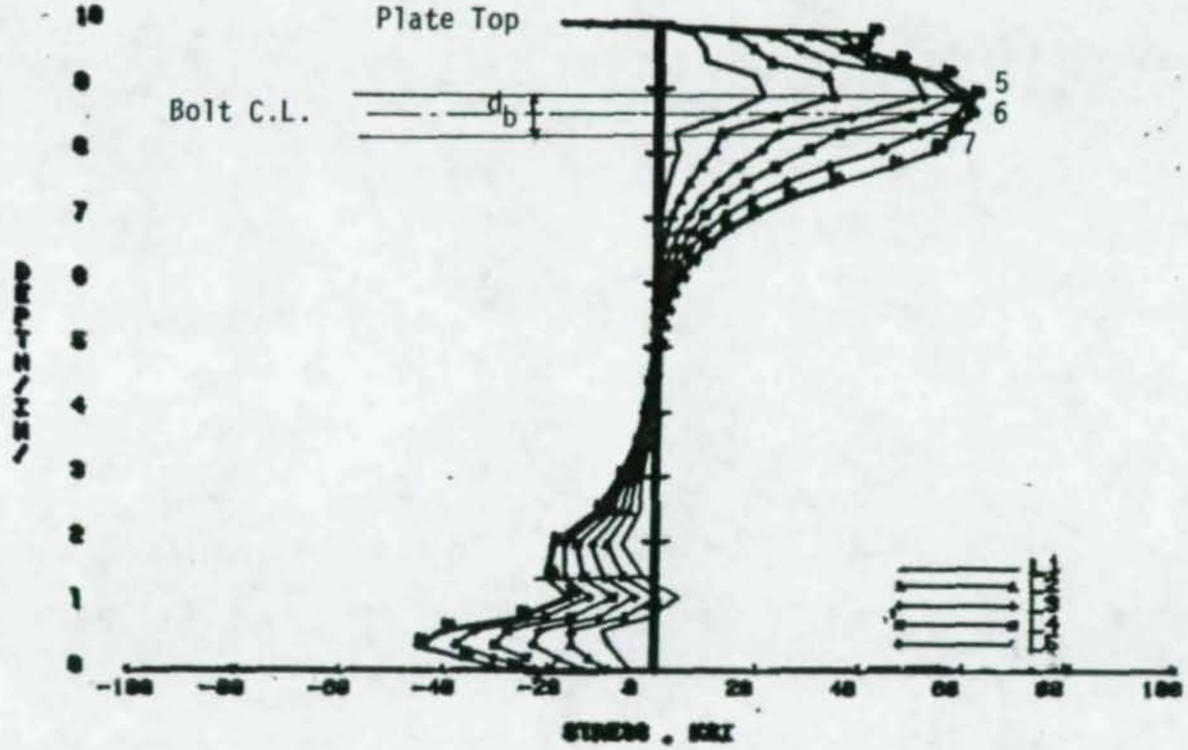

Figure 5.2 Variation of Stress Along Depth for Case 1 of the Parametric Study

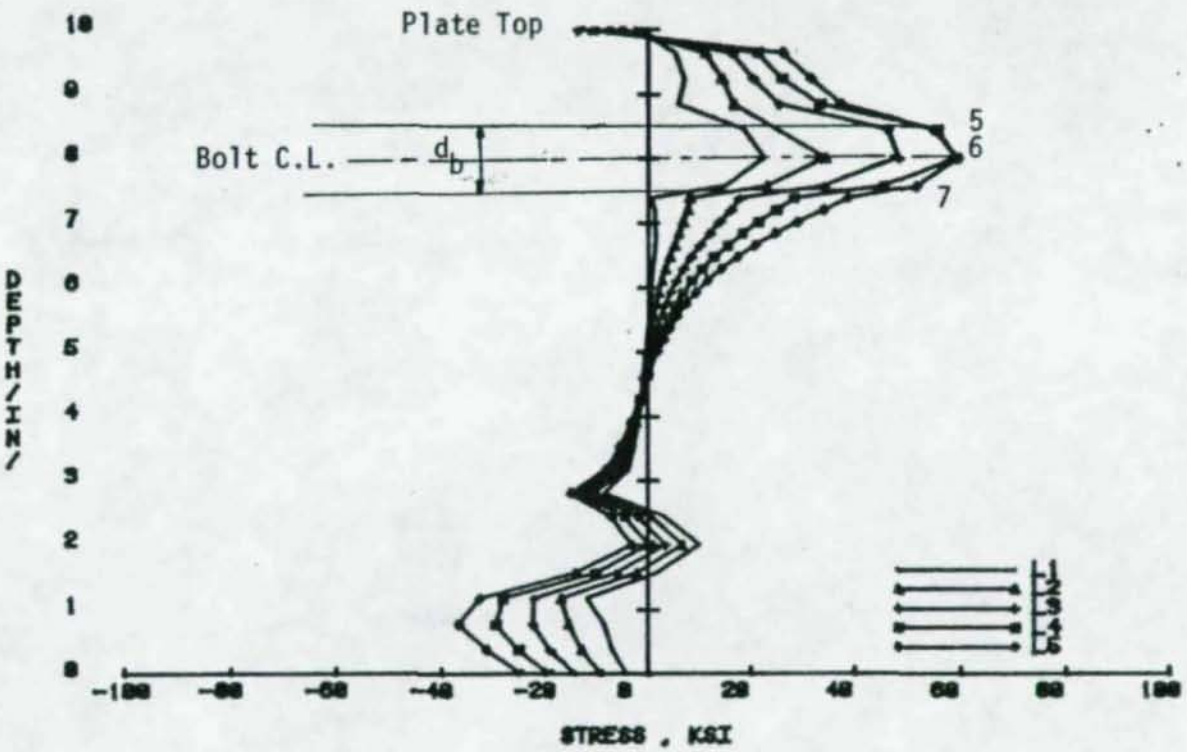

Figure 5.3 Variation of Stress Along Depth for Case 10 of the Parametric Study

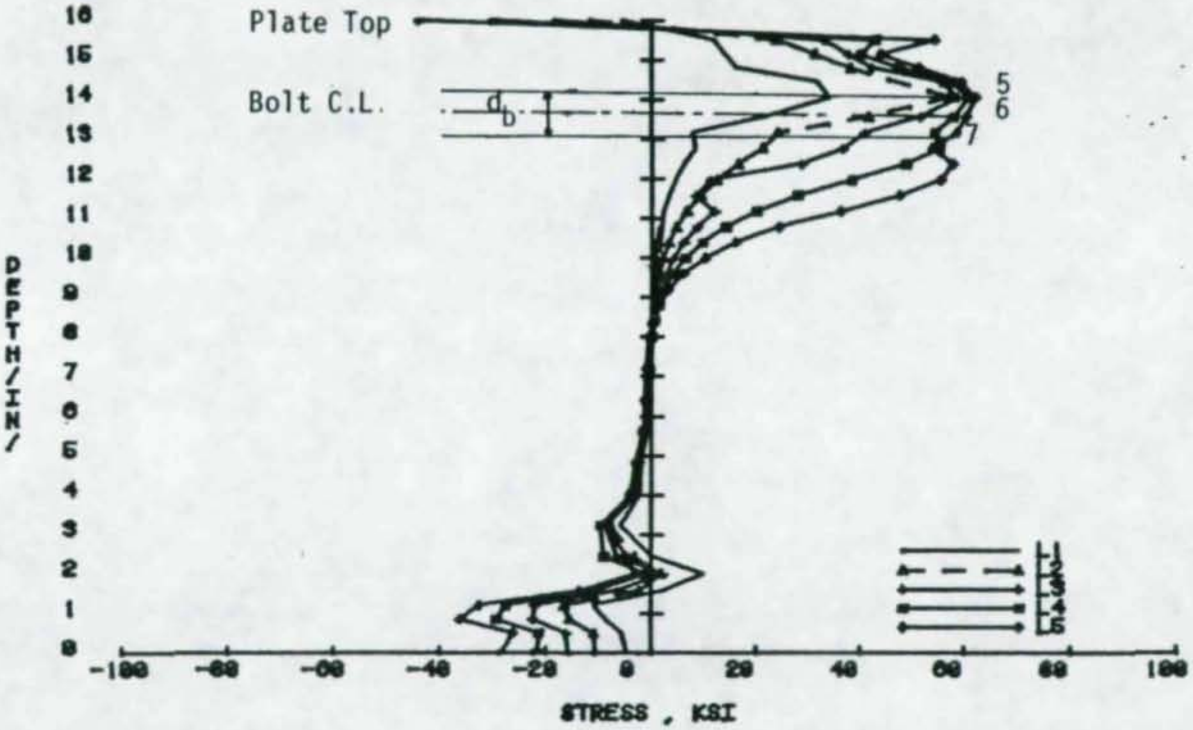

Figure 5.4 Variation of Stress Along Depth for Case 10 of the Parametric Study

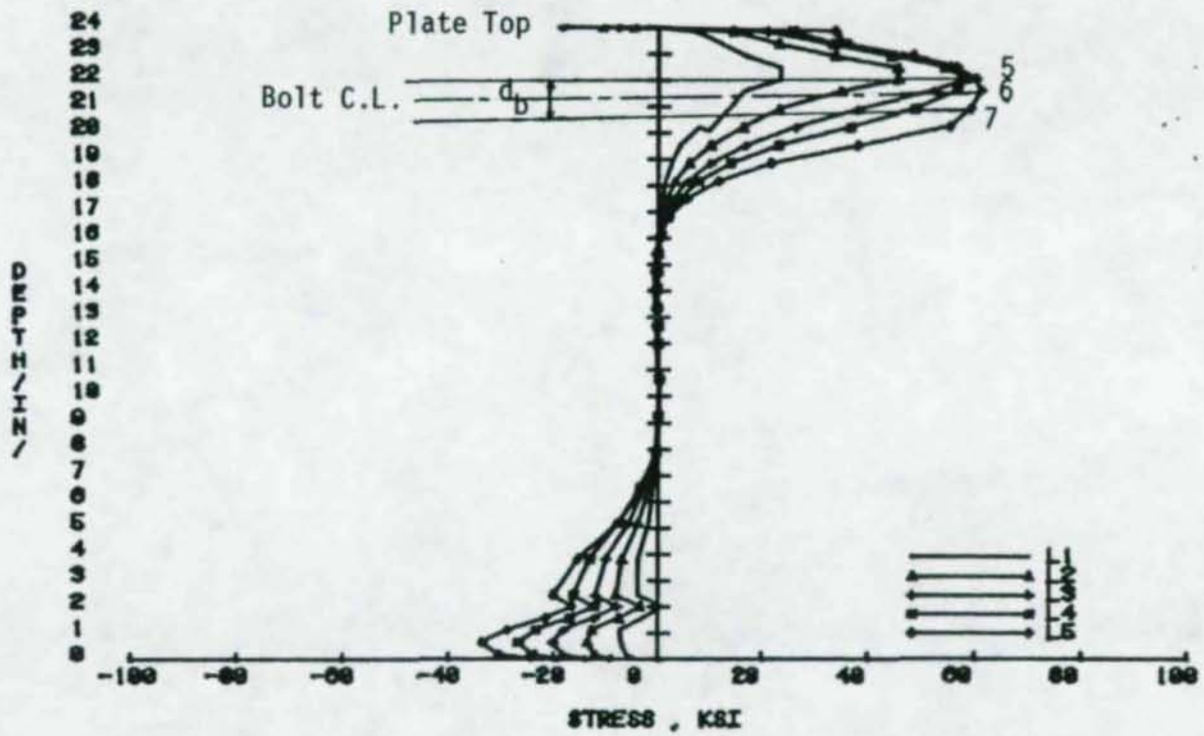

Figure 5.5 Variation of Stress Along Depth for Case 28 of the Parametric Study

Figure 5.6 shows the plot of web thickness, t_w, versus ϕ for the four cases. It is seen from this figure that the four points lie close to the straight line with the following equation:

$$\phi = 1.03\ t_w \tag{5.3.4}$$

Knowing B_F and t_w, then ϕ and T_w can be determined from Equations (5.3.3) and (5.3.4), respectively. The procedure is explained in Section 5.5 for a design example.

5.4 Recommended Design Methodology

Using Equations (5.2.6) and (3.6.16) for end-plate thickness and bolt force, respectively, and equation (5.2.18) for tensile force in the web, a design methodology is developed to design flush end-plate connections with one row of bolts in the tension region. The steps are as follows:

1. Calculate the beam flange force, F_u, from moment, M_u:

$$F_u = M_u/(h-t_f) \tag{5.4.1}$$

where M_u is the ultimate moment. For Type 1 connection, if the working moment, M_w, due to working load is known, then M_u can be computed from [2]:

$$M_u = \frac{M_w}{0.375} \tag{5.4.2}$$

where

M_w = working moment.

2. Estimate the bolt force, T_u for each bolt from T_u :

$$T_u = F_u/2 \tag{5.4.3}$$

3. Select bolt size using Table I-A of the AISC Manual[13].

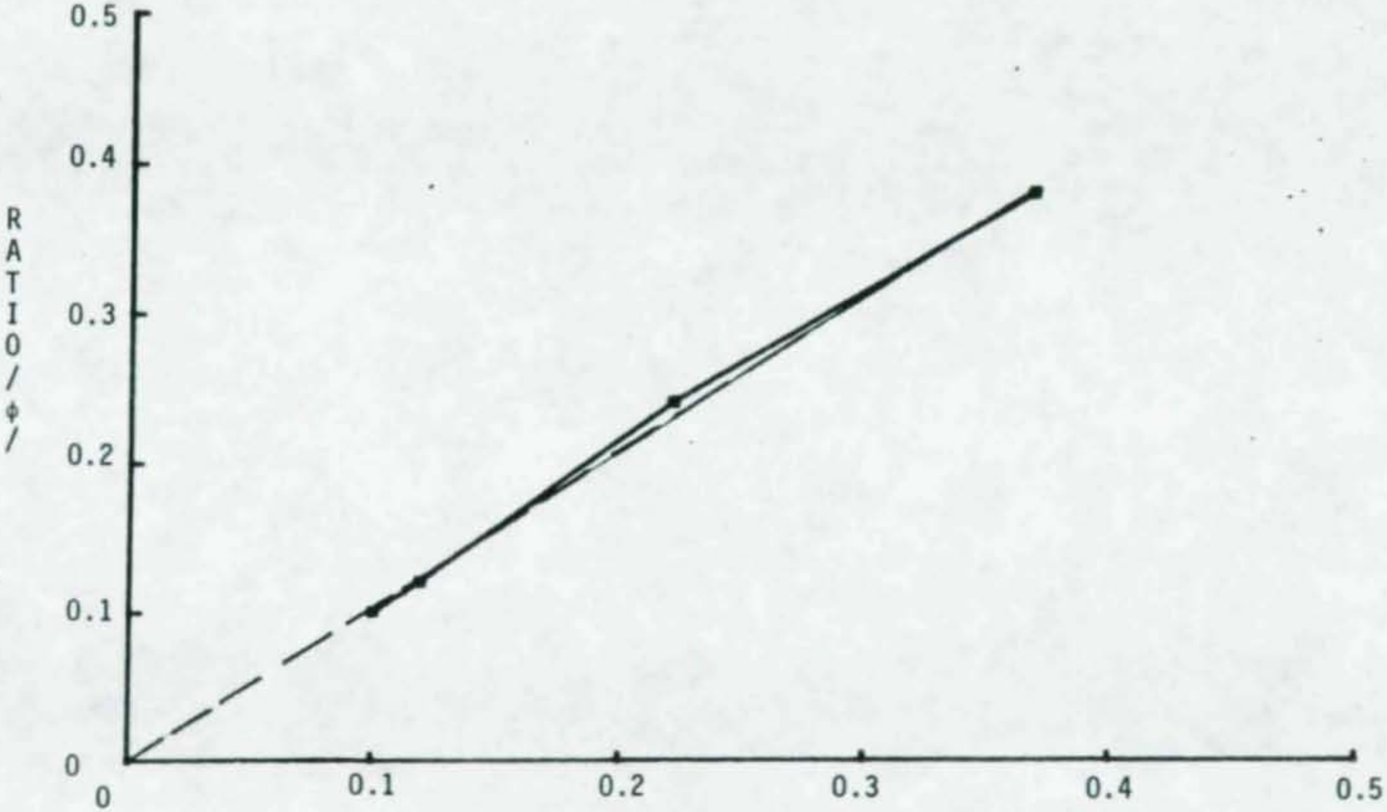

Figure 5.6 Ratio of Maximum Web Tensile Force/Bolt Force Versus Web Thickness

4. Select pitch, p_f, and gage, g. The selected pitch and gage must be within ranges in Table 3.1. The pitch, p_f, can be computed from the following equation (see page 4-111 of Reference 13):

$$p_f = d_b + t_f + 1/2 \tag{5.4.4}$$

where d_b = nominal bolt diameter amd t_f = flange thickness. All units are in inches.

5. Calculate g_b (width of equivalent bolt area in the 2-D finite element model) from Equation (5.2.5), which is repeated here:

$$g_b = \frac{1}{3} \left(\frac{A_B}{d_b}\right) \left(\frac{F_{by}}{F_{yb}}\right) \tag{5.4.5}$$

where A_b = area of beam cross-section, d_b = bolt diameter, F_{by} = yield stress of beam material and F_{yb} = yield stress of bolt material.

6. Using the limiting deflection criterion of $(\delta)_{max}$ = 0.01 in., compute the required end-plate thickness from Equation (5.2.6), which is repeated here:

$$t_p = (0.115526) \frac{(p_f)^{1.447}}{(h)^{1.050}(t_w)^{0.325}(t_f)^{0.024}(d_b)^{0.551}(g_b)^{0.337}(b_p)^{0.141}}(M)^{0.881} \tag{5.4.6}$$

In Equation (5.4.6) the unit of all geometric variables is inches and the unit of moment, M, is kips-ft.

7. Select a practical end-plate thickness greater than or equal to the end-plate thickness calculated in Step 6.

8. For the selected end-plate thickness, compute the bolt force, B_F, from Equation (3.6.13) which can be rearranged as follows:

$$B_F=P_T+(0.1272)\,\frac{(t_f)^{0.049}(g_b)^{0.441}(p_f)^{0.141}}{(t_p)^{0.538}(h)^{2.985}(t_w)^{0.349}(b_p)^{0.023}(d_b)^{2.391}}(M)^{2.568} \qquad (5.4.7)$$

where P_T = pretension force in the bolt from page 5-59 of Reference 13.

9. If the bolt force determined in Step 8 is less than or equal to the capacity of the bolt selected in Step 3, then the bolt size selected is acceptable. If not, choose a larger bolt diameter and repeat Steps 4 to 8.

10. Check tensile force in the web adjacent to bolt as follows:

(i) Calculate the ratio, ϕ, of percentage of maximum tensile force to bolt force using Equation (5.3.4).

$$\phi = 1.03\ t_w \qquad (5.4.8)$$

(ii) Calculate the maximum tensile force, T_w, in the web using

$$T_w = \phi B_F \qquad (5.4.9)$$

(iii) Calculate the tensile capacity of the web using the following equation:

$$T_a = F_{by}\ d_b\ t_w \qquad (5.4.10)$$

(iv) If the maximum tensile force T_w in the web calculated is less than the allowable tensile force, T_a, for the web, then the yield strength of the web is adequate. If not, select a larger bolt diameter and repeat Steps 4 through 10.

5.5 Design Example (Type-I Construction)

To illustrate the design steps in Section 5.4, calculations are now presented.

Example: Determine the bolt size and end-plate thickness for a flush end-plate connection with one row of two bolts at the tension flange M_u = 50.0 kips-ft., h = 16.0 in., t_w = 0.25 in., b_p = 6.00 in. and t_f = 0.25 in.

Step 1. Calculate flange force (Equation 5.4.1):

$$F_u = (50.0 \times 12)/(16-0.25) = 38.10 \text{ kips}$$

Step 2. Calculate required bolt force (Equation 5.4.3):

$$T_u = 38.10/2.0 = 19.05 \text{ kips}$$

Step 3. Select 5/8 in. A325 bolts. Working load for this bolt is 13.5 kips from the AISC Manual (13)

Step 4. Select pitch, p_f = 1 3/4 in. and gage, g = 3 1/2 in.

Step 5. Calculate g_b from Equation (5.4.5):

$$g_b = 1/3 \left(\frac{6.875}{0.625}\right) \left(\frac{50}{80}\right) = 2.30$$

Step 6. Calculate required t_p from Equation (5.4.6)

$$t_p = 0.115526 \frac{(1.75)^{1.447}}{(16)^{1.050}(0.25)^{0.325}(0.25)^{0.024}(0.625)^{0.551}(2.30)^{0.337}(6.0)^{0.141}}(50)^{0.8}$$

$= 0.55$ in.

Step 7. Select t_p = 5/8 in.

Step 8. Calculate bolt force from Equation (5.4.7):

$$B_F = 19.0 + (0.1272) \frac{(0.25)^{0.049}(2.30)^{0.441}(1.75)^{0.141}}{(6.0)^{0.538}(16)^{2.985}(0.25)^{0.349}(6.0)^{0.023}(0.65)^{2.391}}(55)^{2.568}$$

$= 26.81$ kips

Step 9. B_F = 26.81 is less than the factored bolt capacity

(=2 x 13.5 = 27.0 kips), therefore the bolt diameter selected is adequate.

Step 10. Check for yielding in the web.

(i) Calculate the ratio, ϕ, of percent of maximum tensile force to bolt force using Equation (5.4.8):

$$\phi = (1.03)\ (0.25) = 0.2575$$

(ii) Calculate maximum tensile force in the web using Equation (5.4.9):

$$T_w = (0.2575)\ (26.81) = 6.90 \text{ kips}$$

(iii) Calculate allowable tensile force in web using Equation (5.4.10):

$$T_a = (50)\ (0.625)\ (0.25) = 7.81 \text{ kips}$$

(iv) T_w is less than allowable tensile force in the web (=7.81 kips). Therefore, the yield strength of the bolt is adequate.

Use 6.0 in. x 5/8 in. plate with two 5/8 in. diameter A325 bolts.

The end-plate geometry used in the above example is similar to the test specimen F-3/4-1/2-1/16. However, in this test, a 6 in. by 1/2 in. end-plate and 3/4 in. diameter bolts were used. The measured plate separation per side of the connection at 50 kips-ft. was approximately 0.01 in. (see Figure C.7), which corresponds to the values used in the example. If 3/4 in. bolts are used in the above example, the required plate thickness is 0.52 in. Thus, good correlation exists with the test data.

CHAPTER VI

SUMMARY, CONCLUSION, AND RECOMMENDATION

6.1 Summary

This study is an attempt to develop a design methodology for the flush-end-plate connections with one row of bolts in the tension region. The geometric configuration and boundary conditions result in a highly indeterminate problem. Thus it was decided to conduct an analytical study, modeling the connection as an assemblage of finite elements with the objective of developing prediction equations using regression analysis of the finite-element results for the connection behavior.

In modeling, first a 2-D plane stress model passing through plane of web and containing 626 nodes, 560 elements, and 1252 d.o.f. was analyzed. A length of the beam stub equal to the depth of the beam was chosen as adequate for inclusion in the analysis domain. The results of this model for end-plate separation was seen to be stiffer in comparison to experimental results at higher load levels. Therefore, it was decided to select a partial 3-D model to represent the behavior of end-plate. In the partial 3-D model, the end-plate, bolt head, bolt shank and welds connecting beam flanges and web to the end-plate were modeled with 3-D elements, while the web were modeled using 2-D elements. In two of the partial 3-D finite element models, the beam flanges were modeled using 2-D elements, while in the third one modeling was done using 3-D elements. Comparing the partial 3-D finite element model results with experimental results for eight similar experiments it was found that the partial 3-D model with the beam flanges modeled using 3-D elements gave results closest to the experimental results. At failure, the moment carrying capacity of the eight specimens, predicted by the finite element model and experimental result varied between 1% and 15%. This partial 3-D model contains 546 elements, 998 nodes, and 2810 d.o.f. The cpu time for a typical run is 150 minutes. Because of the cost involved with the analysis of the partial 3-D model, it was not feasible to conduct a parametric study based on it. It was decided to use the 2-D model to conduct the parametric study to develop prediction equations characterizing the behavior of a typical flush-end-plate connection and then apply a correction factor to predict the end-plate behavior.

The computer program "NONEPAP" (Nonlinear End-Plate Analysis Program) was used for the finite element analyses. In the program, the effect of the stress-strain behavior of the various steel plates is represented as elastic - perfectly plastic bilinear behavior and of the bolt material as linear elastic behavior. The boundary condition at the back nodes of the end-plate are determined by an iterative procedure so that the nodes were connected when in compression and discontacted when in tension. To consider the inelastic steel behavior in each load cycle, the elastic moduli of the yielded element (i.e. when effective strain exceeds yield strain for steel) is reset to their second values.

Information from sufficient cases was developed from the analytical study to conduct a feasibility and sensitivity study so as to select certain variables from pertinent geometry (end-plate thickness and width bolt pitch, bolt pitch, bolt diameter, beam depth, flange thickness, and web thickness), and force (applied moment and pretension force) related variables governing the connection behavior. The ranges of variables were restricted to practical ranges and fifty cases were selected for the study. Finite element analyses were carried out for these selected cases and results regressed to give prediction equation for maximum end-plate separation and force in the tension bolts. The prediction equation obtained for the maximum end-plate separation using 2-D finite element results was multiplied by a scaling factor to account for the 3-D bending behavior of the end-plate. For verification, analytical results were compared with experimental laboratory tests and it was concluded that partial 3-D model (Mesh-III) with 998 nodes, 546 elements, and 2810 d.o.f. best represents the true behavior of the end-plate. Both the 2-D mesh and the partial 3-D model (Mesh-III) resulted in a good correlation between analytical and experimental results for bolt forces, therefore, no correlation was needed for the bolt force prediction equation from the 2-D model. Also the prediction equations developed from the finite element analyses were shown to adequately explain the behavior of the flush end-plate moment connection.

Two different design procedures are recommended. One considers limiting the maximum allowable end-plate separation and the other considers a specified degree of rigidity for the connection. In the former, it is proposed to limit the end-plate separation to 0.01 in. In the latter, the limiting separation is based on the intersection of the connection curve (i.e. moment-rotation curve) and the beam line. The first procedure is suitable for Type I construction and the second for Type III construction.

Based on plots for variation of stress (σ_x) along the depth of the web from the 2-D model results, an analytical equation was developed to predict the maximum tensile force in the web as a function of web thickness and bolt force. This equation was used to propose a design method for the web so that excessive yielding does not occur in the web.

6.2 Conclusions

From the analytical model investigation it was concluded that the 2-D finite element model containing 560 elements, 616 nodes, and 1252 d.o.f. is suitable for the parametric study if the result of the maximum end-plate separation at failure is multiplied by a factor, C=1.5. A typical 2-D mesh takes 6 minutes of cpu time. This correction factor was determined based on comparison between previously mentioned 2-D and the partial 3-D finite element model results from maximum end-plate deflection criterion is more conservative than that used in test specimen.

6.3 Recommendations

It would be worthwhile to develop a prediction equation for maximum tensile force in the web regressing the finite element results of all the cases selected. The study conducted was limited to Grade 50 steel and A325 bolts. It may also be worthwhile to vary the grade of steel and see how it effects the results.

REFERENCES

1. Douty, R.T. and W. McGuire, "High Strength Bolted Moment Connections", Journal of The Structural Division, ASCE, Vol. 91, No. ST2, April, 1965, pp. 101-128.

2. Srouyi, R. "Yield-Line Analysis of End-Plate Connections with Bolt Force Predictions", A Thesis submitted to the graduate faculty in partial fulfillment of requirements for degree of Master of Science, School of Civil Engineering and Environmental Science, University of Oklahoma.

3. Bockley, D.I., "The Design of Single Story Pitched Roof Portal Frames", BCSA Brochure, 1980.

4. DSTV/DAST, Moment and Plate Connections with HSFG Bolts (in German), IHE 1, 1978.

5. Norme Francaise Enregistree, Metal Construction, Joining by Means Bolts Controlled Tightening, Structural Requirements and Checking of Jointing (in French), NF, 1979, pp. 22-460.

6. Zoetermeiyer, P., "Semi-Rigid Bolted Beam-to-Column Connections with Stiffened Column Flanges and Flush-End-Plate", joints in structural steel work, proceedings of international conference of joints in steel work, held at Middlesbrough, Cleveland, John Wiley and Sons, New York-Toronto, 1981, pp 2.99-2.118.

7. Packer, J.A. and L.J. Morris, "A Limit State Design Method for Tension Region of Bolted Beam-Column Connections", The Structural Engineer, vol. 5, no. 10, October 1977.

8. Phillips, J. and J.A. Packer, "The Effect of Plate Thickness on Flush End-Plate Connections", Joints in Structural Steel Work, proceedings of international conference on joints in steel work, held at Middlesbrough, Cleveland, John Wiley and Sons, New York-Toronto, 1981, pp. 6.77-6.92.

9. Krishnamurthy, N., "Two-Dimensional Finite Element Analysis of Extended and Flush Connections with Multiple Rows of Bolts", Report to AISC and MBMA, no. CE-AISC-MBMA-6, Dept. of Civil Engineering, Auburn University, March 1975.

10. _______________, Manual of Steel Construction, Seventh, Edition, American Institute of Steel Construction, New York, NY, 1969.

11. Kato, B. and W. McGuire, "Analysis of T-Stub Flange-to-Column Connections", Journal of Structural Division, ASCE, vol. 99, no. ST5, May 1973, pp. 865-888.

12. Nair, R.S., P.C. Birkemore and W.H. Munse "High Strength Bolts Subject to Tension and Prying", Journal of Structural Division, ASCE, Vol. 100, No. ST2, February, 1974, pp. 351-372.

13. Fisher, J.W. and J.H.A. Struik, Guide to Design Criteria for Bolted and Riveted Joints. New York: John Wiley and Sons, 1974, Chapters 16-18.

14. Mann, A.P. and Morris, L.J., "Limit Design of Extended-End-Plate Connections", Journal of The Structural Division, ASCE, vol. 105, no. ST3, March 1979, pp. 511-526.

15. Kennedy, N.A., S. Vinnakota and A.N. Sherbourne, "The Split-Tee-Analogy in Bolted Splices and Beam-to-Column Connections", Joints in Structural Steelwork, proceedings of international conference on joints in steel work, held at Middlesbrough, Cleveland, United Kingdom Pentach Press, London, England, 1981, pp. 2.138-2.157.

16. Krishnamurthy, N. and V.R. Krishna, "Behavior of Splice-Plate Connections with Multiple Bolt Rows", Report Submitted to The Metal Building Manufacturers Association, February 1981.

17. ____________, Manual of Steel Construction, Eight edition, American Institute of Steel Construction, Chicago, IL, 1980.

18. Krishnamurthy, N., "Fresh Look at Bolted End-Plate Behavior and Design", Engineering Journal, American Institute of Steel Construction, vol. 15, no. 2, second quarter, 1978, pp. 39-49.

19. Ahuya, V., "Analysis of Stiffened End-Plate Connections using The Finite-Element Method", A Thesis submitted to the graduate faculty in partial fulfillment of the requirements for the degree of Master of Science, School of Civil Engineering and Environmental Science, University of Oklahoma, Norman, Oklahoma, 1982.

20. Ghassemeih, M. "Inelastic Finite Element Analysis of Stiffened-End-Plate Connections", A Thesis submitted to the graduate faculty in partial fulfillment of the requirements for the degree of Master of Science, School of Civil Engineering and Environmental Science, University of Oklahoma.

21. Levy, S., "3-D Isoparametric Finite Element Program", Report No. 71-C-191, General Electric Company, Schenectady, N.Y., June 1971.

22. Turner, M.H., et al, "Stiffness and Deflection Analysis of Complex Structures", Journal of Aeronautical Science, No. 23, September 1956, pp. 815-824.

23. Ugural, A.C. and S.K. Fenster, Advances Strength and Applied Elasticity. New York, NY: Elsevier, 1975.

24. Draper, S. Applied Regression Analysis. New York, N.Y.: Wiley, 1981.

25. __________, Steel Construction/Detail and Relative Costs, the Steel Committee of Northern California.

26. McGuire, W. Steel Structures, Chapter 6, Prentice-Hall, Inc. Englewood Cliffs, N.Y., 1968.

APPENDIX A

NOMENCLATURE

NOMENCLATURE

A_B = area of the beam cross-section

A_b = gross area of the bolt

A_{be} = equivalent area of one row (zone) of bolts

b_p = end-plate width

c = ratio of the three dimensional plate separation to two-dimensional plate separation at failure

d_b = bolt diameter

d_e = edge distance

d_h = bolt head diameter

d_h^1 = equivalent bolt head diameter

E = Young's modulus of elasticity

E_s = Secont modulus

F = flange force per bolt

F_{bf} = effective stress on top fiber

F_{by} = yield stress of beam material

F_{bu} = ultimate stress of the bolt

F_{py} = yield stress of plate material

F_t = tensile strength of bolt material

F_{yb} = yield strength of bolt material

F_u = factored beam flange force = $M_u/(h-t_f)$

g = gage distance between bolts

g_b = width of rectangular bolt zone in two-dimensional model

h = beam depth

h_t = bolt head thickness

I_B = moment of inertia

I_p = moment of inertia of end plate cross-section

L = length of the beam

L_n = length of the yield line, n

M_y = yield moment of the beam cross-section

M_p = plastic moment of the beam cross-section

p_f = pitch measured from top of flange to centerline of bolt row

P_p = bolt proof load

P_T = pretension of bolt

Q = prying force

R_B = radius of gyration of beam cross section

S_F = scaling factor = $\frac{E}{E_s}$

t_f = beam flange thickness

T_a = maximum yield capacity of the beam web

t_p = end-plate thickness

T_u = factored bolt force

T_w = maximum web tensile force

W_s = size of the fillet weld connecting the end plate to beam flange

W_u = ultimate uniform load

Z = plastic section modulus

δ = end-plate separation

$(\delta)_{max}$ = maximum separation in the end-plate

$(\delta_{max})_{2D-3D}$ = maximum end-plate separation obtained from partial 3-D models

$\varepsilon_1, \varepsilon_2, \varepsilon_3$ = principal strains

ε_{eff} = effective strain

ε_y = yield strain

ε_u = ultimate strain

θ_c = connection rotation

θ_{max} = maximum beam and rotation

θ_s = equivalent simple beam end-rotation

ν = Poisson's ratio

Π_i = dependent or independent dimensionless parameter used for regression analysis

$\sigma_1, \sigma_2, \sigma_3$ = prinicipal stress

ϕ = percentage of the ratio of maximum web tensile force to bolt force

APPENDIX B

COMPARISON OF TWO-DIMENSIONAL AND EXPERIMENTAL RESULTS

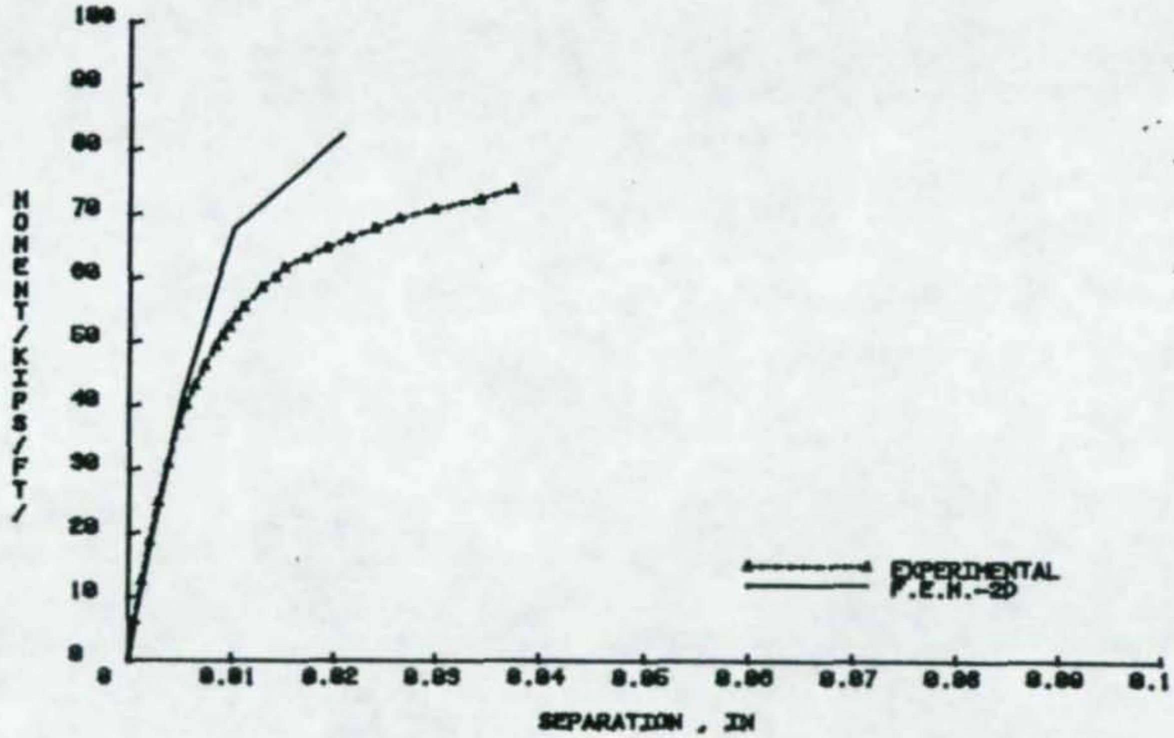

Figure B.1 Moment vs. Plate Separation (F-3/4-1/2-16)

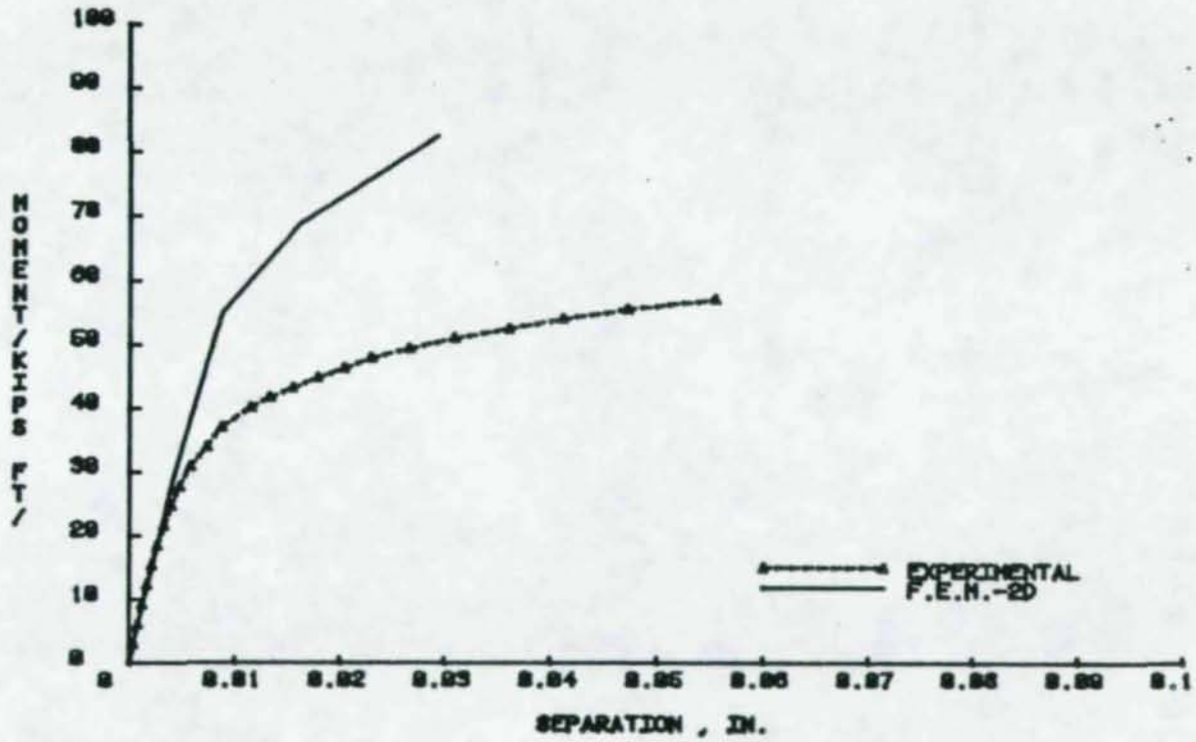

Figure B.2 Moment vs. Plate Separation (F-3/4-3/8-16)

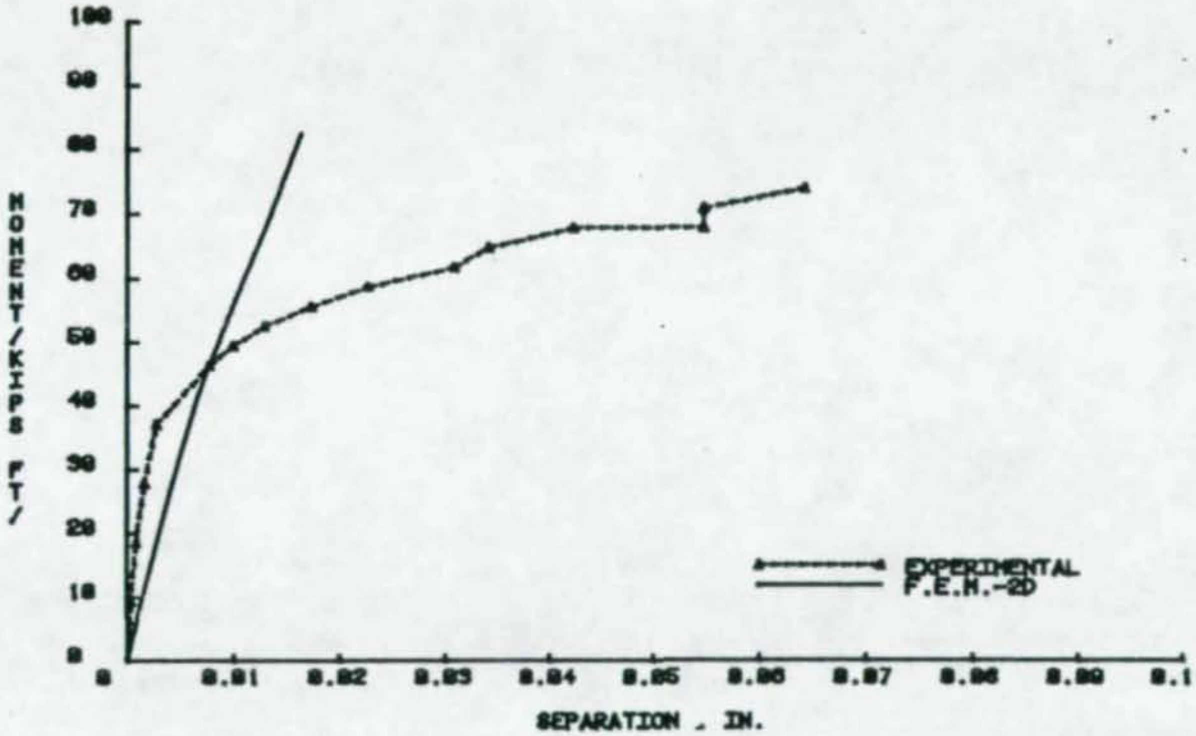

Figure B.3 Moment vs. Plate Separation (F-5/8-1/2-16)

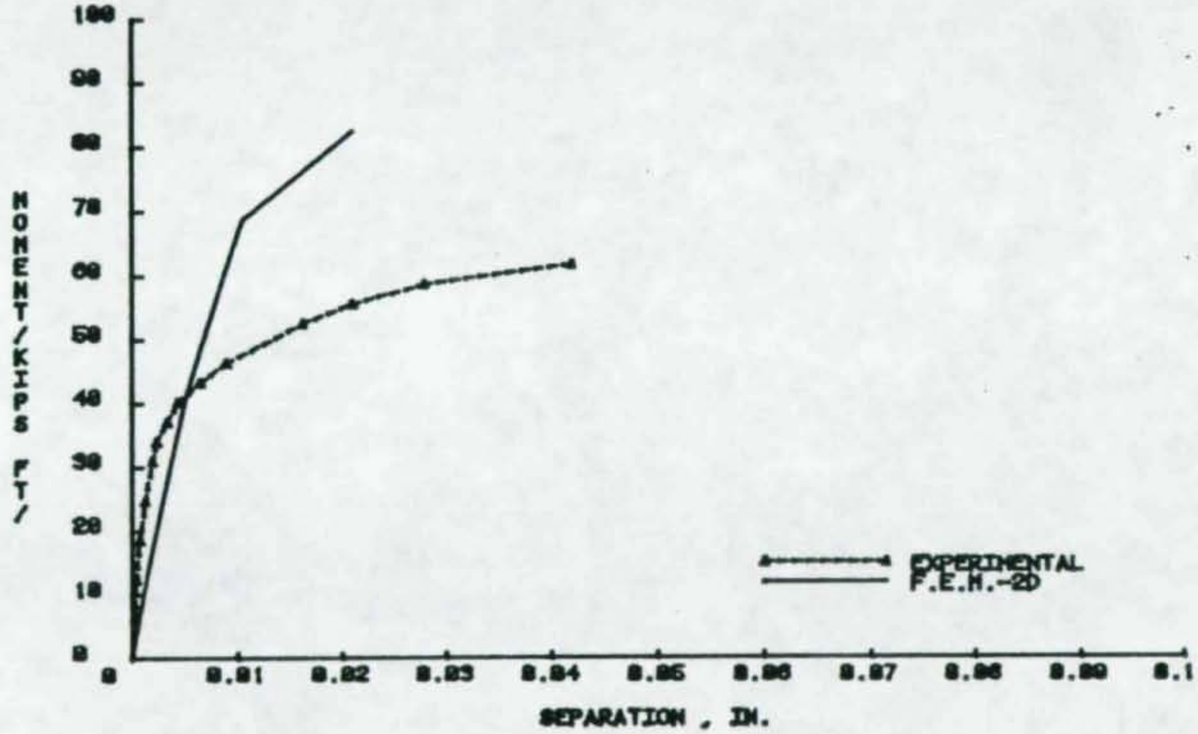

Figure B.4 Moment vs. Plate Separation (F-5/8-3/8-16)

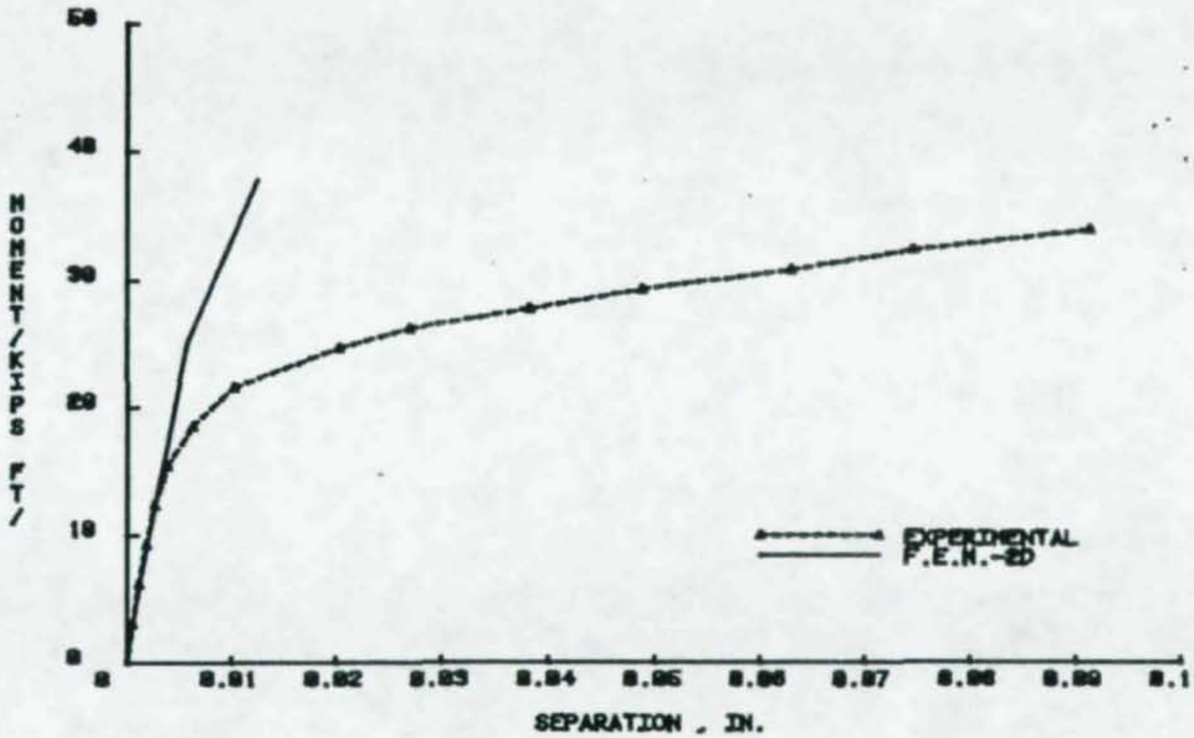

Figure B.5 Moment vs. Plate Separation (F-5/8-3/8-10)

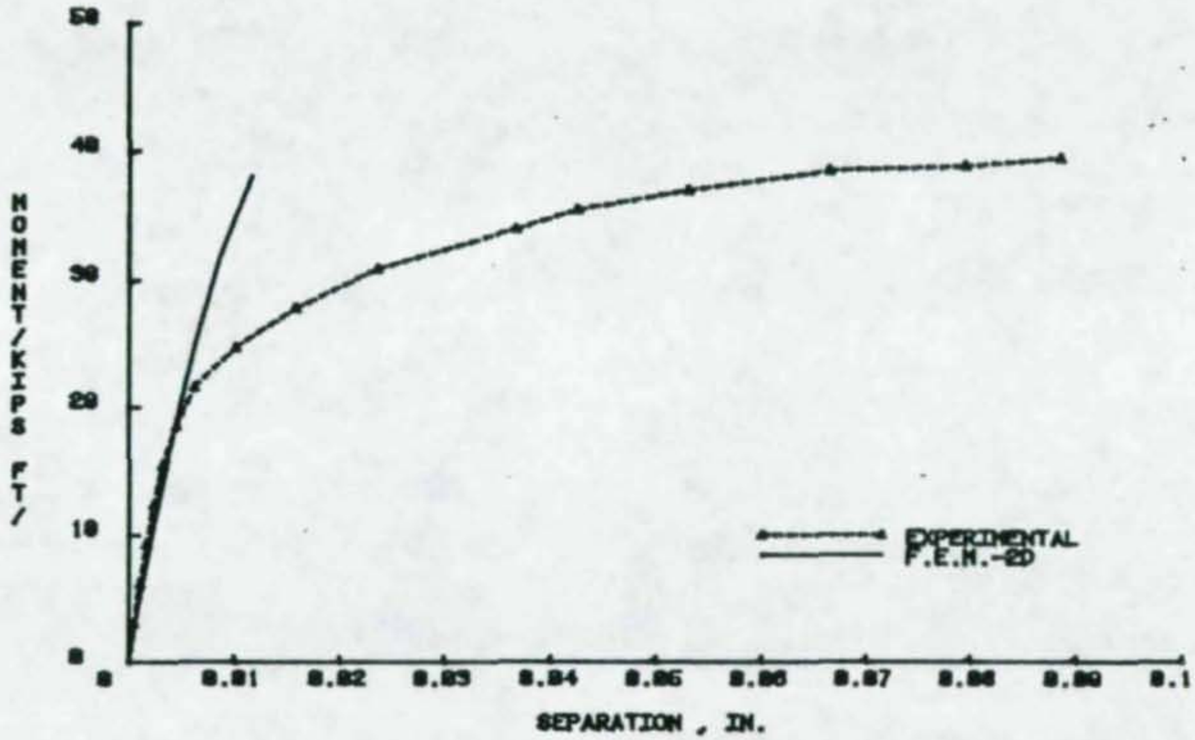

Figure B.6 Moment vs. Plate Separation (F-5/8-1/2-10)

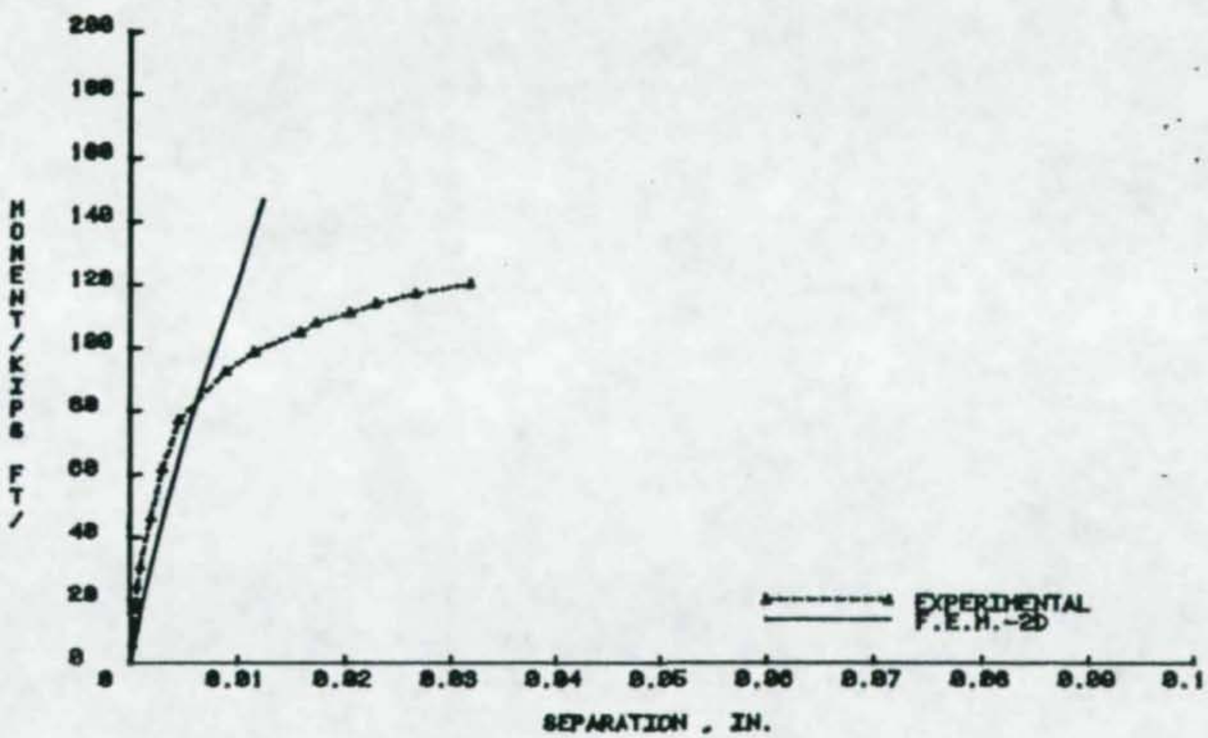

Figure B.7 Moment vs. Plate Separation (F-3/4-1/2-24A)

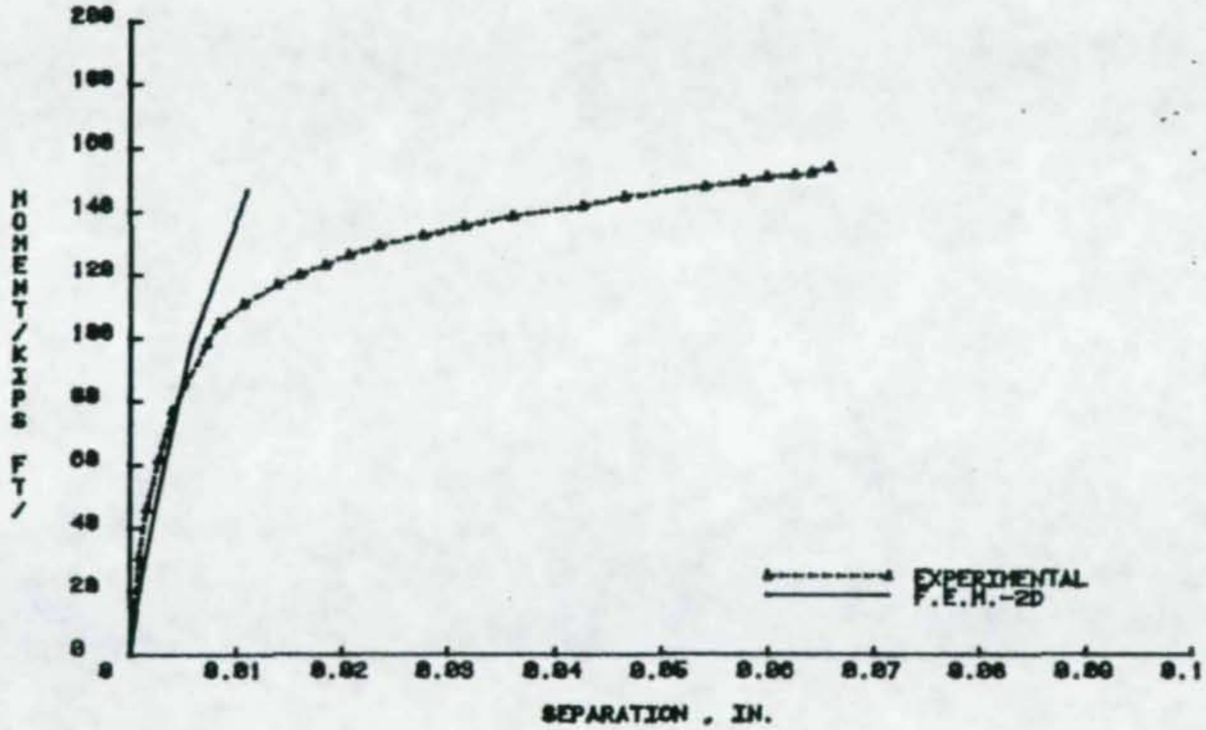

Figure B.8 Moment vs. Plate Separation (F-3/4-1/2-24B)

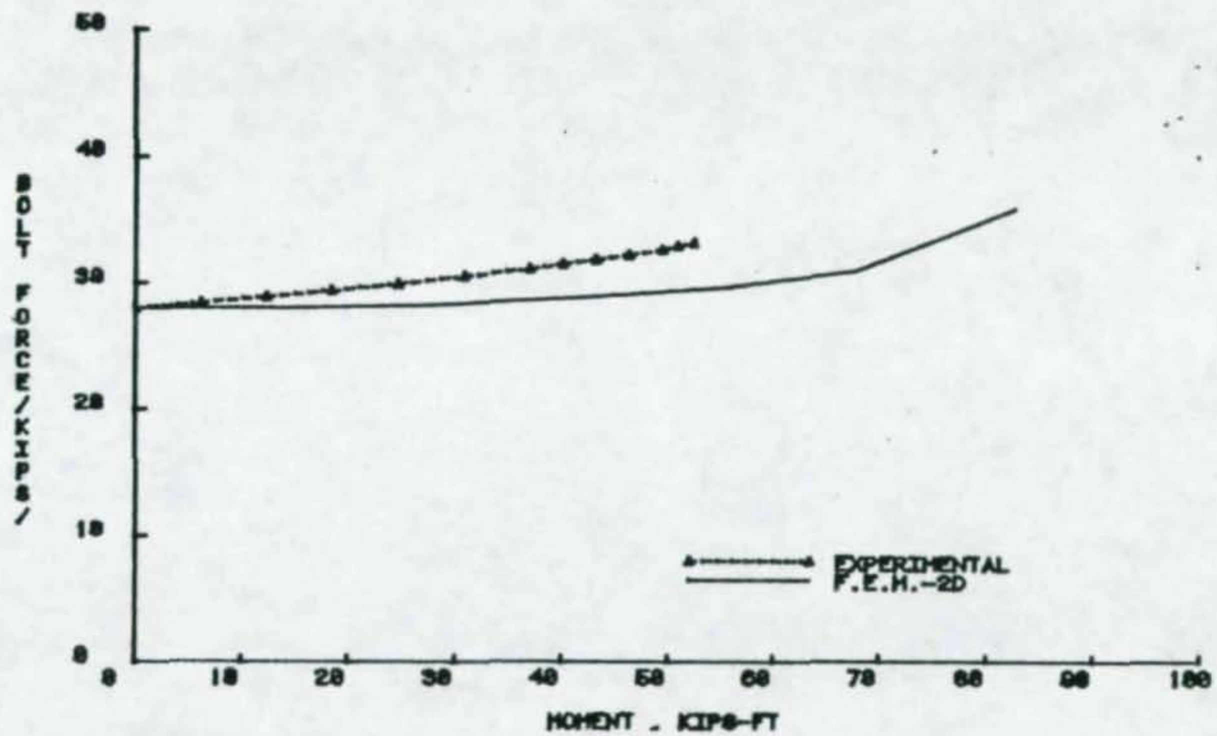

Figure B.9 Bolt Force vs. Moment (F-3/4-1/2-16)

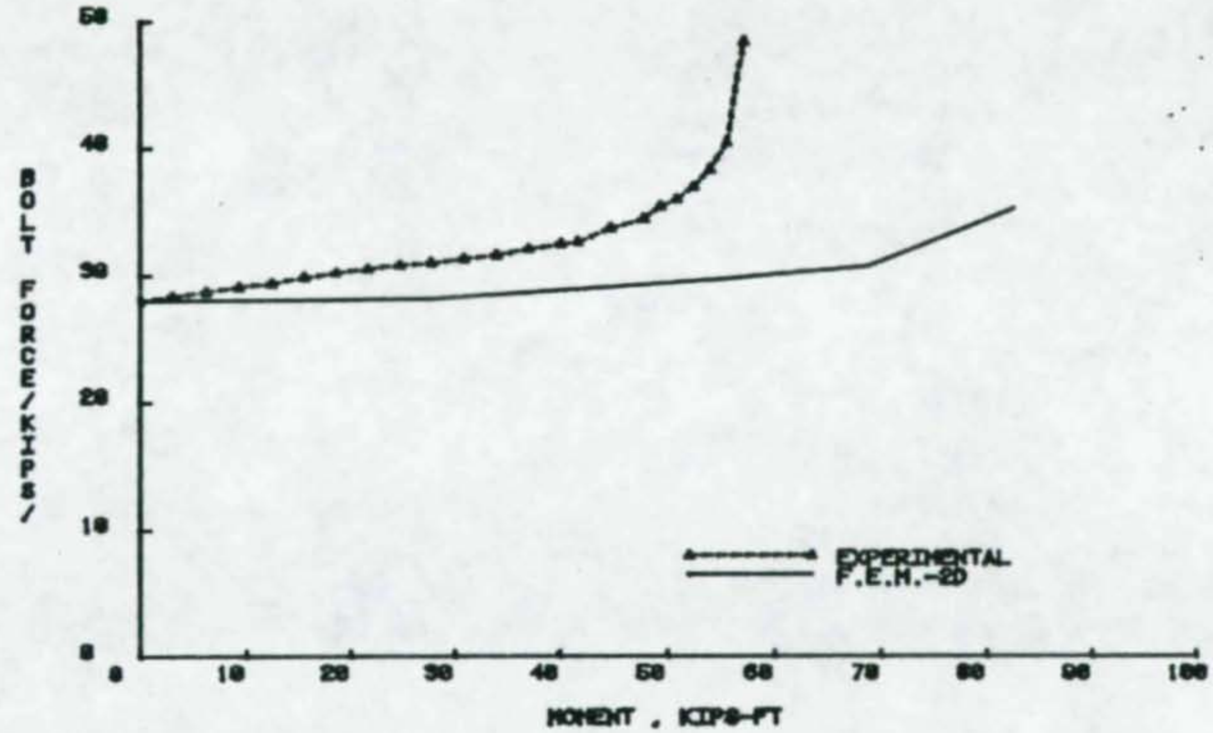

Figure B.10 Bolt Force vs. Moment (F-3/4-3/8-16)

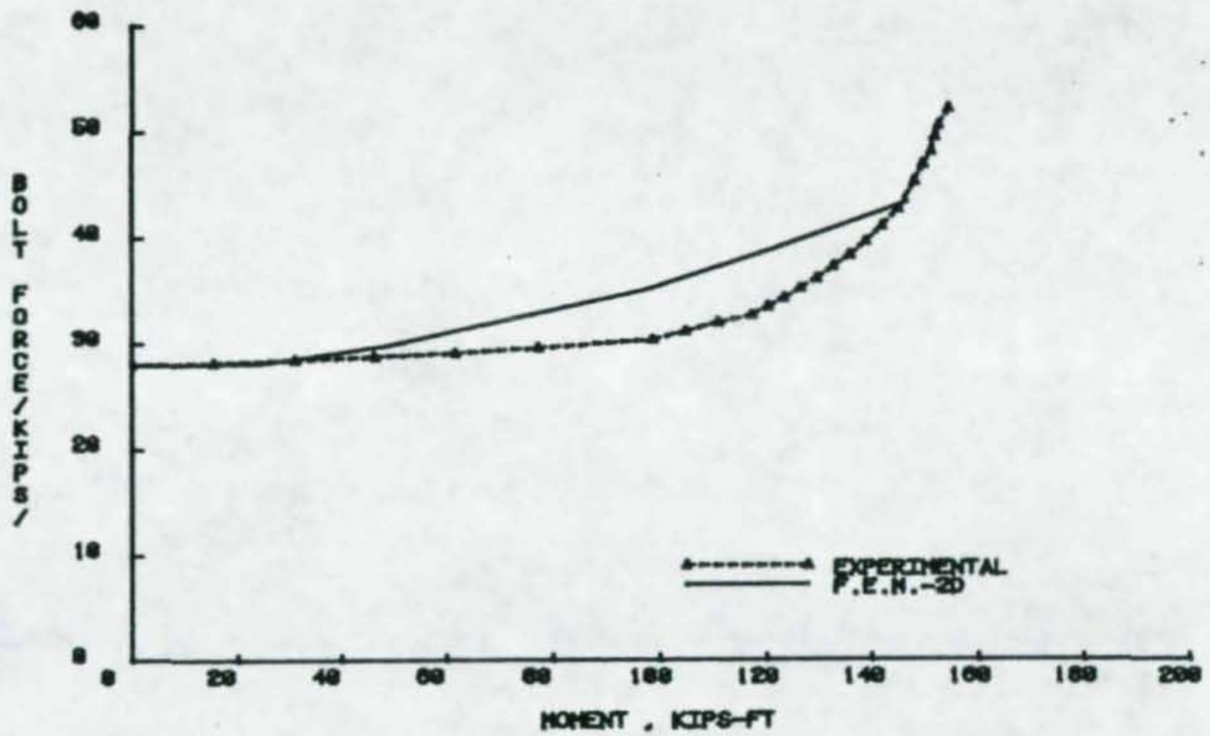

Figure B.16 Bolt Force vs. Moment (F-3/4-1/2-24B)

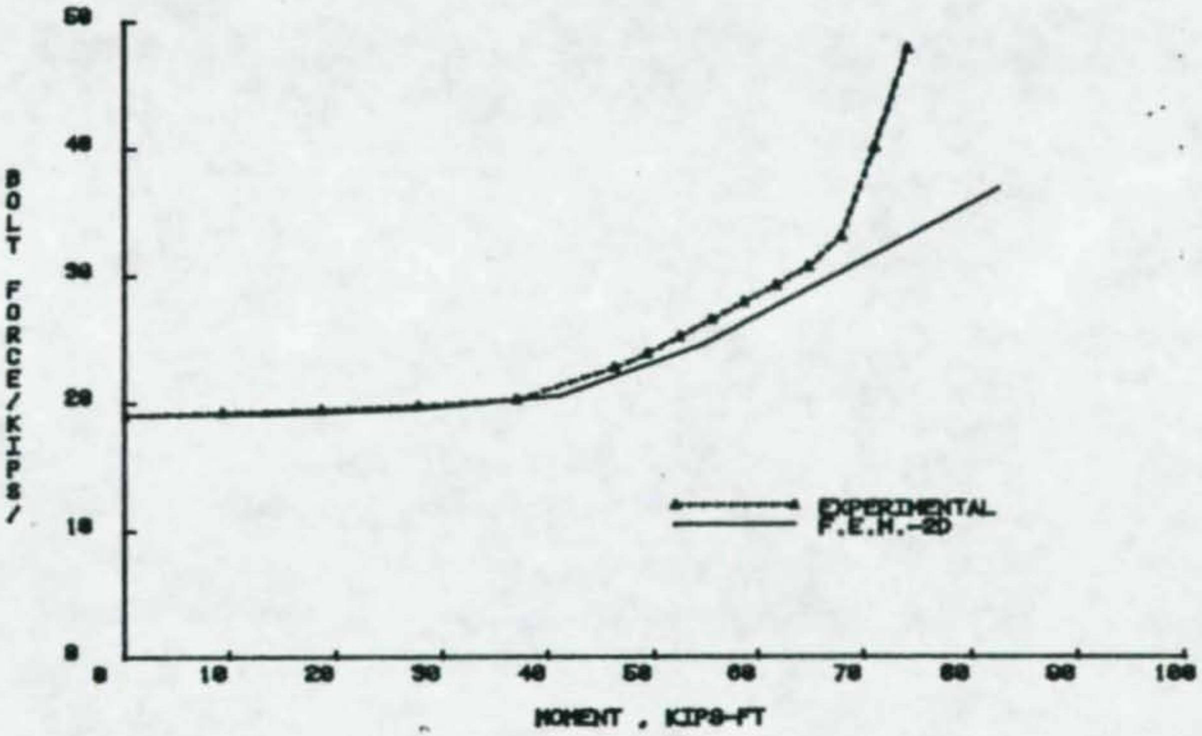

Figure B.11 Bolt Force vs. Moment (F-5/8-1/2-16)

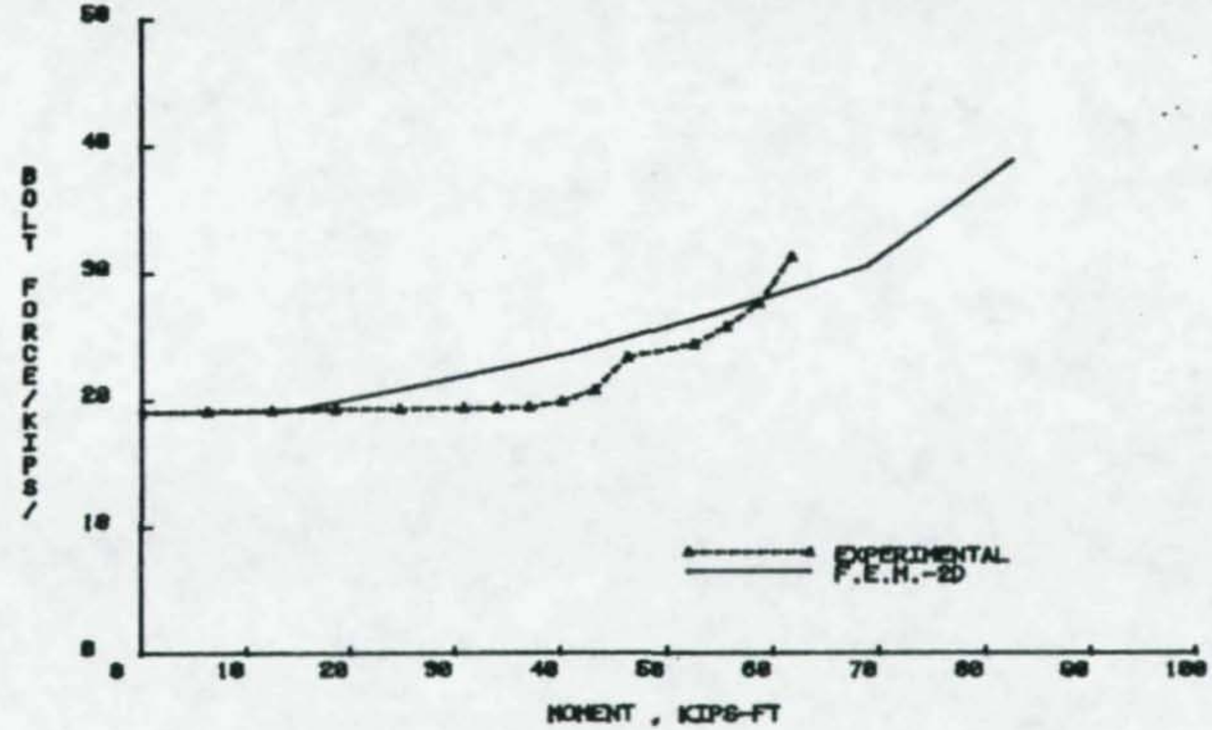

Figure B.12 Bolt Force vs. Moment (F-5/8-3/8-16)

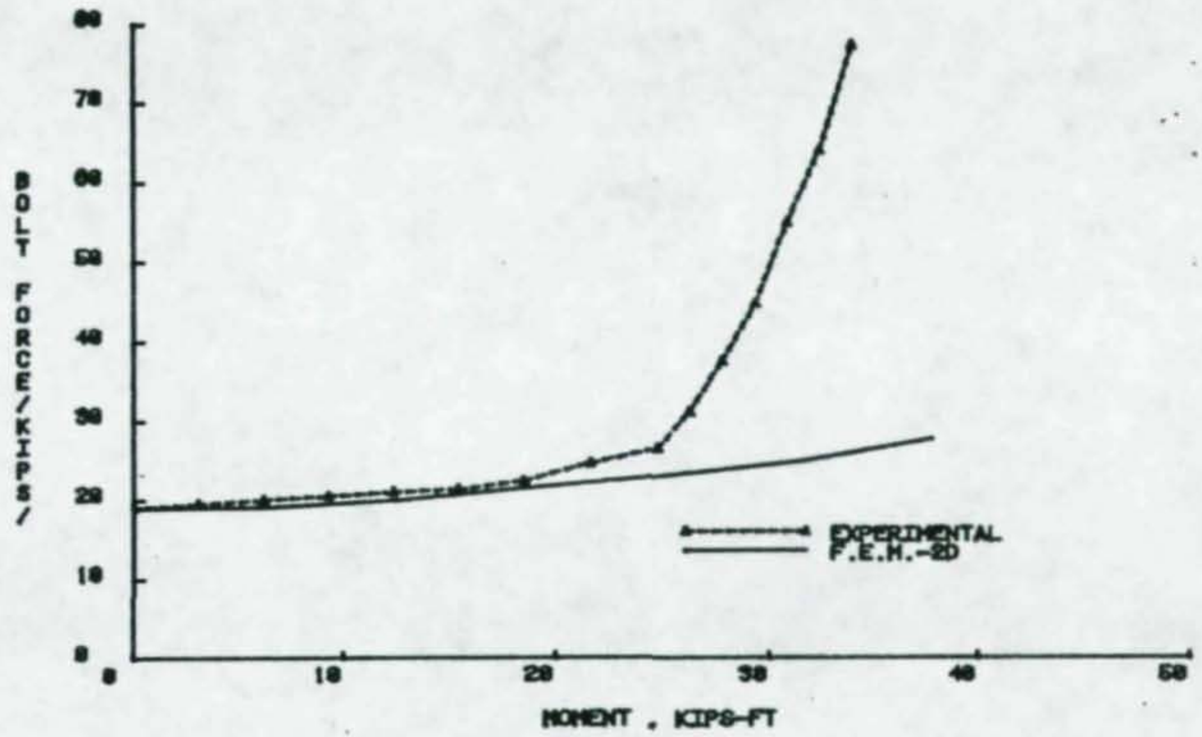

Figure B.13 Bolt Force vs. Moment (F-5/8-3/8-10)

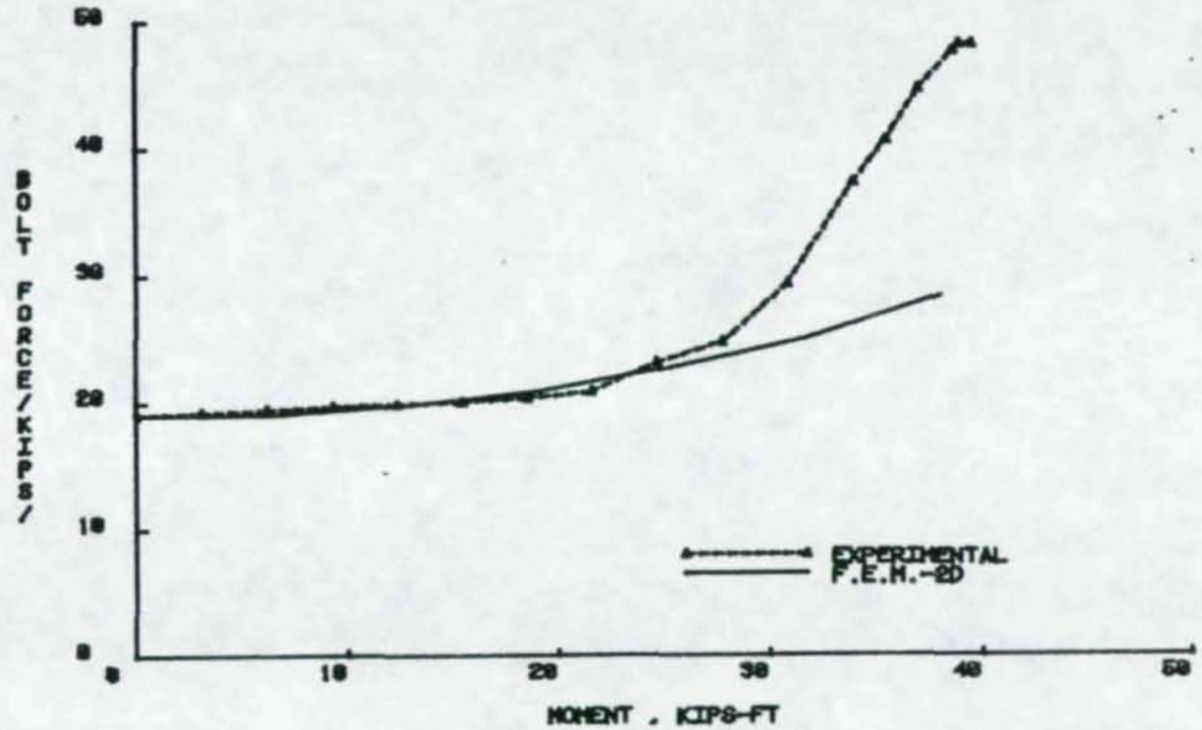

Figure B.14 Bolt Force vs. Moment (F-5/8-1/2-10)

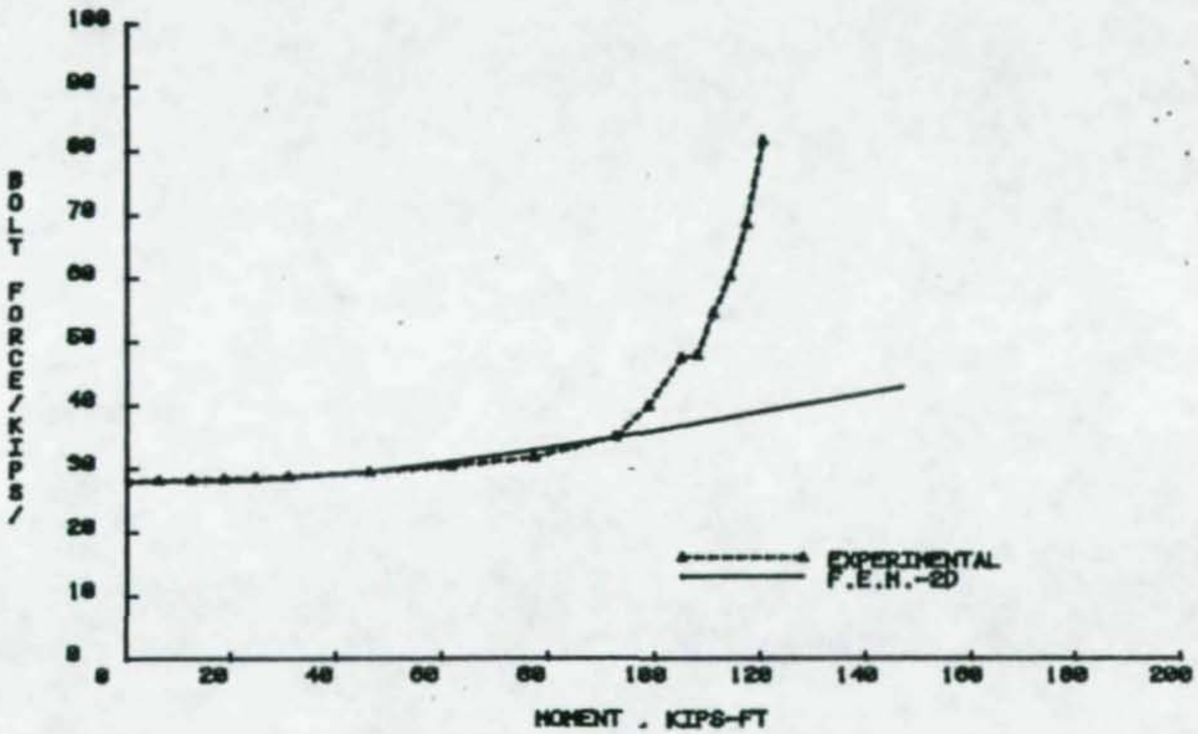

Figure B.15 Bolt Force vs. Moment (F-3/4-1/2-24A)

APPENDIX C

COMPARISON OF TWO-DIMENSION, PARTIAL-THREE DIMENSIONAL AND EXPERIMENTAL RESULTS

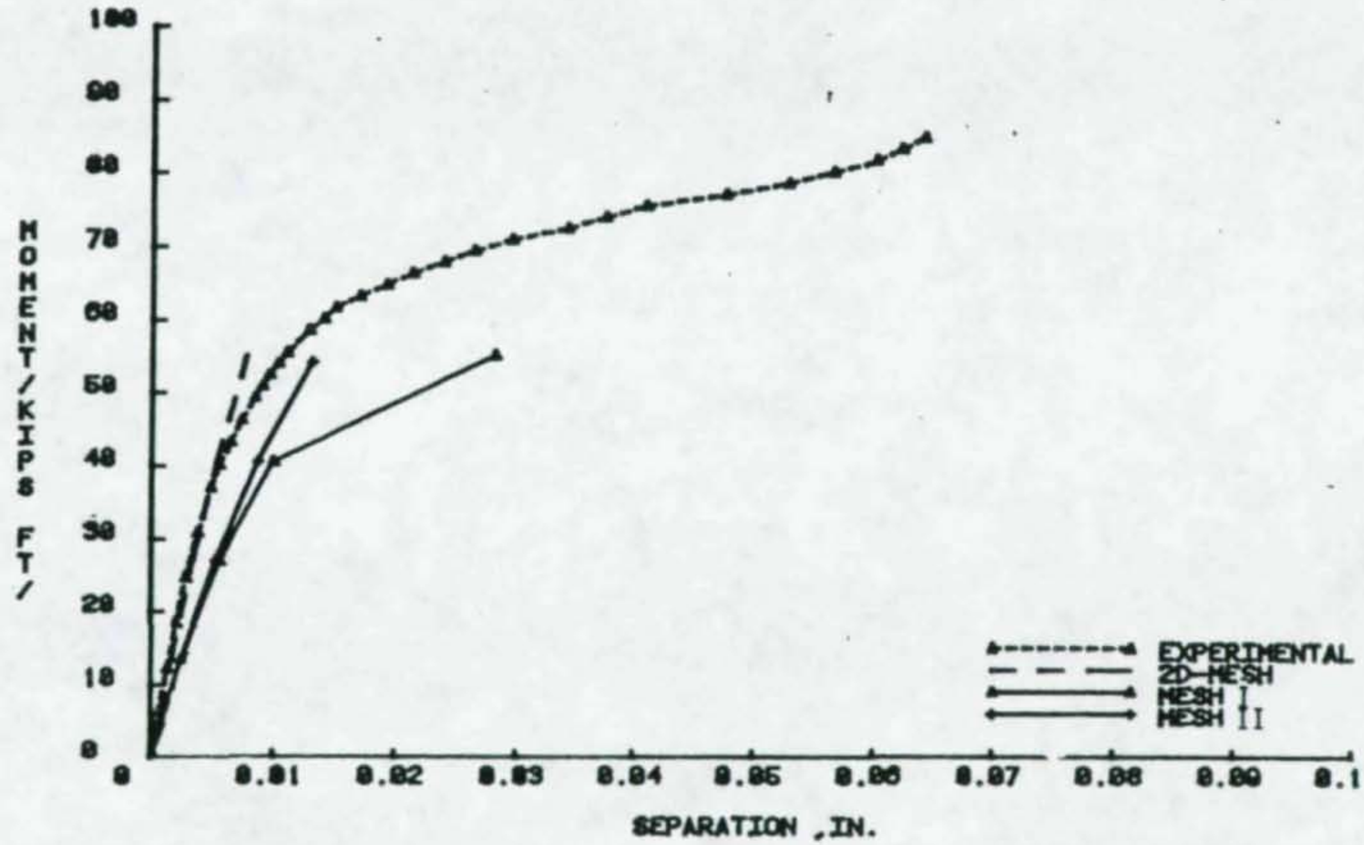

Figure C.1 Moment vs. Plate Separation (F-3/4-1/2-16)

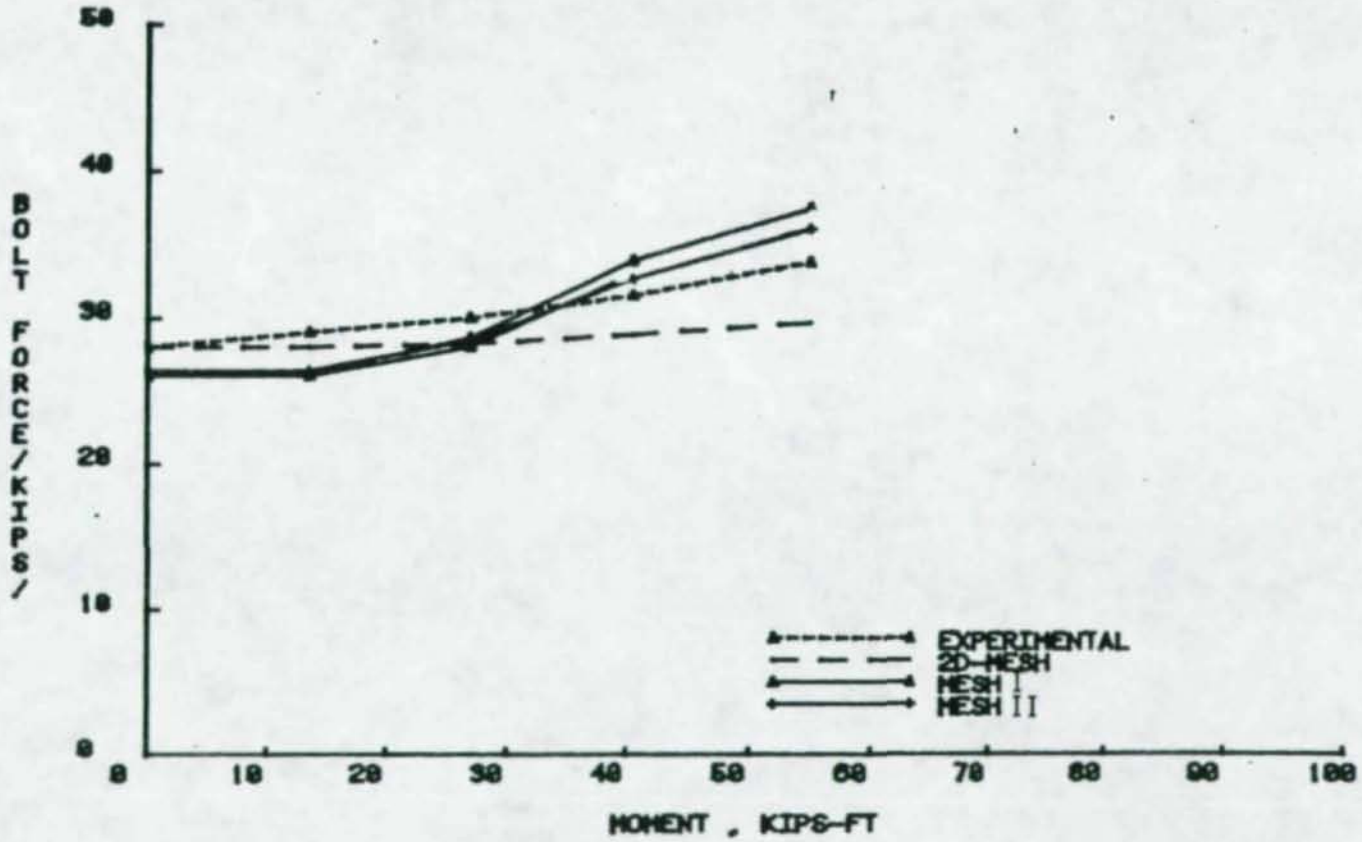

Figure C.2 Bolt Force vs. Moment (F-3/4-1/2-16)

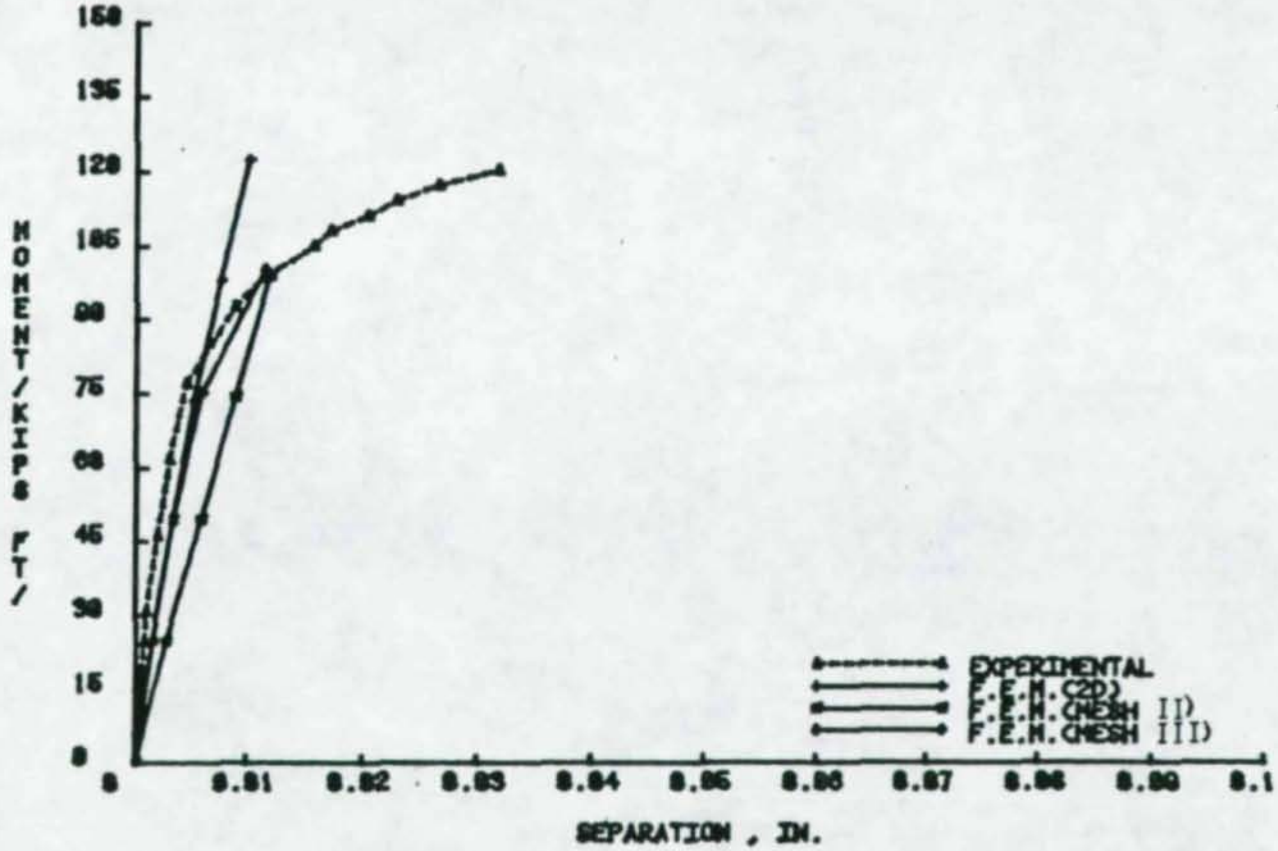

Figure C.3 Moment vs. Plate Separation (F-3/4-1/2-24A)

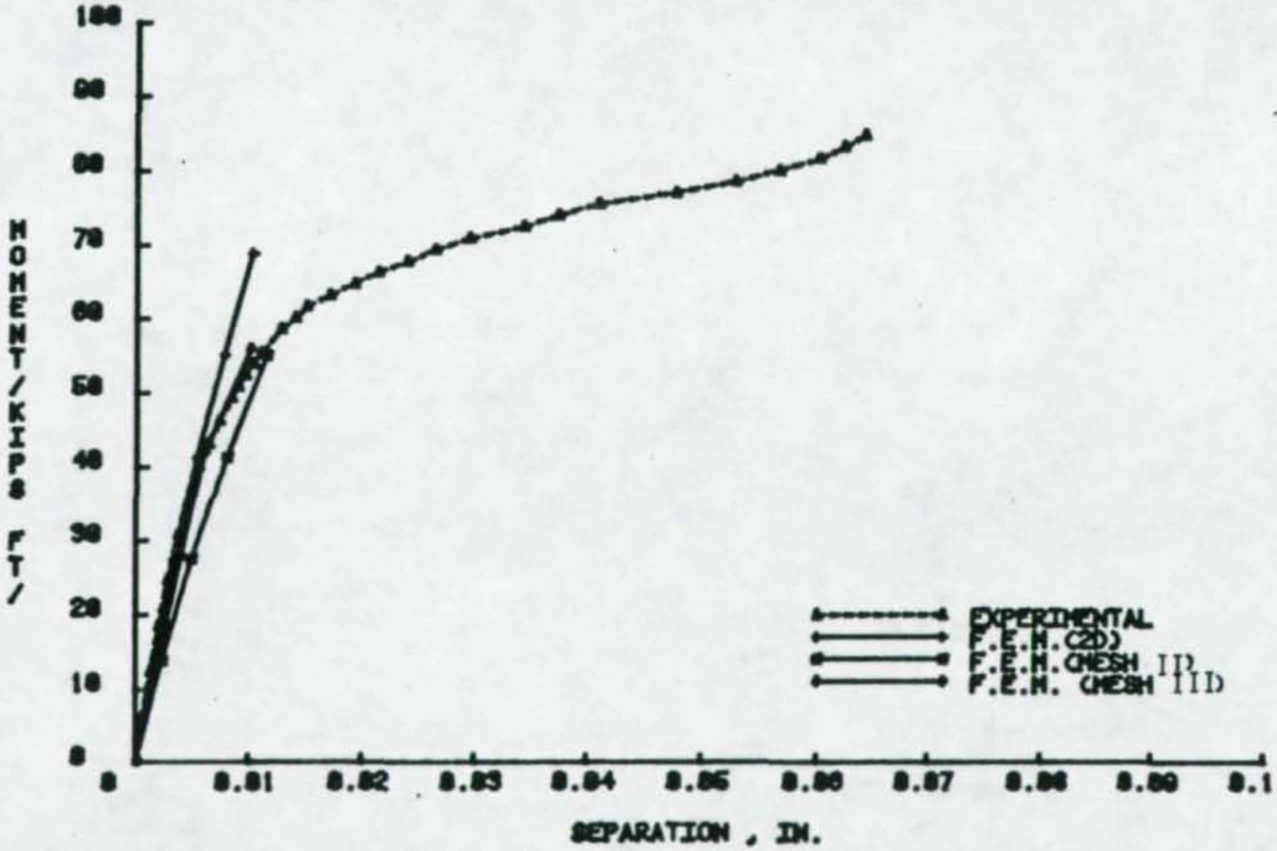

Figure C.4 Moment vs. Plate Separation (F-3/4-1/2-16)

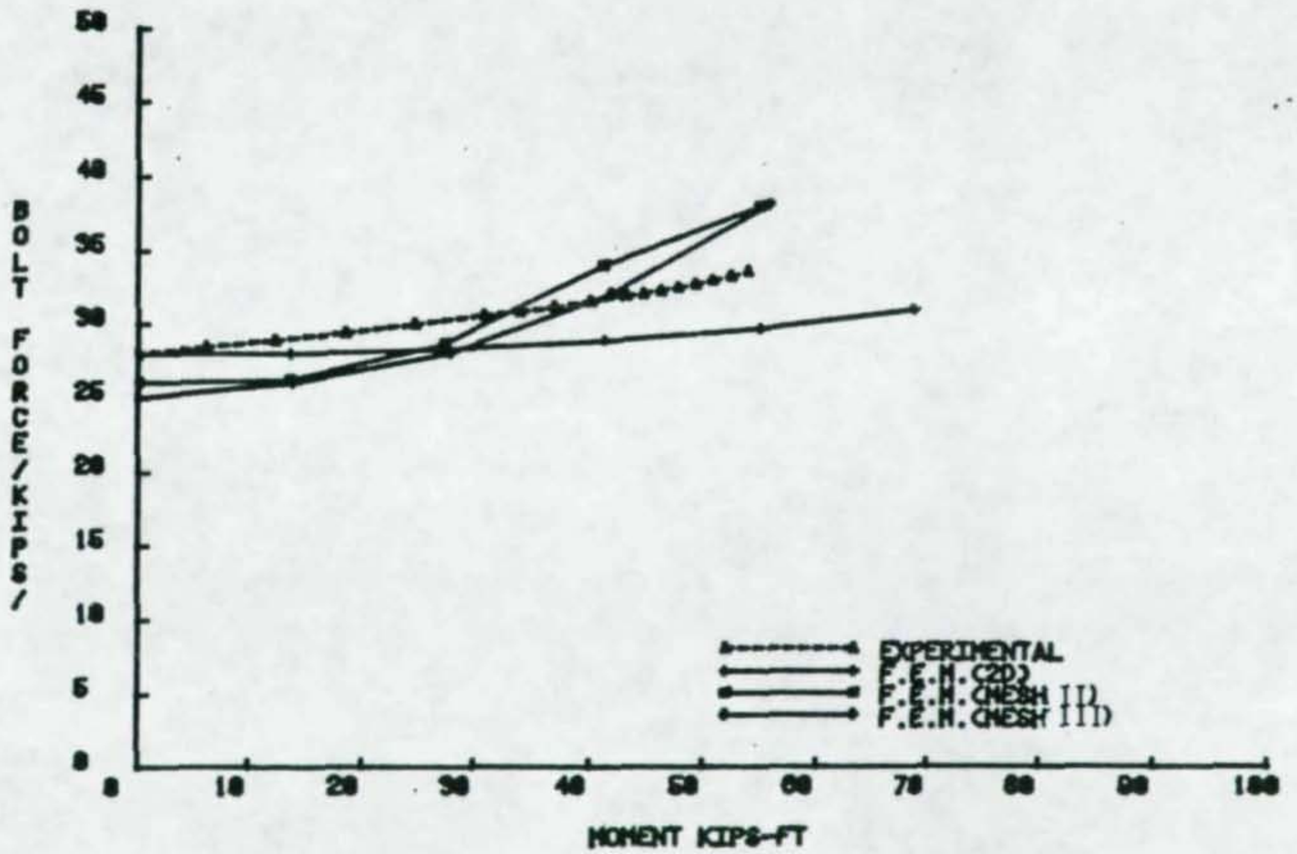

Figure C.5 Bolt Force vs. Moment (F-3/4-1/2-16)

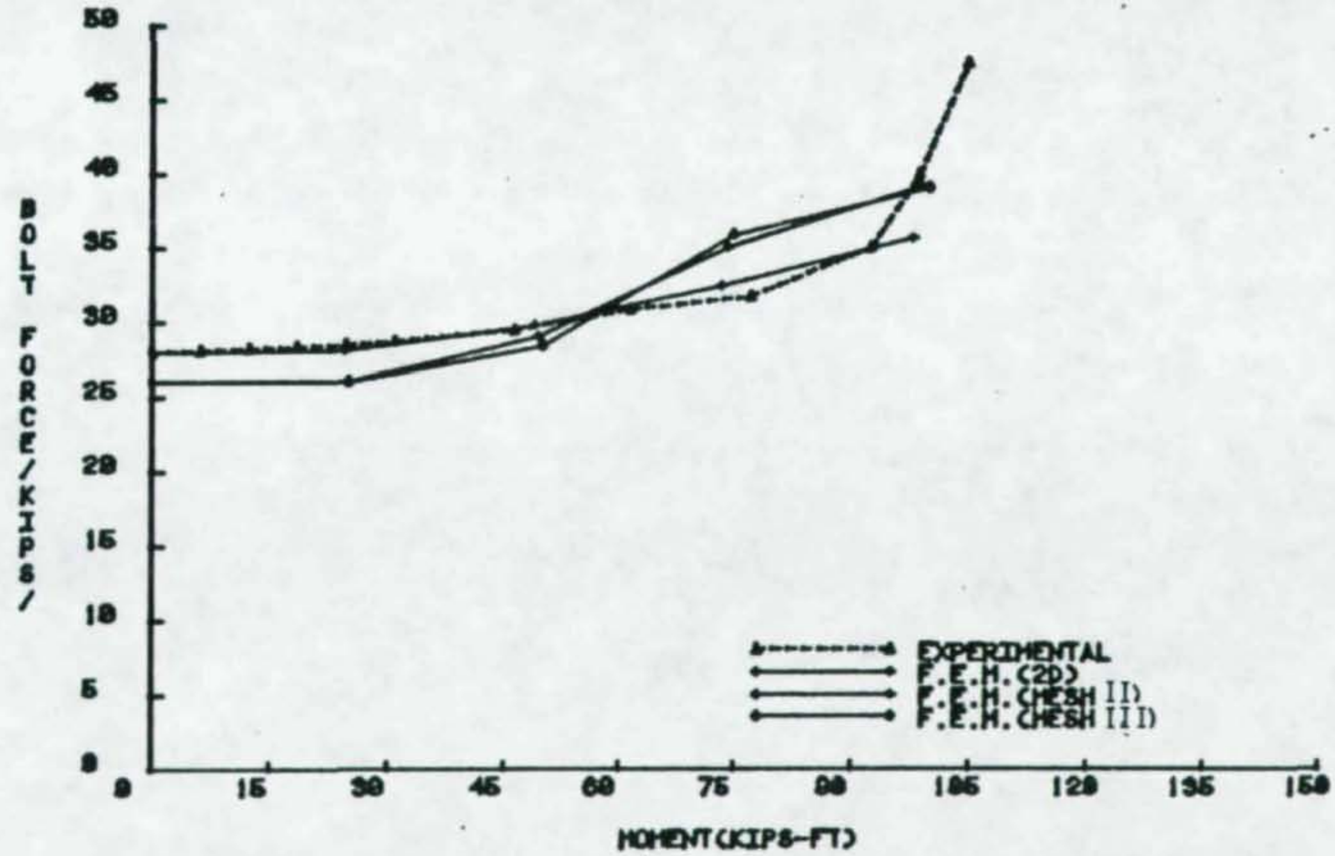

Figure C.6 Bolt Force vs. Moment (F-3/4-1/2-24A)

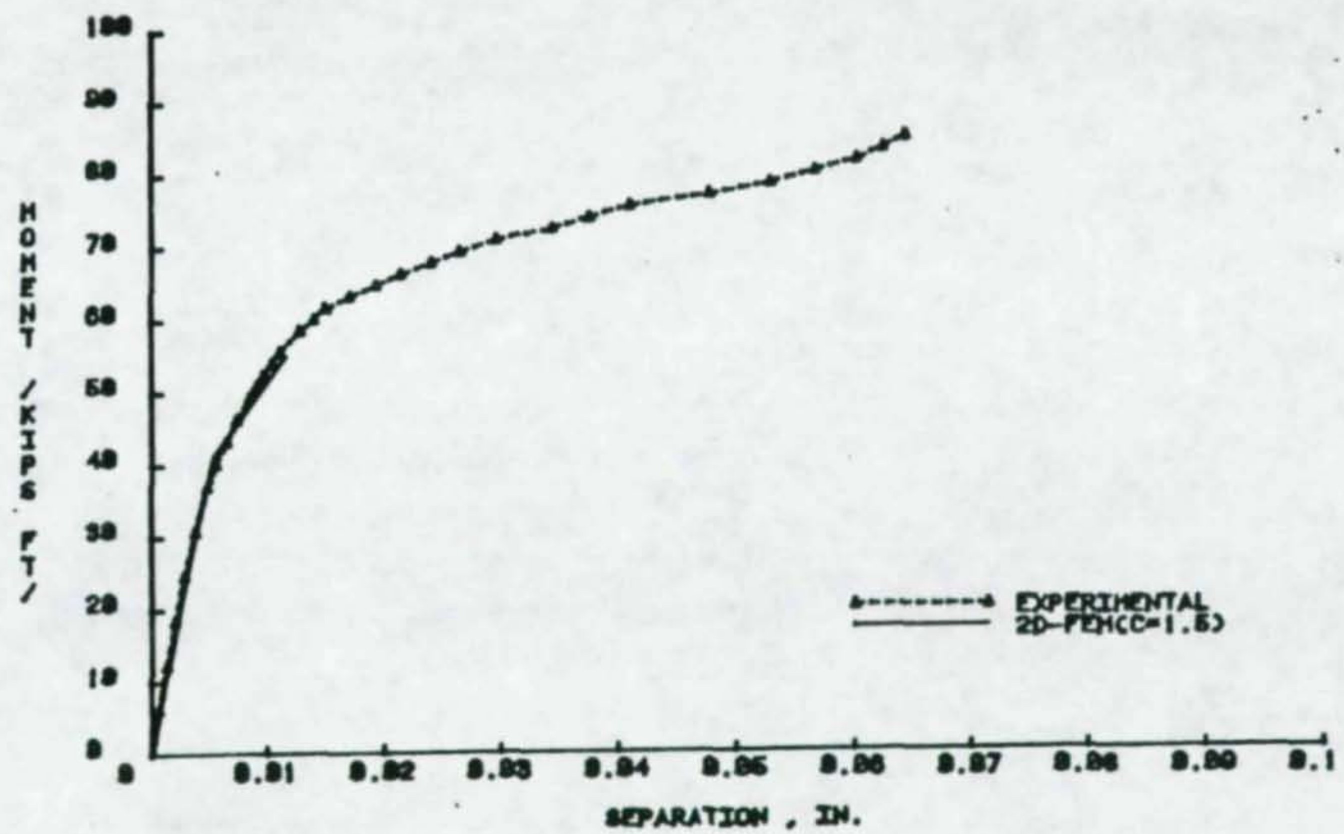

Figure C.7 Moment vs. Plate Separation (F-3/4-1/2-16)

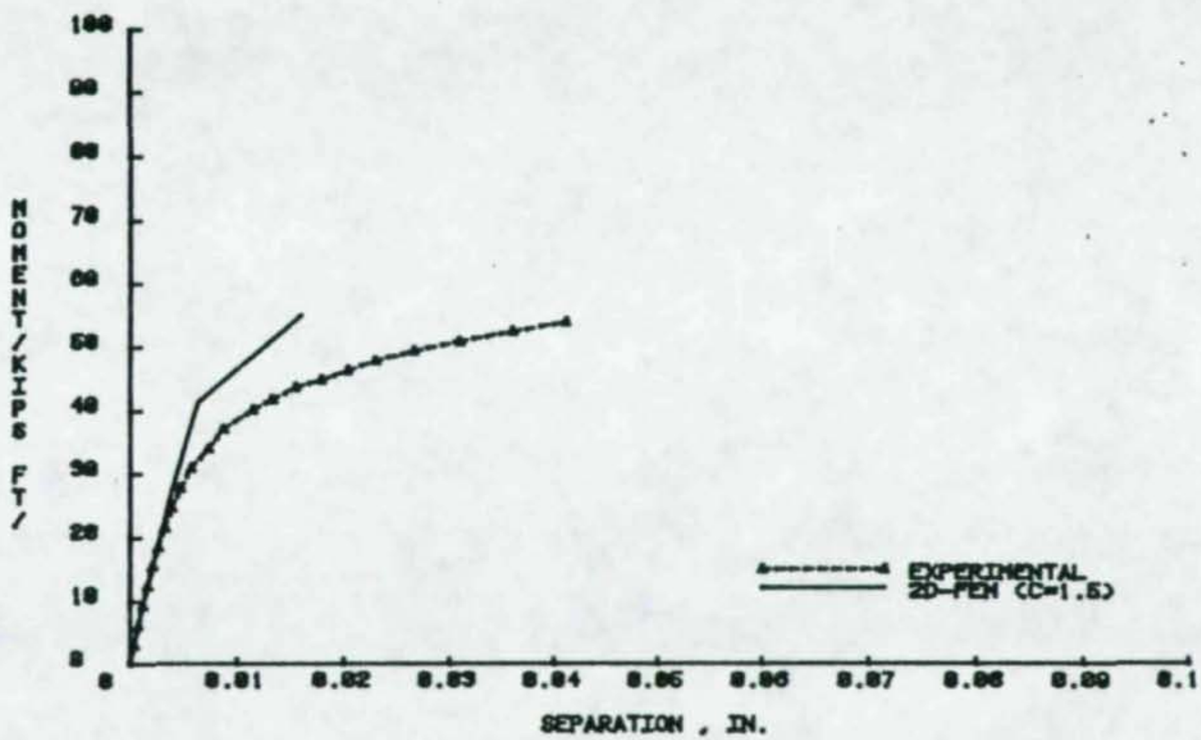

Figure C.8 Moment vs. Plate Separation (F-3/4-3/8-16)

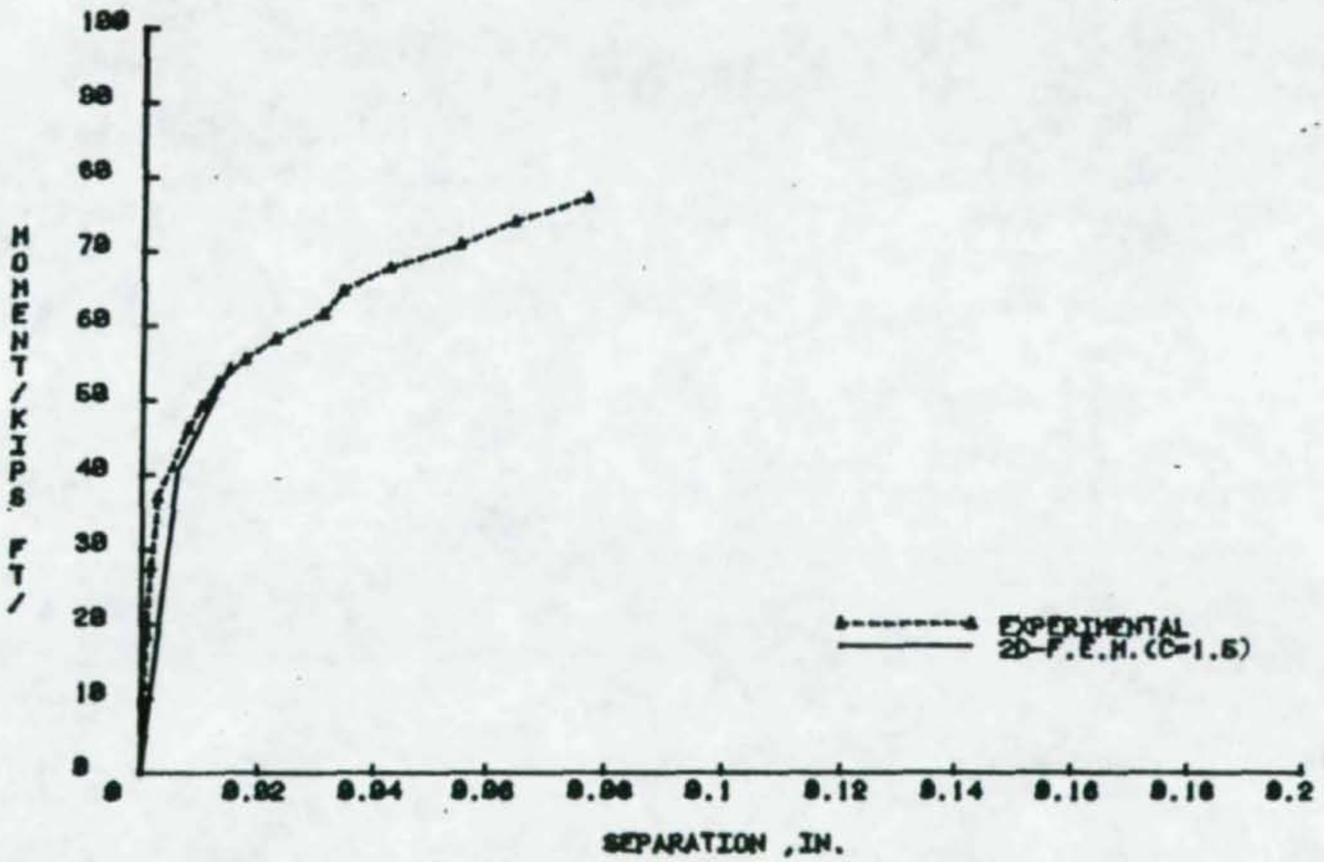

Figure C.9 Moment vs. Plate Separation (F-5/8-1/2-16)

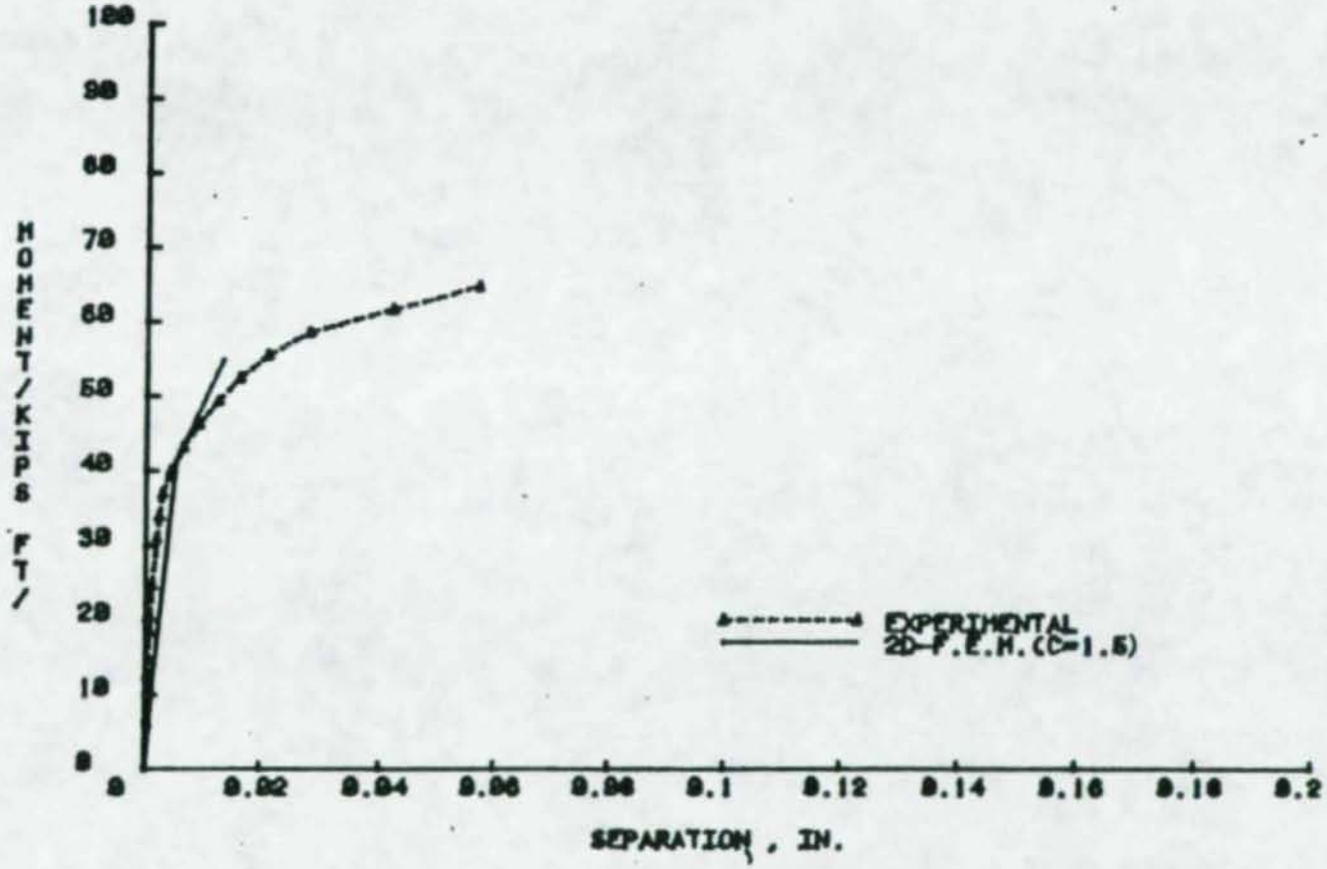

Figure C.10 Moment vs. Plate Separation (F-5/8-3/8-16)

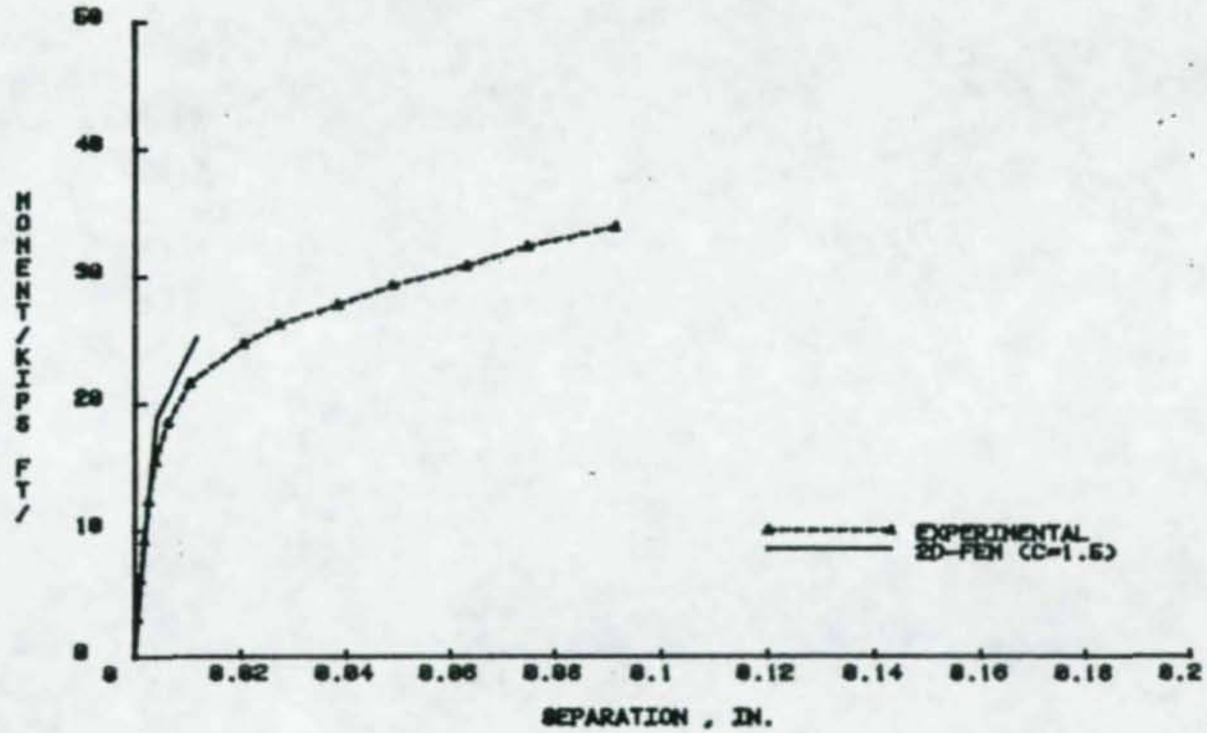

Figure C.11 Moment vs. Plate Separation (F-5/8-3/8-10)

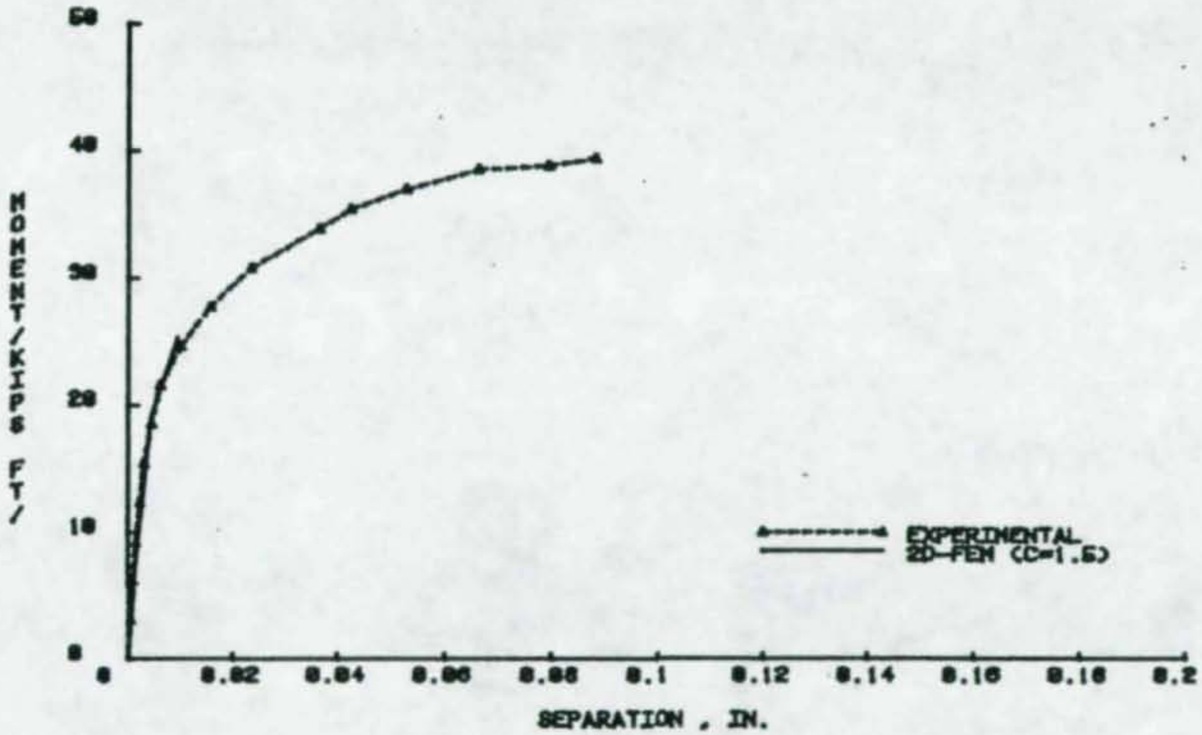

Figure C.12 Moment vs. Plate Separation (F-5/6-1/2-10)

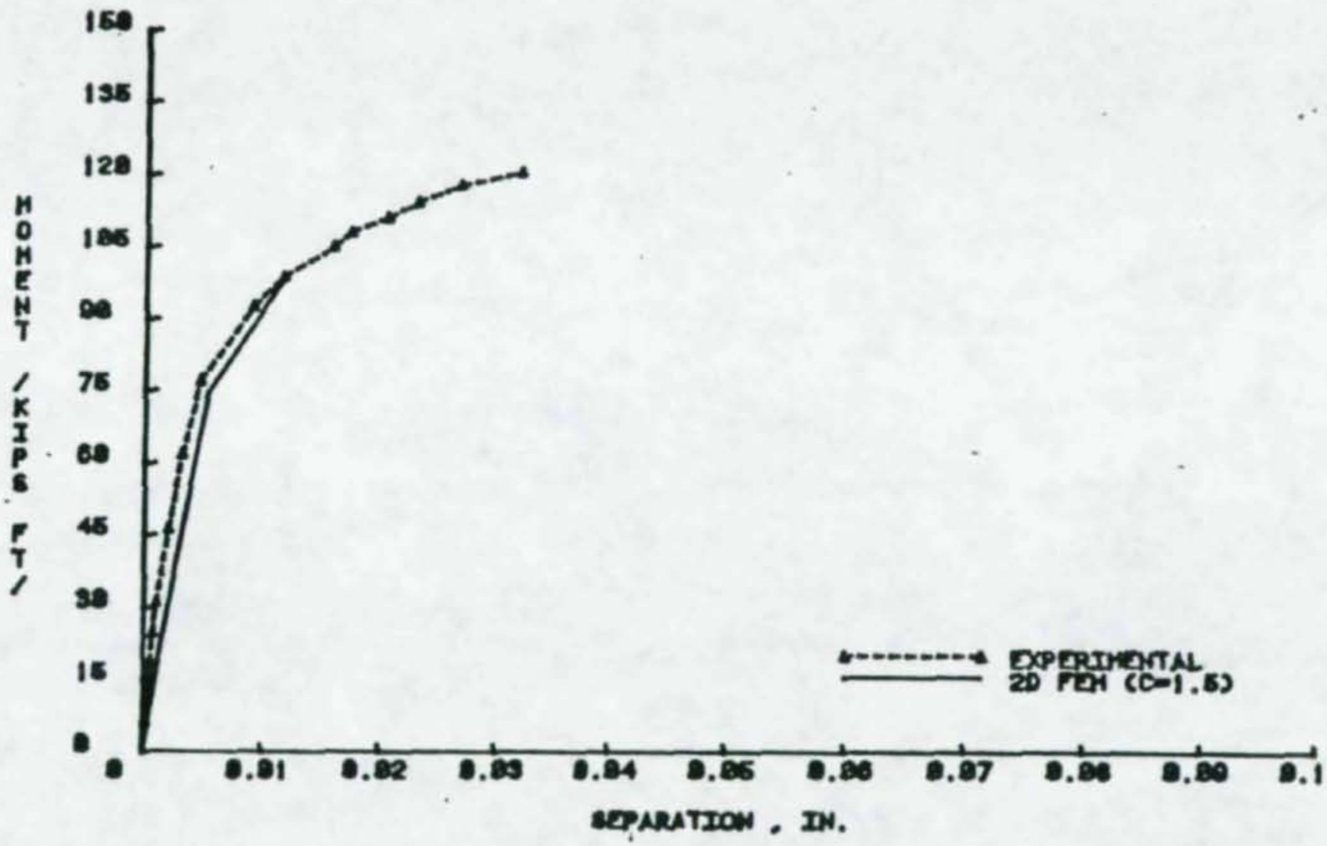

Figure C.13 Moment vs. Plate Separation (F-3/4-1/2-24A)

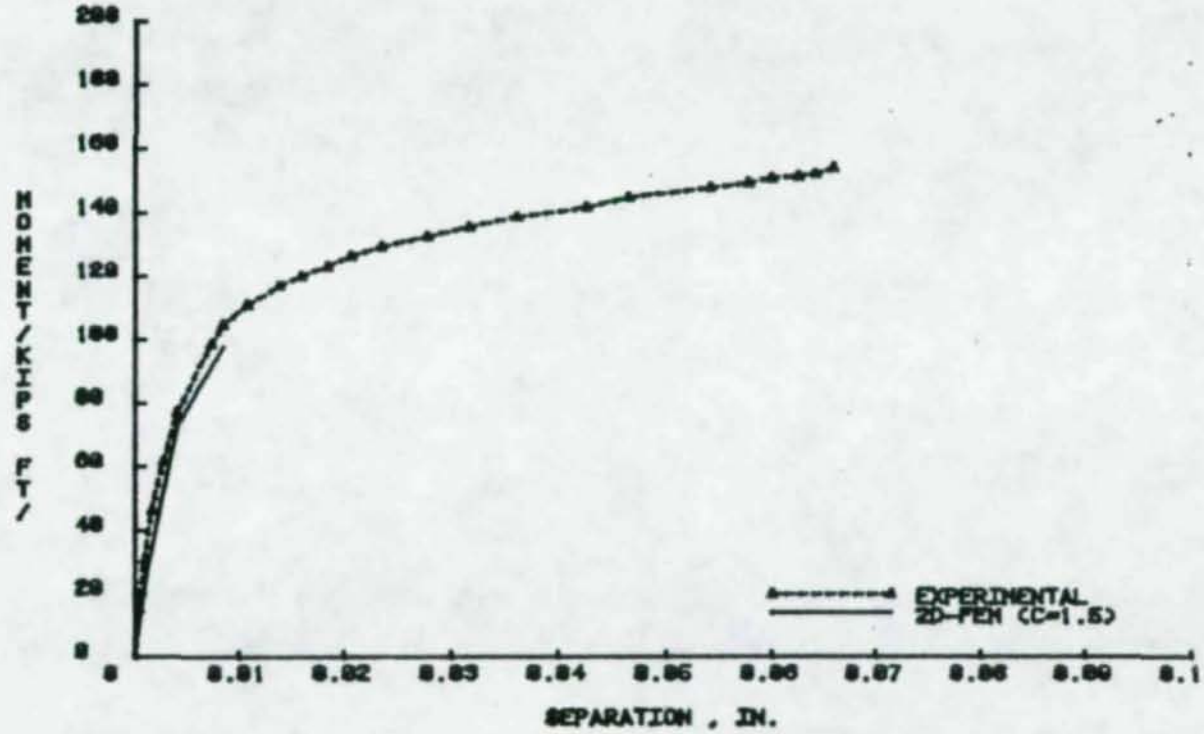

Figure C.14 Moment vs. Plate Separation (F-3/4-1/2-24B)

APPENDIX D

COMPARISON OF PREDICTED AND EXPERIMENTAL RESULTS

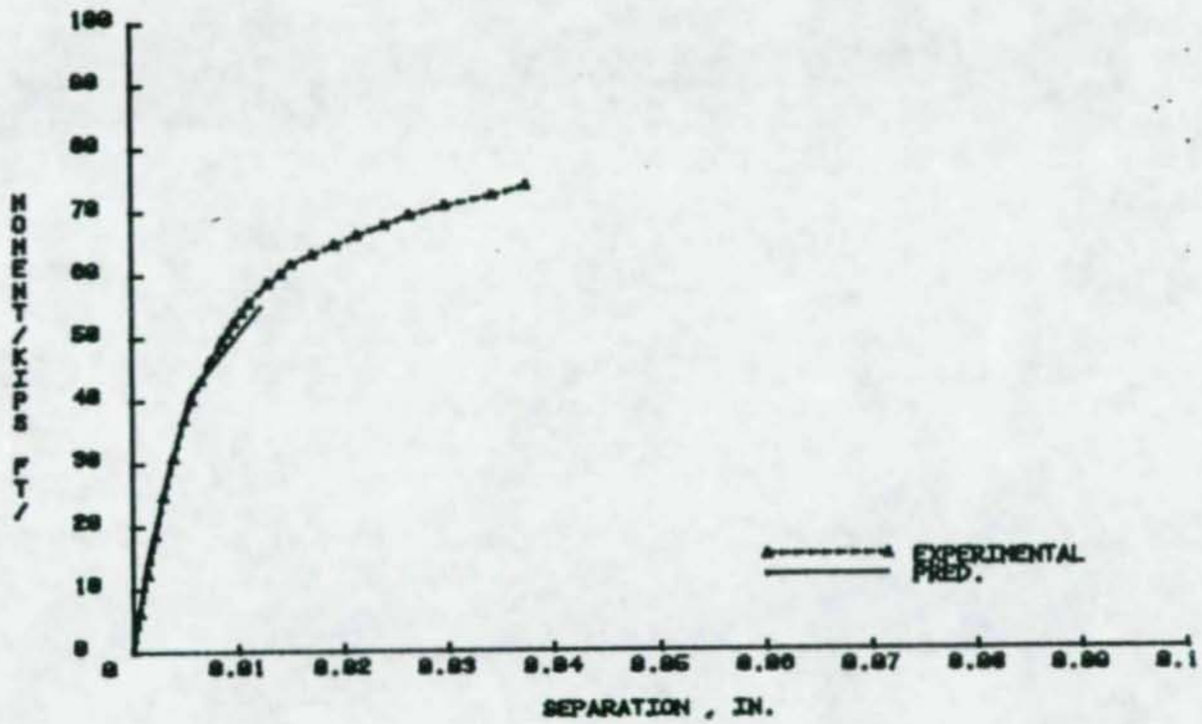

Figure D.1 Moment vs Plate Separation (F-3/4-1/2-16)

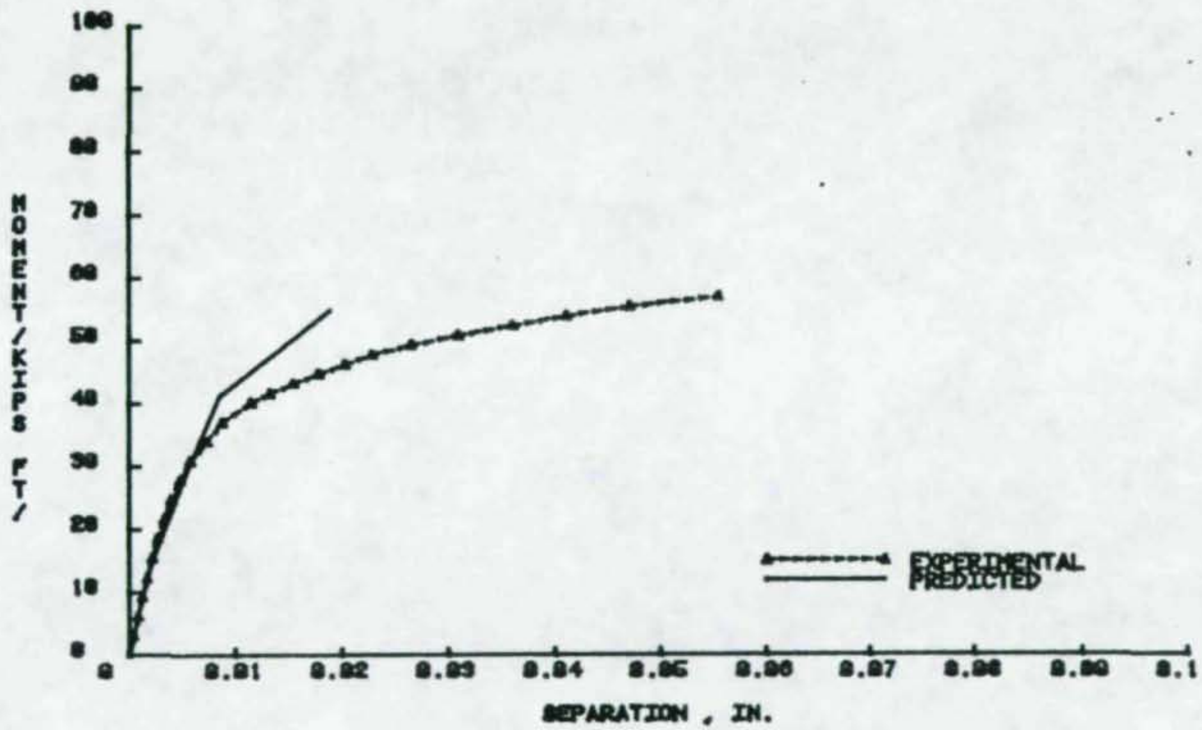

Figure D.2 Moment vs Plate Separation (F-3/4-3/8-16)

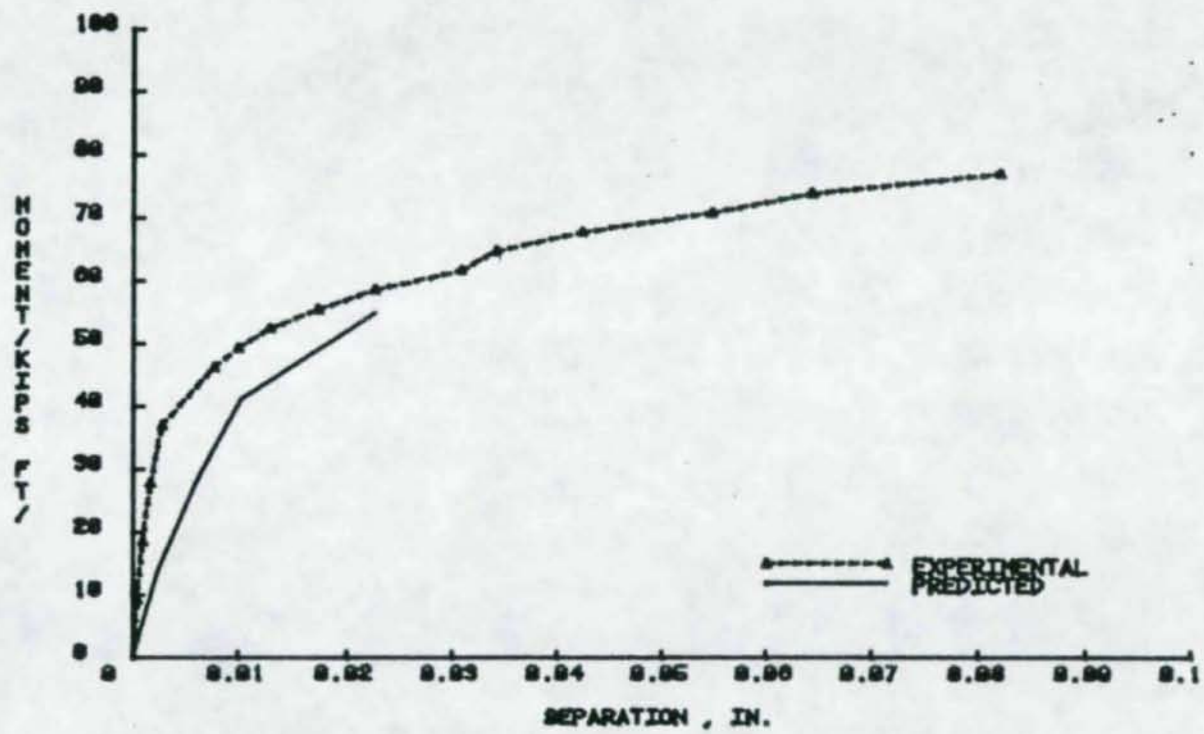

Figure D.3 Moment vs Plate Separation (F-5/8-1/2-16)

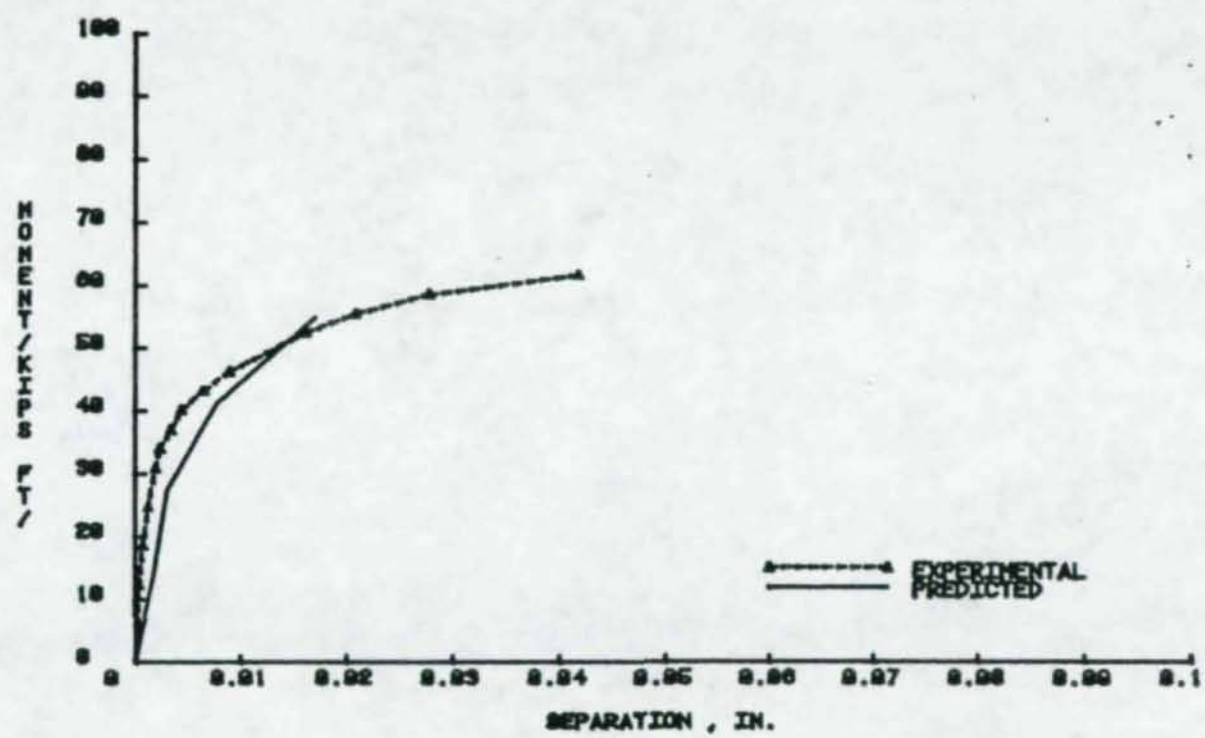

Figure D.4 Moment vs Plate Separation (F-5/8-3/8-16)

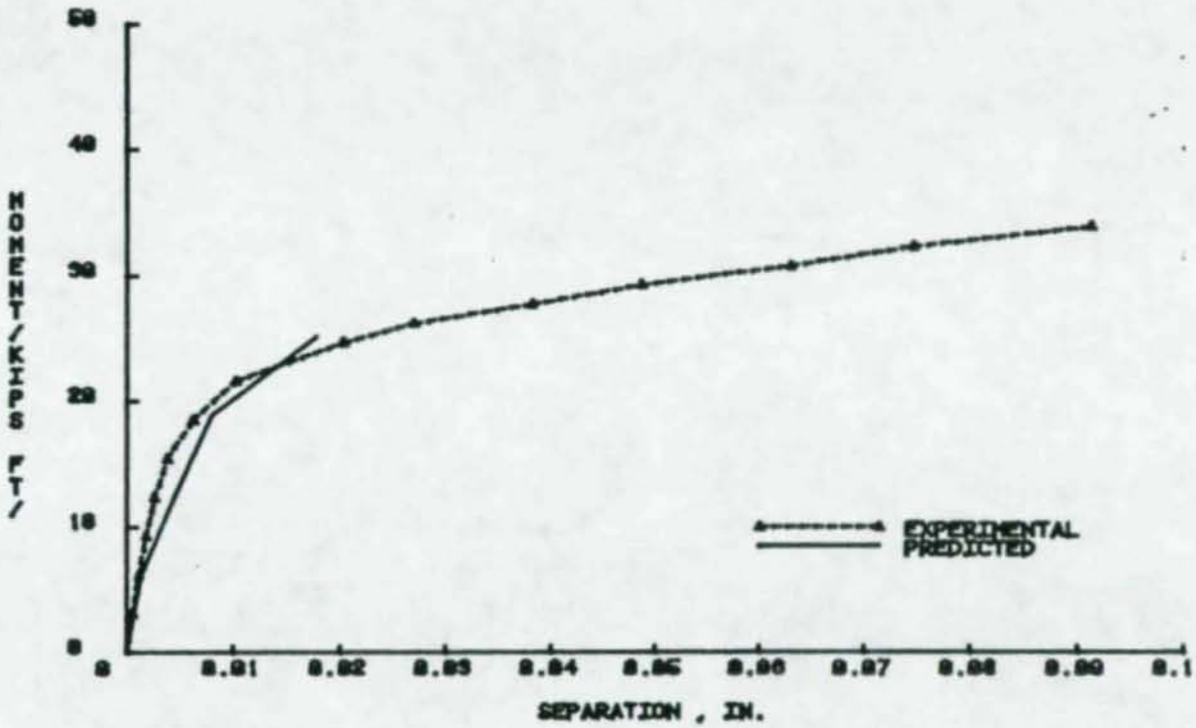

Figure D.5 Moment vs Plate Separation (F-5/8-3/8-10)

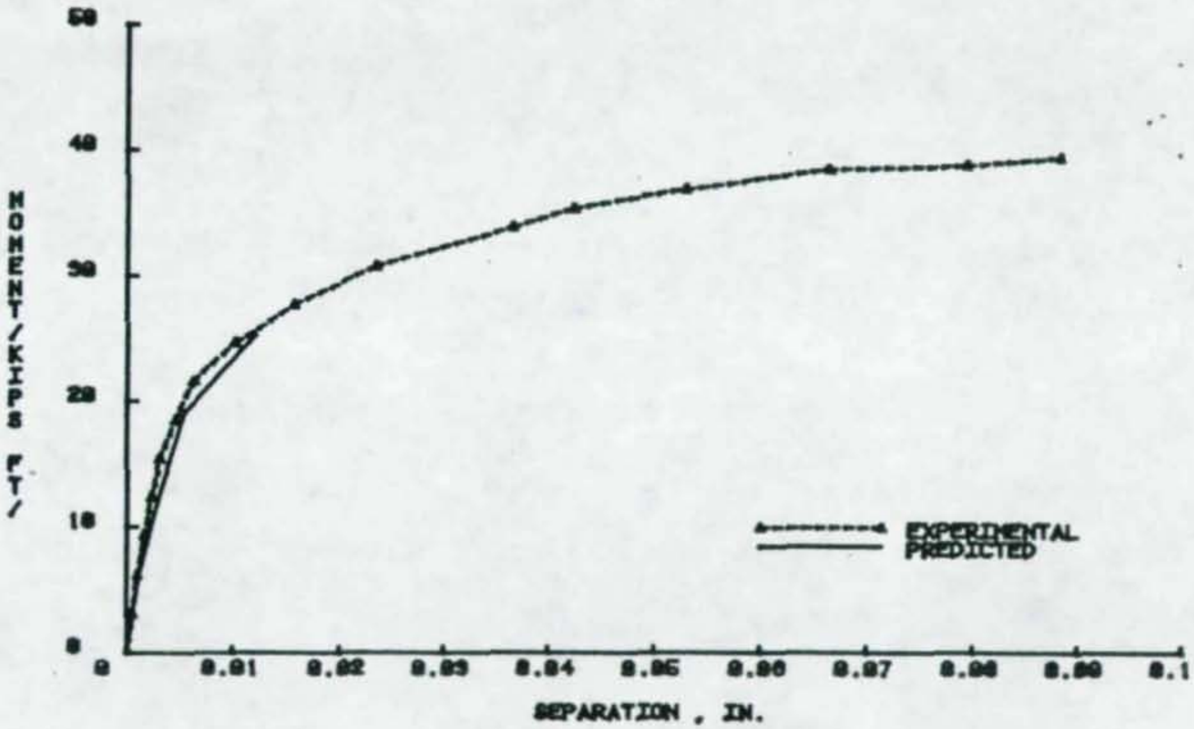

Figure D.6 Moment vs Plate Separation (F-5/8-1/2-10)

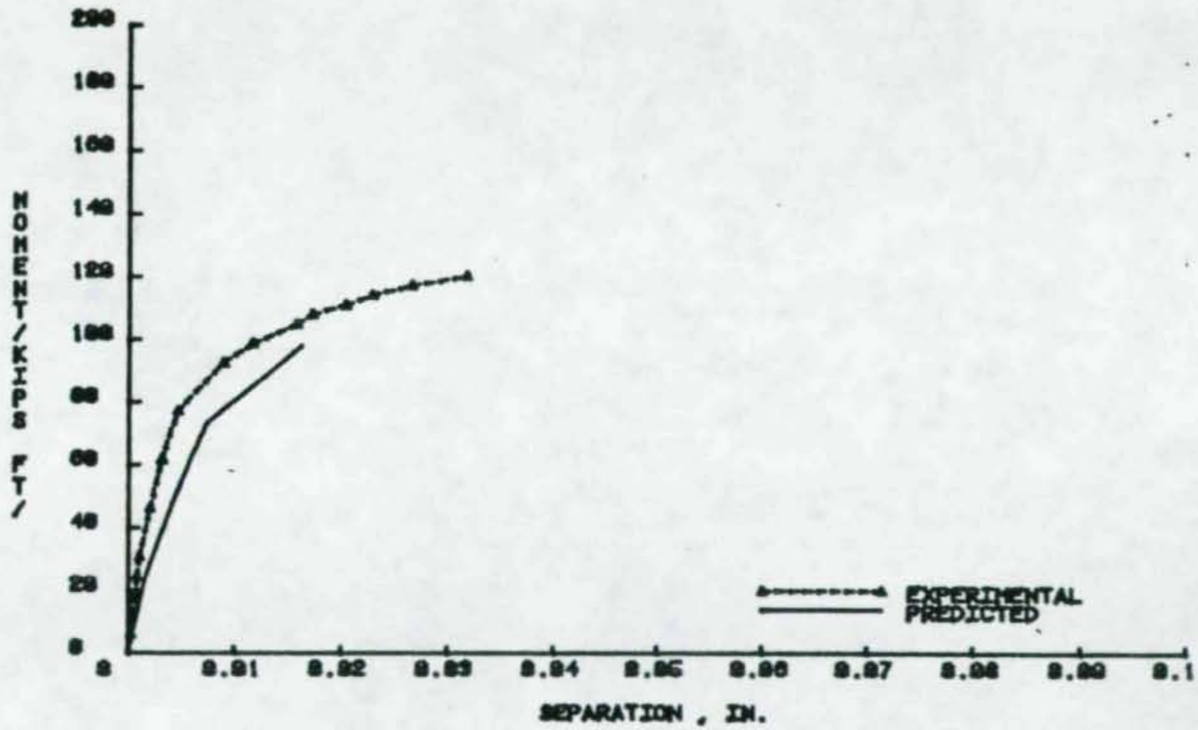

Figure D.7 Moment vs Plate Separation (F-3/4-1/2-24A)

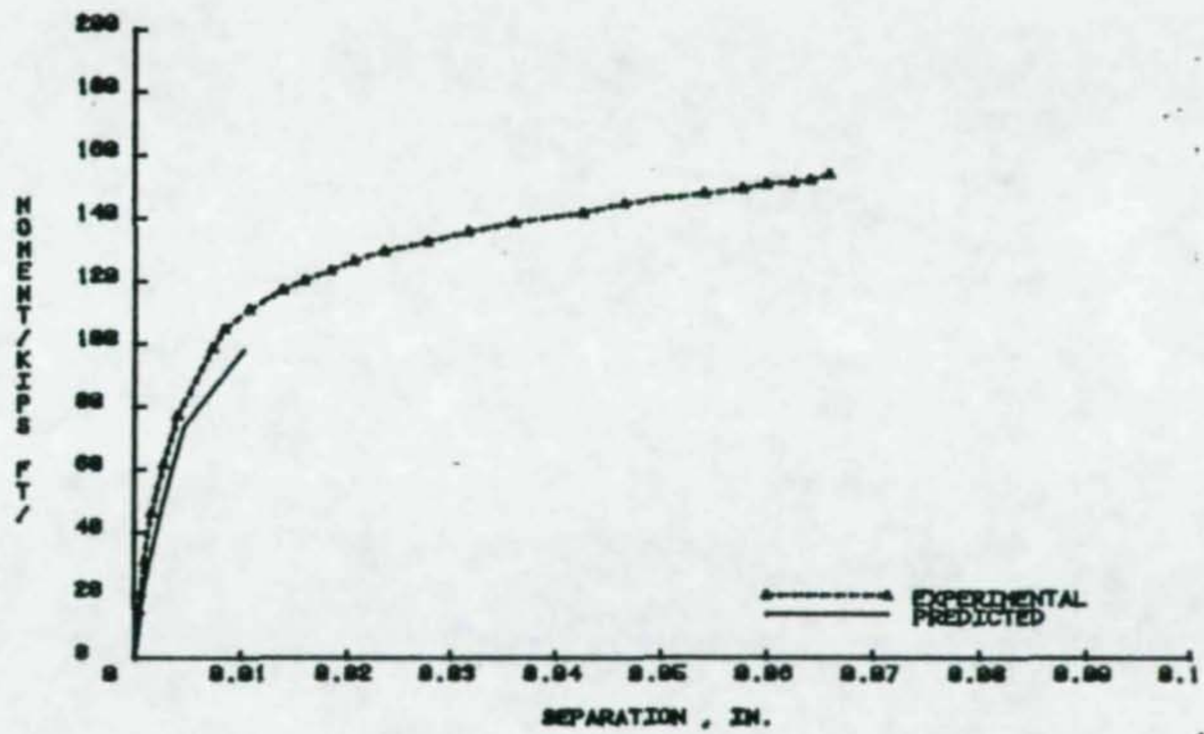

Figure D.8 Moment vs Plate Separation (F-3/4-1/2-24B)

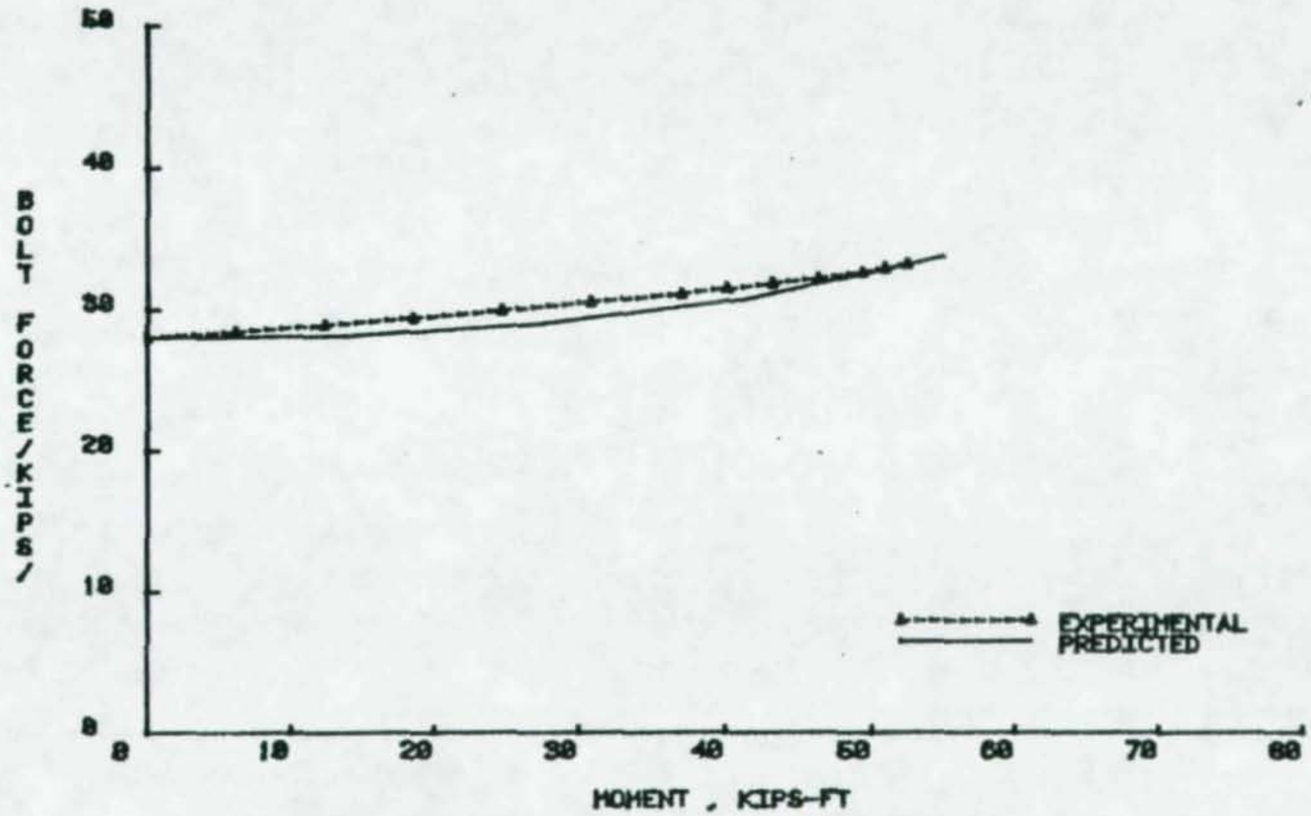

Figure D.9 Bolt Force vs Moment (F-3/4-1/2-16)

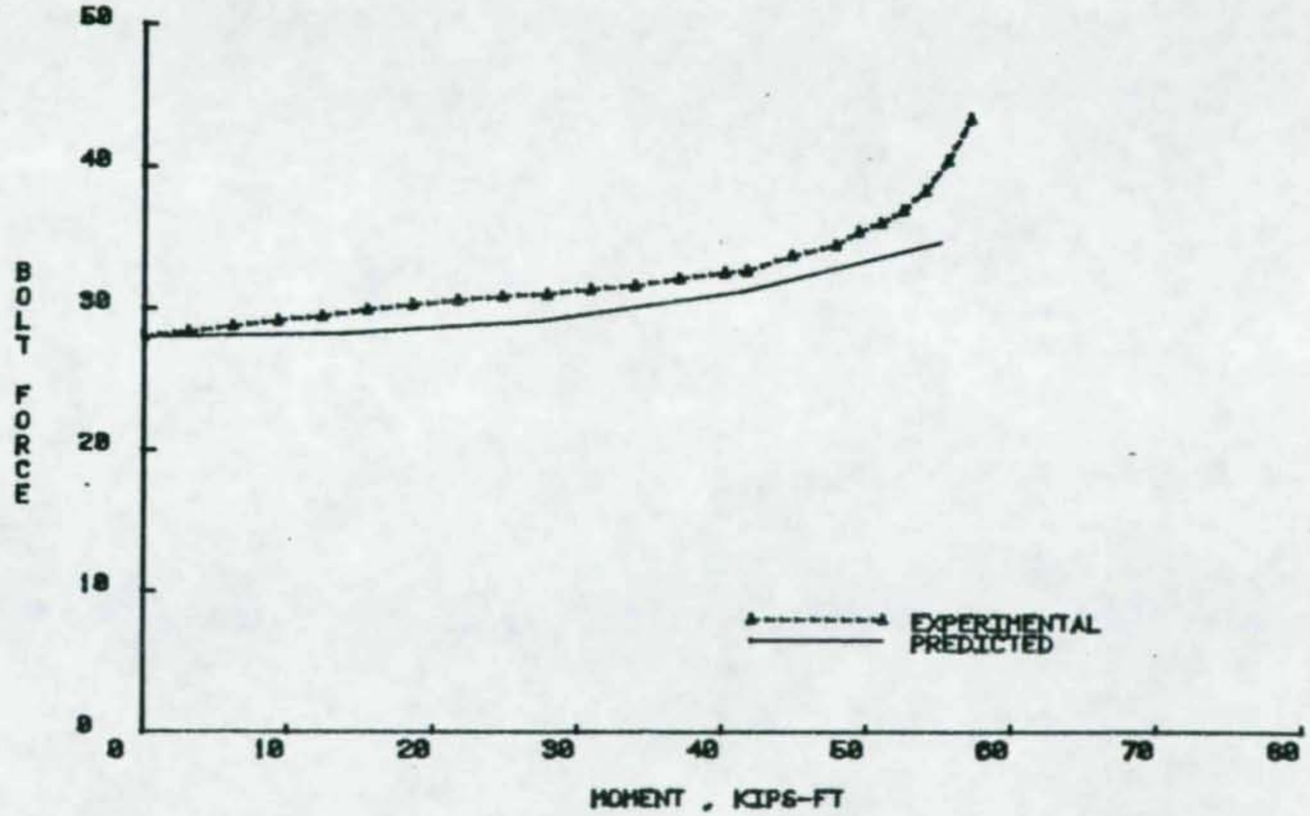

Figure D.10 Bolt Force vs Moment (F-3/4-3/8-16)

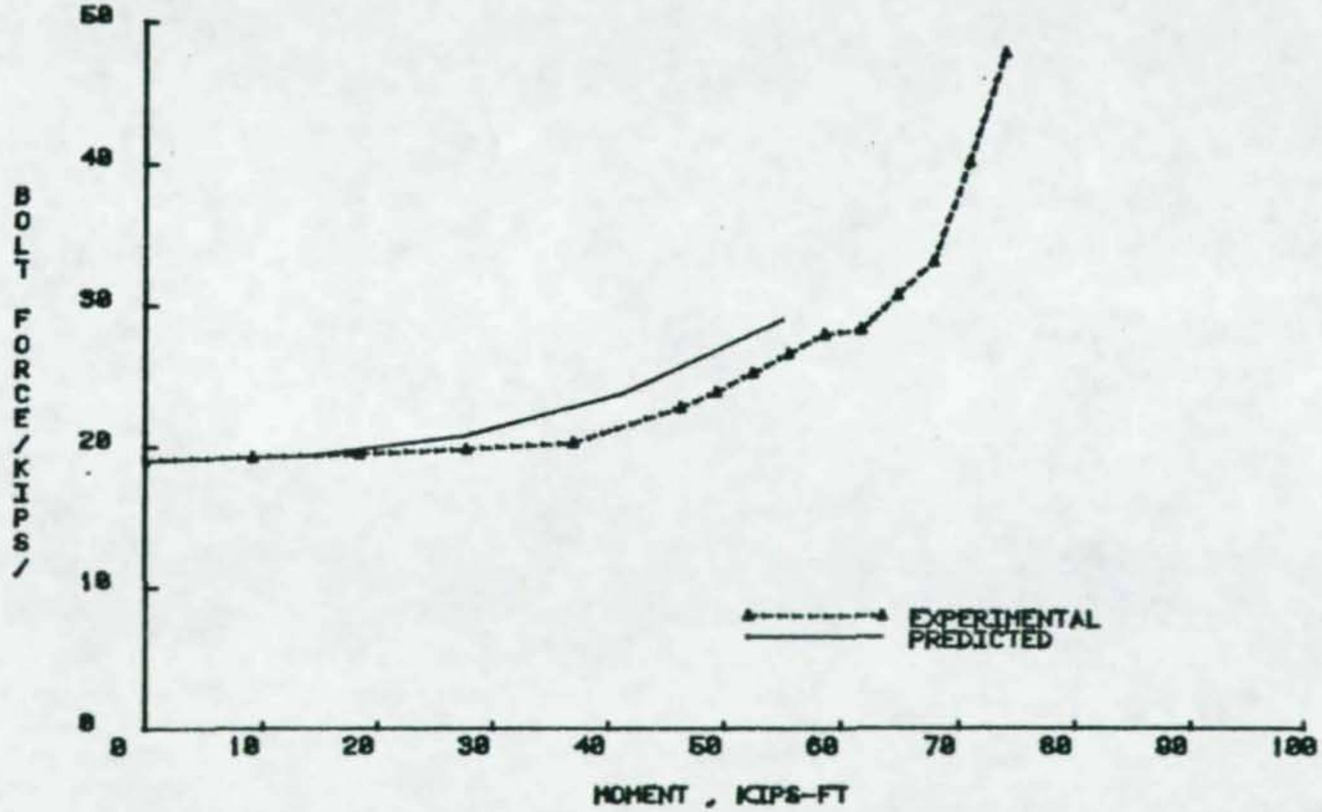

Figure D.11 Bolt Force vs Moment (F-5/8-1/2-16)

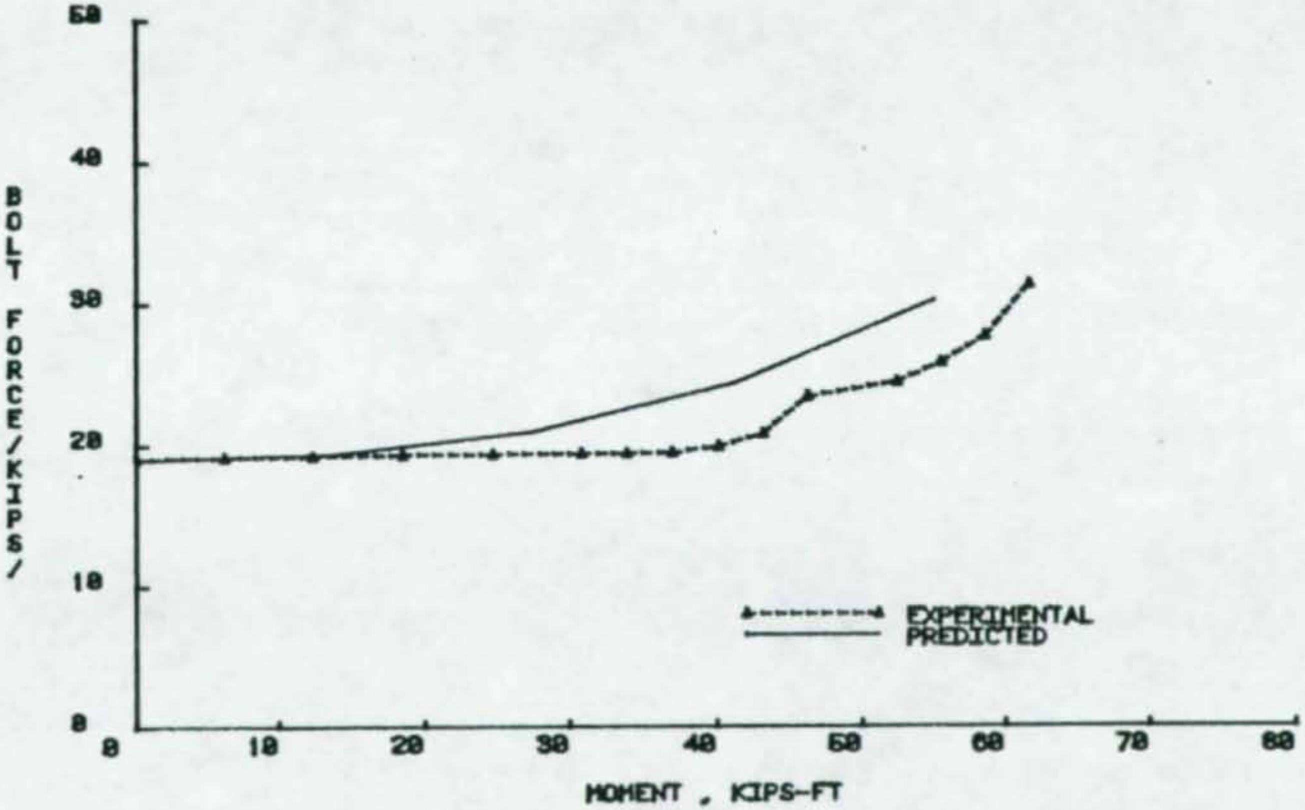

Figure D.12 Bolt Force vs Moment (F-5/8-3/8-16)

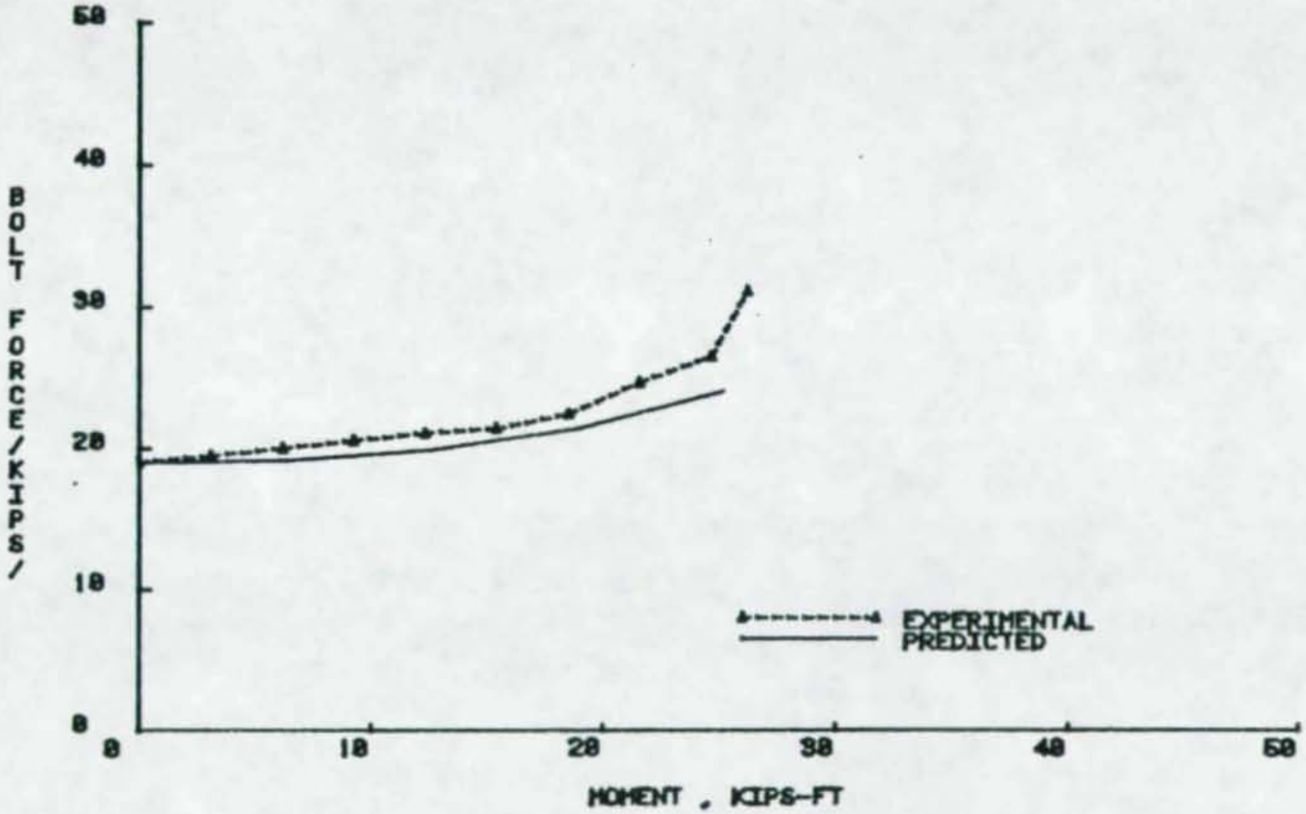

Figure D.13 Bolt Force vs Moment (F-5/8-3/8-10)

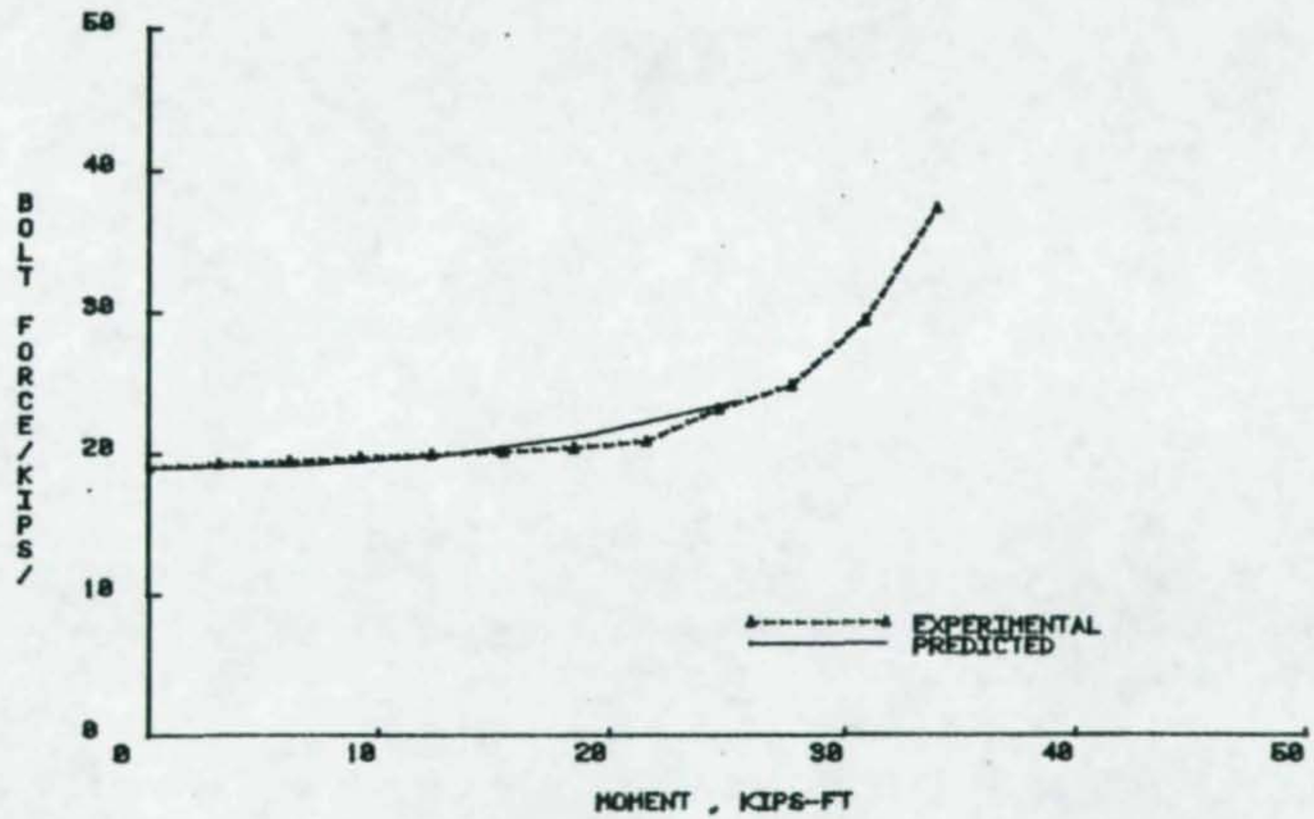

Figure D.14 Bolt Force vs Moment (F-5/8-1/2-10)

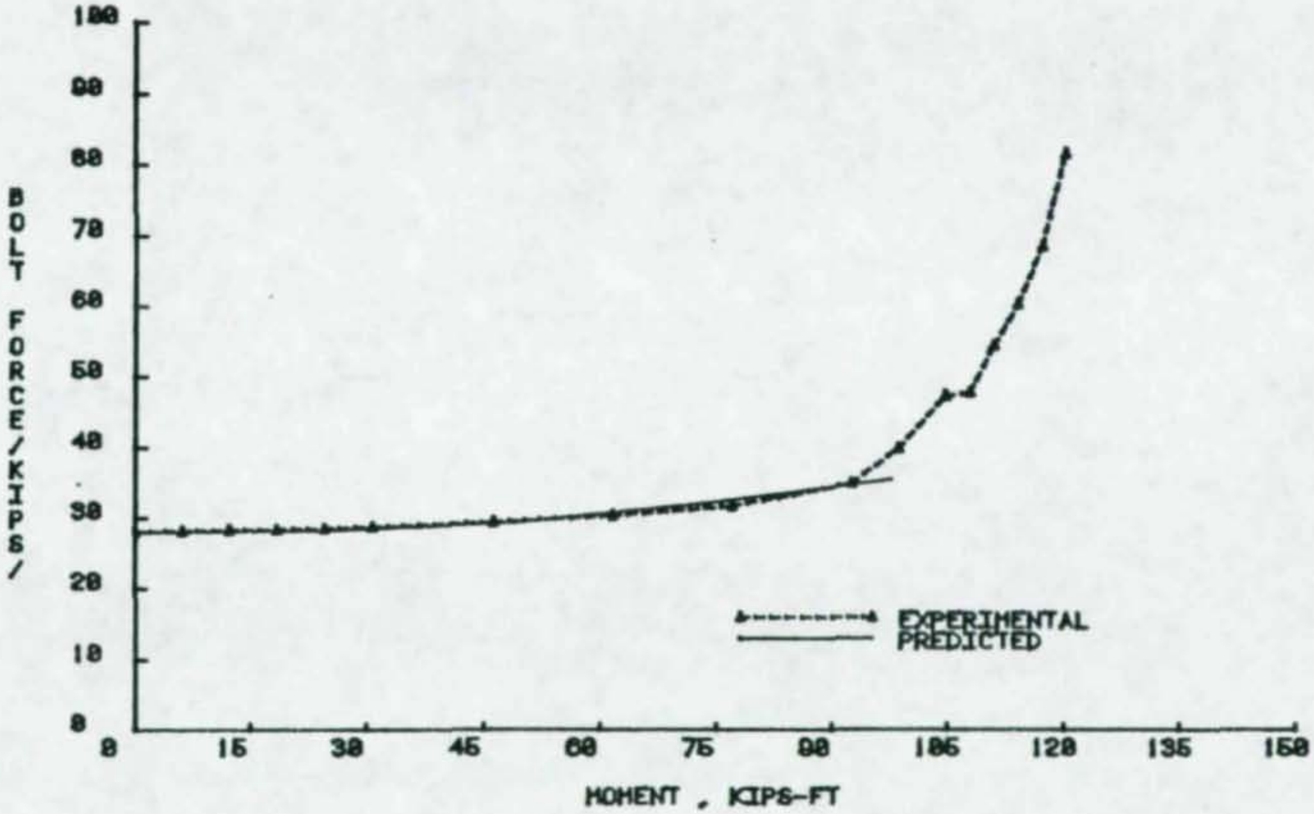

Figure D.15 Bolt Force vs Moment (F-3/4-1/2-24A)

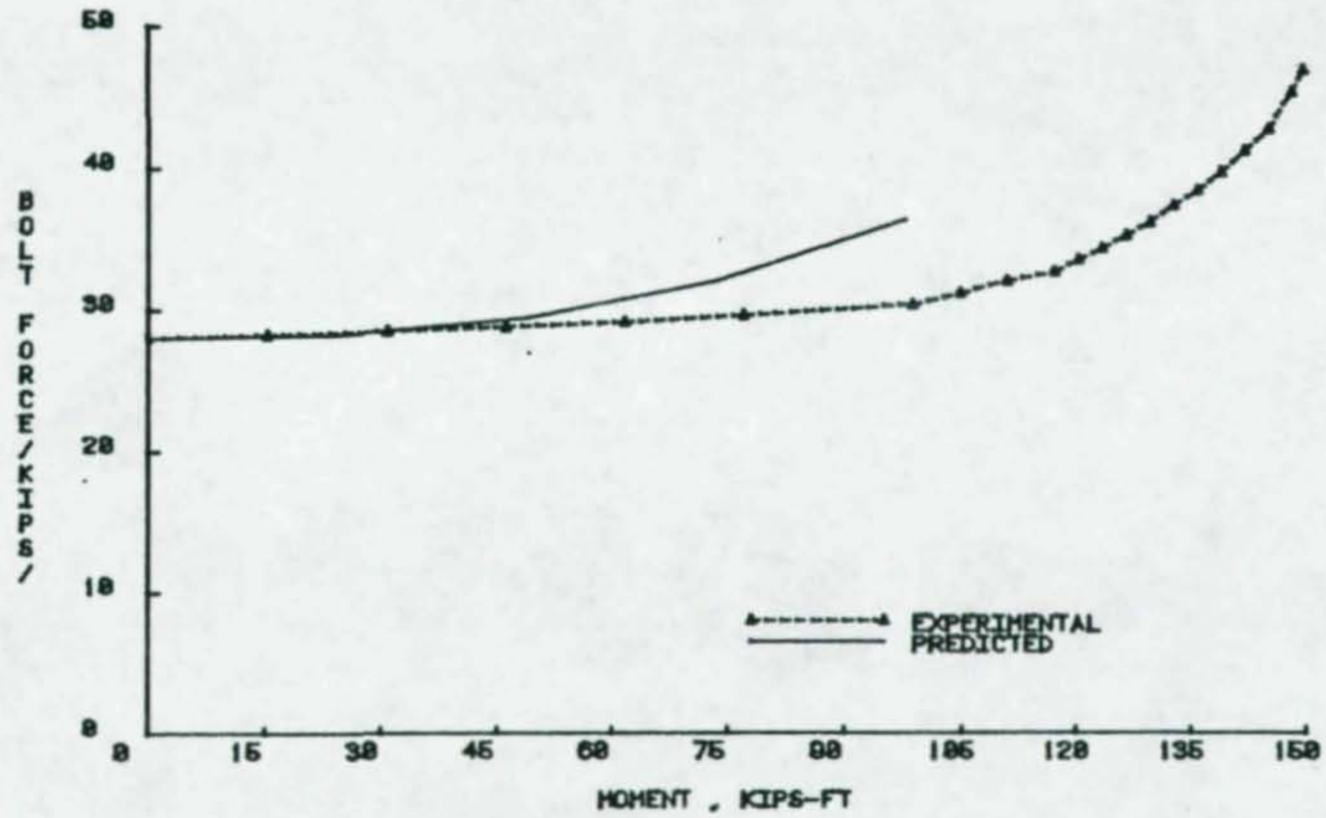

Figure D.16 Bolt Force vs Moment (F-3/4-1/2-24B)

APPENDIX E

DATA USED IN REGRESSION ANALYSES

Table E.1

Data Used in Regression Analyses

Π_1	Π_2	Π_3	Π_4	Π_5	Π_6	δ_{max}	B_F
0.111	0.250	0.026	0.040	2.222	0.139	0.000634	19.000
0.111	0.250	0.026	0.040	2.222	0.139	0.001345	19.130
0.111	0.250	0.026	0.040	2.222	0.139	0.002378	19.775
0.111	0.250	0.026	0.040	2.222	0.139	0.003410	20.420
0.111	0.250	0.026	0.040	2.222	0.139	0.004726	21.280
0.111	0.250	0.026	0.040	2.222	0.139	0.006147	22.880
0.139	0.444	0.049	0.040	2.222	0.139	0.001157	19.050
0.139	0.444	0.049	0.040	2.222	0.139	0.002389	19.210
0.139	0.444	0.049	0.040	2.222	0.139	0.003860	19.900
0.139	0.444	0.049	0.040	2.222	0.139	0.005331	20.600
0.139	0.444	0.049	0.040	2.222	0.139	0.007056	22.070
0.139	0.444	0.049	0.040	2.222	0.139	0.008767	23.590
0.083	0.250	0.017	0.030	1.667	0.104	0.001429	19.000
0.083	0.250	0.017	0.030	1.667	0.104	0.003274	19.670
0.083	0.250	0.017	0.030	1.667	0.104	0.005231	20.540
0.083	0.250	0.017	0.030	1.667	0.104	0.008223	22.600
0.083	0.250	0.017	0.030	1.667	0.104	0.010705	24.900
0.083	0.250	0.017	0.030	1.667	0.104	0.013188	27.190
0.104	0.417	0.020	0.030	1.667	0.104	0.002598	19.000
0.104	0.417	0.020	0.030	1.667	0.104	0.005612	19.640
0.104	0.417	0.020	0.030	1.667	0.104	0.008910	20.860
0.104	0.417	0.020	0.030	1.667	0.104	0.013593	23.860
0.104	0.417	0.020	0.030	1.667	0.104	0.018912	25.450
0.104	0.417	0.020	0.030	1.667	0.104	0.026238	28.830
0.111	0.250	0.082	0.040	2.222	0.139	0.000412	19.100
0.111	0.250	0.082	0.040	2.222	0.139	0.000886	19.310
0.111	0.250	0.082	0.040	2.222	0.139	0.001525	20.220
0.111	0.250	0.082	0.040	2.222	0.139	0.002183	21.200
0.111	0.250	0.082	0.040	2.222	0.139	0.002862	22.230
0.111	0.250	0.082	0.040	2.222	0.139	0.003715	24.280
0.111	0.444	0.022	0.040	3.556	0.139	0.001955	19.000
0.111	0.444	0.022	0.040	3.556	0.139	0.003963	19.130
0.111	0.444	0.022	0.040	3.556	0.139	0.006252	19.850
0.111	0.444	0.022	0.040	3.556	0.139	0.008541	20.560
0.111	0.444	0.022	0.040	3.556	0.139	0.010830	21.280
0.111	0.444	0.022	0.040	3.556	0.139	0.016707	23.880
0.111	0.333	0.022	0.040	3.556	0.139	0.001239	19.000
0.111	0.333	0.022	0.040	3.556	0.139	0.002571	19.195
0.111	0.333	0.022	0.040	3.556	0.139	0.005870	20.660
0.111	0.333	0.022	0.040	3.556	0.139	0.008434	21.530
0.111	0.333	0.022	0.040	3.556	0.139	0.011037	23.340
0.111	0.333	0.022	0.040	3.556	0.139	0.013145	25.070
0.167	0.556	0.049	0.083	2.222	0.194	0.002131	39.080
0.167	0.556	0.049	0.083	2.222	0.194	0.004356	39.250
0.167	0.556	0.049	0.083	2.222	0.194	0.007177	40.80[illegible]

0.167	0.556	0.049	0.083	2.222	0.194	0.009982	42.360
0.167	0.556	0.049	0.083	2.222	0.194	0.014636	44.200
0.167	0.556	0.049	0.083	2.222	0.194	0.018126	47.770
0.050	0.112	0.010	0.018	1.000	0.087	0.000608	39.000
0.050	0.112	0.010	0.018	1.000	0.087	0.001643	39.000
0.050	0.112	0.010	0.018	1.000	0.087	0.003008	41.550
0.050	0.112	0.010	0.018	1.000	0.087	0.004373	43.196
0.050	0.112	0.010	0.018	1.000	0.087	0.006502	47.280
0.050	0.112	0.010	0.018	1.000	0.087	0.008415	51.990
0.167	0.444	0.082	0.083	2.222	0.194	0.001068	39.130
0.167	0.444	0.082	0.083	2.222	0.194	0.002280	39.460
0.167	0.444	0.082	0.083	2.222	0.194	0.003765	40.750
0.167	0.444	0.082	0.083	2.222	0.194	0.005351	42.400
0.167	0.444	0.082	0.083	2.222	0.194	0.006939	44.040
0.167	0.444	0.082	0.083	2.222	0.194	0.009510	46.940
0.063	0.150	0.022	0.018	1.000	0.087	0.000797	39.010
0.063	0.150	0.022	0.018	1.000	0.087	0.001860	39.700
0.063	0.150	0.022	0.018	1.000	0.087	0.003194	41.030
0.063	0.150	0.022	0.018	1.000	0.087	0.004527	42.376
0.063	0.150	0.022	0.018	1.000	0.087	0.006531	46.050
0.063	0.150	0.022	0.018	1.000	0.087	0.008271	49.700
0.104	0.417	0.017	0.030	2.667	0.125	0.002480	28.000
0.104	0.417	0.017	0.030	2.667	0.125	0.005040	28.156
0.104	0.417	0.017	0.030	2.667	0.125	0.007979	28.970
0.104	0.417	0.017	0.030	2.667	0.125	0.010918	29.790
0.104	0.417	0.017	0.030	2.667	0.125	0.017228	31.120
0.104	0.417	0.017	0.030	2.667	0.125	0.021132	33.300
0.139	0.250	0.049	0.111	2.222	0.194	0.000416	39.130
0.139	0.250	0.049	0.111	2.222	0.194	0.000973	39.500
0.139	0.250	0.049	0.111	2.222	0.194	0.002031	41.640
0.139	0.250	0.049	0.111	2.222	0.194	0.003088	43.830
0.139	0.250	0.049	0.111	2.222	0.194	0.004340	46.200
0.139	0.250	0.049	0.111	2.222	0.194	0.005744	50.780
0.125	0.333	0.020	0.063	1.667	0.146	0.002095	39.000
0.125	0.333	0.020	0.063	1.667	0.146	0.004898	40.420
0.125	0.333	0.020	0.063	1.667	0.146	0.008000	42.390
0.125	0.333	0.020	0.063	1.667	0.146	0.012571	47.010
0.125	0.333	0.020	0.063	1.667	0.146	0.018734	53.310
0.125	0.333	0.020	0.063	1.667	0.146	0.025033	59.640
0.167	0.333	0.082	0.111	2.222	0.194	0.000649	39.180
0.167	0.333	0.082	0.111	2.222	0.194	0.001468	39.670
0.167	0.333	0.082	0.111	2.222	0.194	0.002687	41.760
0.167	0.333	0.082	0.111	2.222	0.194	0.003931	43.840
0.167	0.333	0.082	0.111	2.222	0.194	0.005419	46.930
0.167	0.333	0.082	0.111	2.222	0.194	0.007268	51.090

0.167	0.556	0.082	0.040	3.556	0.167	0.001036	28.160
0.167	0.556	0.082	0.040	3.556	0.167	0.002165	28.420
0.167	0.556	0.082	0.040	3.556	0.167	0.003377	29.100
0.167	0.556	0.082	0.040	3.556	0.167	0.004701	30.300
0.167	0.556	0.082	0.040	3.556	0.167	0.006026	31.500
0.167	0.556	0.082	0.040	3.556	0.167	0.007553	33.570
0.139	0.250	0.022	0.083	3.556	0.167	0.000612	28.050
0.139	0.250	0.022	0.083	3.556	0.167	0.001549	28.790
0.139	0.250	0.022	0.083	3.556	0.167	0.002827	30.310
0.139	0.250	0.022	0.083	3.556	0.167	0.004265	32.250
0.139	0.250	0.022	0.083	3.556	0.167	0.005921	35.710
0.139	0.250	0.022	0.083	3.556	0.167	0.007547	39.164
0.104	0.333	0.061	0.083	1.667	0.146	0.001764	39.240
0.104	0.333	0.061	0.083	1.667	0.146	0.003955	41.590
0.104	0.333	0.061	0.083	1.667	0.146	0.006313	44.840
0.104	0.333	0.061	0.083	1.667	0.146	0.009217	49.080
0.104	0.333	0.061	0.083	1.667	0.146	0.013214	55.470
0.104	0.333	0.061	0.083	1.667	0.146	0.016873	62.270
0.063	0.150	0.012	0.018	1.600	0.087	0.000926	39.000
0.063	0.150	0.012	0.018	1.600	0.087	0.002243	39.820
0.063	0.150	0.012	0.018	1.600	0.087	0.003823	41.210
0.063	0.150	0.012	0.018	1.600	0.087	0.005585	42.930
0.063	0.150	0.012	0.018	1.600	0.087	0.007672	46.760
0.063	0.150	0.012	0.018	1.600	0.087	0.009705	50.560
0.063	0.112	0.022	0.038	1.000	0.112	0.000357	56.140
0.063	0.112	0.022	0.038	1.000	0.112	0.001223	58.440
0.063	0.112	0.022	0.038	1.000	0.112	0.002389	62.070
0.063	0.112	0.022	0.038	1.000	0.112	0.003631	66.360
0.063	0.112	0.022	0.038	1.000	0.112	0.005350	75.500
0.063	0.112	0.022	0.038	1.000	0.112	0.007138	84.970
0.167	0.444	0.022	0.111	3.556	0.194	0.002246	39.000
0.167	0.444	0.022	0.111	3.556	0.194	0.005004	40.210
0.167	0.444	0.022	0.111	3.556	0.194	0.008215	42.400
0.167	0.444	0.022	0.111	3.556	0.194	0.012743	45.300
0.167	0.444	0.022	0.111	3.556	0.194	0.018824	51.280
0.167	0.444	0.022	0.111	3.556	0.194	0.024193	56.940
0.075	0.150	0.037	0.038	1.000	0.112	0.000684	56.160
0.075	0.150	0.037	0.038	1.000	0.112	0.001881	58.470
0.075	0.150	0.037	0.038	1.000	0.112	0.003297	61.740
0.075	0.150	0.037	0.038	1.000	0.112	0.004938	67.310
0.075	0.150	0.037	0.038	1.000	0.112	0.006754	75.224
0.075	0.150	0.037	0.038	1.000	0.112	0.009405	84.200
0.194	0.556	0.049	0.111	3.556	0.222	0.001938	51.090
0.194	0.556	0.049	0.111	3.556	0.222	0.004005	51.380
0.194	0.556	0.049	0.111	3.556	0.222	0.006522	53.000

0.194	0.556	0.049	0.111	3.556	0.222	0.009180	55.130
0.194	0.556	0.049	0.111	3.556	0.222	0.011818	56.720
0.194	0.556	0.049	0.111	3.556	0.222	0.017031	60.490
0.167	0.333	0.037	0.030	4.000	0.146	0.000576	39.000
0.167	0.333	0.037	0.030	4.000	0.146	0.001298	39.160
0.167	0.333	0.037	0.030	4.000	0.146	0.002043	39.450
0.167	0.333	0.037	0.030	4.000	0.146	0.003028	40.340
0.167	0.333	0.037	0.030	4.000	0.146	0.004013	41.230
0.167	0.333	0.037	0.030	4.000	0.146	0.005108	42.300
0.104	0.417	0.020	0.030	5.000	0.125	0.002248	28.000
0.104	0.417	0.020	0.030	5.000	0.125	0.004507	28.080
0.104	0.417	0.020	0.030	5.000	0.125	0.007080	29.130
0.104	0.417	0.020	0.030	5.000	0.125	0.009669	30.170
0.104	0.417	0.020	0.030	5.000	0.125	0.012250	31.220
0.104	0.417	0.020	0.030	5.000	0.125	0.021477	33.400
0.167	0.250	0.082	0.040	5.333	0.194	0.000153	39.210
0.167	0.250	0.082	0.040	5.333	0.194	0.000373	39.670
0.167	0.250	0.082	0.040	5.333	0.194	0.000651	40.240
0.167	0.250	0.082	0.040	5.333	0.194	0.000945	40.900
0.167	0.250	0.082	0.040	5.333	0.194	0.001413	42.420
0.167	0.250	0.082	0.040	5.333	0.194	0.001967	44.060
0.063	0.200	0.012	0.018	2.400	0.087	0.001812	39.000
0.063	0.200	0.012	0.018	2.400	0.087	0.004032	40.000
0.063	0.200	0.012	0.018	2.400	0.087	0.006478	41.600
0.063	0.200	0.012	0.018	2.400	0.087	0.008924	43.200
0.063	0.200	0.012	0.018	2.400	0.087	0.013425	47.870
0.063	0.200	0.012	0.018	2.400	0.087	0.019270	54.290
0.139	0.333	0.049	0.040	6.667	0.194	0.001281	39.100
0.139	0.333	0.049	0.040	6.667	0.194	0.002643	39.350
0.139	0.333	0.049	0.040	6.667	0.194	0.004005	39.610
0.139	0.333	0.049	0.040	6.667	0.194	0.005525	40.350
0.139	0.333	0.049	0.040	6.667	0.194	0.007158	41.600
0.139	0.333	0.049	0.040	6.667	0.194	0.008767	42.840
0.167	0.556	0.049	0.040	6.667	0.194	0.001281	39.100
0.167	0.556	0.049	0.040	6.667	0.194	0.002643	39.350
0.167	0.556	0.049	0.040	6.667	0.194	0.004005	39.600
0.167	0.556	0.049	0.040	6.667	0.194	0.005525	40.350
0.167	0.556	0.049	0.040	6.667	0.194	0.007158	41.590
0.167	0.556	0.049	0.040	6.667	0.194	0.008767	42.840
0.167	0.250	0.049	0.083	5.333	0.194	0.000281	39.130
0.167	0.250	0.049	0.083	5.333	0.194	0.000704	39.562
0.167	0.250	0.049	0.083	5.333	0.194	0.001350	40.840
0.167	0.250	0.049	0.083	5.333	0.194	0.002147	42.710
0.167	0.250	0.049	0.083	5.333	0.194	0.002944	44.580
0.167	0.250	0.049	0.083	5.333	0.194	0.004127	47.500

0.075	0.200	0.010	0.038	1.600	0.112	0.002190	56.000
0.075	0.200	0.010	0.038	1.600	0.112	0.005742	60.570
0.075	0.200	0.010	0.038	1.600	0.112	0.009298	65.110
0.075	0.200	0.010	0.038	1.600	0.112	0.014666	76.990
0.075	0.200	0.010	0.038	1.600	0.112	0.019660	88.900
0.075	0.200	0.010	0.038	1.600	0.112	0.024266	100.000
0.125	0.250	0.020	0.063	4.000	0.167	0.000881	51.000
0.125	0.250	0.020	0.063	4.000	0.167	0.001921	51.420
0.125	0.250	0.020	0.063	4.000	0.167	0.003620	53.610
0.125	0.250	0.020	0.063	4.000	0.167	0.005320	55.800
0.125	0.250	0.020	0.063	4.000	0.167	0.007563	58.370
0.125	0.250	0.020	0.063	4.000	0.167	0.009979	63.680
0.125	0.417	0.037	0.030	5.000	0.146	0.001434	39.090
0.125	0.417	0.037	0.030	5.000	0.146	0.002913	39.280
0.125	0.417	0.037	0.030	5.000	0.146	0.004483	39.860
0.125	0.417	0.037	0.030	5.000	0.146	0.006232	414.000
0.125	0.417	0.037	0.030	5.000	0.146	0.007981	42.530
0.125	0.417	0.037	0.030	5.000	0.146	0.009730	43.870
0.167	0.250	0.049	0.111	5.333	0.222	0.000223	51.240
0.167	0.250	0.049	0.111	5.333	0.222	0.000615	51.750
0.167	0.250	0.049	0.111	5.333	0.222	0.001218	53.170
0.167	0.250	0.049	0.111	5.333	0.222	0.002075	55.750
0.167	0.250	0.049	0.111	5.333	0.222	0.002931	58.320
0.167	0.250	0.049	0.111	5.333	0.222	0.003788	60.900
0.063	0.200	0.010	0.018	3.000	0.087	0.001938	39.000
0.063	0.200	0.010	0.018	3.000	0.087	0.004349	40.120
0.063	0.200	0.010	0.018	3.000	0.087	0.007154	41.860
0.063	0.200	0.010	0.018	3.000	0.087	0.010693	44.067
0.063	0.200	0.010	0.018	3.000	0.087	0.014381	48.710
0.063	0.200	0.010	0.018	3.000	0.087	0.017740	53.200
0.063	0.112	0.037	0.018	2.400	0.100	0.000283	51.145
0.063	0.112	0.037	0.018	2.400	0.100	0.000614	51.425
0.063	0.112	0.037	0.018	2.400	0.100	0.001253	53.560
0.063	0.112	0.037	0.018	2.400	0.100	0.001931	55.940
0.063	0.112	0.037	0.018	2.400	0.100	0.002609	58.320
0.063	0.112	0.037	0.018	2.400	0.100	0.003287	60.700
0.146	0.333	0.017	0.083	4.000	0.167	0.000789	51.080
0.146	0.333	0.017	0.083	4.000	0.167	0.002036	52.290
0.146	0.333	0.017	0.083	4.000	0.167	0.003772	54.880
0.146	0.333	0.017	0.083	4.000	0.167	0.005801	58.660
0.146	0.333	0.017	0.083	4.000	0.167	0.008121	64.730
0.146	0.333	0.017	0.083	4.000	0.167	0.010404	70.770
0.194	0.556	0.026	0.111	6.667	0.222	0.002543	51.000
0.194	0.556	0.026	0.111	6.667	0.222	0.005183	51.240
0.194	0.556	0.026	0.111	6.667	0.222	0.008909	53.480

0.194	0.556	0.026	0.111	6.667	0.222	0.012930	55.760
0.194	0.556	0.026	0.111	6.667	0.222	0.015878	58.040
0.194	0.556	0.026	0.111	6.667	0.222	0.027876	64.720
0.167	0.250	0.082	0.111	5.333	0.250	0.000104	56.500
0.167	0.250	0.082	0.111	5.333	0.250	0.000420	57.340
0.167	0.250	0.082	0.111	5.333	0.250	0.000811	58.630
0.167	0.250	0.082	0.111	5.333	0.250	0.001505	61.940
0.167	0.250	0.082	0.111	5.333	0.250	0.002199	65.250
0.167	0.250	0.082	0.111	5.333	0.250	0.002894	68.560
0.125	0.333	0.061	0.030	5.000	0.167	0.000814	51.220
0.125	0.333	0.061	0.030	5.000	0.167	0.001714	51.710
0.125	0.333	0.061	0.030	5.000	0.167	0.002614	52.196
0.125	0.333	0.061	0.030	5.000	0.167	0.003737	54.040
0.125	0.333	0.061	0.030	5.000	0.167	0.004903	56.140
0.125	0.333	0.061	0.030	5.000	0.167	0.006955	58.760
0.167	0.417	0.037	0.083	4.000	0.188	0.001826	56.100
0.167	0.417	0.037	0.083	4.000	0.188	0.003929	57.080
0.167	0.417	0.037	0.083	4.000	0.188	0.006544	59.810
0.167	0.417	0.037	0.083	4.000	0.188	0.009134	62.560
0.167	0.417	0.037	0.083	4.000	0.188	0.013079	67.580
0.167	0.417	0.037	0.083	4.000	0.188	0.018342	74.660
0.167	0.250	0.049	0.111	6.667	0.222	0.000232	51.330
0.167	0.250	0.049	0.111	6.667	0.222	0.000641	51.950
0.167	0.250	0.049	0.111	6.667	0.222	0.001295	53.770
0.167	0.250	0.049	0.111	6.667	0.222	0.002164	56.700
0.167	0.250	0.049	0.111	6.667	0.222	0.003032	59.620
0.167	0.250	0.049	0.111	6.667	0.222	0.004270	63.070
0.194	0.444	0.049	0.111	6.667	0.222	0.001256	51.120
0.194	0.444	0.049	0.111	6.667	0.222	0.002682	51.690
0.194	0.444	0.049	0.111	6.667	0.222	0.004488	53.840
0.194	0.444	0.049	0.111	6.667	0.222	0.006418	56.500
0.194	0.444	0.049	0.111	6.667	0.222	0.008330	59.163
0.194	0.444	0.049	0.111	6.667	0.222	0.012136	63.175
0.075	0.150	0.010	0.038	2.400	0.112	0.000913	56.000
0.075	0.150	0.010	0.038	2.400	0.112	0.002790	59.280
0.075	0.150	0.010	0.038	2.400	0.112	0.004805	62.990
0.075	0.150	0.010	0.038	2.400	0.112	0.007573	71.930
0.075	0.150	0.010	0.038	2.400	0.112	0.010329	81.370
0.075	0.150	0.010	0.038	2.400	0.112	0.013006	90.660
0.125	0.188	0.020	0.083	5.000	0.188	0.000233	56.250
0.125	0.188	0.020	0.083	5.000	0.188	0.000622	56.670
0.125	0.188	0.020	0.083	5.000	0.188	0.001665	59.800
0.125	0.188	0.020	0.083	5.000	0.188	0.002717	62.980
0.125	0.188	0.020	0.083	5.000	0.188	0.005406	74.200
0.125	0.188	0.020	0.083	5.000	0.188	0.006845	81.280

0.075	0.150	0.037	0.018	3.000	0.112	0.000463	56.150
0.075	0.150	0.037	0.018	3.000	0.112	0.000972	56.460
0.075	0.150	0.037	0.018	3.000	0.112	0.001798	58.640
0.075	0.150	0.037	0.018	3.000	0.112	0.002218	89.140
0.222	0.556	0.082	0.111	6.667	0.250	0.001261	56.250
0.222	0.556	0.082	0.111	6.667	0.250	0.002736	57.250
0.222	0.556	0.082	0.111	6.667	0.250	0.004376	59.310
0.222	0.556	0.082	0.111	6.667	0.250	0.006202	62.540
0.222	0.556	0.082	0.111	6.667	0.250	0.008028	65.770
0.222	0.556	0.082	0.111	6.667	0.250	0.011080	68.840
0.194	0.250	0.082	0.111	6.667	0.250	0.000013	56.600
0.194	0.250	0.082	0.111	6.667	0.250	0.000293	57.660
0.194	0.250	0.082	0.111	6.667	0.250	0.000611	58.960
0.194	0.250	0.082	0.111	6.667	0.250	0.001234	62.340
0.194	0.250	0.082	0.111	6.667	0.250	0.001858	65.730
0.194	0.250	0.082	0.111	6.667	0.250	0.002481	69.126
0.167	0.333	0.061	0.063	5.000	0.188	0.000790	56.120
0.167	0.333	0.061	0.063	5.000	0.188	0.001717	56.990
0.167	0.333	0.061	0.063	5.000	0.188	0.002921	59.240
0.167	0.333	0.061	0.063	5.000	0.188	0.004233	62.080
0.167	0.333	0.061	0.063	5.000	0.188	0.005545	64.930
0.167	0.333	0.061	0.063	5.000	0.188	0.007559	69.340
0.087	0.250	0.010	0.038	3.000	0.112	0.003097	56.060
0.087	0.250	0.010	0.038	3.000	0.112	0.007463	59.700
0.087	0.250	0.010	0.038	3.000	0.112	0.012696	65.430
0.087	0.250	0.010	0.038	3.000	0.112	0.018267	74.520
0.087	0.250	0.010	0.038	3.000	0.112	0.023600	83.440
0.087	0.250	0.010	0.038	3.000	0.112	0.028932	92.360

APPENDIX F

COMPARISON BASED ON BEHAVIOR PREDICTION FROM VARYING THE VARIABLES INDIVIDUALLY

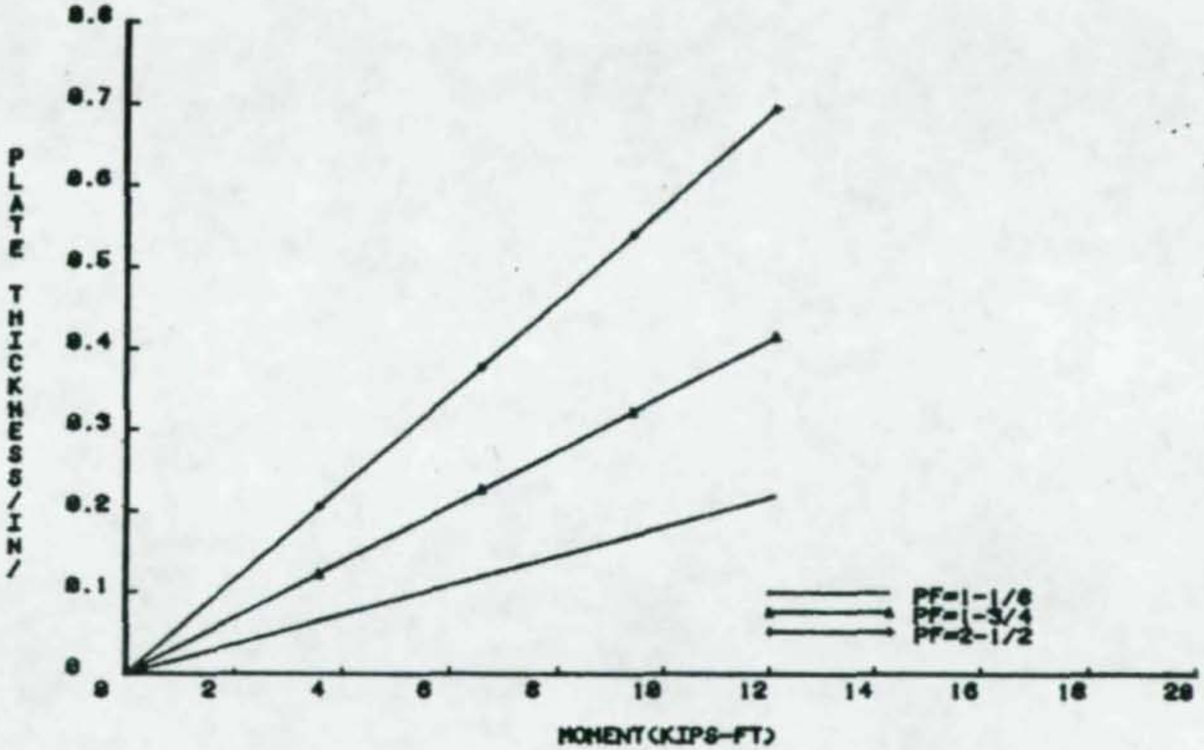

Figure F.1 Plate Thickness vs Moment Plot Obtained from Equation (3.5.1) By Varying P_f Through Low, Intermediate and High Values

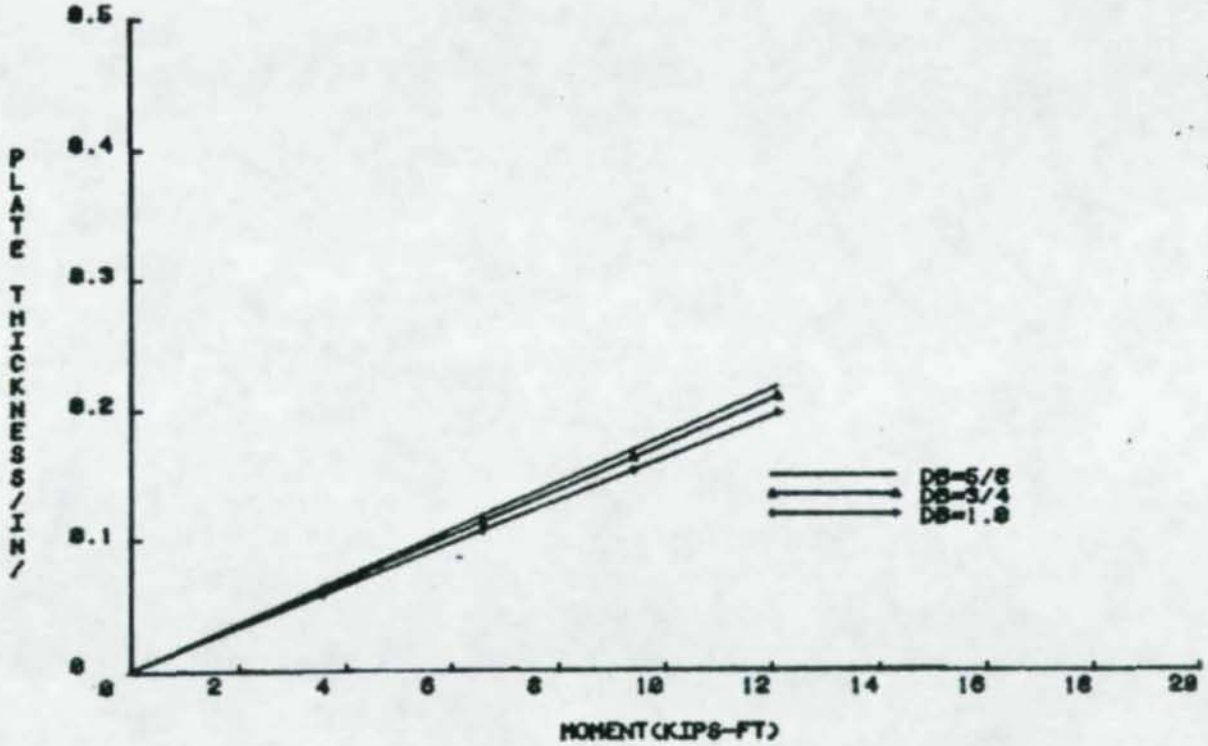

Figure F.2 Plate Thickness vs Moment Plot Obtained from Equation (3.5.11) By Varying d_b Through Low, Intermediate and High Values

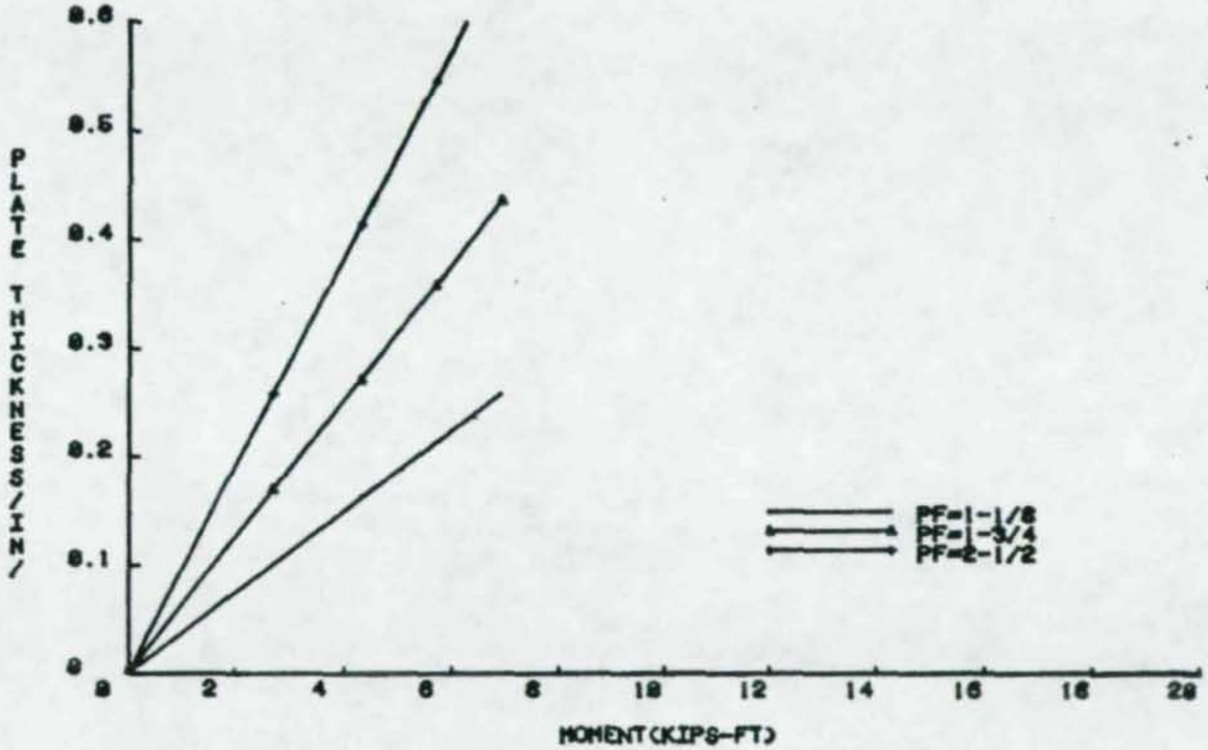

Figure F.3 Plate Thickness vs Moment Plot Obtained from Equation (3.5.15) by Varying P_f Through Low, Intermediate and High Values

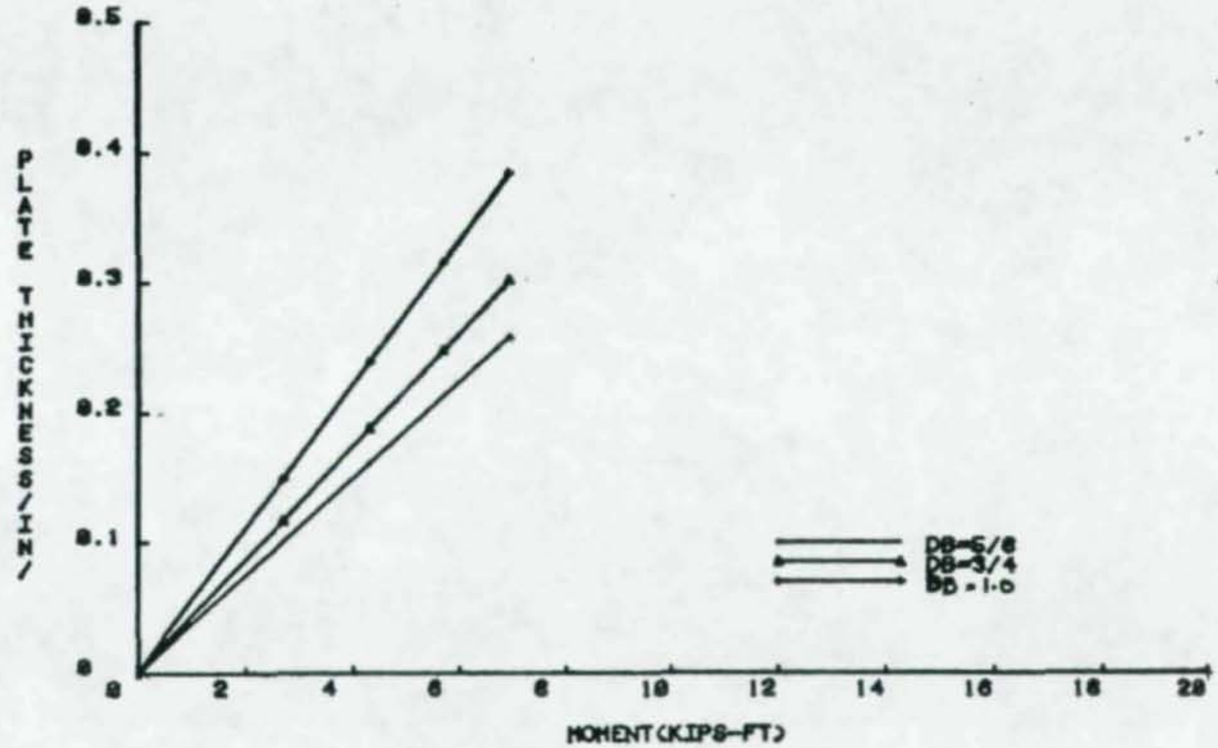

Figure F.4 Plate Thickness vs Moment Plot Obtained from Equation (3.5.15) by Varying d_b Through Low, Intermediate and High Values

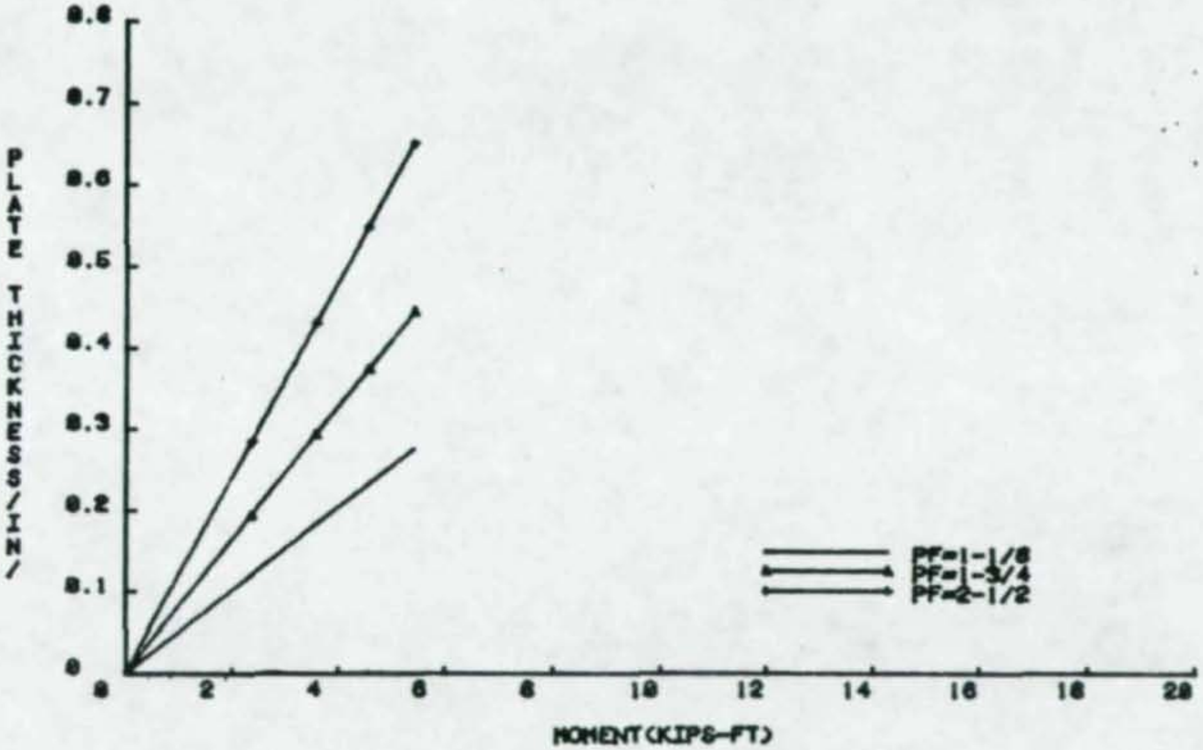

Figure F.5 Plate Thickness vs Moment Plots Obtained from Equation (3.5.17) by Varying P_f Through Low, Intermediate and High Values

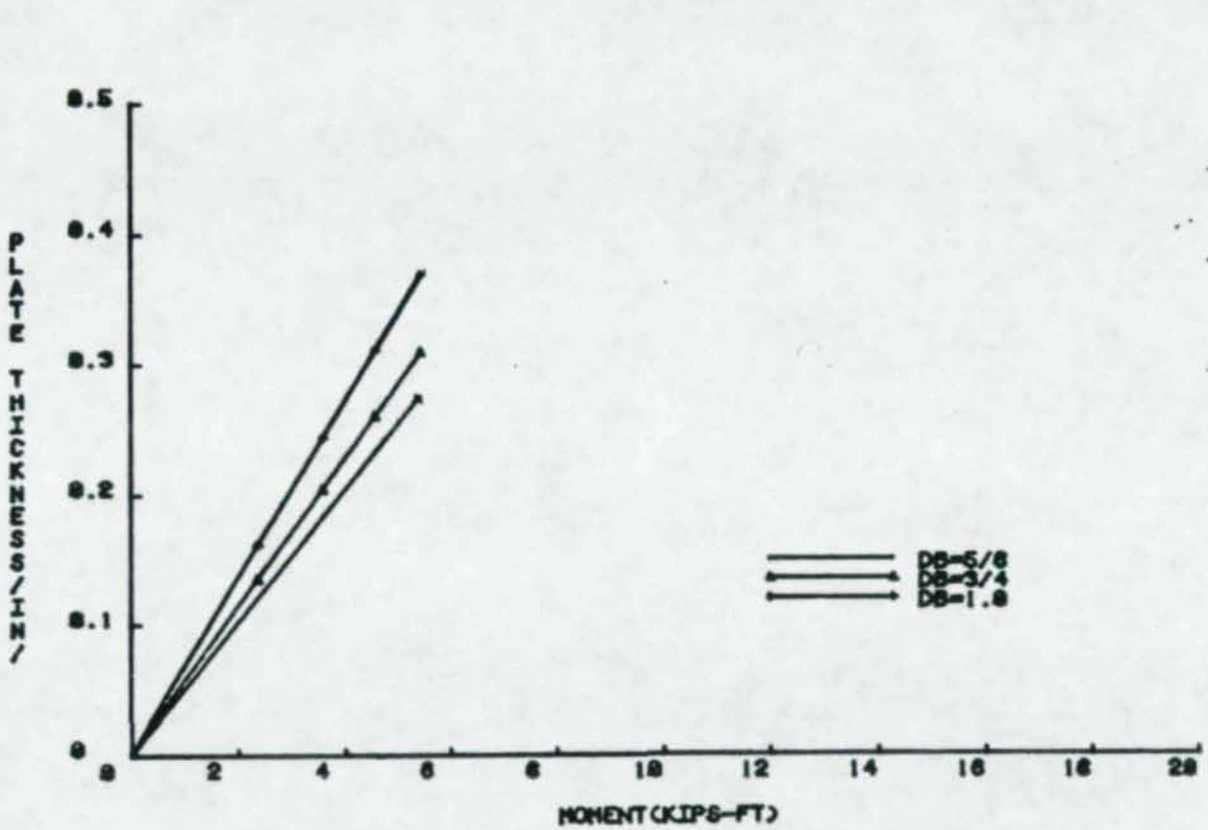

Figure F.6 Plate Thickness vs Moment Plots Obtained from Equation (3.5.17) by Varying d_b Through Low, Intermediate and High Values

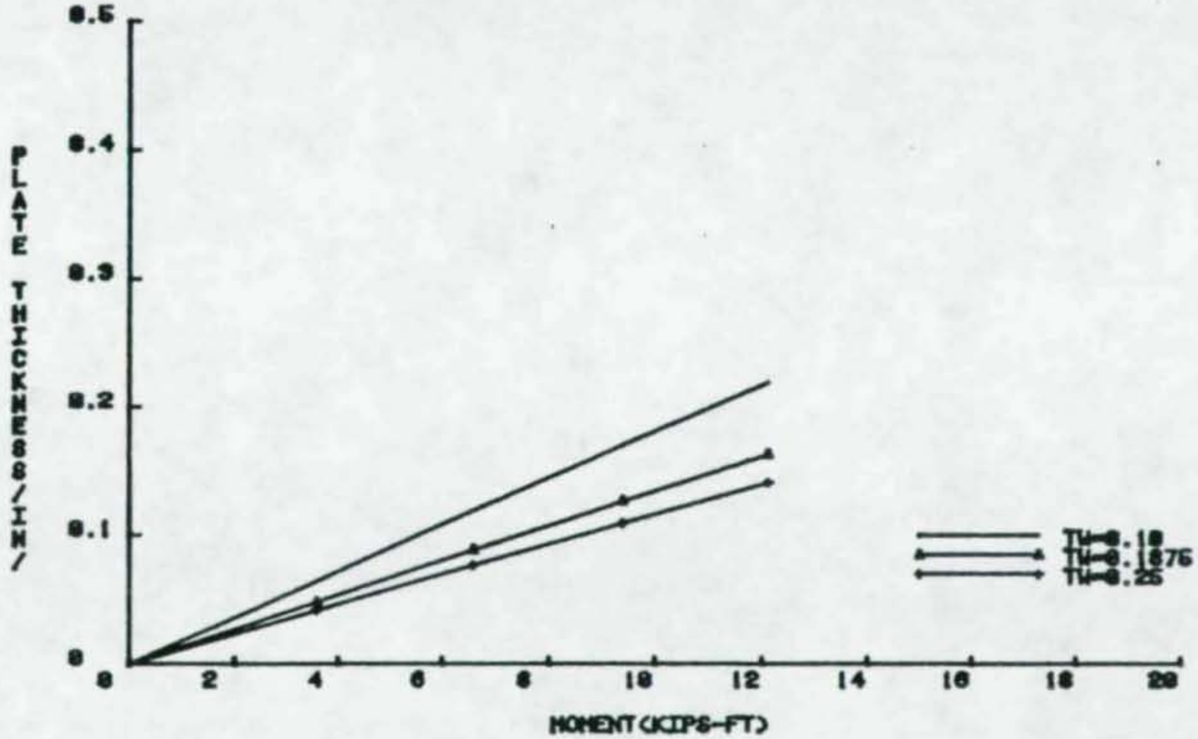

Figure F.7 Plate Thickness vs Moment Obtained from Equation (3.6.11) by Varying t_w Through Low, Intermediate and High Values

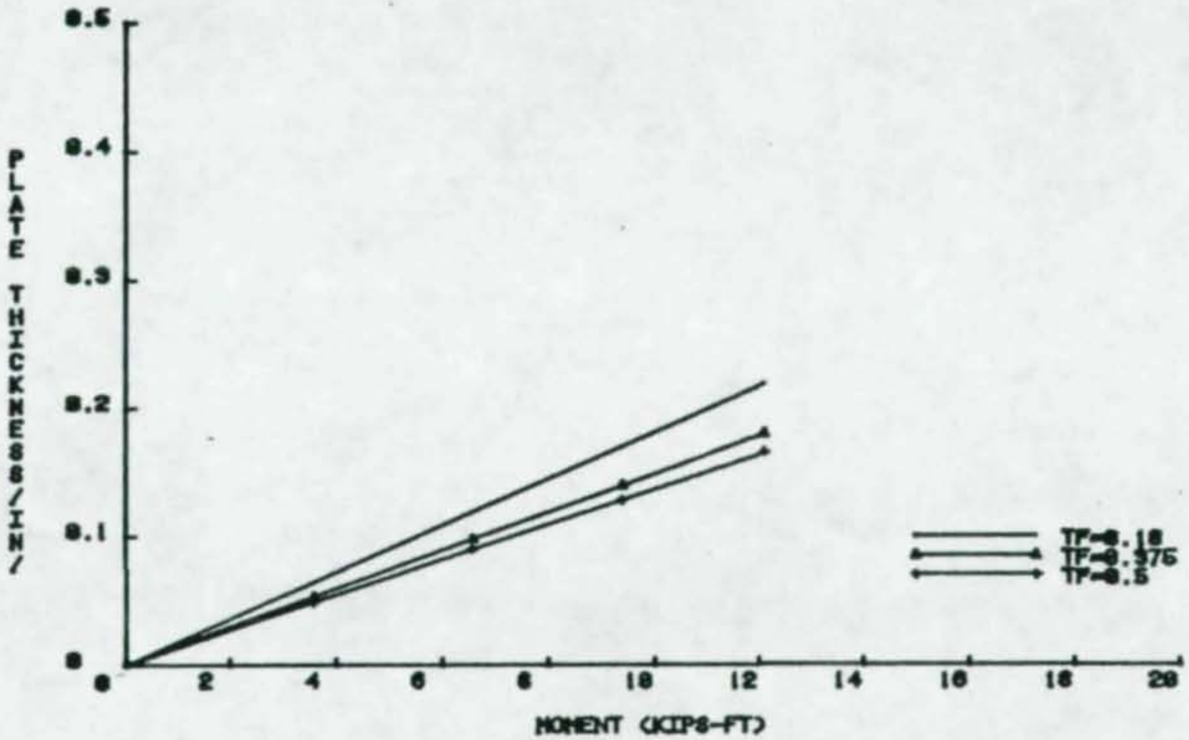

Figure F.8 Plate Thickness vs Moment Obtained from Equation (3.6.11) by Varying t_f Through Low, Intermediate and High Values

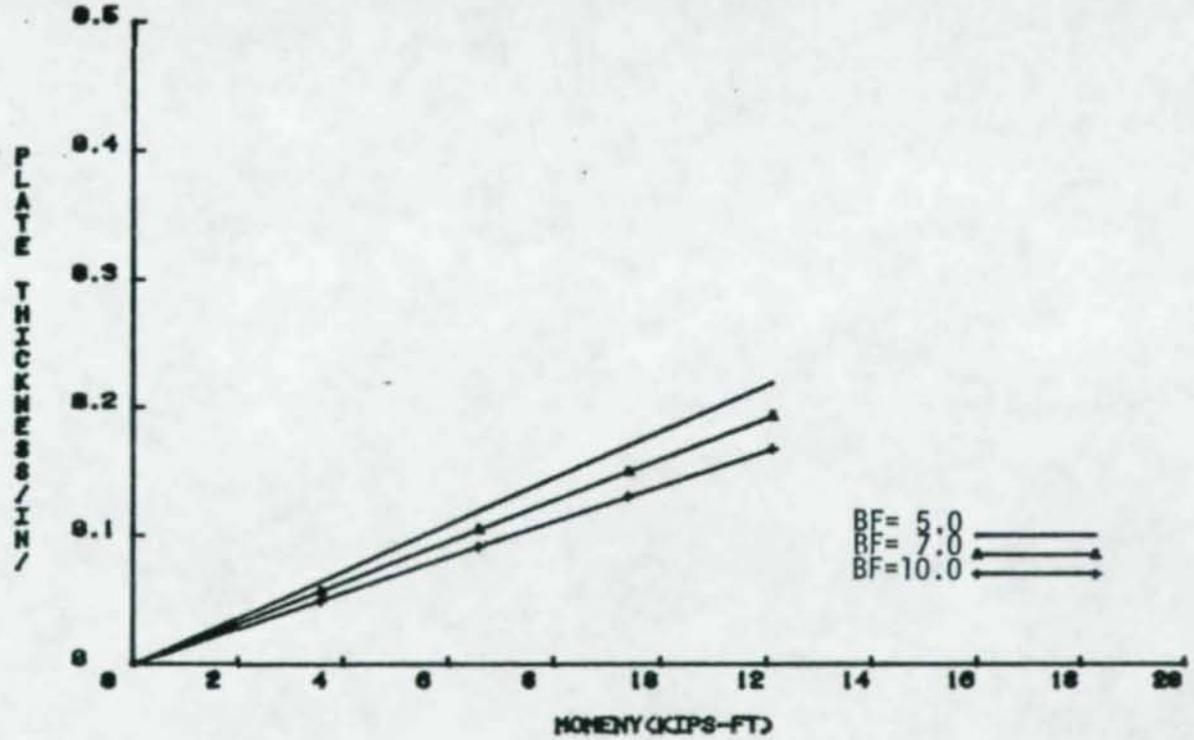

Figure F.9 Plate Thickness vs Moment Obtained From Equation (3.6.11) by Varying b_p Through Low, Intermediate and High $_p$ Values

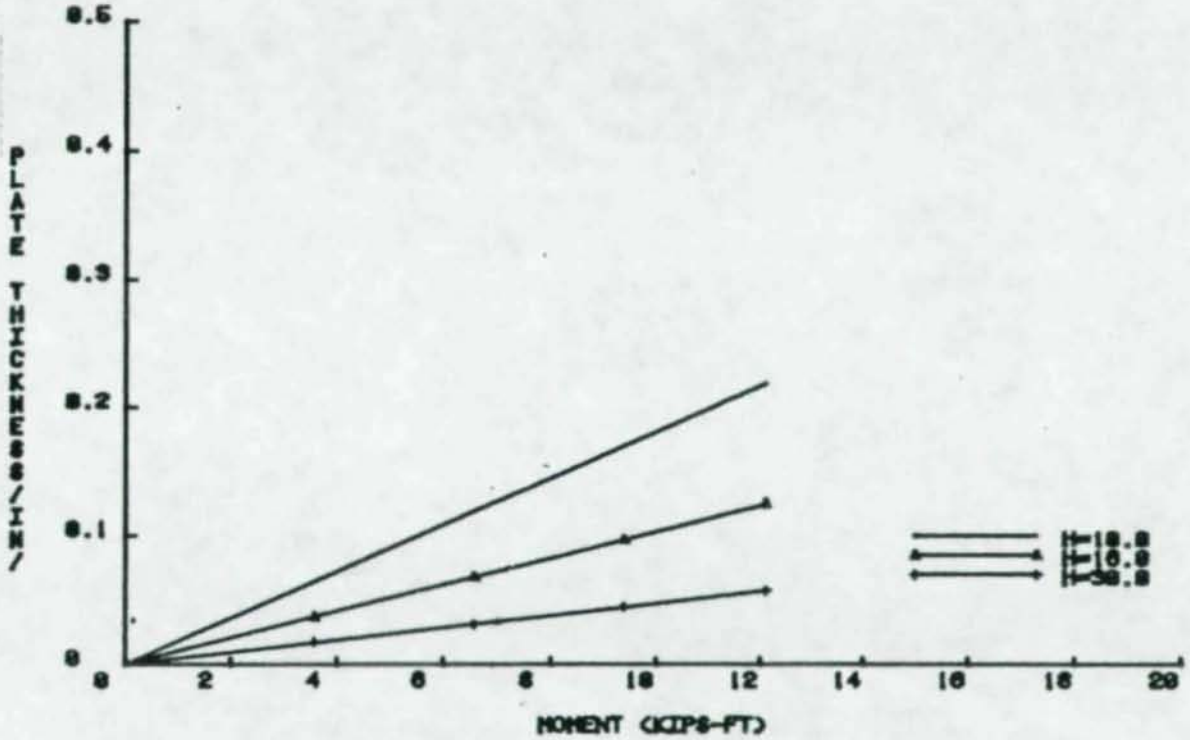

Figure F.10 Plate Thickness vs Moment Obtained from Equation (3.6.11) by Varying h, Through Low, Intermediate and High Values

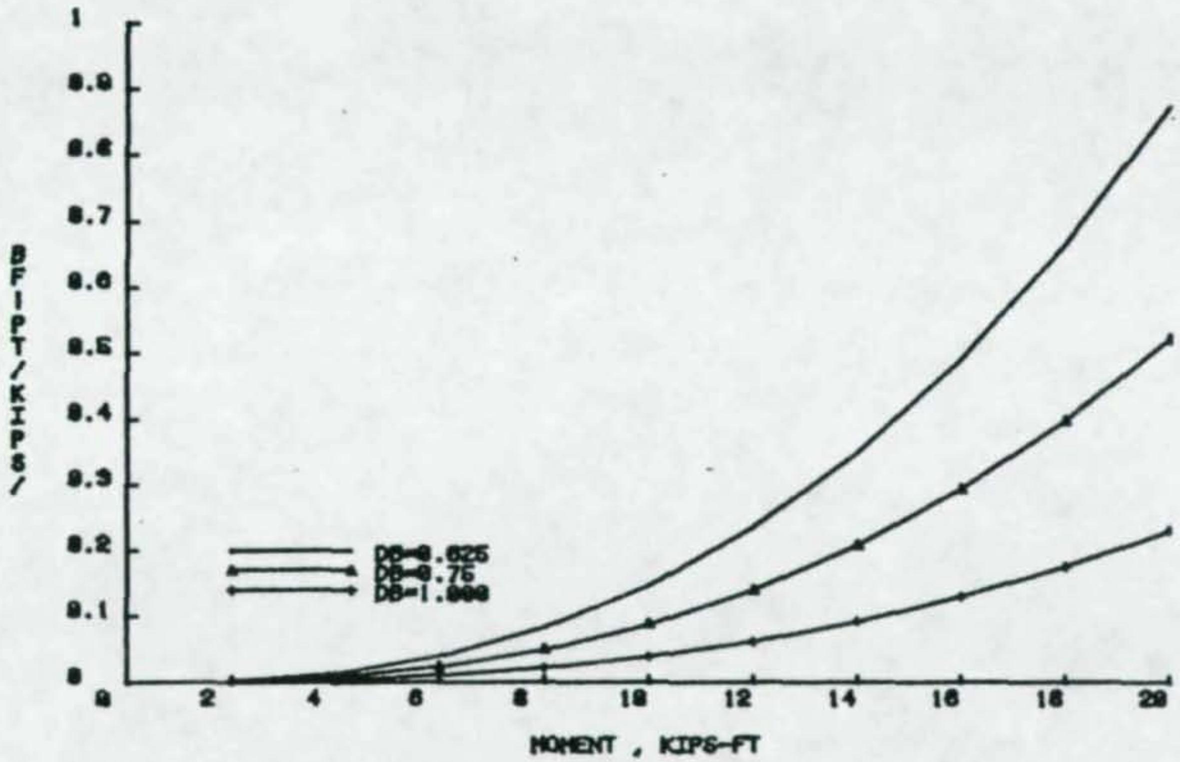

Figure F.11 $(B_F - P_T)$ Versus Moment Obtained from Equation (3.6.13) by Varying d_b Through Low, Intermediate and High Values

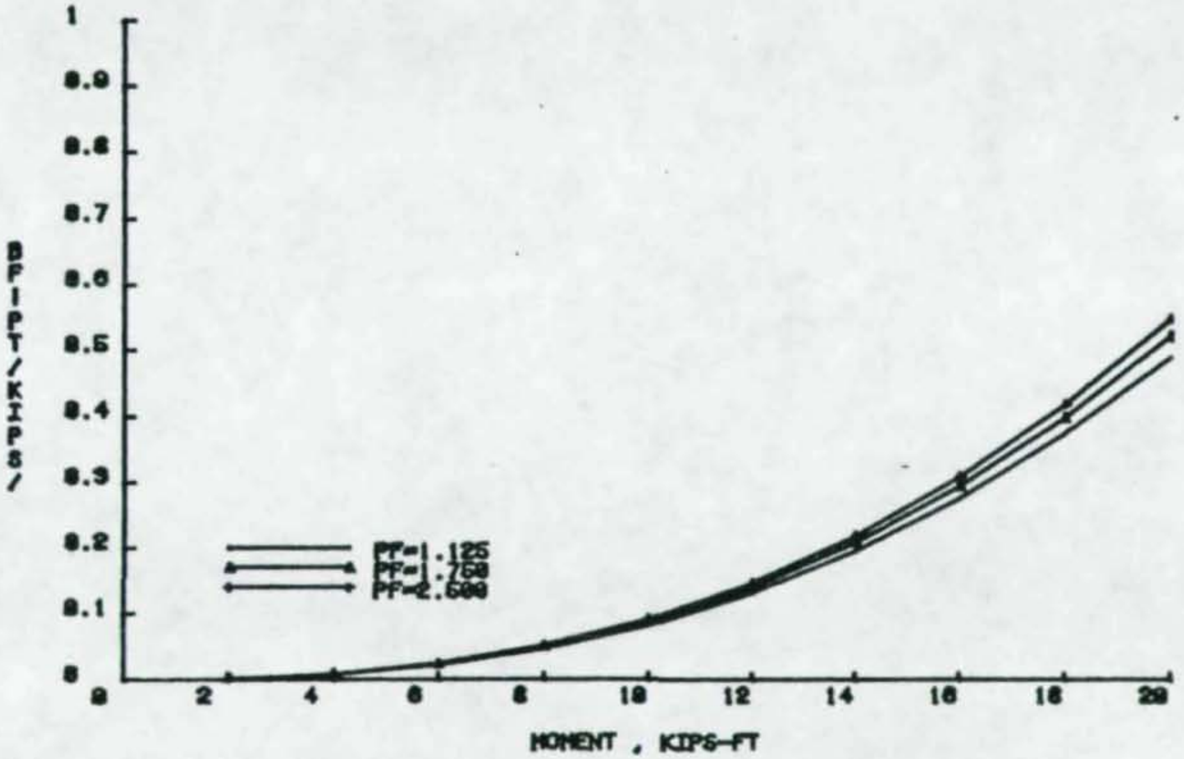

Figure F.12 $(B_F - P_T)$ Versus Moment Obtained from Equation (3.6.13) by Varying P_f Through Low, Intermediate and High

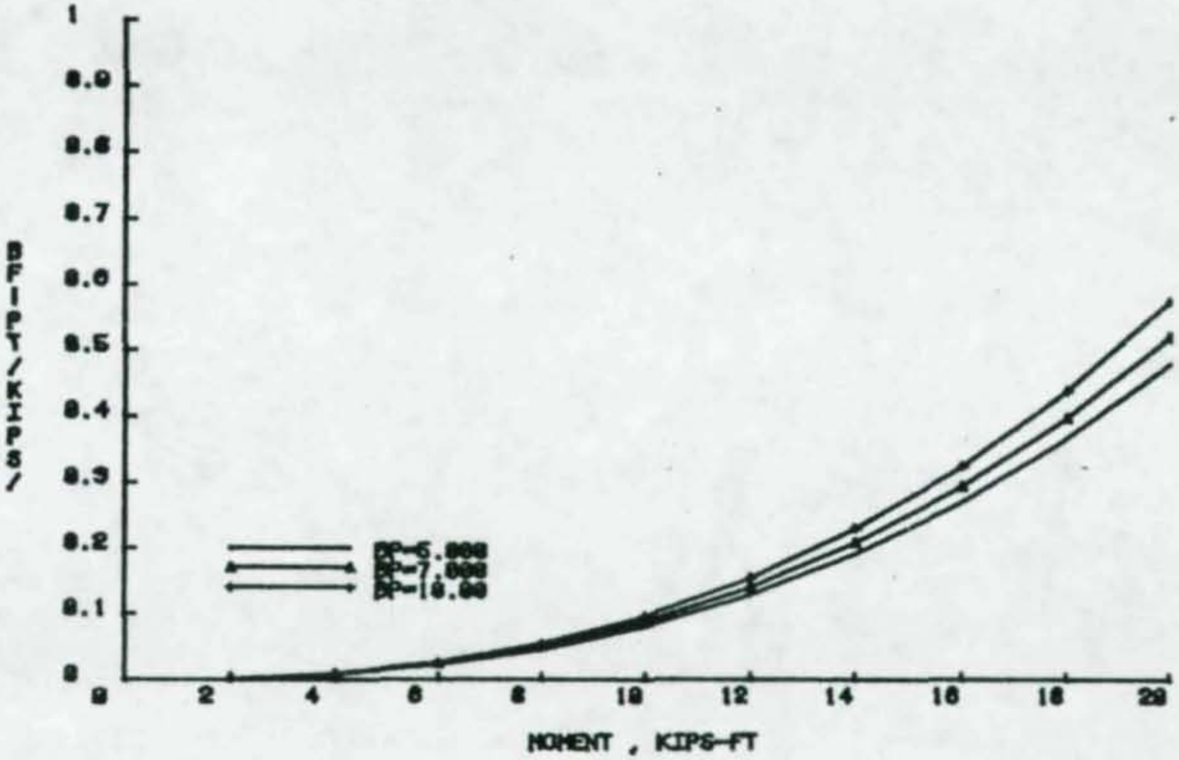

Figure F.13 $(B_F - P_T)$ Versus Moment Obtained from Equation (3.6.13) by Varying B_p Through Low, Intermediate and High

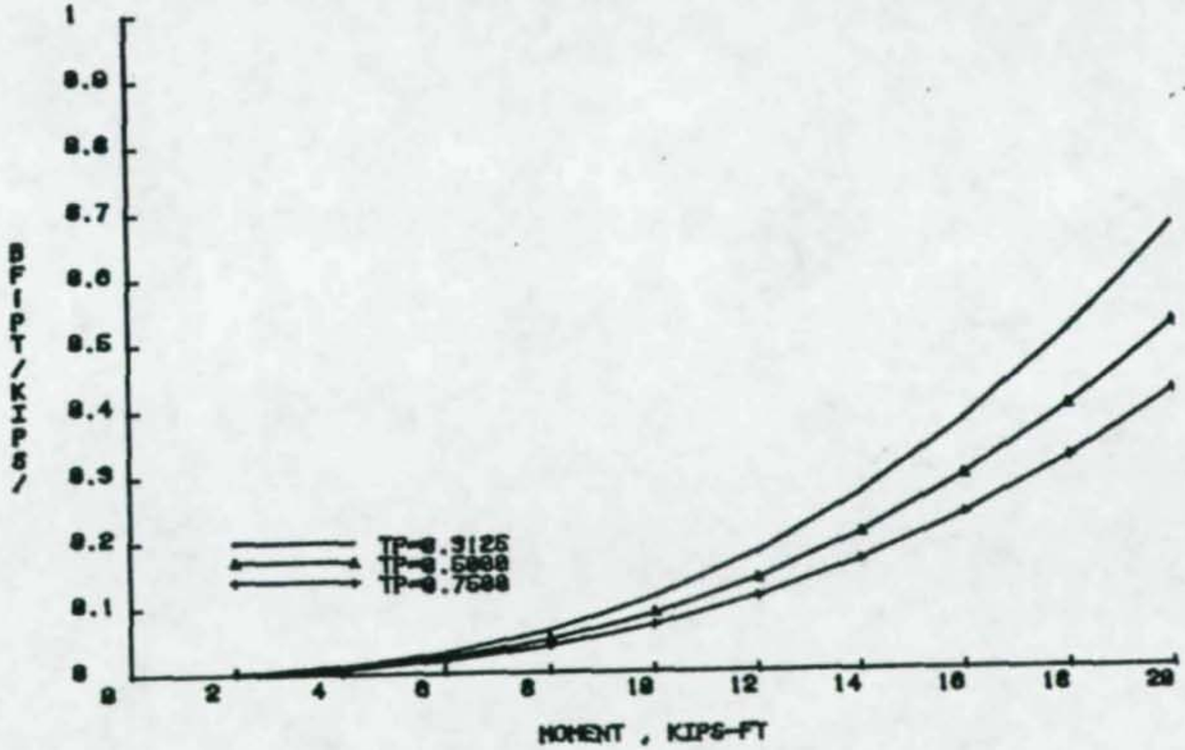

Figure F.14 $(B_F - P_T)$ Versus Moment Obtained from Equation (3.6.13) by Varying t_p Through Low, Intermediate and High

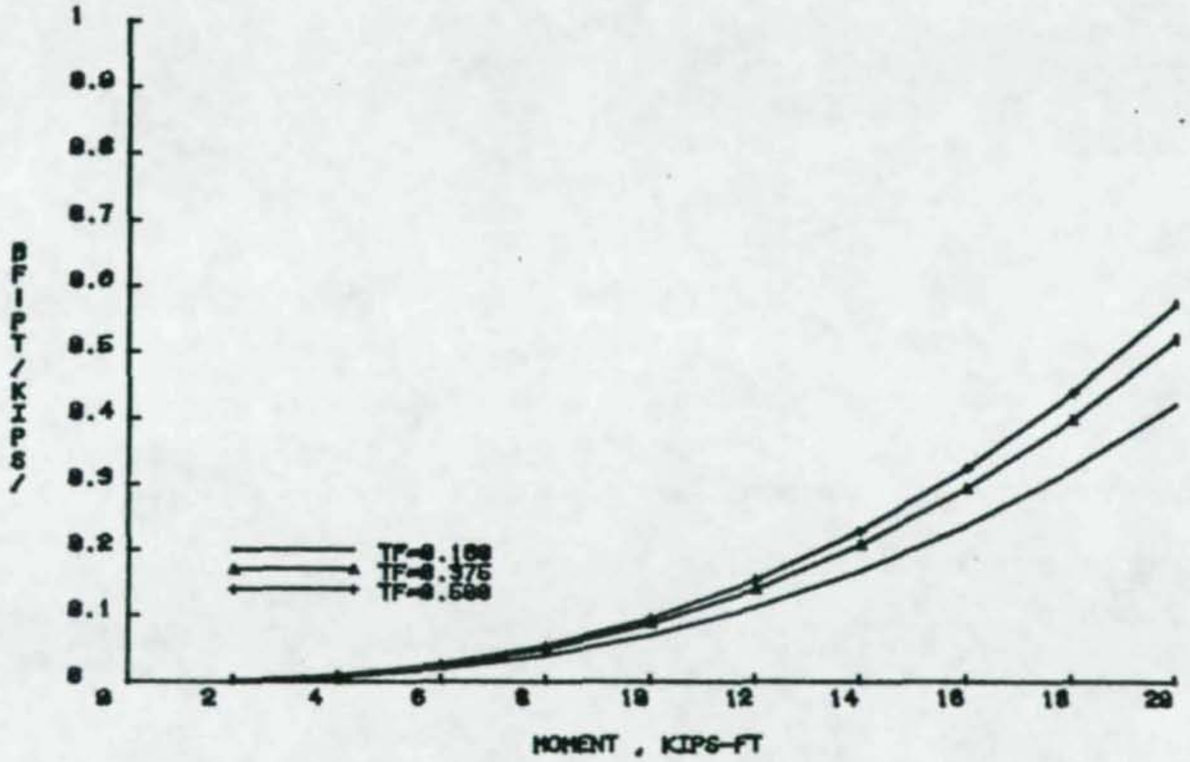

Figure F.15 $(B_F - P_T)$ Versus Moment Obtained from Equation (3.6.13) by Varying t_p Through Low, Intermediate and High

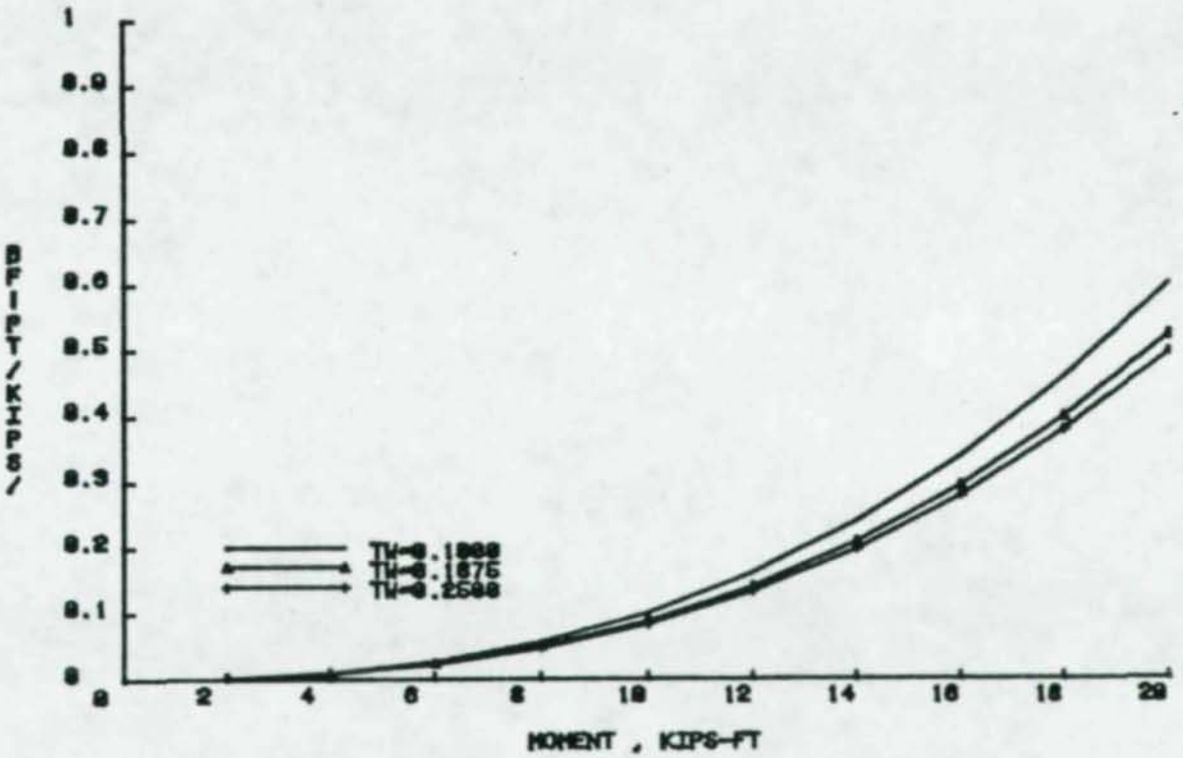

Figure F.16 $(B_F - P_T)$ Versus Moment Obtained from Equation (3.6.13) by Varying t_w, Through Low, Intermediate and High

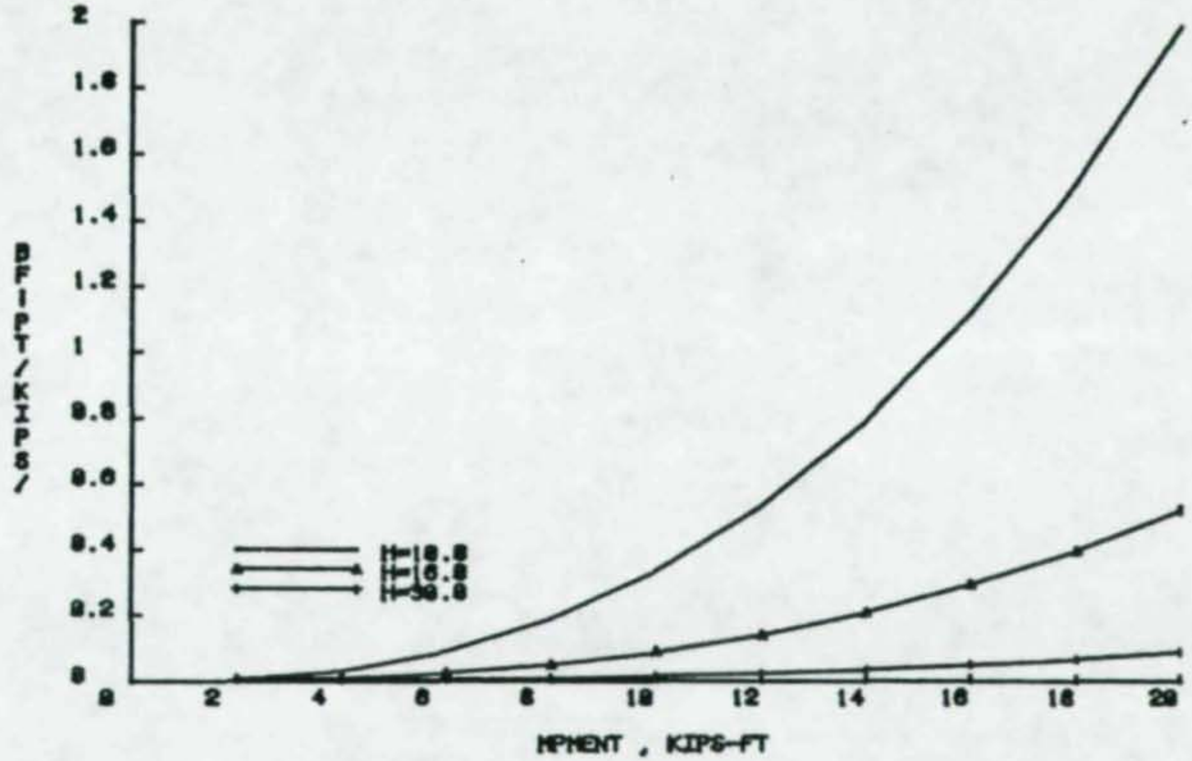

Figure F.17 (B_F - P_T) Versus Moment Obtained from Equation (3.6.13) by Varying h, Through Low, Intermediate and High

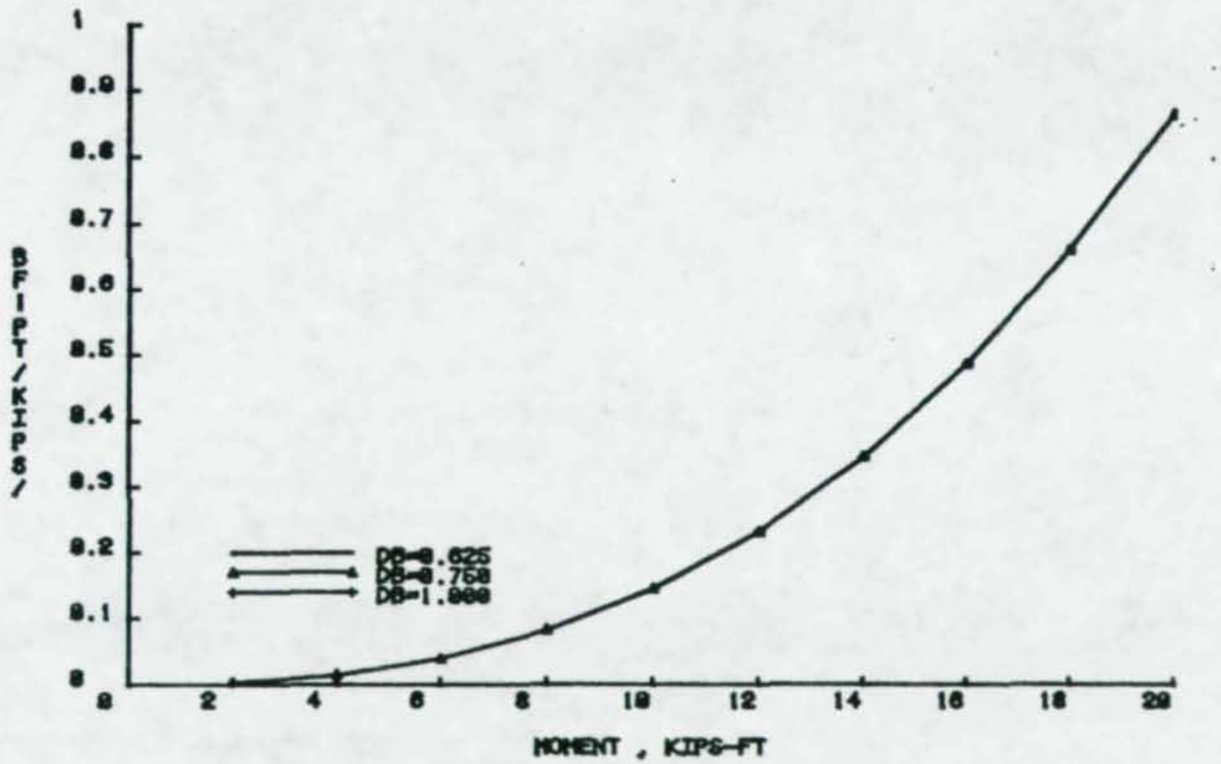

Figure F.18 $(B_F - P_T)$ Versus Moment Obtained from Equation 3.6.16) by varying d_b, Through Low, Intermediate and High

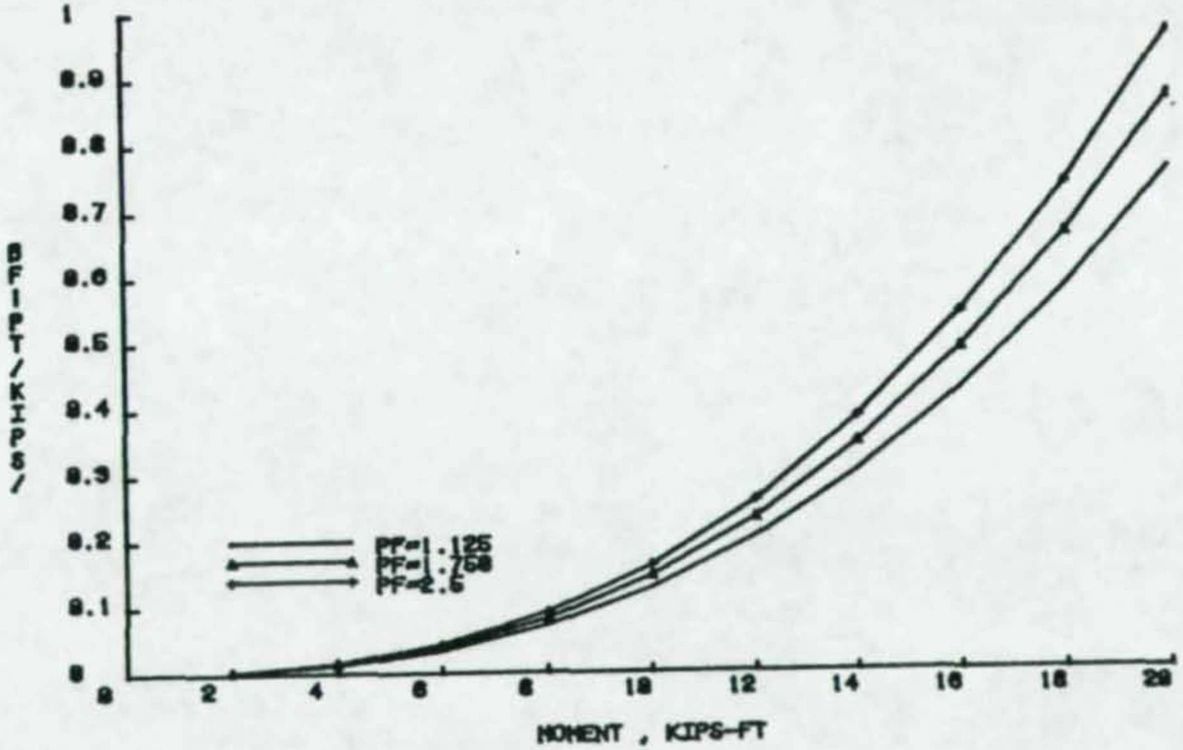

Figure F.19 $(B_F - P_T)$ Versus Moment Obtained from Equation (3.6.16) by Varying P_f, Through Low, Intermediate and High

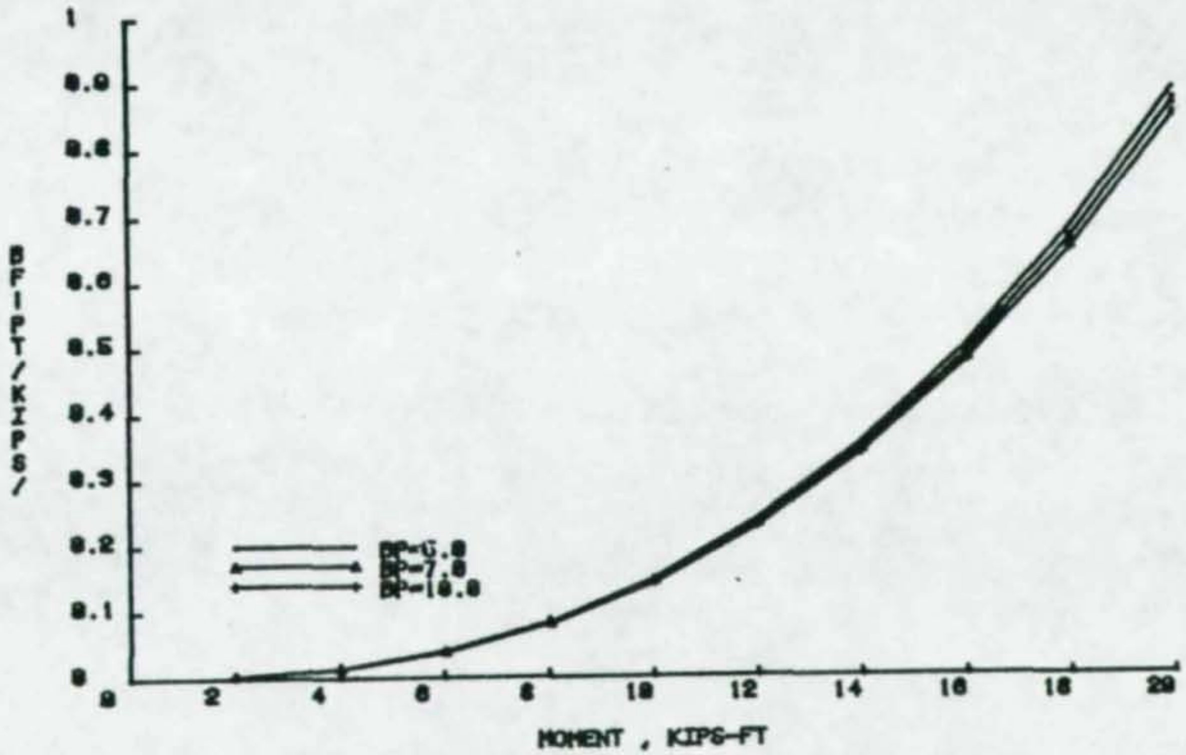

Figure F.20 $(B_F - P_T)$ Versus Moment Obtained from Equation (3.6.16) by Varying b_p, Through Low, Intermediate and High

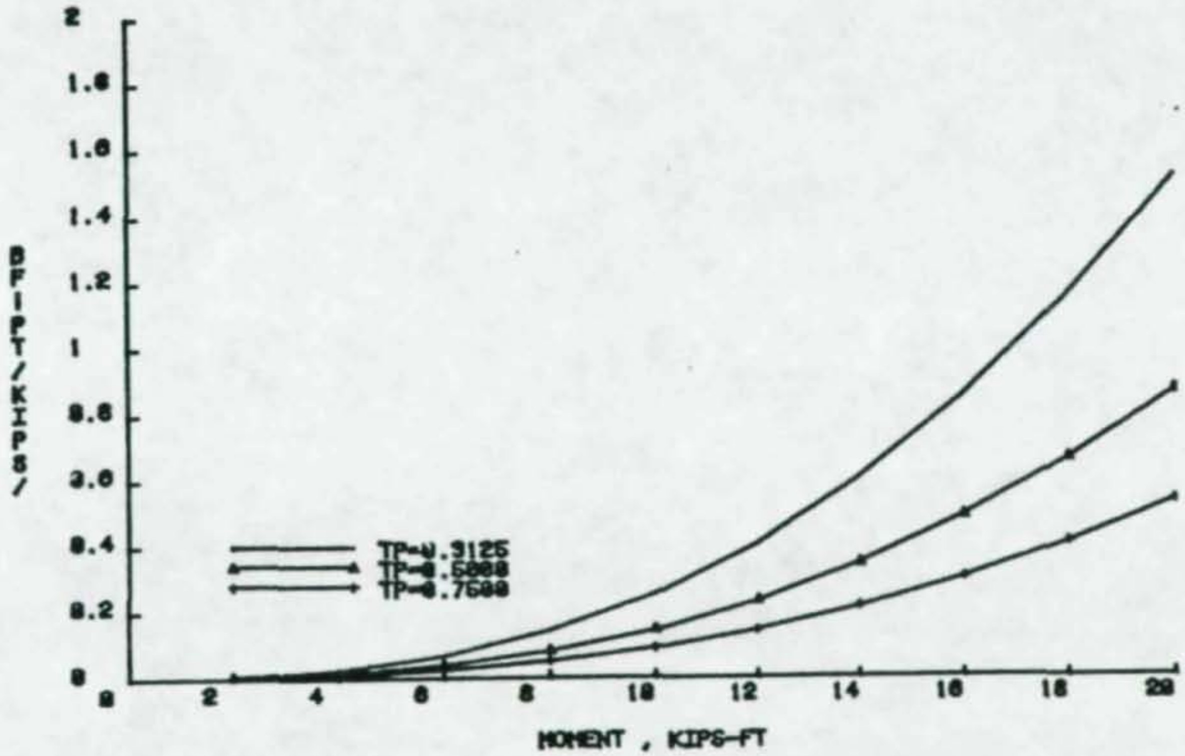

Figure F.21 $(B_F - P_T)$ Versus Moment Obtained from Equation (3.6.16) by Varying t_p, Through Low, Intermediate and High

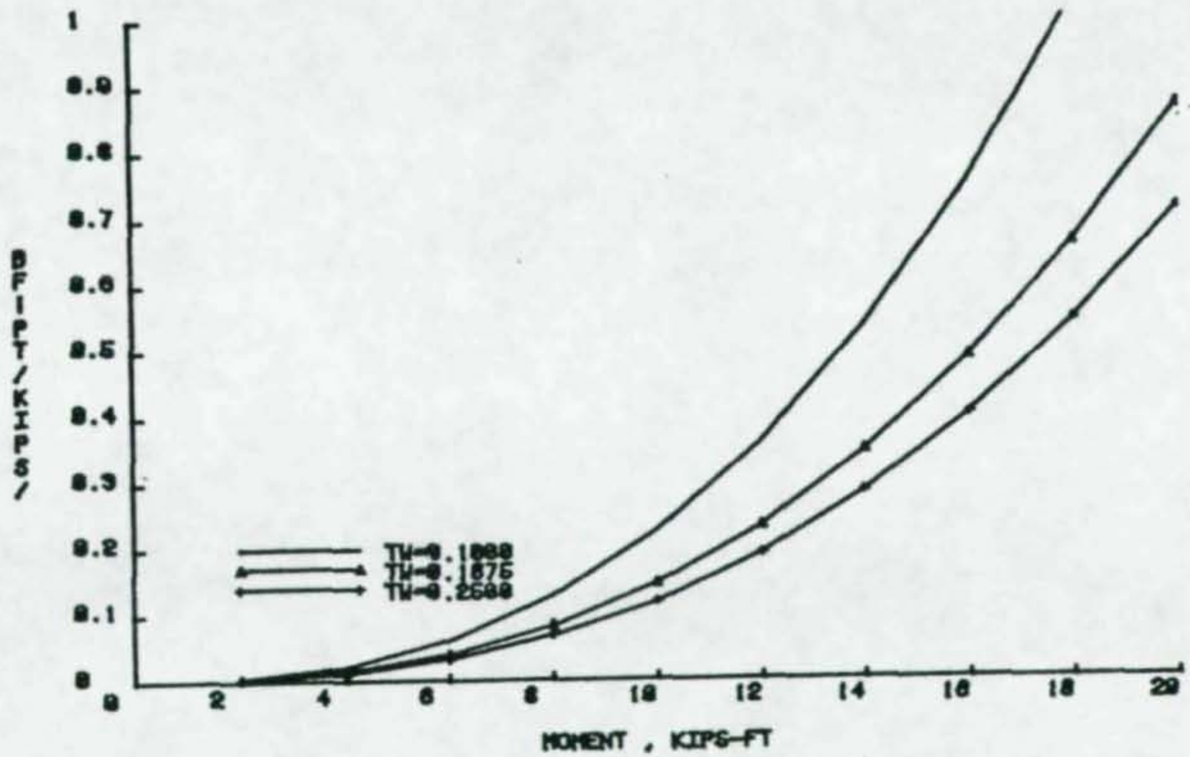

Figure F.22 $(B_F - P_T)$ Versus Moment Obtained from Equation (3.6.16) by Varying t_w, Through Low, Intermediate and High

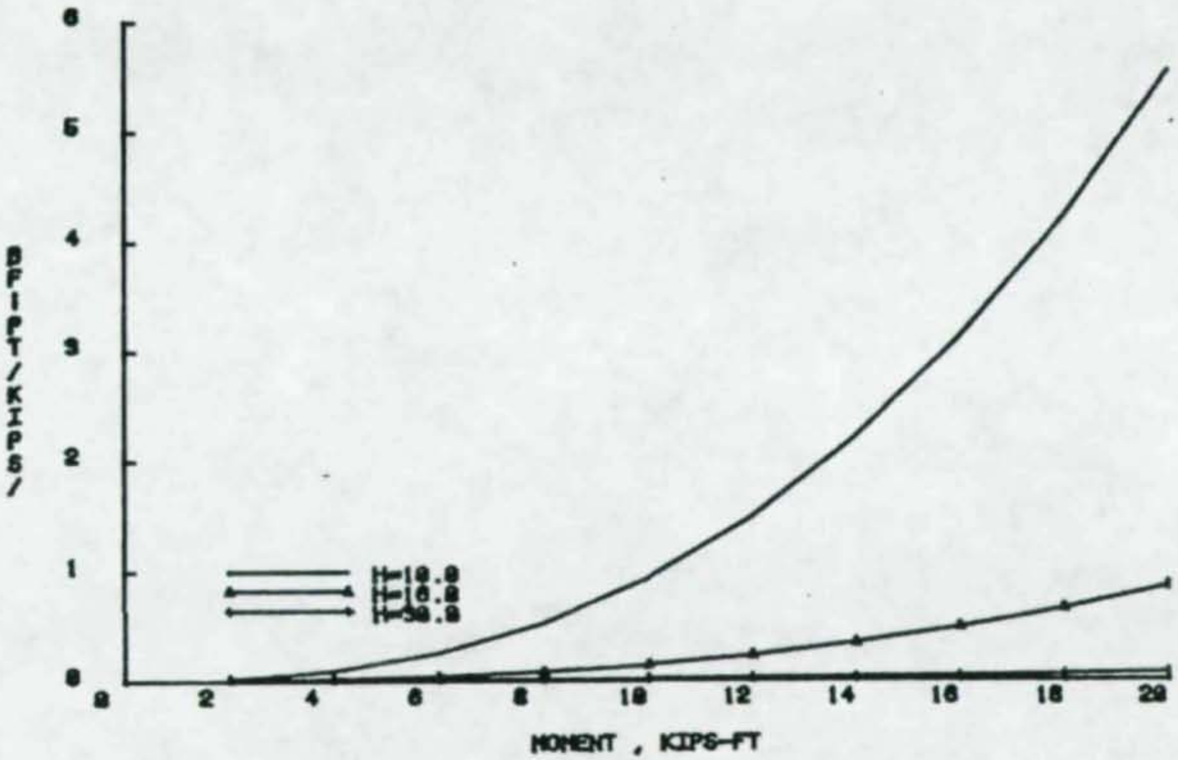

Figure F.23 $(B_F - P_T)$ Versus Moment Obtained from Equation (3.6.16) by Varying h, Through Low, Intermediate and High

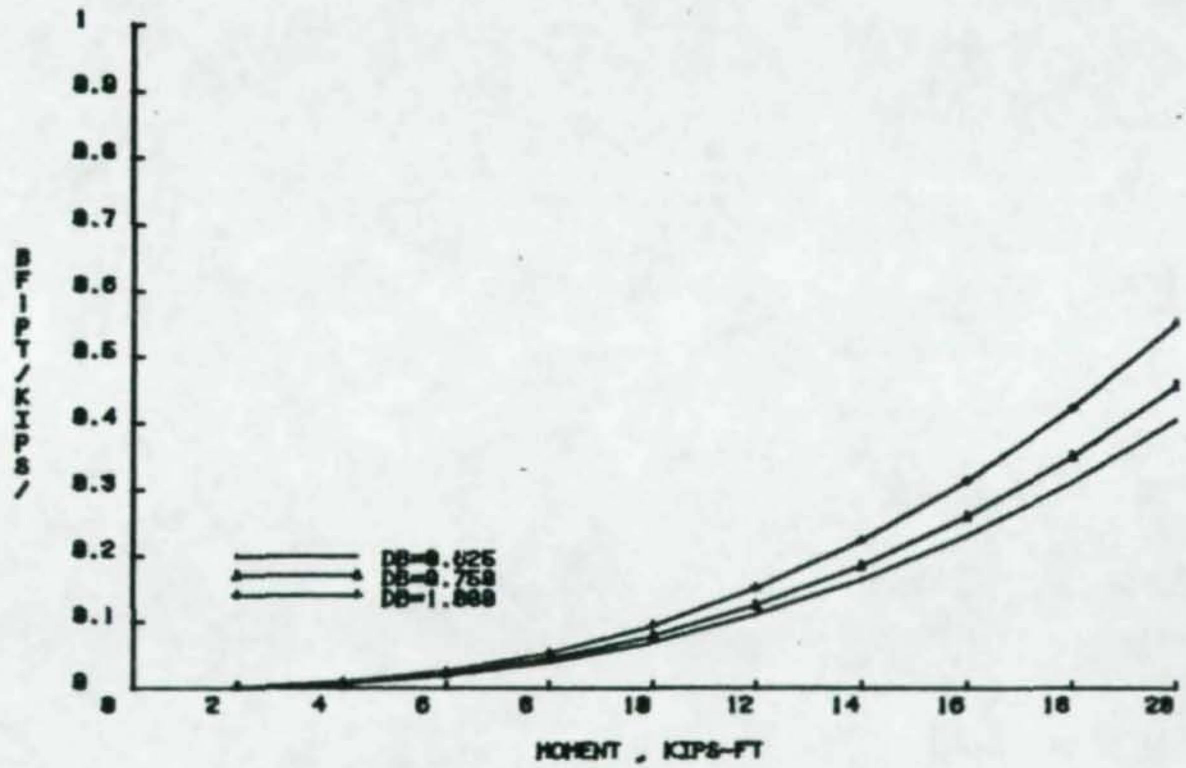

Figure F.24 (B_F - P_T) Versus Moment Obtained from Equation (3.6.18) by Varying d_b Through Low, Intermediate and High

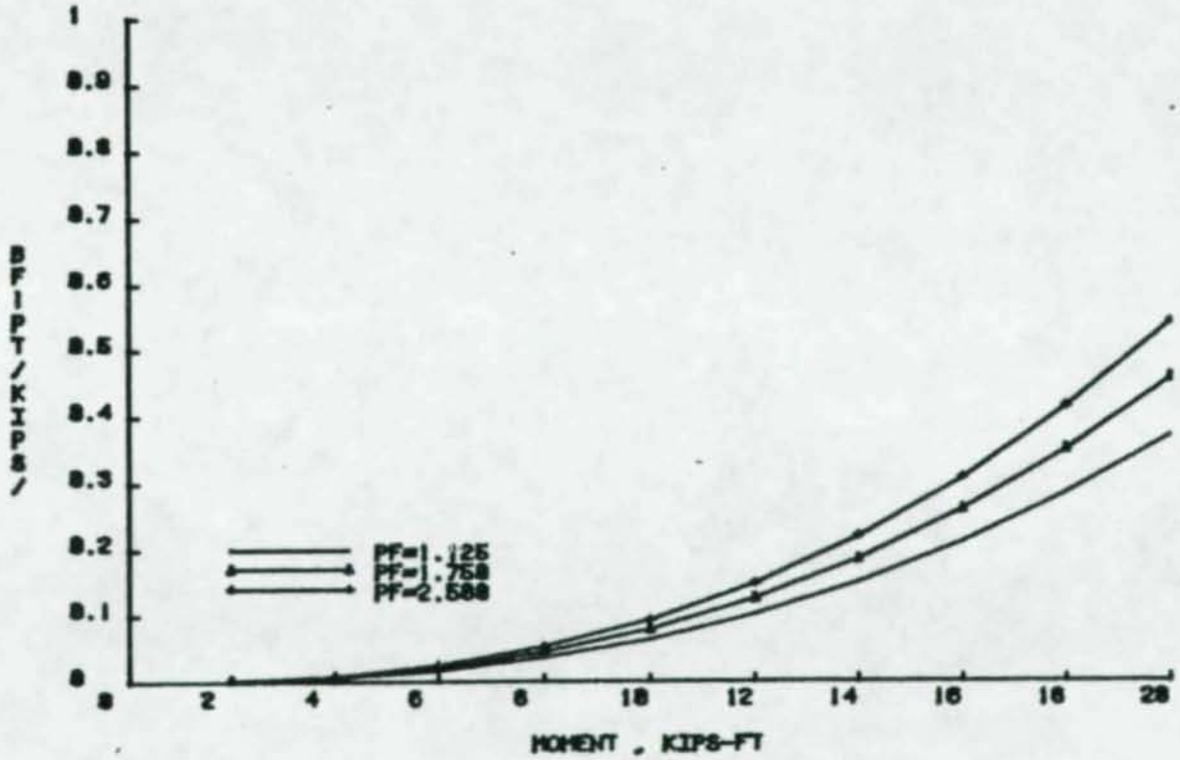

Figure F.25 $(B_F - P_T)$ Versus Moment Obtained from Equation (3.6.18) by Varying p_f Through Low, Intermediate and High

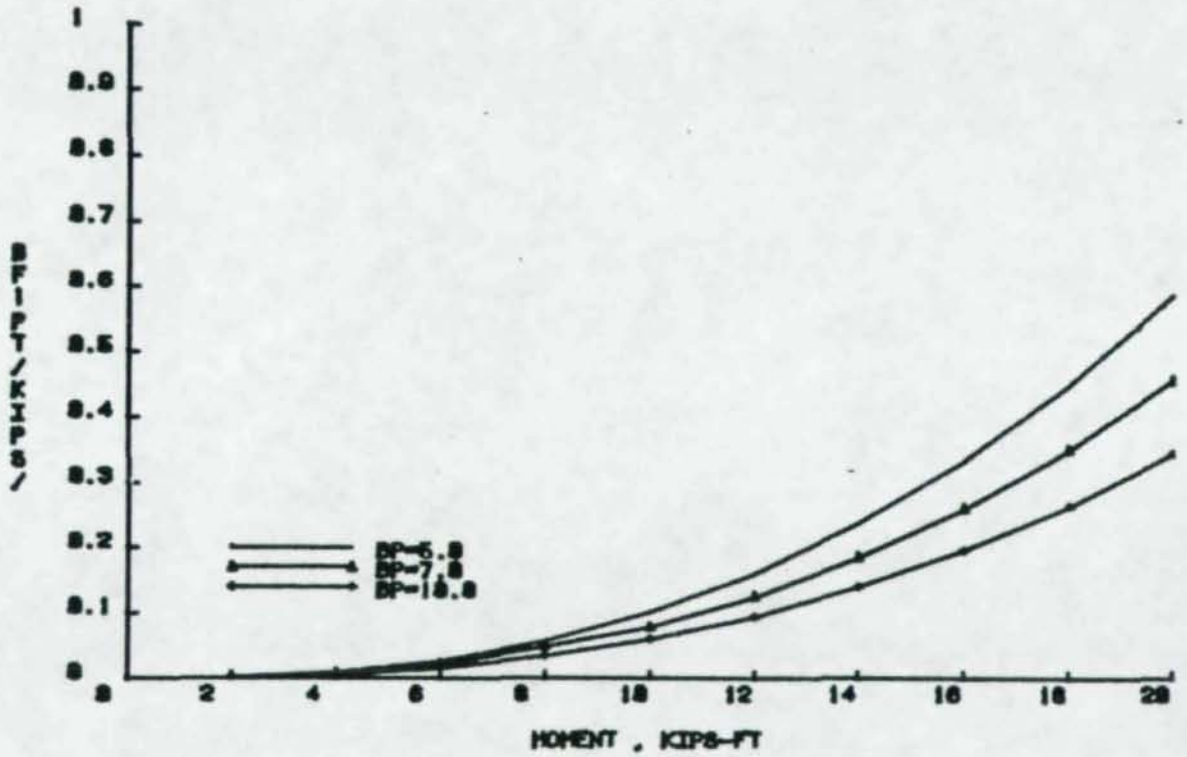

Figure F.26 $(B_F - P_T)$ Versus Moment Obtained from Equation (3.6.18) by Varying b_p, Through Low, Intermediate and High

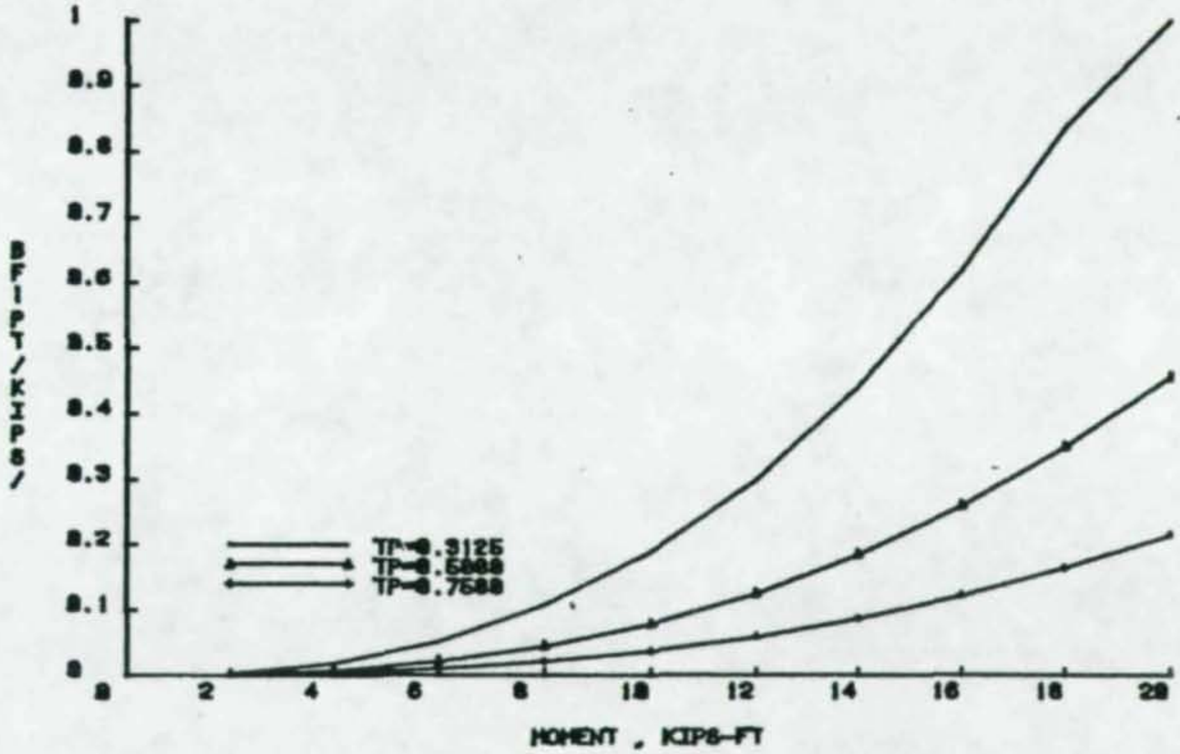

Figure F.27 $(B_F - P_T)$ Versus Moment Obtained from Equation (3.6.18) by Varying b_p, Through Low, Intermediate and High

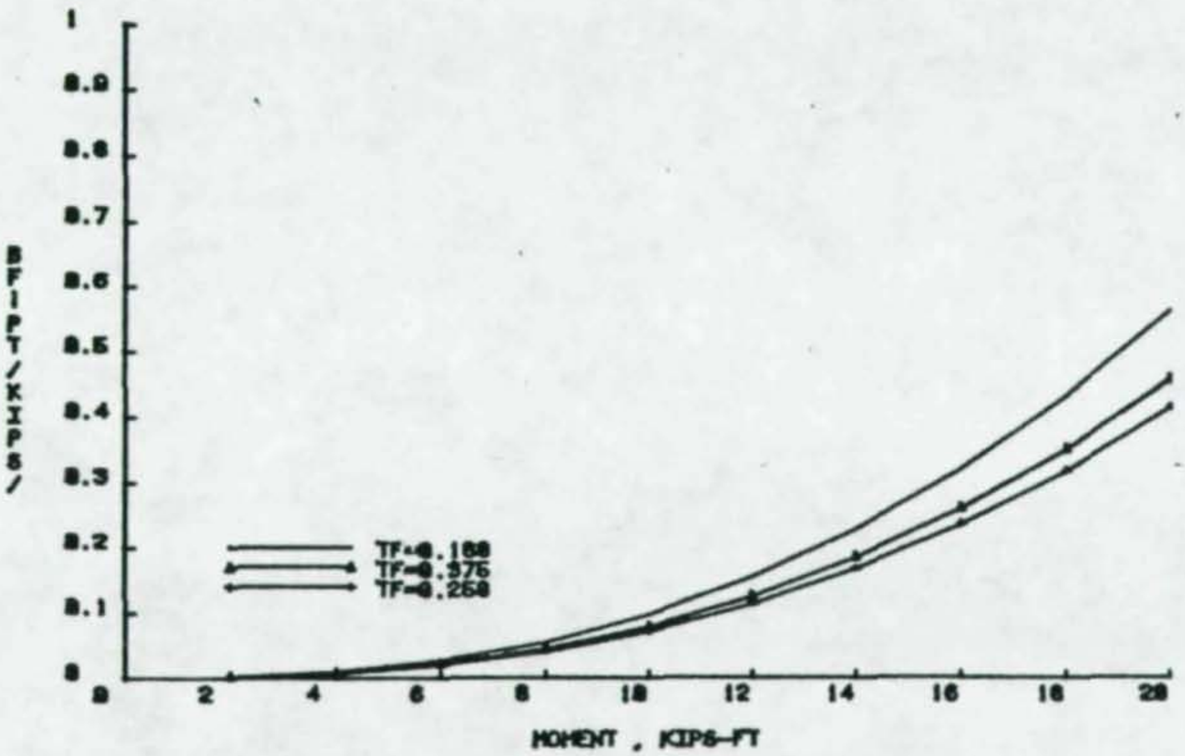

Figure F.28 $(B_F - P_T)$ Versus Moment Obtained from Equation (3.6.18) by Varying t_f, Through Low, Intermediate and High

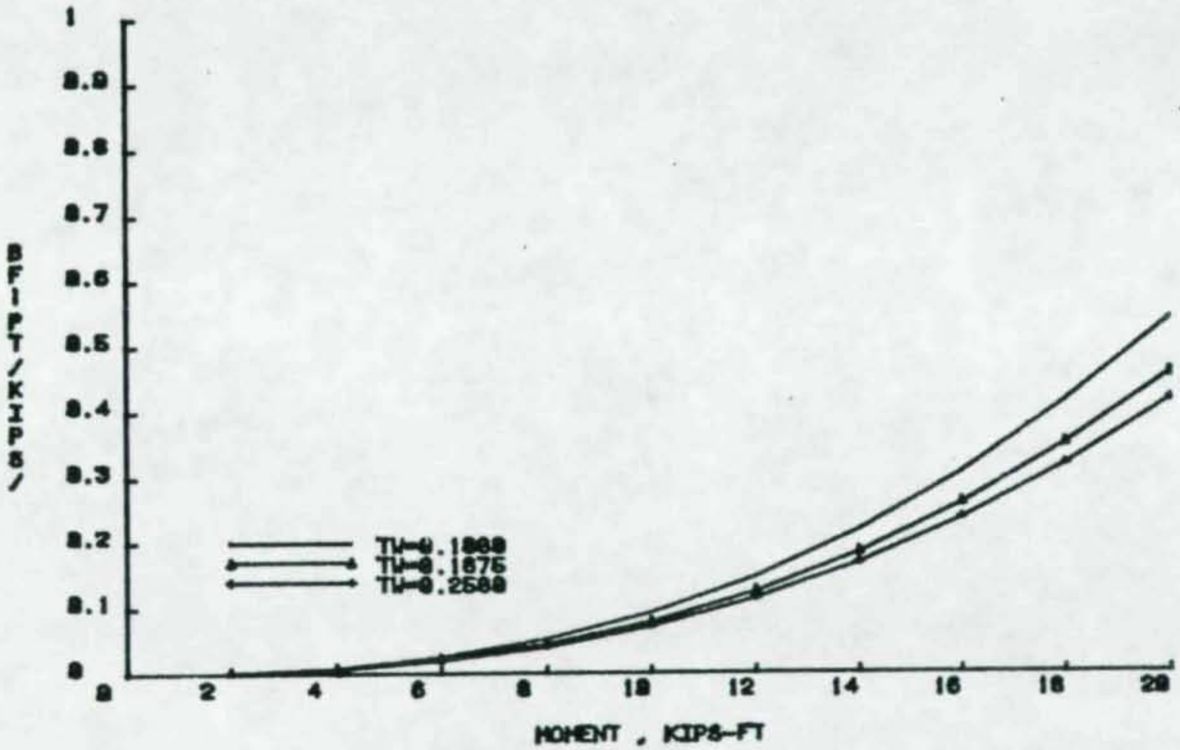

Figure F.29 $(B_F - P_T)$ Versus Moment Obtained from Equation (3.6.18) by Varying t_w, Through Low, Intermediate and High

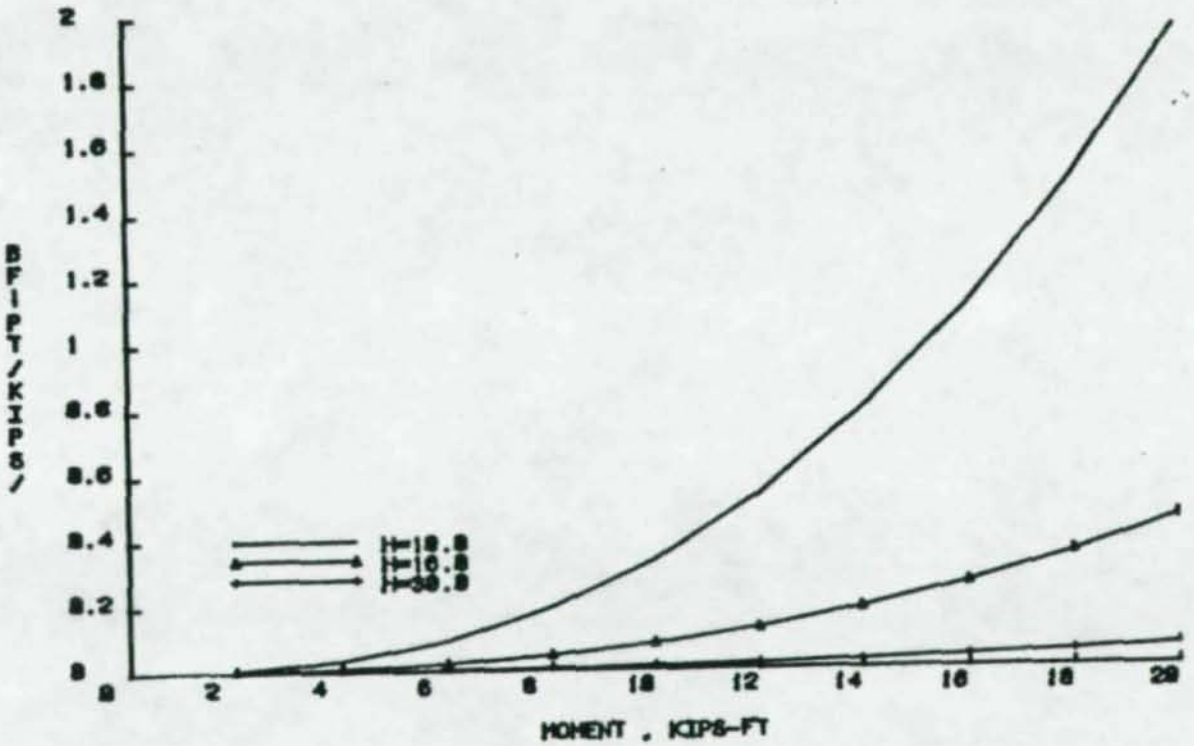

Figure F.30 $(B_F - P_T)$ Versus Moment Obtained from Equation (3.6.18) by Varying h, Through Low, Intermediate and High

APPENDIX G

DEVELOPMENT OF THE EQUATION FOR WIDTH OF RECTANGULAR BOLT ZONE

APPENDIX G

DEVELOPMENT OF THE EQUATION TO CALCULATE WIDTH OF RECTANGULAR BOLT ZONE

To calculate the width of rectangular bolt zone (refer to Section 2.2 of Chapter II), it was decided to correlate the resultant force associated with the tension region of a beam subjected to pure moment, T_t, to the yield strength of the entire beam cross-section, T_y. Figure G.1 represents the connection cross-section along with stress distribution used to develop this correlation. The resultant tension force is defined as follows:

$$T_t = 1/2\ (F_{by}\ (1 + (\frac{h - t_f}{h}))\ b_f + 1/2\ (\frac{h - t_f}{h})\ F_{by}\ t_w \qquad (G.1)$$

Equation (G.1) is to be simplified to the form:

$$\begin{aligned} T_t &= \Gamma\ T_y \\ &= \Gamma\ (A_B\ F_{by}) \end{aligned} \qquad (G.2)$$

where Γ is a scalar factor to be determined, A_B = area of beam cross-section and F_{by} = yield stress of beam material. Using dimensions of the 256 beam cross-sections selected in Chapter III, it was found that the factor Γ varied from 0.30 to 0.37 with an average value of 0.339. Hence, it was decided to use $\Gamma = 1/3$ to compute the resultant tension force subjected to pure moment.

Figure G.2 shows the plot of the right hand side of Equation

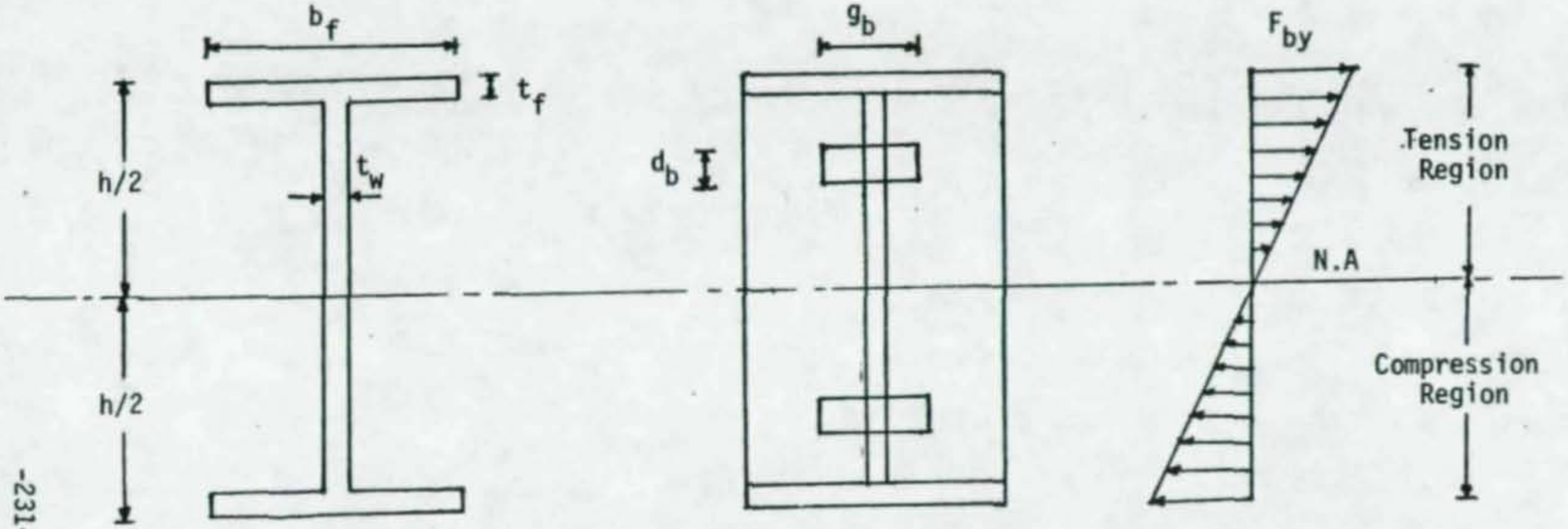

a) Beam Cross-Section

b) Connection Cross-Section

c) Stress Distribution (F_{by} = yield stress of beam material

Figure G.1 Connection Cross-Section and Assumed Stress Distribution

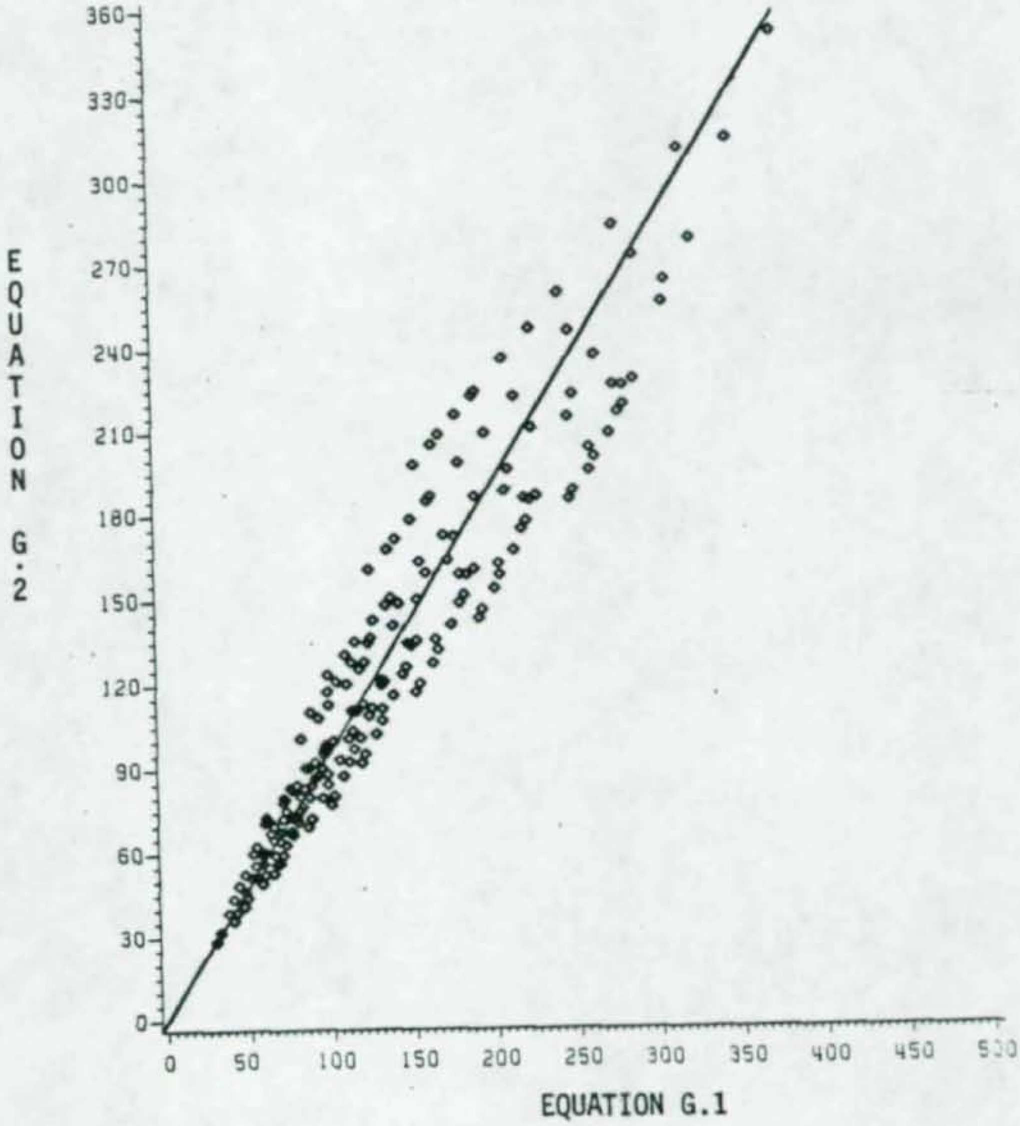

Figure G.2 Relationship Between Equation (G.2) and Equation (G.1)

(G.2) for $r = 1/3$ versus right hand side of Equation (G.1). A line with a slope of 1 to 1 is also drawn in this figure. Points on this line show that exactly same results are obtained from Equations (G.1) and (G.2). It can be noticed from this plot that all the points are close to 1:1 slope line, which is an indication that Equation (G.2) for $r = 1/3$ is a good representation of the Equation (G.1).

To compute the size of the equivalent rectangular area representing the tension bolts in the 2-D model, the ultimate capacity of the tension bolts was set equal to this resultant tension force:

$$(A_B\ F_{by})/3 = A_{be}\ F_{yb} \tag{G.3}$$

or

$$A_{be} = (1/3)\ (A_B\ F_{by})/F_{yb} \tag{G.4}$$

or

$$(g_b)\ (d_b) = (1/3)\ (A_B\ F_{by})/F_{yb} \tag{G.5}$$

where A_{be} = equivalent area of one row (zone) of bolts ($=g_b d_b$), F_{yb} = yield stress of bolt material, g_b = width of equivalent bolt rectangular area and d_b = bolt diameter. Using Equation (G.5), the width g_b of the equivalent bolt area can be obtained and is used as the thickness of the elements representing the bolt shank.